

UCLA

UCLA Electronic Theses and Dissertations

Title

Histones at the Nexus of Eukaryotic Evolution and Biology

Permalink

<https://escholarship.org/uc/item/3v87f2ts>

Author

Attar, Narsis

Publication Date

2017

Peer reviewed|Thesis/dissertation

UNIVERSITY OF CALIFORNIA

Los Angeles

Histones at the Nexus of Eukaryotic Evolution and Biology

A dissertation submitted in partial satisfaction of the requirements for

the degree Doctor of Philosophy

in Molecular Biology

by

Narsis Attar

2017

ABSTRACT OF THE DISSERTATION

Histones at the Nexus of Eukaryotic Evolution and Biology

by

Narsis Attar

Doctor of Philosophy in Molecular Biology

University of California, Los Angeles, 2017

Professor Siavash K. Kurdistani, Chair

Histones have long been known for their functions in packaging the eukaryotic genome and in regulating DNA-based processes. These functions are dependent on physical and chemical properties of histones constructing the nucleosome, the basic structural unit for packaging DNA. The packaging of DNA into chromatin limits DNA accessibility for processes such as transcription and DNA replication, putting the nucleosome in a position to govern and fine-tune these processes. The influence on DNA metabolic processes can be mediated through alterations in nucleosome composition and positioning as well as covalent modification of histones. Variations in nucleosome structure and stability achieved by the use of non-canonical histone variants can lead to changes in DNA wrapping and accessibility. Similarly, covalent modifications of histone N-terminal or core domains can lead to structural changes for the nucleosome and the chromatin fiber. Covalent modification of histone tails also contributes to recruitment and anchoring of protein complexes required for transcription, DNA repair and replication. Changes in histone modifications and

mutations in the enzymes adding and removing them are implicated in a wide-range of pathologies including cancer (discussed in chapters II, III and IV). Histone modifications are dynamically regulated, which makes them suitable for integration of environmental and cellular cues with gene expression. While histone modifications locally participate in orchestrating transcription, global changes in histone modifications can have profound effects on cellular physiology and metabolism. In fact, alterations in cellular levels of histone modifications are observed in diseases such as cancer and can be responsive to changes in physiologic state of the cell like intracellular pH. In addition to the well-recognized structural elements of histones, a less well-known feature of these ancient proteins is their potential metal binding capabilities. Since metals such as copper and iron are required for a variety of important functions, a potential ability of histones to affect cellular metal homeostasis would greatly increase their influence on cellular functions. Indeed we have recently discovered the function of one such metal binding site at the nucleosome core within the H3 dimerization interface in regulating copper homeostasis. Investigating the role of this region of the nucleosome in metal biology revealed an unprecedented molecular function of the nucleosome as an oxidoreductase enzyme, capable of catalyzing the reduction of Cu^{2+} to its bioavailable form Cu^{1+} . This remarkable enzymatic activity significantly affects copper-dependent activities including mitochondrial respiration and Sod1 function, with a profound impact on the molecular biology of eukaryotes and potentially their evolutionary origin. The importance of copper for various physiological and pathological states in humans further underscores the broad implications of copper reductase activity of the nucleosome. These discoveries mark a new frontier into chromatin biology and a function of histones which may have deemed these proteins suitable participants in the emergence of eukaryotes on Earth (discussed in chapters V and VI).

The dissertation of Narsis Attar is approved.

Heather Christofk

Michael Teitell

Hillary Coller

Michael F. Carey

Siavash K. Kurdistani, Committee Chair

University of California, Los Angeles

2017

Table of Contents

I.	Introduction and Literature Survey	1
	a. The Rise of Eukaryotes	3
	b. The Evolutionary Origin of Eukaryotic Histones	6
	c. Properties and Functions Of Histones	9
	i. Histone Variant	
	ii. Post-Translation Modifications	
	iii. Histones and Metals	
II.	Layered Regulation of the Epigenome and Its Links to Cellular Metabolism and Physiology	27
III.	Exploitation of EP300 and CREBBP Lysine Acetyltransferases by Cancer	34
IV.	Histone Deacetylase Inhibitors Provoke a Tumor Supportive Phenotype in Pancreatic Cancer Associated Fibroblasts	50
V.	The Histone H3-H4 Tetramer is a Copper Reductase Enzyme	66
VI.	Nucleosome Copper Reductase Activity is Required for SOD1 Function in Supporting Iron Metabolism	137

List of figures

Figure 1	Page 157
Figure 2	Page 158
Figure 3	Page 159

Acknowledgements

Chapter II appears as a reprint of a work published in the American Association of Cancer Research education book in 2014. Chapter III is a reprint of work published in the Cold Spring Harbor Perspectives in Medicine, 2016. Chapter IV appears as a reprint of work done as collaboration between the Kurdistani, Dawson, Radu and Donahue group directed by Andrew H. Nguyen and published in Oncotarget, 2017. Chapter V is work that is currently under peer-review. I would like to acknowledge the contribution of Oscar A. Campos, Maria Vogelauer, Stefan Schmollinger, Sabeeha Merchant, Yong Xue, Nathan Mallipeddi, Linda Yen, Shivani Thaker, Heather Christofk and Siavash Kurdistani to the work in chapter V and VI. I would like to thank Heather Christofk and Michael Carey for helpful discussions.

Sincere appreciation goes out to the entire Kurdistani group (2012-present) and particularly to Siavash Kurdistani for his support. I would like to express my heartfelt gratitude to my family, friends and life partner for their immense support. Finally, I acknowledge the UCLA-Caltech Medical Scientist Training program, the Molecular Biology Institute Interdepartmental PhD program, the department of Biological Chemistry and the NCI Ruth L. Kirschstein National Research service F30 Award for financial support for a period of three years during the course of my graduate studies.

Curriculum Vitae

Narsis Attar

EDUCATION

- 08/2010 to current UCLA David Geffen School of Medicine
UCLA-Caltech Medical Scientist Training Program, Y7
Class of 2019
- 08/2006 to 05/2008 University of California Berkeley
B.A. Molecular and Cell Biology division of Immunology and
Infectious disease
Honors graduate, Thesis: “Promoter Analysis in Rabbit Retinal
Ganglion Cell Subtypes”
- 09/2004 to 05/2006 Los Angeles Pierce College, Woodland Hills, CA
General education, Biology 2006

PUBLICATIONS:

1. Xue Y, Schmollinger S, **Attar N**, Campos O, Vogelauer M, Carey MF, Merchant SS, Kurdistani SK. Endoplasmic reticulum-mitochondria junction is required for iron homeostasis. *Journal of Biological Chemistry*, June 2017
2. Nguyen AH, Elliott IA, Wu N, Matsumura C, Vogelauer M, **Attar N**, Dann A, Ghukasyan R, Toste PA, Patel SG, Williams JL, Li L, Dawson DW, Radu C, Kurdistani SK, Donahue TR. Histone deacetylase inhibitors provoke a tumor supportive phenotype in pancreatic cancer associated fibroblasts. *Oncotarget*. March 2017
3. **Attar N**, Kurdistani SK. Exploitation of EP300 and CREBBP Lysine Acetyltransferases by Cancer. *Cold Spring Harb Perspect Med*. March 2017
4. von Euw E, Atefi M, **Attar N**, Chu C, Zachariah S, Burgess BL, Mok S, Ng C, Wong DJL, Chmielowski B, Lichter DI, Koya RC, McCannel TA, Izmailova E, Ribas A. Antitumor effects of the investigational selective MEK inhibitor TAK733 against cutaneous and uveal melanoma cell line. *Mol Cancer*. April 2012
5. Atefi M, von Euw E., **Attar N**, Ng C, Chu C, Guo D, Nazarian R, Chmielowski B, Glaspy JA, Comin-Anduix B, Mischel PS, Lo RS, Ribas A. Reversing Melanoma Cross-Resistance to BRAF and MEK Inhibitors by Co-Targeting the AKT/mTOR Pathway. *PLoS One* 2011 December; PMID: PMC3237573
6. Niehr F, von Euw E, **Attar N**, Guo D, Matsunaga D, Sazegar H, Ng C, Glaspy JA, Recio JA, Lo RS, Mischel PS, Comin-Anduix B, Ribas A. Combination therapy with vemurafenib

(PLX4032/RG7204) and metformin in melanoma cell lines with distinct driver mutations. *Journal of Translational Medicine* 2011 May; PMID: PMC3152784

7. Nazarian R, Shi H, Wang Q, Kong X, Koya RC, Lee H, Chen Z, Lee MK, **Attar N**, Sazegar H, Chodon T, Nelson SF, McArthur G, Sosman JA, Ribas A, Lo RS. Melanomas acquire resistance to B-RAF(V600E) inhibition by RTK or N-RAS upregulation. *Nature* 2010 Dec.; PMID: PMC3143360
8. Søndergaard JN, Nazarian R, Wang Q, Guo D, Hsueh T, Mok S, Sazegar H, MacConaill LE, Barretina JG, Kehoe SM, **Attar N**, von Euw E, Zuckerman JE, Chmielowski B, Comin-Anduix B, Koya RC, Mischel PS, Lo RS, Ribas A. Differential sensitivity of melanoma cell lines with BRAFV600E mutation to the specific Raf inhibitor PLX4032. *J Transl Med.* 2010 Apr.; PMID: PMC2876068
9. von Euw E, Chodon T, **Attar N**, Jalil J, Koya RC, Comin-Anduix B, Ribas A. CTLA4 blockade increases Th17 cells in patients with metastatic melanoma. *J Transl Med.* 2009 May; PMID: PMC2697137

PRESENTATIONS

1. **Narsis Attar**, Oscar Campos, Maria Vogelauer, Yong Xue, Stefan Schmollinger, Sabeeha Merchant, Siavash Kurdistani. The nucleosome and metal homeostasis: an evolutionary connection. Gordon Research Conference, Chromatin Structure and Function. May 2016
2. **Narsis Attar**, Matthew A McBrian, Maria Vogelauer, Siavash K Kurdistani. Molecular Mechanism of Global Histone Acetylation for Regulation of Intracellular pH. Cold Spring Harbor Laboratory Meeting, Epigenetics and Chromatin. September 2014
3. Erika von Euw, Mohammad Atefi, **Narsis Attar**, Sybil Zachariah, Barry L. Burgess, Tara McCannel, David I. Lichter, Elena Izmailova, Antoni Ribas. Effects of the investigational selective MEK inhibitor TAK-733 against cutaneous and uveal melanoma cell lines. AACR Annual Conference. April 2011
4. **N. Rahmanattar (Attar)**. Promoter Analysis in Rabbit Retinal Ganglion Cell Subtypes. UC Berkeley Molecular and Cell Biology Honors Poster Session, May 2008

Chapter I

INTRODUCTION

Histones were discovered as structural components of the eukaryotic genome functioning to package the genetic material. In the late 1980s, a series of seminal work provided evidence for the function of histones in regulating transcription and DNA replication, altering the view of the histones as inert DNA binding proteins to dynamic constituents of chromatin¹⁻³. The first level of DNA packaging hierarchy in eukaryotes is the nucleosome consisting of ~147 bp of DNA wrapped around an octameric histone complex composed of two molecules of each 4 core histones (H3, H4, H2A and H2B)⁴. Array of nucleosomes are then folded into higher ordered fibers of 30 nm, which in turn compact progressively to form larger chromatin domains⁵.

The four core histones exhibit substantial sequence and structural conservation across eukaryotic species. They share the common structure of a histone fold domain (HFD) and a highly basic N-terminal tail. The histone fold is an ancient structural motif consisting of 3 alpha helices connected by 2 loops and is thought to have originated in archaea with ubiquitous presence in eukaryotes⁶. This motif is often utilized in protein dimerization as is the case with histone proteins that form heterodimeric structures pairing H3 with H4 and H2A with H2B via a “handshake motif”. These dimeric structures are used to form the nucleosome as a heterotypic tetramer (H3-H4)₂ associated with two H2A-H2B dimers.

Histones through the formation of the nucleosome are inherently involved in DNA-based processes to varying capacities. Transcription through eukaryotic chromatin is a well-orchestrated molecular process that must be coordinated with nucleosome status. As early as 1980 it was observed that nucleosomes can prevent transcription initiation and pose an obstacle to this process

when present at high density⁷. Likewise, replication and repair of DNA need to be coordinated with nucleosome assembly/disassembly and repositioning⁸. Facilitation of such DNA-based processes on chromatin can be mediated by functions of nucleosome remodeling complexes, the use of non-canonical histone variants as well as post-translation modifications of histone N-terminal tails.

In this introductory chapter, I will briefly review the evolution and properties of the eukaryotic nucleosome. The extensive links between chromatin and both DNA-associated functions and other essential cellular processes will be discussed.

I. The Rise of Eukaryotes

The evolutionary events leading to the rise of eukaryotes has fascinated biologists for decades. The representation of Eukarya as the third domain in the tree of life may seem like a simple branching from the archaeal lineage. What is masked in this simple diagram representation is the series of complex events that took place to give rise to the last eukaryotic common ancestor (LECA)⁹. Eukaryotes harbor a number of unique features not found in the prokaryotic domains including the nucleus, the mitochondrion, endomembrane system, sterol synthesis, unique cytokinesis, phagocytic machinery, linear chromosomes with unique features (e.g. telomeres)⁹. The order of events and acquisition of these features leading to the LECA is unclear and a matter of debate. Which of these features were crucial and served as the impetus for eukaryogenesis is also not known. Simultaneous acquisition of these features in a primitive eukaryote seems doubtful because of its exceedingly low likelihood. It is more likely that species with some eukaryotic features coexisted and a key event, the presence of a feature or the appropriate combination of features at some point in time led to the triumph of one and the demise of all other lineages¹⁰. Although no single feature may have been the determining factor for eukaryogenesis, the acquisition of the mitochondrion is considered a critical step. The view that Eukarya arose from the association of an archaeal host, likely a species from the Crenarchaea lineage, and a bacterium, the proto-mitochondrion, is now accepted due to extensive sequence analyses and more comprehensive phylogenetic modeling¹¹. The integration of the bacterial symbiont into the host is a unique endosymbiotic phenomenon. Unlike other symbiotic scenarios, the mitochondria and the archaeal host evolved to replicate as a whole, which may be a reflection of an early interdependence between the two. It is difficult to know the nature and mechanism of this interdependency. However, for the symbiont to be functional in the confines of the host cell, it must have depended on the host for provision of at least some resources.

Among these, we believe transition metals to be major candidates. Specifically, we postulate that the symbiont must have needed copper and iron, metals required by essentially all organisms for many functions including those associated with the mitochondria¹².

Copper in the mitochondria is required for the function of cytochrome c oxidase, a member of the heme-copper oxidase family¹³. These enzymes are involved in respiration, the process of relaying electrons from organic materials to an inorganic molecule such as dioxygen and are found in all three domains of life¹⁴. Copper-heme cytochrome oxidases are ancient membrane-associated complexes that evolved before the divergence of archaea and bacteria and thus prior to oxygenation of Earth¹⁵. The presence of a primitive copper-containing cytochrome oxidase, whether oxygen-reducing or not, in the symbiont bacterium for eukaryogenesis is clear. We propose that the prokaryotic archaeal host must have had evolved a system for the intracellular handling of metals (e.g. iron and copper) which was then used for provision to the acquired intracellular bacterium—at minimum copper for the function of cytochrome c oxidase. It is important to note that most prokaryotes have limit copper use, which is mostly confined to the extracellular or periplasmic space¹⁶. This is in contrast to eukaryotes that require the use of copper not only by the mitochondria but other cellular processes inside the cell.

Intriguingly, the emergence of eukaryotes coincided roughly with accumulation of molecular oxygen on Earth, which led to oxidation of transition metals including iron and copper¹⁷. The oxidized metals (Fe^{3+} and Cu^{2+}) became less usable for biological systems that had evolved in a previously reducing environment¹⁸. In presence of oxygen these essential metals were also becoming more toxic due to their ability to generate oxygen radicals, posing yet another challenge to all organisms¹⁸. Eukaryogenesis was taking place in the face of these major challenges begging the question, “What inventions or features of the emerging eukaryote gave the organism the ability to prevail in these conditions?” Perhaps a unique challenge was faced by the early emerging eukaryote.

This species may have needed a system to be able to maintain copper in its bioavailable cuprous form (Cu^{1+}) intracellularly to supply the symbiont bacterium (i.e. proto-mitochondrion). Recent work by our group has identified a novel copper reductase activity of the eukaryotic histone tetramer and nucleosome (Attar, 2017. Submitted). In light of these findings, the presence of ancestral histones in the archaeal host for eukaryogenesis (see below) may have provided early eukaryotes with a tool to meet the challenges of utilizing copper intracellularly in an oxidizing environment. This idea will be further discussed in chapter V.

II. The Evolution of Eukaryotic Histones

The origin of eukaryotic histones can be traced back to archaea, which are prokaryotes with diverse biology. Histone-like proteins have been discovered in both major branches of archaea, Euryarchaea and Crenarchaea, suggesting their early evolution after the divergence of bacteria and archaea and long before eukaryotic emergence¹⁹. Archaeal histones found to date have sequence similarity to histones H3 and H4, and most strikingly, form structures homologous to the eukaryotic H3-H4 tetramer. Specifically, two histone proteins from *Methanothermobacter ferredoxigenes*, HMfA and HMfB and the histone protein HMk from *Methanopyrus kandleri* form homo or heterodimers and intra-protein dimers using two histone fold domains, respectively^{20,21}. In all cases, the dimeric structures are constituted into tetramers capable of binding ~60 bp of DNA forming a tetrasome. These tetrameric structures can form arrays on archaeal DNA resembling the eukaryotic chromatin²². Although the identity of the archaeal host for the eukaryotic endosymbiosis is still a matter of debate, the presence of primitive histones proteins in the host is certain.

Archaeal histones as the ancestors of eukaryotic histones can provide insight into the functional evolution of the nucleosome. It is thought that an early histone gene duplication event to allow dimer and tetramer formation, and the evolution of histone gene doublets (i.e. end-to-end histone folds) in archaea, were important for the eventual transition to the four eukaryotic histone proteins¹⁹. In the evolutionary timeline of histones, H3 and H4 predate H2A and H2B given the presence of tetramers in archaea and the eventual evolution of an octameric structure in eukaryotes²⁰. This suggests that the H3-H4 tetramer-like structure may have been the minimal required functional unit for the earliest emerging eukaryote.

What are the functions of histones in archaea? Were those functions important for eukaryotic evolution? Archaeal histones contain a core histone fold, but unlike eukaryotic histones

are devoid of extended N-terminal tails. Thus, they lack N-terminal tail post-translational modifications that regulate eukaryotic chromatin structure and DNA processes. Although a function of archaeal histones in DNA compaction has been suggested in some archaeal^{22,23}, histone DNA binding in archaea is not universal. Lack of genome-wide binding of archaeal histones in some cases is observed despite conservation of residues important for the function of eukaryotic histones²⁴. That archaeal genomes are small and do not need to be packaged into a nucleus, questions whether histone-mediated DNA compaction was the early functions of histones. Evidence has also been provided for a potential role of archaeal histones in regulating gene expression^{25,26}. However, it is important to emphasize that the manner by which tail-less archaeal histones mediate such a function differs from that of eukaryotes that employ histone N-terminal tail modifications. These findings challenge the idea that DNA compaction or gene regulation were the fundamental functions of histones in archaea. Dinoflagellates, a large and diverse group of eukaryotes, lack histones despite having in some cases up to 80 fold larger genomes than histone-containing eukaryotes^{27,28}. This further brings into question the notion that genome packaging was the driving force for the evolution of histones and chromatin structure in eukaryotes. However, it is possible that once histones had evolved and were present in the early eukaryote, additional features such as extended N-terminal tails and post-translational modifications aided in genome packaging and DNA-mediated processes throughout the expansion of eukaryotes.

To achieve the chromatin structure present in almost all eukaryotes today, the primordial tetrasome (i.e. histone tetramer associated with DNA) evolved to contain features required for eukaryotic biology. The transition from a tetramer to an octamer containing histone H2A and H2B is by far the most substantial alteration to the histone-containing globular structure^{19,20}. It is suggested that the transition to an octamer was needed to achieve a greater degree of DNA compaction in eukaryotes; however, this cannot be fully reconciled when considering the small

genome of primitive eukaryotes and the larger genome size of certain archaeal species. Nevertheless, an octameric structure can be more feasible for compacting larger genomes. Additionally, incorporation of H2A-H2B dimer can modulate the structural flexibility of the tetrasome providing a layer of structural regulation²⁹.

While maintaining a high degree of structural conservation, the complexity of the nucleosome has expanded throughout eukaryotic evolution. Numerous variants of canonical histones have been appropriated that play roles in mediating chromosome dynamics and transcription³⁰. Functional specialization of nucleosome is further achieved through the acquisition of highly modifiable extended N-terminal tails in all four core eukaryotic histones. These specialized features of the nucleosomes will be briefly discussed in the following sections.

III. The Properties and Functions of Histones

i. Histone Variants

Most eukaryotes possess multiple copies of each canonical histone gene usually arranged in clusters. The expression of canonical histones is tightly coupled to the S phase of the cell cycle; therefore, these constitute the majority of histones incorporated in nucleosomes genome-wide.³¹ Genes encoding non-canonical histone variants are usually found singly and are expressed throughout the cell cycle. Variants are the major source of histones outside of S phase and in non-dividing cells³². Multiple variants for histones H3, H2A and H2B have been identified in most lineages of eukaryotes, with limited presence in some lower eukaryotic species such as *Saccharomyces Cerevisiae*. Specific molecular functions have been ascribed to certain histone variants ranging from gene activation/repression to DNA-repair and X chromosome inactivation³⁰.

a. Histone H3 variants with varied levels of divergence

The deviation from canonical histones is in most cases minimal and restricted to a few residues, but more divergent variants are also present. An examples of highly divergent histone variants present in nearly all eukaryotes is the centromeric histone H3 having only ~50% similarity to the histone fold of canonical H3 and minimal conservation of the N-terminal tail³¹. Nucleosomes at the eukaryotic centromeres are highly enriched for the centromeric H3 variant as this variant is required, but not sufficient, for the special centromeric chromatin architecture, kinetochore formation and proper chromosome segregation³³. In fact, the rapid evolution of centromeric H3 across eukaryotes and its divergence from H3 may be due to the requirement for binding to and anchoring various components of the kinetochore and mitotic machinery²⁰.

Histone H3 variants with significantly higher conservation include the replication-independent H3.3, differing for example at only five amino acid residues from replicative H3 (H3.1

and H3.2) in mammals³⁴. With the exception of *Acetomyces* including *Saccharomyces Cerevisiae* that contains a sole histone H3 resembling H3.3, when present as a non-replicative variant, H3.3 is associated with transcriptionally-active chromatin replacing canonical H3 during gene activation³⁵. Highlighting the function of H3.3 in gene activation, this variant harbors post-translational modifications associated with gene activity in humans, flies and plants³⁶.

Unique to mammals is the presence of an additional replication-dependent histone H3 (H3.1), differing at one amino acid position from H3.2³⁴. This corresponds to cysteine and serine 96 in H3.1 and H3.2, respectively. Although the significance of this subtle specification is not yet clear, the nature of this amino acid in H3.1 is intriguing, as cysteine residues can participate in oxidation and reduction cycles. How or whether C96 is linked to the redox state of the cell and what this could mean requires further investigation.

b. Histone H2A variants and nucleosome stability

Similar to histone H3, histone H2A has several variants with varying levels of divergence from canonical H2A. Of these, histone H2A.Z and H2A.X are conserved through most eukaryotic lineages and have specialized functions in gene activation and DNA repair, respectively³⁰. Histone H2A variants differ mostly in the sequence and length of the C-terminal tail³⁷. This is interesting given the interactions between this region of histone H2A and the H3-H4 dimer and can affect the stability and flexibility of the H3-H4 tetramer³⁸. In fact, nucleosomes containing H2A.Z show destabilization of the interaction between H2A.Z-H2B and the H3-H4 dimers leading to a looser packaging of the DNA protecting only ~120 bp³⁹. It is also possible that the rate of histone H2A.Z-H2B turnover and exchange is higher than that of H2A-H2B dimers. Therefore, H2A.Z-containing nucleosomes can be more dynamic in transitioning between the tetrasome and nucleosome states. The association of H2A.Z with transcriptional activation can provide a justification for this property. However, more recent studies have described enrichment of H2A.Z with heterochromatin

(i.e. inactive chromatin) and a function of this variant in suppression of antisense transcription^{40,41}. Although, it is possible that the functions of H2A.Z are context-dependent, the instability of H2A.Z vs. canonical nucleosomes may be involved in regulating a function(s) of nucleosome other than transcription.

c. Principles and functions of histone variants

How are the functions of histone variants mediated? One regulatory step is the timing of histone variant expression. In regards to more divergent variants, major amino acid changes, especially of exposed residues, can modulate interactions with histone modifying enzymes, transcriptional or DNA-repair machinery mediating specialized functions. Structural deviations from canonical nucleosomes have also been noted for such divergent variants, such as centromeric H3, MacroH2A and H2A.Z^{42,43}. However, despite the striking sequence conservation between some canonical histones and their variants, the variant histone is required for specific functions on a cellular or even organismal level. For instance, in some multi-cellular organisms, the abundance of histone H3 variants can vary from tissue to tissue⁴⁴. The only tissue-specific histone H3 variant that is well established is the testis-specific H3.1, which is essential for spermatogenesis⁴⁵. Whether maintaining a specific histone variant composition in somatic cell types is required for cellular identity or certain functional demands of such cells is unclear.

The presence of histone variants results in spatial and temporal nucleosome structural heterogeneity across the genome. It is clear that locally histone variants can impart structural and functional changes on chromatin. An intriguing question is whether this heterogeneity is dynamic genome-wide and functionally meaningful on a global level for certain cellular functions. For example, what roles, if any, do histone variants play in the regulation of the copper reductase activity of the nucleosome or the tetrasome? Differences in structural flexibility can result in confirmation changes or lack-there-of that may be required for or modulate the catalytic activity. Conceivably,

protein-protein interactions facilitated by the histone variant surface-exposed residues can recruit components of the reaction such as chaperons for copper delivery to or liberation from the nucleosome. Investigating these ideas by integrating our current knowledge of histone variants and the novel enzymatic activity of nucleosomes is imperative to understanding the full spectrum of chromatin function.

ii. Histone N-Terminal Tails and Core Post-Translational Modifications

a. The contributions of N-terminal tails and their modifications to nucleosome structure

The N-terminal tails of core histones are targets for a multitude of covalent post-translational modifications (PTMs) including acetylation, methylation and phosphorylation⁴⁶. Histone modifications are heavily studied for their functions in changing the local chromatin landscape. Combinatorial presence of tail modifications, which has been well-appreciated in the last decade, index the genome and provide highly specific regulation of the chromatin state^{47,48}. This is partly achieved through recruitment and anchoring of various protein complexes at specific loci to mediate DNA-based processes. Tail modifications function as docking sites for chromatin readers, proteins harboring domains that specifically recognize these modifications, and include components of the transcription, DNA replication and chromatin remodeling machinery⁴⁹. Recent studies have now provided a greater appreciation for the role of such PTMs in altering nucleosome structure and dynamics.

Acetylation of lysine residues is one of the earliest histone modifications identified and was recognized as a means to neutralize the positive charge of numerous lysines in the N-terminal tails. Acetylation is thought to relax the electrostatic interactions between these basic residues and DNA and contributes to enhanced accessibility. Methylation of lysine and arginine residues involved in

histone-DNA interactions and to some extent serine phosphorylation can affect chromatin structure through diverse mechanisms such as recruitment of chromatin factors and introduction of a negative charge, respectively⁵⁰.

In the last two decades, multiple crystal structures of the nucleosome have provided insight into the effect of histone tails on chromatin structures⁵¹. These structures reveal histone N-terminal tails extend out from the face of the nucleosome and lack organized domains⁵². However, several contact sites between distal, less heavily modified regions of histone tails, specifically for histone H3 and H2B, and the octamer-wrapped DNA are present⁵². The distal domain of the N-terminal tail for all four histones have also been shown to contribute to DNA wrapping around the nucleosome⁵³. In addition, histone tails interact with linker DNA and the neighboring nucleosomes, which regulates higher-order chromatin fiber structure⁵⁴.

Structural analysis of nucleosomes reconstituted with one of the four histones lacking the N-terminal tail, have determined the contribution of histone tails. Although these findings can be extended to predict the effect of chemical alterations of the tail via specific PTMs, more direct evidence is needed to precisely define the role of specific post-translational modifications. Mutations of lysine residues mimicking acetylated (glutamine) or non-acetylated (arginine) states have provided enormous insight into the function of these modifiable sites. Such studies have pinpointed specific contributions of lysine residues, for example, the link between H4 K5/K12 diacetylation and nucleosome assembly and the role of H4 K16 acetylation in heterochromatin formation among others⁴⁷. It is important to note that acetylation-mimicking mutations, which address the presence or absence of the charge associated with lysine, are not perfect since they do not possess the structural property of an acetyl-lysine. Biochemical studies using acetylated histones have revealed the particular effect of this PTM on nucleosome dynamics. Interestingly, the effect of histone acetylation or deletion of histone tail was shown to be minimal for the nucleosome but producing

significant alteration of the H3-H4 tetrasome structure⁵⁵. Hyperacetylated H3-H4 tetrasomes but not nucleosomes undergo structural changes adopting a relaxed conformation and altered DNA supercoiling⁵⁵. These findings strongly suggest the effect of tail hyperacetylation may be mediated through transiently formed flexible H3-H4 tetramers *in vivo*.

The prevalence and significance of tetrasomes *in vivo* is unclear. Transient formation of intermediate nucleosome states including tetrasome occurs during nucleosome assembly/disassembly but this is not shown to depend on histone tail hyperacetylation^{56,57}. Transcription by RNA polymerase II on highly acetylated active chromatin may specifically rely on transient formation of flexible tetrasomes⁵⁸. It is also possible that tetrasome formation *in vivo* is more prevalent than previously assumed through the combined functions of enhanced H2A-H2B dimer exchange and histone tail acetylation. This notion can broadly impact our understanding of the many functions associated with the nucleosome. One such a function is the copper reductase activity observed for nucleosomes, which is not limited to the octameric complex as is observed with H3-H4 tetramers *in vitro*. A major question for future investigations is whether *in vivo* the enzymatic activity is associated with just the nucleosome, the tetrasome or both. Dynamic nucleosome-tetrasome transition, potentially through histone acetylation, may regulate this function of histones. In the same scope of ideas, the role of histone tail acetylation either via provoking other structural changes or serving as docking sites for protein recruitment can impact the kinetics of copper reductase activity.

b. Post-translational modifications of histone core domains

For decades studies on covalent histone modifications focused largely on those occurring at the N-terminal tail. Modifications of the core domain, depending on the position, can have diverse effects at the level of the nucleosome as well as chromatin architecture. Core PTMs can be divided into those at protein-protein or protein-DNA interfaces and at the nucleosome surface, greatly

impacting nucleosome structure and participating in recruitment of other proteins to chromatin, respectively⁵⁹. Among solvent-accessible surface PTMs is histone H3K79 methylation that has been extensively studied for its influence on heterochromatin gene silencing⁶⁰. Interestingly, it is thought that this function is indirect as this modification is more abundant on euchromatin. Based on studies in yeast it was proposed that H3K79 methylation functions to prevent the association of components of silent chromatin with the nucleosome ensuring the availability of these factors for assembly of silent chromatin elsewhere⁶¹.

The widespread application of mass spectrometry for detecting protein modifications, has led to the discovery of numerous PTMs on histone core domains. Although most have not been extensively studied, a large number of these modifications fall at the lateral surface of the nucleosome near the dyad. A number of these residues are contributed by the c-terminal region of histone H3 and by histone H4 and include H3T118, H3K115, H3K122 and H4S47⁶⁰. This region is of interest since it contains many histone-DNA interaction sites. Modifications of these residues that for the most part are highly conserved can regulate the kinetics of octameric DNA unwrapping⁶⁰. Given that the H3 residues mentioned above are within the 4 helix bundle that holds the H3-H4 tetramer together, their modifications can also potentially affect protein-protein interactions⁵². Therefore, PTMs at these sites can affect nucleosome dynamics, DNA accessibility and nucleosome mobility.

More recently, amino acid modifications with larger chemical moieties such as ubiquitin and glutathione have been identified in the core domains of histones. Mono-ubiquitination of lysine 119 in H2A and lysine 120 in H2B in mammals with equivalent residues found in yeast and plant H2B are among the most well-recognized of these modifications. These are associated with gene silencing and transcription initiation, respectively⁶². The conserved lysine 122 in histone H3 has also been shown to be ubiquitinated and can impact nucleosome dynamics and assembly given its position as

previously highlighted⁶³. Ubiquitin is a large molecule and would be expected to induce physical changes in the nucleosome conformation. Further investigations of the specific structural consequences of core lysine ubiquitination are needed.

A less bulky, yet relatively large, protein adduct is glutathione (γ -L-Glutamyl-L-cysteinylglycine). Glutathione is known for its function in maintaining the redox equilibrium of the cell but its reactivity with thiolate anions of cysteine residues in target proteins can regulate many protein functions⁶⁴. Evidence for S-glutathionylation of a well-conserved cysteine residue (C110) of histone H3 has been found in mammals⁶⁵. This cysteine residue lies at the core of the nucleosome at the interface of the two histone H3 molecules, and its modification by glutathione destabilizes the nucleosome *in vitro*⁶⁵. Alterations of C110 through S-glutathionylation is correlated with proliferation in mammalian cells and is associated with young age in mice⁶⁵. Oxidation and disulfide bridge formation between the two C110 residues, one from each H3 molecule, were reported as early as 1977⁶⁶. The potential presence of a disulfide bridge at this site *in vivo* is likely biologically meaningful; however, further investigation is needed to address this. Although a disulfide bridge would be structurally and chemically different from glutathionylation of cysteines, the ability of this cysteine to undergo redox reactions with glutathione or with the opposing cysteine hints at an interesting but unknown function of this residue.

c. Histone modifying enzymes and the link between chromatin and cellular metabolism

Covalent modification of histone tail and core residues is mediated by a diverse group of histone-modifying enzymes (HMFs). The enzymatic activity is in most cases contained in large multi-protein complexes that can also harbor histone chaperon, nucleosome remodeling, PTM recognition or DNA-binding activities⁶⁷. The varied nature of these complexes allows for coupling of chemical modification of histone with physical alterations such as assembly and remodeling.

The reversibility of almost all histone modifications in an enzyme-dependent manner allows for dynamic regulation of the nucleosome and functions linked to PTMs. The rate of turnover for various modifications is set by the action of enzymes writing and removing the modification, with lysine acetylation having the highest rate of turnover⁶⁸. This is an important concept for understanding the fluidity of chromatin states and the integration of cellular cues with chromatin. An emerging body of work has revealed links between histone modifications and metabolic networks facilitated in part by histone-modifying enzymes. Cellular metabolites can serve as regulatory co-factors such as the case with NAD-dependent Sir2 family of deacetylases or as the source of the chemical moiety (i.e. acetyl-CoA for acetylation reactions)⁶⁹. Primary metabolism and the secondary metabolites derived from metabolic pathways can be theoretically linked to almost all functions of chromatin. Evidence for the converse relationship namely chromatin state altering the metabolome, has been put forth. The most recognized mode of mediating this is through regulation of expression of metabolic genes in response to sensing a relevant secondary metabolite by chromatin modifiers.⁷⁰ More direct crosstalk can involve consumption or generation of a certain metabolic factor through establishing or removing certain histone modifications, respectively, either locally or genome-wide. For example, generation of acetate anions upon histone deacetylation can represent a substantial source of carbon and impact metabolism⁷¹. Although more investigation is required to understand such effects of chromatin on cellular metabolism, it is easy to imagine many instances of this type of crosstalk.

Considering the evolutionary origin of the nucleosome, one might postulate the inheritance of the repertoire of histone-modifying enzymes from ancient archaea. Surprisingly, evidence suggests a proteobacterial origin of primitive histone modifying enzymes in eukaryotes⁷². Sequencing of a great number of bacterial genomes has identified genes with similarity to chromatin modifying enzymes of eukaryotes⁷³. Conversely, archaea lack histone modifications and therefore do not have

the repertoire of modifier enzymes. The bacterial homologues of eukaryotic chromatin modifiers enrich for functions in secondary metabolism and bacterial defense system, which in some cases rely on modifying peptides, DNA and small molecules of the competing organisms⁷². Diversification of these enzymes is speculated to have occurred in bacteria partly due to the expansion of secondary metabolism as a result of the Great Oxygenation Event⁷². Interestingly, this includes the invention of oxygen-utilizing enzymes that are homologous to oxygen-dependent histone demethylases such as LSD1 present in eukaryotes⁷³. Although the adaptation and advantage of these bacterial inventions are apparent in modern eukaryotes, that may not have been the case for the archaea host for eukaryogenesis. It has been proposed that active manipulation of the host's DNA and protein by the bacteria endosymbiont may have in fact driven the emergence of the nucleus, a protective barrier to foreign modifications.

iii. Histones and Transition Metals

As early as 1980s it was postulated that metal ions may play a role in chromatin structure and organization⁷⁴. This postulate came after a series of investigations revealed potential metal binding motifs for numerous DNA-binding transcription factors. Zinc binding was demonstrated for some of those proteins and was shown to mediate their stabilization and association with DNA⁷⁵. The idea that an analogous binding site was present in the nucleosome and could mediate interactions between histones and transcription regulators was entertained. The structure of the nucleosome core particle had in fact revealed the presence of a similar metal binding motif. This comprised of residues 110-113 in the C-terminal region of histone H3 generating a potential metal binding pocket upon H3 dimerization⁷⁴. Decades later the ability of this region of the H3-H3' dimerization interface to bind various metal ions was demonstrated *in vitro*⁷⁶. Whether metal binding occurs *in vivo*, and the

biological significance of such binding had not been investigated. Our recent work (see chapter V) reveals a novel function of this region of the nucleosome in transition metal, specifically copper, homeostasis. The function of the nucleosome to support copper-dependent processes through the enzymatic reduction of copper ion, is affected by mutation of His113 to an asparagine in this region of histone H3. Interestingly, mutating the cysteine residue (C110), which together with histidine 113 form the metal binding motif, to an alanine, almost abolishes the copper reductase activity of the H3-H4 tetramer *in vitro*. Altogether suggesting a role of this metal binding motif potentially as a site for copper coordination during catalytic reduction. More investigation into the mechanistic contribution of this metal binding domain to copper reductase activity as well as its link to other properties of the nucleosome is needed.

In addition to the H3-H3' dimerization interface, a metal binding site on the surface of the nucleosome was revealed in one of the early high resolution structures of the nucleosome core particle containing the histone variant H2A.Z³⁸. Two well-conserved histidine residues, His112 and His114, in the H2A.Z docking domain mediate coordination of a manganese ion in the structure^{38,77}. The identity of a potential metal at this site *in vivo* is not clear, but copper or zinc are plausible given the coordination chemistry. These histidine residues are not found in canonical H2A and are absent from *Saccharomyces Cerevisiae* H2A.Z⁷⁷ suggesting a specialized function in some eukaryotes. The function of this metal binding site has not been examined thoroughly but a role for the two histidine residues in *Xenopus laevis* development has been shown. Specifically, a defect in mesoderm formation is observed in embryos with H2A.Z containing histidine mutations⁷⁸. Of note, mutations of the copper transporter (Ctr1) in *Xenopus laevis* has been shown to result in a mesoderm induction defect⁷⁹. Does this hint at the identity of the metal coordinated by H2A.Z *in vivo*? More work needs to be conducted to answer such questions and to further understand whether H2A.Z putative metal binding affects cellular copper metabolism. Lastly, this property of histone H2A.Z may be linked to

the copper reductase function of the nucleosome. The docking site of H2A.Z which contains the metal binding pocket is in close proximity to the N-terminal region of histone H3³⁸. It is possible that copper binding by H2A.Z can participate in transfer of copper to/from the enzyme catalytic site, which is postulated to be at H3-H3' dimerization interface. However, these two regions in a fully formed nucleosome are far apart and such direct interaction is improbable. However, the dynamic exchange of H2A-H2B dimers and structural transitions of the nucleosome may transiently mediate such an interaction. The co-localization of H2A.Z and histone H3.3 observed in the same genomic regions or nucleosome for transcriptional activation may hint at a specific interaction, physical or functional, between these variants in regards to copper reduction by the nucleosome. Extending this idea one can imagine differences in the copper reductase activity at various regions of chromatin. Changes in enzymatic activity can be associated with changes in histone variants or histone modifications, and even more broadly, with heterochromatic or euchromatic states.

References

1. Grunstein, M. HISTONE FUNCTION IN TRANSCRIPTION. *Annu. Rev. Cell Biol.* 643–678 (1990). doi:10.1146/annurev.cb.06.110190.003235
2. Gary Felsenfeld. Chromatin as an essential part of the transcriptional mechanism. *Nature* **355**, (1992).
3. Stillman, B. Chromatin Assembly during S/40 DNA Replication In Vitro. **45**, 555–565 (1986).
4. McGhee, J. D. & Felsenfeld, G. Nucleosome structure. *Ann. Rev. Biochem.* (1980). doi:10.1146/annurev.bi.49.070180.005343
5. Leonardo Mariño-Ramírez, Maricel G Kann, Benjamin A Shoemaker, and D. L. Histone structure and nucleosome stability. *Expert Rev Proteomics* **2**, 719–729 (2005).
6. Arents, G. & Moudrianakis, E. N. The histone fold: a ubiquitous architectural motif utilized in DNA compaction and protein dimerization. *Proc. Natl. Acad. Sci. U. S. A.* **92**, 11170–4 (1995).
7. Knezetic, J. A. & Luse, D. S. The Presence of Nucleosomes on a DNA Template Prevents Initiation by RNA Polymerase II In Vitro. *Cell* **45**, 95–104 (1986).
8. Ransom, M., Dennehey, B. K. & Tyler, J. K. Chaperoning histones during DNA replication and repair *Monica*. **140**, 183–195 (2010).
9. Gribaldo, S., Poole, A. M., Daubin, V., Forterre, P. & Brochier-Armanet, C. The origin of eukaryotes and their relationship with the Archaea: are we at a phylogenomic impasse? *Nat. Rev. Microbiol.* **8**, 743–752 (2010).
10. Booth, A. & Doolittle, W. F. Eukaryogenesis, how special really? *Proc. Natl. Acad. Sci.* **112**, 10278–10285 (2015).
11. Williams, T. A. & Embley, T. M. Archaeal ‘dark matter’ and the origin of eukaryotes. *Genome Biol. Evol.* **6**, 474–481 (2014).
12. Tracy Nevitt¹, Helena Öhrvik¹, and D. J. T. Charting the travels of copper in eukaryotes from yeast to mammals. **1823**, 1580–1593 (2013).
13. Horn, D. & Barrientos, A. Mitochondrial copper metabolism and delivery to cytochrome C oxidase. *IUBMB Life* **60**, 421–429 (2008).
14. Sousa, F. L. *et al.* The superfamily of heme–copper oxygen reductases: Types and evolutionary considerations ✱. (2012). doi:10.1016/j.bbabi.2011.09.020

15. Castresana, J., Lübben, M., Saraste, M. & Higgins, D. G. Evolution of cytochrome oxidase, an enzyme older than atmospheric oxygen. *EMBO J.* **13**, 2516–2525 (1994).
16. Festa, R. A. & Thiele, D. J. Copper: An essential metal in biology. *Current Biology* **21**, (2011).
17. Anbar, A. D. OCEANS: Elements and Evolution. *Science (80-.)*. **322**, 1481–1483 (2008).
18. Hong Enriquez, R. P. & Do, T. N. Bioavailability of Metal Ions and Evolutionary Adaptation. *Life* **2**, 274–285 (2012).
19. Dryhurst, D. & Ausio, J. *Evolutionary Biology*. (2009). doi:10.1007/978-3-642-00952-5
20. Malik, H. S. & Henikoff, S. Phylogenomics of the nucleosome. **10**, 882–891 (2003).
21. Sandman, K., Krzycki, J. A., Dobrinski, B., Lurz, R. & Reeve, J. N. Hmf, a DNA-binding protein isolated from the hyperthermophilic archaeon *Methanothermus fervidus*, is most closely related to histones (DNA-protein complex/thermal stability/molecular evolution/histone sequence conservation). *Biochemistry* **87**, 5788–5791 (1990).
22. Dé, F., Marc, R., Sandman, K., Lurz, R. & Reeve, J. N. Archaeal Histone Tetramerization Determines DNA Affinity and the Direction of DNA Supercoiling*. (2002). doi:10.1074/jbc.M203674200
23. Higashibata, H., Siddiqui, M. A., Takagi, M., Imanaka, T. & Fujiwara, S. Surface histidine residue of archaeal histone affects DNA compaction and thermostability. (2003). doi:10.1016/S0378-1097(03)00358-6
24. Dulmage, K. A., Todor, H. & Schmid, A. K. Growth-phase-specific modulation of cell morphology and gene expression by an archaeal histone protein. *MBio* **6**, (2015).
25. Ammar, R. *et al.* Chromatin is an ancient innovation conserved between Archaea and Eukarya. *Elife* **1**, e37 (2012).
26. Soares, D. *et al.* Archaeal histone stability, DNA binding, and transcription inhibition above 90 degrees C. *Extremophiles* **2**, 75–81 (1998).
27. Rizzo, J. Those amazing dinoflagellate chromosomes. **13**, 215–217 (2003).
28. Talbert, P. B. & Henikoff, S. Chromatin: Packaging without Nucleosomes. (2012). doi:10.1016/j.cub.2012.11.004
29. Hamiche, A. The Switch in the Helical Handedness of the Histone (H3-H4) 2 Tetramer within a Nucleoprotein Particle Requires a Reorientation of the H3-H3 Interface *. **273**, 9261–9269 (1998).
30. Kamakaka, R. T. Histone variants: deviants? *Genes Dev.* **19**, 295–316 (2005).

31. Talbert, P. B. & Henikoff, S. Histone variants — ancient wrap artists of the epigenome. **11**, (2010).
32. Maze, I., Noh, K.-M., Soshnev, A. A. & David Allis, C. Every amino acid matters: essential contributions of histone variants to mammalian development and disease. *Nat. Publ. Gr.* **15**, (2014).
33. Verdaasdonk, J. S. & Bloom, K. Centromeres: unique chromatin structures that drive chromosome segregation. *Nat. Rev. Mol. Cell Biol.* **12**, 320–332 (2011).
34. Hake, S. B. & Allis, C. D. Histone H3 variants and their potential role in indexing mammalian genomes : The “ H3 barcode hypothesis ”. **103**, (2006).
35. Ahmad, K. & Henikoff, S. The Histone Variant H3.3 Marks Active Chromatin by Replication-Independent Nucleosome Assembly ment are not clear. A study in Tetrahymena concluded that no protein difference between histone H3 variants was required for replacement histone deposition and. *Mol. Cell* **9**, 1191–1200 (2002).
36. McKittrick, E., Gafken, P. R., Ahmad, K. & Henikoff, S. From The Cover: Histone H3.3 is enriched in covalent modifications associated with active chromatin. *Proc. Natl. Acad. Sci.* **101**, 1525–1530 (2004).
37. B??nisch, C. & Hake, S. B. Histone H2A variants in nucleosomes and chromatin: More or less stable? *Nucleic Acids Res.* **40**, 10719–10741 (2012).
38. Suto, R. K., Clarkson, M. J., Tremethick, D. J. & Luger, K. Crystal structure of a nucleosome core particle containing the variant histone H2A.Z. *Nat. Struct. Biol.* **7**, 1121–1124 (2000).
39. Tolstorukov, M. Y., Kharchenko, P. V, Goldman, J. A., Kingston, R. E. & Park, P. J. Comparative analysis of H2A . Z nucleosome organization in the human and yeast genomes. 967–977 (2009). doi:10.1101/gr.084830.108. Identification
40. Rangasamy, D., Berven, L., Ridgway, P. & Tremethick, D. J. Pericentric heterochromatin becomes enriched with H2A.Z during early mammalian development. *EMBO J.* **22**, 1599–1607 (2003).
41. Zofall, M. *et al.* Histone H2A.Z cooperates with RNAi and heterochromatin factors to suppress antisense RNAs. *Nature* **461**, 419–422 (2009).
42. Chakravarthy, S. *et al.* Structural Characterization of the Histone Variant macroH2A. *Mol. Cell. Biol.* **25**, 7616–7624 (2005).
43. Tachiwana, H. *et al.* Crystal structure of the human centromeric nucleosome containing CENP-A. *Nature* **476**, 232–235 (2011).
44. Maehara, K. *et al.* Tissue-specific expression of histone H3 variants diversified after species separation. *Epigenetics Chromatin* **8**, 35 (2015).

45. Ueda, J. *et al.* Testis-Specific Histone Variant H3t Gene Is Essential for Entry into Spermatogenesis. *CellReports* **18**, 593–600 (2017).
46. Kouzarides, T. Chromatin modifications and their function. *Cell* **128**, 693–705 (2007).
47. Bannister, A. J. & Kouzarides, T. Regulation of chromatin by histone modifications. *Cell Res.* **21**, 381–395 (2011).
48. Su, Z. & Denu, J. M. Reading the Combinatorial Histone Language. *ACS Chemical Biology* **11**, 564–574 (2016).
49. Yun, M., Wu, J., Workman, J. L. & Li, B. Readers of histone modifications. *Cell Res.* **21**, 564–578 (2011).
50. Gabriel E Zentner & Steven Henikoff. Regulation of nucleosome dynamics by histone modifications. doi:10.1038/nsmb.2470
51. Chakravarthy, S., Park, Y.-J., Chodaparambil, J., Edayathumangalam, R. S. & Luger, K. Structure and dynamic properties of nucleosome core particles. *FEBS Lett.* **579**, 895–898 (2005).
52. Luger, K., Mä, A. W., Richmond, R. K., Sargent, D. F. & Richmond, T. J. Crystal structure of the nucleosome core particle at 2.8 Å resolution. *Nature* **389**, (1997).
53. Lenfant, F., Mann, R. K., Thomsen, B., Ling, X. & Grunstein, M. All four core histone N-termini contain sequences required for the repression of basal transcription in yeast. *EMBO J.* **15**, 3974–85 (1996).
54. Iwasaki, W. *et al.* Contribution of histone N-terminal tails to the structure and stability of nucleosomes. *FEBS Open Bio* **3**, 363–369 (2013).
55. Morales, V. & Richard-Foy, H. Role of Histone N-Terminal Tails and Their Acetylation in Nucleosome Dynamics. *Mol. Cell. Biol.* **20**, 7230–7237 (2000).
56. Torigoe, S. E., Urwin, D. L., Ishii, H., Smith, D. E. & Kadonaga, J. T. Identification of a Rapidly Formed Nonnucleosomal Histone-DNA Intermediate that Is Converted into Chromatin by ACF. (2011). doi:10.1016/j.molcel.2011.07.017
57. Mazurkiewicz, J., Kepert, J. F. & Rippe, K. On the Mechanism of Nucleosome Assembly by Histone Chaperone NAP1 * □ S. (2006). doi:10.1074/jbc.M511619200
58. Kireeva, M. L. *et al.* Nucleosome Remodeling Induced by RNA Polymerase II: Loss of the H2A/H2B Dimer during Transcription. *Mol. Cell* **9**, 541–552 (2002).
59. Tessarz, P. & Kouzarides, T. Histone core modifications regulating nucleosome structure and dynamics. *Nat. Rev. Mol. Cell Biol.* **15**, 703–708 (2014).

60. Mersfelder, E. L. & Parthun, M. R. The tale beyond the tail: Histone core domain modifications and the regulation of chromatin structure. *Nucleic Acids Res.* **34**, 2653–2662 (2006).
61. Van Leeuwen, F. & Gottschling, D. E. Genome-wide histone modifications: Gaining specificity by preventing promiscuity. *Current Opinion in Cell Biology* **14**, 756–762 (2002).
62. Weake, V. M. & Workman, J. L. Histone Ubiquitination: Triggering Gene Activity. doi:10.1016/j.molcel.2008.02.014
63. Han, J. *et al.* A Cul4 E3 ubiquitin ligase regulates histone hand-off during nucleosome assembly. doi:10.1016/j.cell.2013.10.014
64. L Cooper, A. J. Reversible and irreversible protein glutathionylation: biological and clinical aspects. doi:10.1517/17425255.2011.577738
65. García-Giménez, J. L. *et al.* Histone H3 Glutathionylation in Proliferating Mammalian Cells Destabilizes Nucleosomal Structure. *Antioxid. Redox Signal.* **19**, 1305–1320 (2013).
66. Daniel Camerini-Otero, R. & Felsenfeld, G. Histone H3 disulfide dimers and nucleosome structure (nuclease digestion/supercoiling of DNA/sedimentation velocity/nucleoprotein gel electrophoresis/chromatin). *Biochemistry* **74**, 5519–5523 (1977).
67. Desjarlais, R. & Tummino, P. J. Role of Histone-Modifying Enzymes and Their Complexes in Regulation of Chromatin Biology. *Biochemistry* **55**, 1584–1599 (2016).
68. Zee, B. M., Levin, R. S., Dimaggio, P. A. & Garcia, B. A. Global turnover of histone post-translational modifications and variants in human cells. *Epigenetics Chromatin* **3**, 22 (2010).
69. Fan, J., Krautkramer, K. A., Feldman, J. L. & Denu, J. M. Metabolic regulation of histone post-translational modifications. doi:10.1021/cb500846u
70. Van Der Knaap, J. A. & Verrijzer, C. P. Undercover: gene control by metabolites and metabolic enzymes. doi:10.1101/gad.289140
71. Schug, Z. T., Voorde, J. Vande & Gottlieb, E. The metabolic fate of acetate in cancer. *Nat. Publ. Gr.* **16**, 708–717 (2016).
72. Aravind, L., Maxwell Burroughs, A., Zhang, D. & Iyer, L. M. Protein and DNA modifications: Evolutionary imprints of bacterial biochemical diversification and geochemistry on the provenance of eukaryotic epigenetics. *Cold Spring Harb. Perspect. Biol.* **6**, 1–23 (2014).
73. Aravind, L., Abhiman, S. & Iyer, L. M. in 105–176 (2011). doi:10.1016/B978-0-12-387685-0.00004-4
74. Saavedra, R. Histones and metal-binding domains. (1589). doi:10.1126/science.3787266

75. Berg, J. Potential metal-binding domains in nucleic acid binding proteins. *Science* (80-.). **232**, (1986).
76. Adamczyk, M., Poznański, J., Kopera, E. & Bal, W. A zinc-finger like metal binding site in the nucleosome. *FEBS Lett.* **581**, 1409–16 (2007).
77. Zlatanova, J. & Thakar, A. H2A.Z: View from the Top. doi:10.1016/j.str.2007.12.008
78. Ridgway, P., Brown, K. D., Rangasamy, D., Svensson, U. & Tremethick, D. J. Unique Residues on the H2A . Z Containing Nucleosome Surface Are Important for *Xenopus laevis* Development * **279**, 43815–43820 (2004).
79. Haremaki, T., Fraser, S. T., Kuo, Y., Baron, M. H. & Weinstein, D. C. Vertebrate Ctr1 coordinates morphogenesis and progenitor cell fate and regulates embryonic stem cell differentiation. **104**, 12029–12034 (2007).

Chapter II

Layered regulation of the epigenome and its links to cellular metabolism and physiology

This chapter was published in 2014 titled “Layered regulation of the epigenome and its links to cellular metabolism and physiology”. It appears as a chapter in the American Association of Cancer Research education book for the AACR annual meeting in 2014. Briefly, this chapter reviews the literature concerning the role of epigenetic changes including DNA methylation and histone modifications with special attention given to global histone acetylation, in cellular metabolism and cancer progression. The connection of epigenetic changes to clinical outcome in cancer is also discussed.

I authored this chapter and was responsible for the literature review, writing the manuscript and the analysis of the primary data included.

Layered regulation of the epigenome and its links to cellular metabolism and physiology

Narsis Attar^{1,2} and Siavash K. Kurdistani^{1,2,3,4}

Background

Epigenetics is the study of heritable changes in patterns of gene expression mediated by mechanisms other than alterations in primary DNA sequence. The main determinants of the gene expression state are sequences-specific DNA binding transcription factors; but methyl-ation of DNA, covalent modifications of the histones, nucleosome composition and posi-tioning as well as large and small noncoding RNAs are thought to influence the epigenetic information (1). Aberrations in the epigenome occur frequently in essentially all cancers and may contribute to cancer initiation or progression (1). Epigenetic abnormalities in cancer, especially patterns of histone modifications, occur at single gene level but also globally, at the cellular level. Global changes in the levels of histone modifications have proved to be surprisingly common prognosticators of clinical outcome in a variety of cancers types regardless of the tissue of origin (2). The aberrations in histone modifications are studied primarily for their deregulatory effects on DNA-based processes such as transcription and DNA repair but recent evidence suggest that histone modifications may also have unanticipated links to cellular metabolism and physiology. These novel links have important and practical implications for the use of epigenetic therapeutics in cancer.

Discussion

DNA methylation

One of the early epigenetic alterations observed in malignancies involves global loss of 5-methylcytosine (5mC) on CpG dinucleotides (3). This global DNA hypomethylation preferentially affects repetitive sequences including heterochromatic repeats and endogenous retroviral elements, potentially leading to genomic instability and transcription of regions that are otherwise silent in normal cells (3). The exact contribution of DNA hypomethylation to cancer initiation or progression is still unclear but studies of mice deficient in DNA methylation suggest a causal role of DNA hypomethylation in cancer predisposition and tumorigenesis, in particular in the development of lymphomas (4). Recurrent inactivating mutations in the *de novo* methyltransferase DNMT3A is also seen in some leukemias and is associated with DNA hypomethylation and poor prognosis (5).

Authors' Affiliations: ¹Department of Biological Chemistry, ²Molecular Biology Institute, ³Department of Pathology and Laboratory Medicine, and ⁴Eli and Edythe Broad Center of Regenerative Medicine and Stem Cell Research, David Geffen School of Medicine, University of California, Los Angeles, California, USA

Corresponding Author: Siavash Kurdistani, Phone: 310-794-5194; E-mail: skurdistani@mednet.ucla.edu

©2014 American Association for Cancer Research.

AACR Education Book • <http://educationbook.aacrjournals.org>

Cancer genomes are also characterized by localized hypermethylation of CpG islands, which are often associated with gene promoters (3). Many promoters containing CpG islands are hypermethylated, leading to epigenetic silencing of genes whose expression may adversely affect tumor growth (3). In fact, methylation status of certain gene promoters have been used as molecular biomarkers of cancer prognosis (6). Notably, a significant proportion of DNA methylation changes occur in regions flanking CpG islands designated as "shores" which are normally differentially methylated in a tissue-type specific manner (7, 8). These shore regions exhibit striking DNA methylation hyper-variability among tumors of the same cancer type, raising the possibility that epigenetic plasticity at sites governing normal tissue differentiation may confer an adaptive advantage to cancer cells.

Histone modifications

Alterations of histone modifications can occur locally, at specific genomic loci via inappropriate activity or recruitment of histone modifying enzymes. When found in gene-regulatory regions such as promoters or enhancers, these alterations are linked to mis-regulation of downstream genes which may contribute to cancer development or progression. For instance, EZH2-mediated H3K27 trimethylation at gene promoters is associated with silencing of a number of tumor suppressor genes (9). Redistribution of H3K4me1, a histone modification found preferentially at enhancer elements, in colon cancer is associated with improper usage of enhancer elements to promote a carcinogenic gene expression program (10).

Histone modification levels can also be regulated globally at the cellular level. Individual cells or tissues display dramatic differences in the total levels of histone modifications contained within chromatin, quantitatively demonstrated by immunohistochemistry or Western blotting. For example, cells of skeletal muscle, heart and stomach contain much lower levels of histone acetylation compared to other tissues such as lung or colon (11). Cancer cells in primary patients' tumors also exhibit marked differences in their global levels of histone acetylation and methylation (12). Unlike alterations of histone modifications at specific genomic loci, differences in the global levels of histone modifications are prognostic of clinical outcome in many types of cancers (2, 14–17) (Table 1). In general, lower global levels of histone acetylation and/or methylation, regardless of their general correlations with gene expression or repression, are associated with more aggressive cancers and poor clinical outcome (13–16). The ability of global histone modification levels to categorize different types of cancers into clinically cohesive groups, presumably independent of gene expression states or mutational profiles, has been a surprisingly common feature of all cancers examined to date. In most cases, the prognostic of global histone modifications has been independent of key clinical or pathological variables patterns, informing on an aspect of cancer pathobiology that is not reflected by other clinic-pathological variables.

At the genomic level, extensive loss of H4K16 acetylation and H4K20 trimethylation at DNA repetitive elements is observed in many cancer types and correlates with tumor progression in mouse models of multistage tumorigenesis (17). But very little is known about what functions the changes in global levels of histone modifications serve for the cell or how the global regulation of histone modifications is linked to more aggressive cancers.

Table 1. Changes in global levels histone modifications are prognostic of clinical outcome in various types of cancers

Cancer type	Modification	Clinical correlates
Renal cell carcinoma	↓H3K18ac	Increased recurrence
	↓H3K9me2	Reduced cancer-related survival
	↓H3K4me1, 2, 3	Increased recurrence/reduced survival
Lung adenocarcinoma	↓H3K4me2, H3K18ac	Reduced cancer-related survival
	↓H3K9ac, H3K9me3, H4K16ac	Increased recurrence
Prostate cancer	↓H3K18ac, H3K4me2	Increased recurrence
	↓H3K9me2	Increased recurrence
	↓H3K4me1	Increased recurrence
Pancreatic cancer	↓H3K27me3	Reduced cancer-related survival
	↓H3K18ac, H3K4me2, H3K9me2	Reduced disease-free survival
Ovarian cancer	↓H3K27me3	Reduced cancer-related survival
Breast cancer	↓H3K27me3	Reduced cancer-related survival
	↓H3K18ac, H3K9ac, H3K4me2	Reduced disease-free survival
	↓H4K12ac, H3K4me2, H4K20me3, H4R3me2, H4K16ac	Poor prognosis subtype
Hepatocellular carcinoma	↑H3K27me3	Reduced survival
	↑H3K4me3	Poor prognosis
Gastric carcinoma	↑H3K9me3	Reduced survival

In the case of global acetylation, recent work from our lab has revealed an unanticipated function in the context of cellular physiologic homeostasis, specifically intracellular pH (pH_i) (18). We found that global histone acetylation and deacetylation is in flux with the extracellular acetate through monocarboxylate transporters (MCTs) which are obligate proton symporters. In acidic environments, histones become globally deacetylated and the liberated acetate molecules are co-transported along with protons out of the cell through the MCTs, decreasing the intracellular proton load. This cellular response to acidity is an active process marked by increased histone deacetylation, resulting in the continuous generation of free acetate molecules to be used for proton export. Conversely, histones are globally acetylated as pH_i becomes more alkaline in order to prevent undesired increases in pH_i . Inhibitions of histone deacetylases (HDACs) or MCTs, which respectively prevent the release of acetate from chromatin or its efflux from the cell, compromise cellular pH maintenance. These findings suggest that acetylation of chromatin acts as a rheostat for pH_i control. Since cancer tissues commonly exhibit low pH *in vivo* (19), cancer cells with lower levels of histone acetylation may be using this mechanism as a means to maintain a viable pH_i in acidic microenvironments. Such acidic conditions can select for resilient cells that are resistant to chemotherapy and/or radiation (19), potentially explaining the association of low histone acetylation with aggressive cancers. At the molecular level, the global regulation of acetylation is tied to coordinate control of thousands of individual acetylation peaks throughout the genome (18) (Fig. 1). This indicates that histone acetyltransferases (HATs) and HDACs must integrate the processes of pH_i control with gene expression by dynamically shaping the abundance and distribution of genome-wide acetylation on histones.

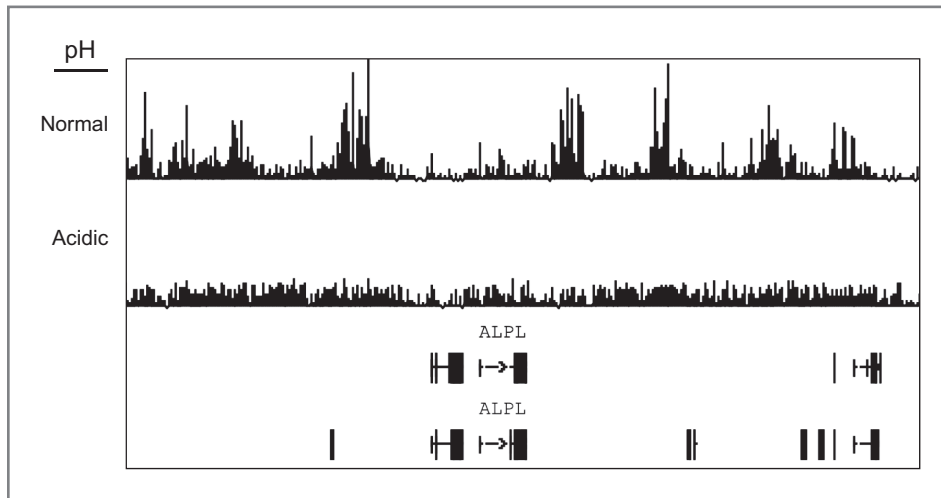


Fig. 1. Histones are globally and dynamically deacetylated in acidic conditions. Shown are genomic tracks displaying levels of histone acetylation across a region of chromosome 1 in HeLa cells grown briefly in normal or low pH. Most deacetylated regions regain acetylation in presence of HDACi's suggesting that the deacetylation is favored over acetylation, leading to the appearance of deacetylated histones. Dynamic acetylation and deacetylation of histones, when favored toward the latter at low pH, generates free acetate molecules for proton export through the monocarboxylate transporters and buffers intracellular pH.

Disruption of pH_i maintenance by HDAC inhibitors (HDACi's) suggests a novel mechanism of action for these drugs. By compromising cellular pH buffering capacity, HDACi's may render their companion drugs essentially ineffective because most drugs are developed for function at neutral to slightly alkaline pH. These considerations could lead to more informed use of HDACi's in oncology.

The mechanisms by which histone modifications levels are regulated globally are not very well understood. For example, it is unclear how the balance of histone acetylation and deacetylation is favored toward the latter in acidic conditions. One possible mechanism may be through modulation of activities of epigenetic enzymes by co-factor availability or small molecule allosteric regulators that link metabolic or physiologic states to epigenetic maintenance. Such possibility has been highlighted by the discovery of mutations in isocitrate dehydrogenase (IDH)1 and 2 in a subset of oligodendroglioma and leukemias that result in production of 2-hydroxyglutarate (2HG) instead of 2-oxoglutarate. 2HG functions as a competitive inhibitor of α -ketoglutarate-dependent dioxygenases including the jumonji family of histone demethylases, leading to genomewide increases in various histone methylation marks in cancer cells harboring IDH mutations (5). Essentially all other histone modifying enzymes require and/or are regulated by metabolic cofactors (20, 21), raising the possibility of additional links between global regulation of histone modifications and specific physiological and metabolic processes within the cell.

Future Directions

Understanding the distributions of histone modifications across the genome has led to significant investment in comprehensive mapping efforts (e.g., NIH Epigenome Roadmap). These maps are used to infer the functions of histone modifications by comparing the location of modified histones to genomic landmarks or nearby molecular processes such as gene expression. Implicit in this approach is the assumption that histone modifications are regulated locally and function mainly to regulate nearby DNA-based events. It is now clear that in addition to the locus specific regulation of histone modifications, cells regulate levels of histone modifications at a global scale in response to metabolic or physiologic cues. By changing the fraction of total histones that are modified in a cell, global regulation of histone modifications may affect numerous genomic loci at once (18), enabling coordinate regulation of cellular metabolism/physiology and genomewide gene expression through large-scale epigenetic reprogramming. Whatever the case maybe, global levels of histone modifications in primary cancer tissues have proved to be reliable molecular biomarkers for stratification of tumors into more clinically homogeneous subgroups that could be used to increase the specificity of cancer therapies (22).

References

1. Dawson MA, Kouzarides T. Cancer epigenetics: From mechanism to therapy. *Cell* [Internet]. 2012 [cited 2014 Jan 6];150:12–27. Available from: <http://www.sciencedirect.com/science/article/pii/S0092867412007623>.
2. Seligson DB, Horvath S, McBrien MA, Mah V, Yu H, Tze S, et al. Global levels of histone modifications predict prognosis in different cancers. *Am J Pathol* [Internet]. 2009 May [cited 2013 Aug 1];174:1619–28. Available from: <http://www.pubmedcentral.nih.gov/articlerender.fcgi?artid=2671251&tool=pmcentrez&rendertype=abstract>.
3. Esteller M. Cancer epigenomics: DNA methylomes and histone-modification maps. *Nat Rev Genet* [Internet]. 2007 Apr [cited 2013 Jul 30];8:286–98. Available from: <http://dx.doi.org/10.1038/nrg2005>.
4. Gaudet F, Hodgson JG, Eden A, Jackson-Grusby L, Dausman J, Gray JW, et al. Induction of tumors in mice by genomic hypomethylation. *Science (New York, N.Y.)* [Internet]. 2003 May 18 [cited 2013 Dec 31];300:489–92. Available from: <http://www.sciencemag.org/content/300/5618/489.long#F2>.
5. Plass C, Pfister SM, Lindroth AM, Bogatyrova O, Claus R, Lichter P. Mutations in regulators of the epigenome and their connections to global chromatin patterns in cancer. *Nat Rev Genet* [Internet]. Nature Publishing Group, a division of Macmillan Publishers Limited. All Rights Reserved; 2013 Nov [cited 2014 Jan 11];14:765–80. Available from: <http://dx.doi.org/10.1038/nrg3554>.
6. Szyf M. DNA methylation signatures for breast cancer classification and prognosis. *Genome Med* [Internet]. 2012 Mar 30 [cited 2014 Jan 9];4:26. Available from: <http://genomemedicine.com/content/4/3/26>.
7. Irizarry RA, Ladd-Acosta C, Wen B, Wu Z, Montano C, Onyango P, et al. The human colon cancer methylome shows similar hypo- and hypermethylation at conserved tissue-specific CpG island shores. *Nat Genet* [Internet]. Nature Publishing Group; 2009 Feb [cited 2013 Dec 17];41:178–86. Available from: <http://dx.doi.org/10.1038/ng.298>.
8. Hansen KD, Timp W, Bravo HC, Sabuncian S, Langmead B, McDonald OG, et al. Increased methylation variation in epigenetic domains across cancer types. *Nat Genet* [Internet]. Nature Publishing Group; 2011 Aug 26 [cited 2013 Dec 17];43:768–75. Available from: <http://www.nature.com/ng/journal/v43/n8/full/ng.865.html#supplementary-information>.
9. Kondo Y, Shen L, Cheng AS, Ahmed S, Boumber Y, Charo C, et al. Gene silencing in cancer by histone H3 lysine 27 trimethylation independent of promoter DNA methylation. *Nat Genet* [Internet]. Nature Publishing Group; 2008 Jun 18 [cited 2014 Jan 10];40:741–50. Available from: <http://www.nature.com/ng/journal/v40/n6/full/ng.159.html#B2>.

10. Kurdistani SK. Enhancer dysfunction: How the main regulators of gene expression contribute to cancer. *Genome Biol* [Internet]. 2012 [cited 2014 Jan 11];13:156. Available from: <http://genomebiology.com/2012/13/5/156>.
11. Iwabata H, Yoshida M, Komatsu Y. Proteomic analysis of organ-specific post-translational lysine-acetylation and -methylation in mice by use of anti-acetyllysine and -methyllysine mouse monoclonal antibodies. *Proteomics* [Internet]. 2005 Dec [cited 2014 Jan 19];5:4653–64. Available from: <http://www.ncbi.nlm.nih.gov/pubmed/16247734>.
12. Kurdistani SK. Histone modifications as markers of cancer prognosis: A cellular view. *Br J Cancer* [Internet]. 2007 Jul 2 [cited 2014 Jan 11];97:1–5. Available from: <http://www.pubmedcentral.nih.gov/articlerender.fcgi?artid=2359665&tool=pmcentrez&rendertype=abstract>.
13. Manuyakorn A, Paulus R, Farrell J, Dawson NA, Tze S, Cheung-Lau G, et al. Cellular histone modification patterns predict prognosis and treatment response in resectable pancreatic adenocarcinoma: Results from RTOG 9704. *J Clin Oncol* [Internet]. 2010 Mar 10 [cited 2013 Aug 1];28:1358–65. Available from: <http://www.pubmedcentral.nih.gov/articlerender.fcgi?artid=2834495&tool=pmcentrez&rendertype=abstract>.
14. Elsheikh SE, Green AR, Rakha EA, Powe DG, Ahmed RA, Collins HM, et al. Global histone modifications in breast cancer correlate with tumor phenotypes, prognostic factors, and patient outcome. *Cancer Res* [Internet]. 2009 May 1 [cited 2013 Jul 30];69:3802–9. Available from: <http://cancerres.aacr-journals.org/content/69/9/3802.long>.
15. Mosashvilli D, Kahl P, Mertens C, Holzapfel S, Rogenhofer S, Hauser S, et al. Global histone acetylation levels: Prognostic relevance in patients with renal cell carcinoma. *Cancer Sci* [Internet]. 2010 Dec [cited 2013 Aug 1];101:2664–9. Available from: <http://www.ncbi.nlm.nih.gov/pubmed/20825416>.
16. Greer EL, Shi Y. Histone methylation: A dynamic mark in health, disease and inheritance. *Nat Rev Genet* [Internet]. Nature Publishing Group; 2012 May 3 [cited 2014 Jan 9];13:343–57. Available from: http://www.nature.com/nrg/journal/v13/n5/full/nrg3173.html?WT.ec_id=NRG-201205.
17. Fraga MF, Ballestar E, Villar-Garea A, Boix-Chornet M, Espada J, Schotta G, et al. Loss of acetylation at Lys16 and trimethylation at Lys20 of histone H4 is a common hallmark of human cancer. *Nat Genet* [Internet]. Nature Publishing Group; 2005 Apr 13 [cited 2014 Jan 10];37:391–400. Available from: <http://www.nature.com/ng/journal/v37/n4/full/ng1531.html#B23>.
18. McBrien MA, Behbahan IS, Ferrari R, Su T, Huang T-W, Li K, et al. Histone acetylation regulates intracellular pH. *Mol Cell* [Internet]. 2013 Jan 24 [cited 2013 Aug 1];49:310–21. Available from: <http://dx.doi.org/10.1016/j.molcel.2012.10.025>.
19. Webb BA, Chimenti M, Jacobson MP, Barber DL. Dysregulated pH: A perfect storm for cancer progression. *Nat Rev Cancer* [Internet]. Nature Publishing Group; 2011 Sep [cited 2013 Aug 1];11:671–7. Available from: <http://www.ncbi.nlm.nih.gov/pubmed/21833026>.
20. Denu JM. Linking chromatin function with metabolic networks: Sir2 family of NAD⁺-dependent deacetylases. *Trends Biochem Sci* [Internet]. 2003 [cited 2014 Jan 19];28:41–8. Available from: <http://www.sciencedirect.com/science/article/pii/S0968000402000051>.
21. Vogelauer M, Krall AS, McBrien MA, Li J-Y, Kurdistani SK. Stimulation of histone deacetylase activity by metabolites of intermediary metabolism. *J Biol Chem* [Internet]. 2012 Sep 14 [cited 2013 Aug 1];287:32006–16. Available from: <http://www.jbc.org/content/287/38/32006.long>.
22. Chervona Y, Costa M. Histone modifications and cancer: Biomarkers of prognosis? *Am J Cancer Res* [Internet]. 2012 Jan [cited 2013 Aug 1];2:589–97. Available from: <http://www.pubmedcentral.nih.gov/articlerender.fcgi?artid=3433108&tool=pmcentrez&rendertype=abstract>.

Chapter III

Exploitation of EP300 and CREBBP Lysine

Acetyltransferases by Cancer

This chapter was published in 2017 in the Cold Spring Harbor Perspectives in Medicine in the issue titled “Cancer and Chromatin”. Briefly, the biological functions of p300/CBP are discussed with an emphasis on how disruption of these functions by mutations and alterations in expression or subcellular localization contributes to the cancer phenotype.

I was responsible for the review of the literature, drafting the article, critical revision of the article and managing the review process for publication.

Exploitation of EP300 and CREBBP Lysine Acetyltransferases by Cancer

Narsis Attar^{1,2} and Siavash K. Kurdistani^{1,2,3,4}

¹Department of Biological Chemistry, David Geffen School of Medicine, University of California, Los Angeles, California 90095

²Molecular Biology Institute, David Geffen School of Medicine, University of California, Los Angeles, California 90095

³Department of Pathology and Laboratory Medicine, David Geffen School of Medicine, University of California, Los Angeles, California 90095

⁴Eli and Edythe Broad Center of Regenerative Medicine and Stem Cell Research, David Geffen School of Medicine, University of California, Los Angeles, California 90095

Correspondence: skurdistani@mednet.ucla.edu

p300 and CREB-binding protein (CBP), two homologous lysine acetyltransferases in metazoans, have a myriad of cellular functions. They exert their influence mainly through their roles as transcriptional regulators but also via nontranscriptional effects inside and outside of the nucleus on processes such as DNA replication and metabolism. The versatility of p300/CBP as molecular tools has led to their exploitation by viral oncogenes for cellular transformation and by cancer cells to achieve and maintain an oncogenic phenotype. How cancer cells use p300/CBP in their favor varies depending on the cellular context and is evident by the growing list of loss- and gain-of-function genetic alterations in p300 and CBP in solid tumors and hematological malignancies. Here, we discuss the biological functions of p300/CBP and how disruption of these functions by mutations and alterations in expression or subcellular localization contributes to the cancer phenotype.

EP300 (hereafter referred to as p300) and its closely related paralog CREB-binding protein (CREBBP, hereafter CBP) are ubiquitously expressed transcriptional coactivators and major lysine acetyltransferases (KATs) in metazoans. They regulate transcription by serving as scaffolds that bridge sequence-specific DNA-binding factors and the basal transcriptional machinery (Chan and La Thangue 2001), and facilitate transcription through acetylation of histones, transcription factors, and autoacetyla-

tion (Sterner and Berger 2000; Black et al. 2006; Pugh 2006; Das et al. 2014). p300 and CBP are large proteins with multiple functional domains accommodating diverse protein–protein interactions. This has enabled a large number of disparate transcription factors to use p300/CBP as cofactors in regulating the expression of thousands of genes in essentially all cell types (Chan and La Thangue 2001). The large number of proteins that interact with p300 and CBP underscore the widespread influence of these

Editors: Scott A. Armstrong, Steven Henikoff, and Christopher R. Vakoc
Additional Perspectives on Chromatin Deregulation in Cancer available at www.perspectivesinmedicine.org

Copyright © 2016 Cold Spring Harbor Laboratory Press; all rights reserved
Advanced Online Article. Cite this article as *Cold Spring Harb Perspect Med* doi: 10.1101/cshperspect.a026534

coactivators on essential cellular functions. p300 and CBP regulate several fundamental biological processes including proliferation, cell cycle, cell differentiation, and the DNA damage response (Shi and Mello 1998; Goodman and Smolik 2000; Grossman 2001; Poleskaya et al. 2001). But the versatility of these proteins has also made it difficult to discern their specific involvements in distinct biological processes and pathophysiological states. Another impediment to understanding the roles of p300 and CBP is the overlapping contribution of these proteins to the same molecular processes such as gene regulation, hence, the commonly used designation “p300/CBP”

Although p300/CBP have been implicated in cancer development, the specific contributions of each acetyltransferase to the cancer phenotype have been less precisely defined. This is in part attributable to the participation of p300/CBP in diverse and, at times, antagonistic cellular pathways such as tumor-suppressive and pro-oncogenic processes. The challenge is even greater when attempting to understand the consequences of mutations in p300 and CBP, which have been identified in numerous cancer genome studies. To fully understand how genetic or epigenetic alterations of p300/CBP contribute to the cancer phenotype, it is important to determine which cellular pathways are specifically affected by mutations in p300 or CBP. One important consideration is that p300 and CBP, despite significant sequence homology, also perform nonoverlapping cellular functions and can cooperate with distinct binding partners. In this review, we discuss the major functions of p300/CBP in the cell and how cancer cells exploit these functions to their advantage.

p300/CBP ORCHESTRATE THE CELL CYCLE AND REGULATE PROLIFERATION

p300 was initially identified through its physical association with the adenovirus transforming protein E1A and determined to be essential for adenovirus-mediated oncogenic transformation (Whyte et al. 1989; Sawada et al. 1997). Soon after, the E1A–p300 interaction

was shown to be critical for the G₁–S phase transition in adenovirus-infected cells (Howe et al. 1990). A number of other oncogenic viral proteins (e.g., SV40/polyoma LT, HPV E7) were subsequently shown to also target p300 or CBP to promote cellular transformation (Eckner et al. 1996; Zimmermann et al. 1999; Bernat et al. 2003). The frequent exploitations of p300/CBP as cofactors for viral oncoproteins highlighted the fundamental role of these proteins in regulating cellular proliferation, and raised the possibility that alterations of p300/CBP may also contribute to nonviral mechanisms of tumorigenesis.

E1A was initially reported to inhibit p300/CBP-mediated KAT activity and transcriptional activation, which led to a hypothesis that p300 may normally function as a negative regulator of S phase entry (Arany et al. 1995; Yang et al. 1996; Chakravarti et al. 1999). However, many studies have since revealed a major role for p300/CBP in promoting growth and cell-cycle progression. In fact, on adenoviral infection p300 is recruited to genes with functions in cell cycle and proliferation to promote their full activation and S phase entry in otherwise nondividing cells (Ferrari et al. 2008, 2014).

The functions of p300 and CBP in regulating cell-cycle progression are partly mediated through their influence on transcription by being recruited to gene regulatory regions, such as enhancers and promoters, via sequence-specific DNA-binding transcription factors. Once bound, they facilitate subsequent regulatory events to ultimately direct RNA polymerase II activation. p300 in particular contributes to the formation of the transcription pre-initiation complex, a large multiprotein complex required for expression of genes. p300 does this partly through dynamic association with and dissociation from the transcriptional machinery, which is facilitated by p300 auto-acetylation activity (Black et al. 2006). The pervasive participation of p300 and CBP in transcriptional regulation is evident in their binding to >16,000 genes in human cells (Smith et al. 2004; Ramos et al. 2010). Not all binding events lead to transcriptional activation and a growing body of evidence indicates a gene-repressive role for

p300/CBP in certain contexts (Santoso and Kadonaga 2006; Sankar et al. 2008; Ferrari et al. 2014). p300 and CBP also regulate the cell cycle through interactions with or acetylation of proteins involved in cell-cycle progression, such as the DNA replication machinery and histones for the purpose of DNA replication through chromatin.

Transcriptional Coactivation and the Cell Cycle

One of the earliest cell-based models showing the role of p300/CBP in cell-cycle progression involved depletion of p300 and CBP, through microinjection of an antibody against both proteins, which was found to limit S phase entry (Ait-Si-Ali et al. 2000). This defect was reversed by overexpression of exogenous CBP, indicating a direct function of CBP in promoting cell-cycle progression. p300 and CBP serve as transcriptional coactivators for the E2F transcription factor family, which are central for expression of genes required for G₁/S transition (Trouche and Kouzarides 1996; Trouche et al. 1996; Wang et al. 2007). In addition, p300/CBP acetylate the E2F proteins themselves (e.g., E2F1), leading to enhanced DNA-binding and gene activation (Martínez-Balbás et al. 2000; Marzio et al. 2000). The acetyltransferase activity of CBP is regulated in a cell-cycle-dependent manner and peaks at the G₁/S boundary possibly as a consequence of cyclin/Cdk-mediated phosphorylation of CBP before initiation of S phase (Ait-Si-Ali et al. 1998). Cell-cycle-dependent transcription of the major histone genes for DNA replication is also dependent on p300/CBP, which are recruited by NPAT, the general histone expression regulator (He et al. 2011). Therefore, the transcriptional coactivator functions of p300/CBP mediate S phase entry through proper expression of DNA replication and cellular growth genes.

Nontranscriptional Effects of p300/CBP on Cell Cycle

p300/CBP may regulate DNA replication through modifying the histones surrounding

the DNA replication origins. These two acetyltransferases are responsible for the bulk of histone H3 lysine 18 acetylation (H3K18ac) and H3K27ac, modifications associated with active promoters and enhancers (Horwitz et al. 2008; Jin et al. 2011). H3K18ac is also associated with active DNA replication in certain cell types (Li et al. 2014). p300/CBP may also directly regulate the DNA replication machinery by acetylating two major endonucleases involved in Okazaki fragment processing, FEN1 and Dna2, inhibiting and stimulating their activities, respectively (Hasan et al. 2001; Balakrishnan et al. 2010). This differential regulation is suggested to lead to increased accuracy of DNA replication (Balakrishnan et al. 2010). Complementing these results, pharmacological inhibition of p300 KAT activity prolongs S phase because of reduced replication fork velocity and defects in timing of replication origin firing and synchronization (Prieur et al. 2011). Altogether, p300/CBP regulate various aspects of the DNA replication process, including the choice and timing of origin firing and the assembly of the newly synthesized DNA into chromatin.

p300/CBP function in other phases of the cell cycle as well. Depletion of CBP leads to a delay in mitosis and accumulation of cells in G₂/M because of the aberrant activity of the anaphase-promoting complex (APC/C), an E3 ubiquitin ligase required for progression through mitosis (Turnell et al. 2005). Taken together with the above, these findings place p300 and CBP at multiple positions along the cell cycle and emphasize the functions of these proteins in promoting progression through the entire cell cycle (Fig. 1).

Consistent with the critical roles of p300/CBP in cell-cycle regulation, significant growth defects are observed when these proteins are depleted in cells or organisms. Mouse models null for p300 or CBP are embryonic lethal and, although p300-null cells obtained from these embryos are viable, they show reduced proliferation (Yao et al. 1998). This also occurs when p300 is transiently or stably depleted (Yuan et al. 1999; Iyer et al. 2007). Therefore, loss of p300/CBP in most contexts leads to decreased proliferation.

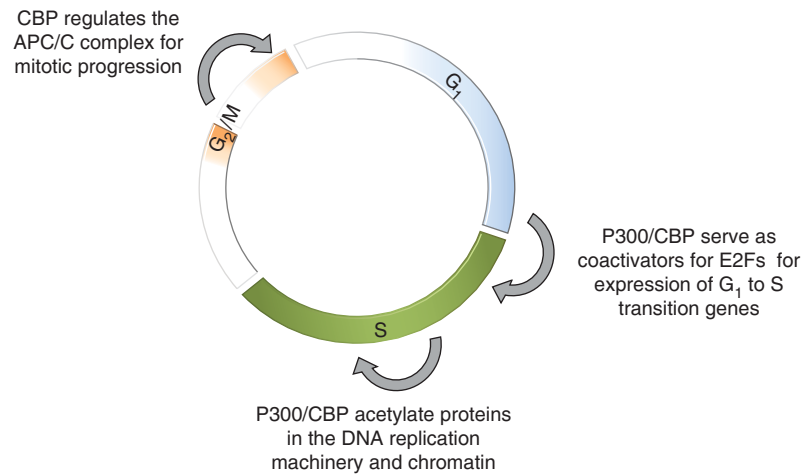


Figure 1. p300/CREB-binding protein (CBP) regulate the cell cycle at multiple points. The diagram summarizes the known functions of p300/CBP at different points along the cell cycle. The E2F family of transcription factors uses p300/CBP as transcriptional coactivators to facilitate expression of E2F target genes that orchestrate the transition from G₁ to S. p300 also facilitates S phase progression by acetylating the DNA replication machinery (e.g., FEN1 and Dna2) and the histones surrounding the replication origins (e.g., H3K18). CBP promotes progression through mitosis by regulating the function of the anaphase-promoting complex (APC)/C complex.

p300 AND CBP IN CANCER

p300/CBP as Classic Tumor Suppressors

Early indications of tumor suppression by p300/CBP came from findings in a rare congenital developmental disorder, Rubinstein–Taybi syndrome (RTS). Germline heterozygous mutations in CBP and less frequently in p300 are observed in RTS and may play a role in the pathogenesis of this disease. RTS patients have an increased incidence of cancer with ~5% diagnosed with childhood tumors of neural crest origin (Miller and Rubinstein 1995). p300/CBP mutations in RTS are variable and encompass microdeletions, truncating mutations as well as point mutations in different domains (Petrij et al. 1995; Roelfsema and Peters 2007). A number of these genetic lesions reduce acetyltransferase and/or transcriptional activities of p300/CBP implicating the reduction of these functions in the etiology of RTS-associated malignancies (Roelfsema and Peters 2007), a contention that is supported by studies in mice (Tanaka et al. 1997; Rebel et al. 2002; Alarcón et al. 2004).

Investigations of primary tumor samples helped to strengthen the tumor-suppressive functions of p300/CBP in humans. Work by

Gayther et al. identified the first cancer-associated inactivating genetic lesions in p300 in breast and colorectal primary tumors and cell lines (Gayther et al. 2000). The majority of cases harbored inactivation or deletion of the second allele of p300. Studies of larger cohorts of solid tumors including colorectal, gastric, ovarian, and hepatocellular carcinomas also detected loss of heterozygosity (LOH) at the p300 or CBP loci at frequencies ranging from 1% to 50% (Bryan et al. 2002; Tillinghast et al. 2003; Koshiishi et al. 2004; Dancy and Cole 2015). A small fraction of p300/CBP LOH events in these studies were accompanied by somatic mutations in the second allele confirming earlier findings. Tumors showing LOH indicate that haploinsufficiency of p300/CBP may be a factor in the pathogenesis of cancer. This is consistent with the idea that a limiting cellular pool of p300/CBP may be a biological determinant of their effects on the cell. In fact there is evidence that these proteins are haploinsufficient because p300/CBP heterozygote null embryos have reduced survival (Yao et al. 1998). Therefore, different molecular pathways have to compete for a limited pool of p300/CBP to regulate their target genes (Kamei et al. 1996; Huang et al. 2007). So

the reduced availability of p300/CBP through LOH may contribute to cancer development or progression by altering the equilibrium between the various p300/CBP-dependent pathways. Additional evidence suggesting a tumor-suppressive function for p300/CBP came from oral and cervical carcinoma cell lines. These cell lines, which harbor either a homozygous mutation in p300 or a heterozygous truncation of p300 with inactivation of the normal allele, show reduced proliferation on introduction of a normal copy of p300 (Suganuma et al. 2002).

p300/CBP may exert tumor-suppressive effects through promoting the functions of other bona fide tumor suppressors, such as p53, RB1, BRCA1, or through inducing transforming growth factor β (TGF- β)-responsive genes (Nishihara et al. 1998; Pao et al. 2000; Chan et al. 2001; Grossman 2001). The involvement of p300/CBP in p53-mediated functions is extensively studied and occurs at multiple levels. In response to DNA damage, p300/CBP augment p53-dependent transcriptional activation of genes required for cell-cycle arrest and DNA repair (Grossman 2001). In addition, p300 promotes the nuclear accumulation and stability of p53 in response to genotoxic stress. Interestingly, in unstressed conditions and during recovery from DNA damage, p300 is thought to ensure degradation of p53 for resumption of the cell cycle after DNA repair (Grossman et al. 1998; Grossman 2001; Kawai et al. 2001). BRCA1, which is frequently mutated in familial breast and ovarian cancers, plays a role in cell-cycle checkpoint, DNA damage repair, and transcriptional regulation (Monteiro et al. 1996; Wu et al. 2010). The latter role has linked BRCA1 to p300/CBP, which enhance BRCA1-mediated transcriptional activation (Pao et al. 2000; Mullan et al. 2006). Similarly p300/CBP mediate the effects of TGF- β signaling by serving as transcriptional coactivators for Smad3, a downstream effector of this tumor-suppressive pathway (Feng et al. 1998; Derynck et al. 2001).

p300/CBP as Drivers of Cancer Growth

Despite the tumor-suppressive roles of p300/CBP, several lines of evidence suggest that these

KATs can also participate in promoting cancer. Although inactivating mutations in p300/CBP are found in certain cancers (Kalkhoven 2004; Pasqualucci et al. 2011), some cancer-linked point mutations are in fact gain-of-function alterations in p300/CBP that could contribute to cancer development (Ringel and Wolberger 2013). In addition to the acetyltransferase domains, important structural features of p300/CBP include three cysteine/histidine-rich zinc-binding domains (CH1-3), a bromodomain, and a recently identified RING (Really Interesting New Gene) domain within the larger CH2 region. The RING domain contacts the active site of the KAT domain blocking substrate binding and decreasing acetyltransferase activity in vitro. Disruption of the RING domain enhances p300 KAT activity (Delvecchio et al. 2013). Mutations in the p300 RING domain are found in malignancies including melanoma, endometrial and colorectal carcinoma (Forbes et al. 2015), as well as in RTS, and may boost p300 KAT activity in these settings (Delvecchio et al. 2013). How increased KAT activity of p300 or CBP promotes malignancy is not clear. In addition to acetylation of H3K18 and H3K27, p300/CBP also mediate the acetylation of histone H3 lysine 56, a modification associated with nucleosome assembly in yeast and DNA replication and repair in mammals (Li et al. 2008; Yuan et al. 2009; Vempati et al. 2010). Increased cellular levels of histone H3K56ac are observed in a number of epithelial tumors and relate to tumor stage and an undifferentiated phenotype (Das et al. 2009). Enhanced KAT activity of p300 or CBP may lead to increased acetylation of H3K56 in certain cancers.

Another mode of p300/CBP acetyltransferase gain-of-function involves translocation events in hematological malignancies such as myelodysplastic syndrome and acute myeloid leukemia. These translocations occur between p300 or CBP and monocytic leukemia zing-finger (MOZ), MOZ-related factor (MORF), or myeloid/lymphoid or mixed-lineage leukemia (MLL) (Kitabayashi et al. 2001; Panagopoulos et al. 2001). The translocation events more commonly generate a fusion protein containing the carboxy-terminal region of CBP with or with-

out its KAT domain. The MOZ/MORF-CBP as well as MOZ-p300 fusion proteins maintain the KAT domains from both parent proteins potentially resulting in highly active lysine acetyltransferases (Yang and Ullah 2007). In essentially all translocation events, the amino-terminal region of CBP is excluded from the fusion protein. The novel functions that are gained by the fusion protein can contribute to the oncogenic nature of these translocations. Mutations in the KAT-inhibitory RING domain of p300 are also detected in myelodysplastic syndrome (Forbes et al. 2015). This further suggests a key role for increased p300/CBP KAT activity in the pathogenesis of these hematological malignancies.

Mutations in p300/CBP Are Nonrandom

The widespread application of next generation sequencing has revealed an abundance of somatic genetic mutations with frequencies of up to 30% in p300 and CBP in various types of cancer. Although earlier studies of p300/CBP had uncovered gross or partial gene deletions, only a relatively small fraction of all p300/CBP genetic lesions in cancer are of this nature. The majority of alterations are, in fact, missense point mutations (Fig. 2) that occur essentially throughout the p300 and CBP proteins with a higher frequency in the KAT domains, suggesting a selective pressure in cancers for alteration of this activity (Fig. 3A). Certain residues in the KAT domain of p300 and CBP (e.g., D1399 and

Y1467 for p300 and Y1450 and Y1503 for CBP) that are known to reduce or abolish the KAT activity when mutated are among the most frequent mutations in cancer (Delvecchio et al. 2013; Forbes et al. 2015). It is unclear, however, whether and how the other frequently mutated residues in this domain are important for the KAT activity. The top four and five most frequent missense mutations in p300 and CBP, respectively, are highlighted in Fig. 3B. These mutations in p300 including those thought to reduce KAT activity are clustered near the site of acetyl-CoA binding (Fig. 3B) (Liu et al. 2008; Maksimoska et al. 2014). The location of the other uncharacterized mutations near this site suggests these may also have an effect on the KAT activity.

Tables 1 and 2 list the cancers with p300 and CBP mutation frequencies, respectively, of 5% or higher as reported in the COSMIC (Catalogue of Somatic Mutations in Cancer) database (Forbes et al. 2015). Both p300 and CBP are frequently mutated in skin squamous cell carcinoma followed by certain types of lymphomas. Alterations of p300/CBP may therefore be key contributory milestones to the development or progression of these cancers. Alternatively, these specific cellular contexts may provide a more permissive background for accumulation of genetic lesions in p300/CBP with no selective pressure to avoid them. Tables 3 and 4 include lists of cancers with $\leq 1\%$ frequency of p300 or CBP mutations, respectively. Of interest in these

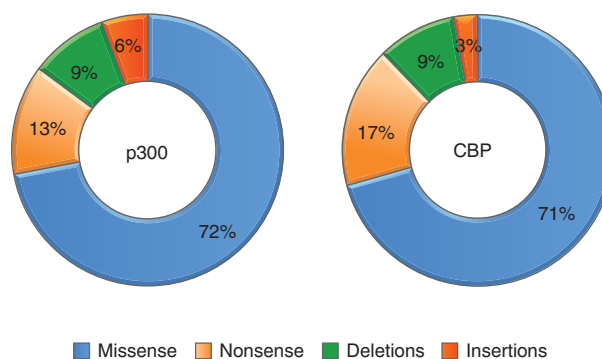


Figure 2. Frequency of the different types of mutations in p300 and CBP in cancer. The majority of genetic lesions to p300 or CBP in cancer are missense mutations followed by nonsense mutations, deletions, and a small number of insertions.

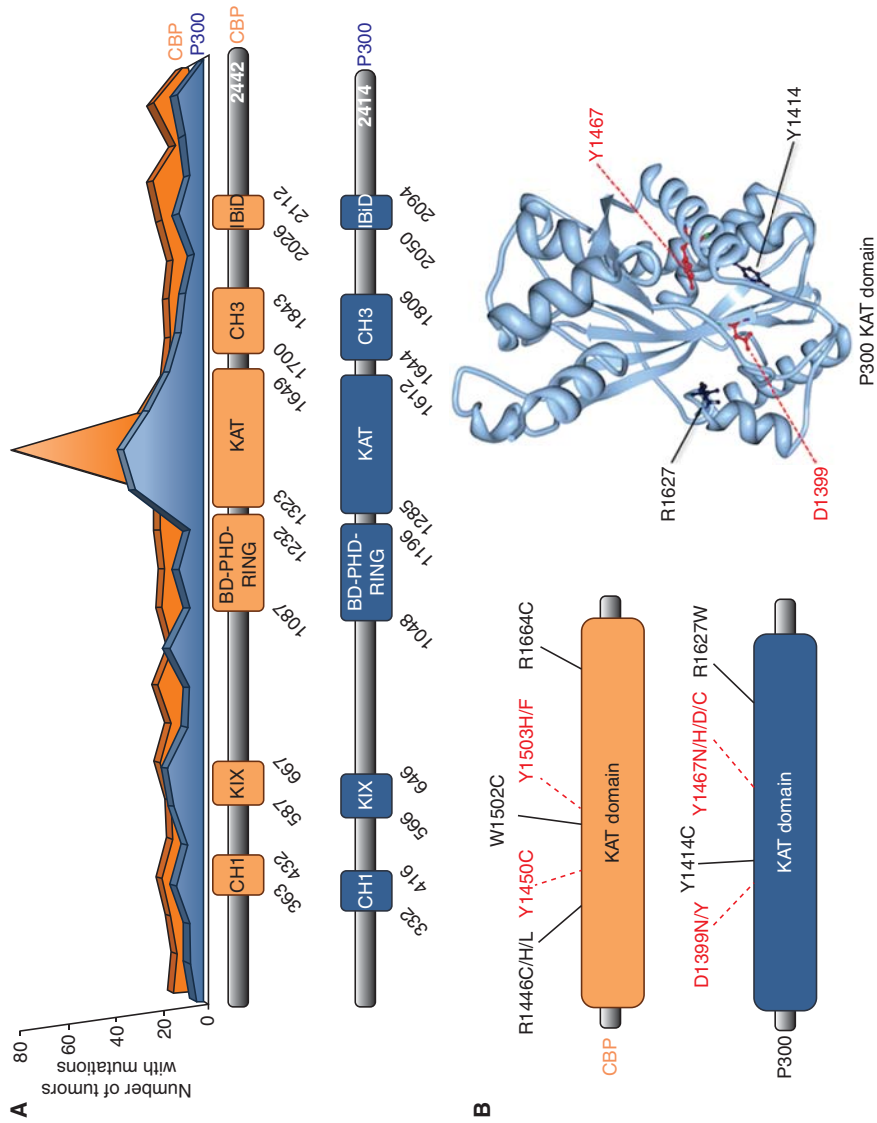


Figure 3. The acetyltransferase domains of p300 and CBP are hotspots for mutations in cancer. (A) The number of tumors of different origins with missense mutations along the p300 and CBP proteins domain structures is shown (Forbes et al. 2015). CH1, Cysteine/histidine-rich region 1; BR, bromodomain; PHD, plant homeodomain finger; RING, Really Interesting New Gene finger domain; KAT, lysine acetyltransferase domain; CH3, cysteine/histidine-rich region 3 (also referred to as TAZ2); IBID, IRE3-binding domain. (B) The residues in the KAT domains of p300 and CBP that are frequently mutated in cancer are indicated. Residues in red are important for the KAT activity. The four most common residues mutated in p300 reside close to the acetyl-CoA-binding site as indicated in the crystal structure (Liu et al. 2008; Maksimoska et al. 2014).

Table 1. Cancer subtypes with higher frequency of p300 mutations

Cancer subtype	N	Samples mutated (%)
Skin squamous cell carcinoma	82	26.8
Marginal zone B-cell lymphoma	15	13.3
Bladder carcinoma	425	9.4
Follicular lymphoma	68	8.8
Lung small-cell carcinoma	48	8.3
Endometrial carcinoma	387	7.2
Esophageal squamous cell carcinoma	511	5.9
Cervical squamous cell carcinoma	193	5.2
Breast carcinoma (estrogen-receptor-positive)	80	5.0

Data were obtained from the publicly available COSMIC database (cancer.sanger.ac.uk).

groups are prostate and pancreas carcinomas, which may be under selective pressure to preserve the normal functions of p300/CBP for growth or may alter the functions of p300 or CBP through nongenetic means.

Beyond Genetic Alterations

In the absence of genetic defects, mechanisms such as changes in expression or subcellular localization can alter p300/CBP-associated functions in cancer. Analysis of The Cancer Genome Atlas (TCGA) data indicates differences in expression levels of p300 and CBP in multiple types of carcinomas and hematological malignancies. The effects of these changes in mediating the neoplastic phenotype cannot be described under one umbrella as both higher and lower levels of p300/CBP are found. These expression differences in some cases are accompanied by changes in gene copy number as a result of gross gene amplifications or deletions. Several studies of primary tumors of varying origins have also revealed changes in p300/CBP protein levels, which in either direction are prognostic in many cases. A study of 95 prostate cancer lesions revealed that increased p300 protein levels, as compared with adjacent

normal tissue, correlate with increased proliferation, tumor volume, and extraprostatic involvement (Debes et al. 2003). A function of p300 in the progression of prostate cancer has also been proposed as it mediates androgen-dependent as well as independent transactivation of the androgen receptor (Debes et al. 2002). Additionally, increased p300 expression correlates with poor survival and aggressive phenotypes in breast, hepatocellular, esophageal, and cutaneous squamous cell carcinoma (Li et al. 2011a,b; Xiao et al. 2011; Chen et al. 2014). Consistently, pharmacological inhibition of p300/CBP KAT activities in a panel of primary melanoma cell lines sensitizes cells to DNA-damaging chemotherapeutic agents (Yan et al. 2013). Higher nuclear CBP protein levels have also been detected in precancerous hyperplastic and dysplastic laryngeal lesions, suggesting overexpression of p300/CBP may contribute to different steps of cancer development and growth (Karamouzis et al. 2002). Conversely, reduced levels of p300/CBP have been detected in certain cancers. Pasqualucci et al. (2011) detected loss of p300 and/or CBP expression in 8% of diffuse large B-cell lymphoma with no genetic lesion in these genes. The significance of these changes has been underscored by the prognostic value of this information. A study of

Table 2. Cancer subtypes with higher frequency of CBP mutations

Cancer subtype	N	Samples mutated (%)
Follicular lymphoma	66	33.3
Skin squamous cell carcinoma	77	28.6
Marginal zone B-cell lymphoma	15	13.3
Diffuse large B-cell lymphoma	242	12.0
Salivary gland carcinoma	63	9.5
Bladder carcinoma	438	8.9
Endometrial carcinoma	337	8.0
Lung small-cell carcinoma	52	7.7
Breast carcinoma (estrogen-receptor-positive)	80	7.5

Data were obtained from the publicly available COSMIC database (cancer.sanger.ac.uk).

Table 3. Cancer subtypes with low frequency of p300 mutations

Cancer subtype	<i>N</i>	Samples mutated (%)
Acute lymphoblastic leukemia	438	0.9
Clear cell renal cell carcinoma	692	0.9
Hepatocellular carcinoma	628	0.8
Chronic lymphocytic leukemia	798	0.5
Ovarian carcinoma	693	0.3
Prostate adenocarcinoma	755	0.3
Pancreatic carcinoma	593	0.2

Data were obtained from the publicly available COSMIC database (cancer.sanger.ac.uk).

327 melanoma samples found that decreased nuclear levels of p300 associated with disease progression and poor overall survival (Rotte et al. 2013).

Interestingly, an increase in cytoplasmic levels of p300 was observed in melanoma and correlated significantly with tumor size and disease progression in early stages (Rotte et al. 2013; Bhandaru et al. 2014). These findings suggest that a shift in the subcellular localization of p300 may be involved in the progression of this cancer and highlight the importance of p300/CBP cytoplasmic functions. However, few investigations addressing cytoplasmic functions of p300/CBP have been conducted. Among these are studies that provide evidence for a p53-directed E4 ligase activity associated with cytoplasmic p300/CBP leading to polyubiquitination and degradation of cytoplasmic p53 (Grossman et al. 2007; Shi et al. 2009). The compartmentalized regulation of p53 by p300/CBP provides an explanation for previously reported opposing effects of these KATs on p53, namely, destabilization of the protein and promoting its nuclear functions. Hence, the physical separation of p300/CBP's nuclear transcriptional function from the cytosolic E3/E4 ligase activity is an important aspect of p53 regulation by p300/CBP. Extranuclear functions of p53 involve triggering apoptosis through interactions with mitochondrial outer membrane proteins, which contribute to its tu-

mor-suppressive effects (O'Brate and Giannakakou 2003). Inappropriate accumulation of cytosolic p300/CBP can, therefore, suppress p53-mediated apoptosis in response to stress signals.

The Effects of p300/CBP on Chromatin in Cancer

Deregulated chromatin targeting by p300/CBP can have profound effects in cancer. For instance, alterations of H3K27ac, a major *in vivo* target of p300/CBP at enhancer loci, is observed in numerous cancers indicating disrupted activities of p300/CBP at specific enhancer elements (Akhtar-Zaidi et al. 2012). These "variant enhancer loci" (VELs) as they were termed, correlate with aberrant expression of their putative target genes. The enhancers with inappropriately acquired H3K27ac associate frequently with genes that have known contributions to many phenotypic hallmarks of cancer (Hnisz et al. 2013). Thus, alterations in the distribution of H3K27ac (and likely H3K18ac, the other major target of p300/CBP) and, hence, enhancer activity in cancer can promote tumorigenesis through promoting an oncogenic gene expression program. Possible mechanisms of deregulated chromatin targeting may involve mutant or inappropriately expressed p300/CBP as well as changes in transcription factors that recruit these coactivators to gene regulatory elements. For example, genetic lesions in the acetyllysine-binding bromodomain of p300/CBP can lead

Table 4. Cancer subtypes with low frequency of CBP mutations

Cancer subtype	<i>N</i>	Samples mutated (%)
Pancreatic carcinoma	593	1.0
Breast carcinoma (triple-negative)	121	0.8
Clear cell renal cell carcinoma	692	0.6
Chronic lymphocytic leukemia	798	0.5
Prostate adenocarcinoma	762	0.4
Acute myeloid leukemia	785	0.4

Data were obtained from the publicly available COSMIC database (cancer.sanger.ac.uk).

to alterations in specificity or strength of chromatin binding and to redistribution of H3K18/27ac across the genome. Such a scenario could also occur through gene amplifications or translocations, giving rise to aberrant formation of enhancer loci in some tumors (Hnisz et al. 2013).

Functions of p300/CBP on chromatin can also be co-opted by viral oncogenes leading to cellular transformation. Adenovirus small E1A (e1a), a splice variant of E1A that is responsible for reprogramming the expression of thousands of host genes, relies on interactions with p300/CBP to coerce normal, primary cell-cycle-arrested fibroblasts into S phase (Howe et al. 1990). The e1a protein causes the recruitment of p300/CBP to and increased H3K18ac (but not H3K27ac) at promoter regions of cell-cycle genes for full transcriptional activation. In parallel, e1a also actively represses cell-type-specific genes by opposing the functions of p300/CBP at promoters and enhancers of these genes as evident by substantial deacetylation of H3K18 and H3K27 at these sites on e1a expression (Ferrari et al. 2010, 2014). Furthermore, e1a represses cellular defense response genes by forming a trimeric complex between e1a, RB1, and, surprisingly, p300 itself, which acetylates RB1 to prevent its normal inactivation by phosphorylation (Ferrari et al. 2014). The repressive RB1-e1a-p300 complex binds to the promoter and gene body regions of defense response genes, and in some cases fully coating entire gene loci and preventing their activation by the host cell. This repression is accompanied by condensation of the local chromatin environment (Ferrari et al. 2014). The overall effect of e1a in the 24 h after entry into a cell is to turn off cell identity and the antiviral cellular defense genes, and to turn on genes that are required for entry into S phase and DNA replication. The bulk of this oncogenic reprogramming depends on interactions of e1a with p300/CBP and RB1. These findings provide a blueprint for understanding how nonviral oncogenesis may also depend on precise exploitations of p300/CBP to achieve similar cellular outcomes.

HISTONE ACETYLATION BALANCE AND ITS IMPLICATIONS FOR CANCER

In addition to targeted recruitment and acetylation of specific genomic loci, histone acetyltransferases function globally throughout the genome in a seemingly nontargeted manner by mechanisms that are not yet clear (Vogelauer et al. 2000). When coupled to the global actions of lysine deacetylases (KDACs), the opposing but continual functions of KATs and KDACs result in fast turnover of histone acetylation (Waterborg 2001), which consumes acetyl coenzyme A and generates acetate anions. In primary tumor tissues, cancer cells show marked differences in the global levels of histone modifications including acetylation, which are prognostic of clinical outcome in many types of solid tumors (Kurdistani 2007). Specifically, lower global level of H3K18ac is associated with cancer-related mortality and/or morbidity in prostate, kidney, lung, pancreatic, and breast cancers (Seligson et al. 2005, 2009; Manuyakorn et al. 2010; Mosashvilli et al. 2010; Kurdistani 2011). Cancer-associated genetic lesions in p300/CBP resulting in reduced KAT activity can certainly lead to the global loss of H3K18/27ac. However, recent work from our laboratory has revealed an unanticipated function for global histone acetylation in regulating intracellular pH (McBrien et al. 2013). We found that in multiple cancer or normal cell lines, the balance of KAT and KDAC activities is shifted toward the latter in response to acidic cellular environment, resulting in histones that are globally and continuously deacetylated. This leads to liberated acetate anions that are in turn used by the membrane-bound monocarboxylate transporters to export protons out of the cell, thus buffering the intracellular pH. Proliferating cells including cancer cells need to maintain an alkaline intracellular pH relative to the outside for cell growth and division (Webb et al. 2011). Because cancer tissues commonly show low pH *in vivo*, it is possible that enhanced global histone deacetylation serves to maintain a viable intracellular pH in these tumors, providing a growth advantage (Parks et al. 2011). This chromatin response to acidity is an active process resulting in the con-

tinuous generation of free acetate molecules through enhanced deacetylation and thus depends on intact or even enhanced histone acetylation. Therefore, the function of KATs in maintaining global histone acetylation is imperative to this pH-regulatory function of chromatin. In this regard, loss of KAT function may in fact reduce fitness in tumors exposed to an acidic environment.

LINKING CELLULAR ENERGETICS AND THE EPIGENOME

p300 and CBP target a significant number of nonhistone proteins for acetylation, including cytosolic proteins involved in essential metabolic processes. This can potentially coordinate cytoplasmic and chromatin-related functions of p300/CBP. The involvement of p300 in regulating metabolism via targeting the M2 isoform of pyruvate kinase, PKM2, is one such example (Lv et al. 2013). A majority of cancers express PKM2, which unlike the constitutively active PKM1 isoform, shows lower activity and is allosterically activated by an upstream glycolytic intermediate (Christofk et al. 2008; Wong et al. 2015). The slower enzymatic rate of PKM2 is thought to essentially serve as a road blockage that causes a logjam in upstream glycolytic reactions, forcing glycolysis intermediates into branching pathways, the products of which, such as nucleotide precursors, are required for general cellular biosynthesis. p300 acetylates a lysine residue (K433) unique to PKM2, which abolishes allosteric activation and enhances nuclear localization of this PK isoform. The switch between cytoplasmic metabolic function and nuclear protein kinase activity of PKM2 regulated by p300 occurs in response to mitogens and oncogenic signals and may be involved in tumorigenesis (Lv et al. 2013). In the nucleus PKM2 phosphorylates histone H3 at threonine 11, a modification shown to be required for cell-cycle progression and tumorigenesis (Yang et al. 2012). These findings indicate a role of p300 in mediating the proliferative program in cancer cells through switching a metabolic enzyme to a nuclear kinase to create a chromatin state conducive for cell replication. The regula-

tion of PKM2 localization and activity is just one recent indication of the broader influence of p300/CBP beyond their nuclear functions as transcriptional coactivators.

FUTURE DIRECTIONS AND THERAPEUTIC APPLICATIONS

The central roles of p300/CBP in regulating cell proliferation have spurred efforts to develop specific inhibitors of the enzymatic activities as well as protein–protein interactions of p300/CBP. KAT inhibitors with higher specificity toward p300/CBP show antiproliferative effects in preclinical studies of cancer (Santer et al. 2011; Yang et al. 2013). Small molecules that inhibit p300/CBP interactions with other proteins also show promising clinical use. ICG-001, which specifically inhibits CBP binding to β -catenin, a component of the Wnt signaling pathway, reduces tumorigenic phenotypes and enhances drug sensitivity in both acute lymphoblastic leukemia (ALL) and nasopharyngeal carcinoma (Emami et al. 2004; Gang et al. 2014; Chan et al. 2015). This approach is thought to take advantage of differential co-activator usage by β -catenin. β -catenin may mediate the opposing outcomes of Wnt signaling by using CBP or p300 to either stimulate proliferation or initiate differentiation, respectively (Ma et al. 2005; Teo and Kahn 2010). Interestingly, the effect of ICG-001 is independent of CBP mutational status in ALL (Gang et al. 2014). Most CBP mutations in ALL are found carboxy terminal to the β -catenin binding site where ICG-001 binds (Mullighan et al. 2011). These findings suggest that the preservation of CBP- β -catenin interaction and not the mutations in other regions of CBP may underlie progression of ALL.

CONCLUDING REMARKS

The many functions of p300/CBP can be differentially exploited in cancer depending on the context, cellular identity, and perhaps environmental cues to confer a growth advantage. The paradigm of cancer as an evolutionary system suggests the sequential acquisition of somatic mutations in a fluctuating microenvironment

to gain fitness. Considering such a system, the order and nature of other oncogenic events can dictate the selection for or against p300/CBP alterations that are most advantageous for survival and growth, therefore branding these proteins as tumor suppressors or oncogenes.

ACKNOWLEDGMENTS

We thank Michael Carey and Trent Su for valuable input and discussions in preparing this manuscript. N.A. is supported by a Ruth L. Kirschstein National Research Service Award (CA186619-02) and S.K.K. by a National Institutes of Health Grant (CA178415).

REFERENCES

- Ait-Si-Ali S, Ramirez S, Barre FX, Dkhissi F, Magnaghi-Jaulin L, Girault JA, Robin P, Knibiehler M, Pritchard LL, Ducommun B, et al. 1998. Histone acetyltransferase activity of CBP is controlled by cycle-dependent kinases and oncoprotein E1A. *Nature* **396**: 184–186.
- Ait-Si-Ali S, Polesskaya A, Filleur S, Ferreira R, Duquet A, Robin P, Vervish A, Trouche D, Cabon F, Harel-Bellan A. 2000. CBP/p300 histone acetyl-transferase activity is important for the G₁/S transition. *Oncogene* **19**: 2430–2437.
- Akhtar-Zaidi B, Cowper-Sal-lari R, Corradin O, Saiakhova A, Bartels CF, Balasubramanian D, Myeroff L, Lutterbaugh J, Jarrar A, Kalady MF, et al. 2012. Epigenomic enhancer profiling defines a signature of colon cancer. *Science* **336**: 736–739.
- Alarcón JM, Malleret G, Touzani K, Vronskaya S, Ishii S, Kandel ER, Barco A. 2004. Chromatin acetylation, memory, and LTP are impaired in CBP^{+/-} mice: A model for the cognitive deficit in Rubinstein–Taybi syndrome and its amelioration. *Neuron* **42**: 947–959.
- Arany Z, Newsome D, Oldread E, Livingston DM, Eckner R. 1995. A family of transcriptional adaptor proteins targeted by the E1A oncoprotein. *Nature* **374**: 81–84.
- Balakrishnan L, Stewart J, Polaczek P, Campbell JL, Bambara RA. 2010. Acetylation of Dna2 endonuclease/helicase and flap endonuclease 1 by p300 promotes DNA stability by creating long flap intermediates. *J Biol Chem* **285**: 4398–4404.
- Bernat A, Avvakumov N, Mymryk JS, Banks L. 2003. Interaction between the HPV E7 oncoprotein and the transcriptional coactivator p300. *Oncogene* **22**: 7871–7881.
- Bhandaru M, Ardekani GS, Zhang G, Martinka M, McElwee KJ, Li G, Rotte A. 2014. A combination of p300 and Braf expression in the diagnosis and prognosis of melanoma. *BMC Cancer* **14**: 398.
- Black JC, Choi JE, Lombardo SR, Carey M. 2006. A mechanism for coordinating chromatin modification and pre-initiation complex assembly. *Mol Cell* **23**: 809–818.
- Bryan EJ, Jokubaitis VJ, Chamberlain NL, Baxter SW, Dawson E, Choong DYH, Campbell IG. 2002. Mutation analysis of EP300 in colon, breast and ovarian carcinomas. *Int J Cancer* **102**: 137–141.
- Chakravarti D, Ogryzko V, Kao HY, Nash A, Chen H, Nakatani Y, Evans RM. 1999. A viral mechanism for inhibition of p300 and PCAF acetyltransferase activity. *Cell* **96**: 393–403.
- Chan HM, La Thangue NB. 2001. p300/CBP proteins: HATs for transcriptional bridges and scaffolds. *J Cell Sci* **114**: 2363–2373.
- Chan HM, Krstic-Demonacos M, Smith L, Demonacos C, La Thangue NB. 2001. Acetylation control of the retinoblastoma tumour-suppressor protein. *Nat Cell Biol* **3**: 667–674.
- Chan KC, Chan LS, Ip JCY, Lo C, Yip TTC, Ngan RKC, Wong RNS, Lo KW, Ng WT, Lee AWM, et al. 2015. Therapeutic targeting of CBP/ β -catenin signaling reduces cancer stem-like population and synergistically suppresses growth of EBV-positive nasopharyngeal carcinoma cells with cisplatin. *Sci Rep* **5**: 9979.
- Chen MK, Cai MY, Luo RZ, Tian X, Liao QM, Zhang XY, Han JD. 2014. Overexpression of p300 correlates with poor prognosis in patients with cutaneous squamous cell carcinoma. *Br J Dermatol* **172**: 111–119.
- Christofk HR, Vander Heiden MG, Harris MH, Ramathan A, Gerszten RE, Wei R, Fleming MD, Schreiber SL, Cantley LC. 2008. The M2 splice isoform of pyruvate kinase is important for cancer metabolism and tumour growth. *Nature* **452**: 230–233.
- Dancy BM, Cole PA. 2015. Protein lysine acetylation by p300/CBP. *Chem Rev* **115**: 2419–2452.
- Das C, Lucia MS, Hansen KC, Tyler JK. 2009. CBP/p300-mediated acetylation of histone H3 on lysine 56. *Nature* **459**: 113–117.
- Das C, Roy S, Namjoshi S, Malarkey CS, Jones DNM, Kutateladze TG, Churchill ME, Tyler JK. 2014. Binding of the histone chaperone ASF1 to the CBP bromodomain promotes histone acetylation. *Proc Natl Acad Sci* **111**: E1072–E1081.
- Debes JD, Schmidt LJ, Huang H, Tindall DJ. 2002. P300 mediates androgen-independent transactivation of the androgen receptor by interleukin 6. *Cancer Res* **62**: 5632–5636.
- Debes JD, Sebo TJ, Lohse CM, Murphy LM, Haugen DAL, Tindall DJ. 2003. p300 in prostate cancer proliferation and progression. *Cancer Res* **63**: 7638–7640.
- Delvecchio M, Gaucher J, Aguilar-Gurrieri C, Ortega E, Panne D. 2013. Structure of the p300 catalytic core and implications for chromatin targeting and HAT regulation. *Nat Struct Mol Biol* **20**: 1040–1046.
- Derynck R, Akhurst RJ, Balmain A. 2001. TGF- β signaling in tumor suppression and cancer progression. *Nat Genet* **29**: 117–129.
- Eckner R, Ludlow JW, Lill NL, Oldread E, Arany Z, Modjtahedi N, DeCaprio JA, Livingston DM, Morgan JA. 1996. Association of p300 and CBP with simian virus 40 large T antigen. *Mol Cell Biol* **16**: 3454–3464.
- Emami KH, Nguyen C, Ma H, Kim DH, Jeong KW, Eguchi M, Moon RT, Teo J, Oh SW, Kim HY, et al. 2004. A small

- molecule inhibitor of β -catenin/CREB-binding protein transcription. *Proc Natl Acad Sci* **101**: 12682–12687.
- Feng XH, Zhang Y, Wu RY, Derynck R. 1998. The tumor suppressor Smad4/DPC4 and transcriptional adaptor CBP/p300 are coactivators for Smad3 in TGF- β -induced transcriptional activation. *Genes Dev* **12**: 2153–2163.
- Ferrari R, Pellegrini M, Horwitz GA, Xie W, Berk AJ, Kurdistani SK. 2008. Epigenetic reprogramming by adenovirus e1a. *Science* **321**: 1086–1088.
- Ferrari R, Berk AJ, Kurdistani SK. 2010. Viral manipulation of the host epigenome for oncogenic transformation. *Nat Rev Genet* **10**: 290–294.
- Ferrari R, Gou D, Jawdekar G, Johnson SA, Nava M, Su T, Yousef AF, Zemke NR, Pellegrini M, Kurdistani SK, et al. 2014. Adenovirus small E1A employs the lysine acetylases p300/CBP and tumor suppressor Rb to repress select host genes and promote productive virus infection. *Cell Host Microbe* **16**: 663–676.
- Forbes SA, Beare D, Gunasekaran P, Leung K, Bindal N, Boutselakis H, Ding M, Bamford S, Cole C, Ward S, et al. 2015. COSMIC: Exploring the world's knowledge of somatic mutations in human cancer. *Nucleic Acids Res* **43**: D805–D811.
- Gang EJ, Hsieh YT, Pham J, Zhao Y, Nguyen C, Huantes S, Park E, Naing K, Klemm L, Swaminathan S, et al. 2014. Small-molecule inhibition of CBP/catenin interactions eliminates drug-resistant clones in acute lymphoblastic leukemia. *Oncogene* **33**: 2169–2178.
- Gayther SA, Batley SJ, Linger L, Bannister A, Thorpe K, Chin SF, Daigo Y, Russell P, Wilson A, Sowter HM, et al. 2000. Mutations truncating the EP300 acetylase in human cancers. *Nat Genet* **24**: 300–303.
- Goodman RH, Smolik S. 2000. CBP/p300 in cell growth, transformation, and development. *Genes Dev* **14**: 1553–1577.
- Grossman SR. 2001. p300/CBP/p53 interaction and regulation of the p53 response. *Eur J Biochem* **268**: 2773–2778.
- Grossman SR, Perez M, Kung AL, Joseph M, Mansur C, Xiao ZX, Kumar S, Howley PM, Livingston DM. 1998. p300/MDM2 complexes participate in MDM2-mediated p53 degradation. *Mol Cell* **2**: 405–415.
- Grossman SR, Grossman SR, Deato ME, Tagami H, Nakatani Y, Livingston DM. 2007. Polyubiquitination of p53 by a ubiquitin ligase activity of p300. *Science* **342**: 342–345.
- Hasan S, Stucki M, Hassa PO, Imhof R, Gehrig B, Hunziker P, Hübscher U, Hottiger MO. 2001. Regulation of human flap endonuclease-1 activity by acetylation through the transcriptional coactivator p300. *Mol Cell* **7**: 1221–1231.
- He H, Yu FX, Sun C, Luo Y. 2011. CBP/p300 and SIRT1 are involved in transcriptional regulation of S phase specific histone genes. *PLoS ONE* **6**: e22088.
- Hnisz D, Abraham BJ, Lee TI, Lau A, Saint-André V, Sigova AA, Hoke HA, Young RA. 2013. Super-enhancers in the control of cell identity and disease. *Cell* **155**: 934–947.
- Horwitz GA, Zhang K, McBrien MA, Grunstein M, Kurdistani SK, Berk AJ. 2008. Adenovirus small e1a alters global patterns of histone modification. *Science* **321**: 1084–1085.
- Howe JA, Mymryk JS, Egan C, Branton PE, Bayley ST. 1990. Retinoblastoma growth suppressor and a 300-kDa protein appear to regulate cellular DNA synthesis. *Proc Natl Acad Sci* **87**: 5883–5887.
- Huang WC, Ju TK, Hung MC, Chen CC. 2007. Phosphorylation of CBP by IKK α promotes cell growth by switching the binding preference of CBP from p53 to NF- κ B. *Mol Cell* **26**: 75–87.
- Iyer NG, Xian J, Chin SF, Bannister AJ, Daigo Y, Aparicio S, Kouzarides T, Caldas C. 2007. p300 is required for orderly G₁/S transition in human cancer cells. *Oncogene* **26**: 21–29.
- Jin Q, Yu LR, Wang L, Zhang Z, Kasper LH, Lee JE, Wang C, Brindle PK, Dent SYR, Ge K. 2011. Distinct roles of GCN5/PCAF-mediated H3K9ac and CBP/p300-mediated H3K18/27ac in nuclear receptor transactivation. *EMBO J* **30**: 249–262.
- Kalkhoven E. 2004. CBP and p300: HATs for different occasions. *Biochem Pharmacol* **68**: 1145–1155.
- Kamei Y, Xu L, Heinzel T, Torchia J, Kurokawa R, Glass B, Lin SC, Heyman RA, Rose DW, Glass CK, et al. 1996. A CBP-integrator complex mediates transcriptional activation and AP-1 inhibition by nuclear receptors. *Cell* **85**: 403–414.
- Karamouzis MV, Papadas T, Varakis I, Sotiropoulou-Bonikou G, Papavassiliou AG. 2002. Induction of the CBP transcriptional co-activator early during laryngeal carcinogenesis. *J Cancer Res Clin Oncol* **128**: 135–140.
- Kawai H, Nie L, Wiederschain D, Yuan ZM. 2001. Dual role of p300 in the regulation of p53 stability. *J Biol Chem* **276**: 45928–45932.
- Kitabayashi I, Aikawa Y, Yokoyama A, Hosoda F, Nagai M, Kakazu N, Abe T, Ohki M. 2001. Fusion of MOZ and p300 histone acetyltransferases in acute monocytic leukemia with a t(8;22)(p11;q13) chromosome translocation. *Leukemia* **15**: 89–94.
- Koshiishi N, Chong JM, Fukasawa T, Ikeno R, Hayashi Y, Funata N, Nagai H, Miyaki M, Matsumoto Y, Fukayama M. 2004. P300 gene alterations in intestinal and diffuse types of gastric carcinoma. *Gastric Cancer* **7**: 85–90.
- Kurdistani SK. 2007. Histone modifications as markers of cancer prognosis: A cellular view. *Br J Cancer* **97**: 1–5.
- Kurdistani S. 2011. CRCnetBASE—Histone modifications in cancer biology and prognosis. *Prog Drug Res* **67**: 91–106.
- Li Q, Zhou H, Wurtele H, Davies B, Horazdovsky B, Verreault A, Zhang Z. 2008. Acetylation of histone H3 lysine 56 regulates replication-coupled nucleosome assembly. *Cell* **134**: 244–255.
- Li M, Luo RZ, Chen JW, Cao Y, Lu JB, He JH, Wu QL, Cai MY. 2011a. High expression of transcriptional coactivator p300 correlates with aggressive features and poor prognosis of hepatocellular carcinoma. *J Transl Med* **9**: 5.
- Li Y, Yang HX, Luo RZ, Zhang Y, Li M, Wang X, Jia WH. 2011b. High expression of p300 has an unfavorable impact on survival in resectable esophageal squamous cell carcinoma. *Ann Thorac Surg* **91**: 1531–1538.
- Li B, Su T, Ferrari R, Li JY, Kurdistani SK. 2014. A unique epigenetic signature is associated with active DNA replication loci in human embryonic stem cells. *Epigenetics* **9**: 257–267.

- Liu X, Wang L, Zhao K, Thompson PR, Hwang Y, Marmorstein R, Cole PA. 2008. The structural basis of protein acetylation by the p300/CBP transcriptional coactivator. *Nature* **451**: 846–850.
- Lv L, Xu YP, Zhao D, Li FL, Wang W, Sasaki N, Jiang Y, Zhou X, Li TT, Guan KL, et al. 2013. Mitogenic and oncogenic stimulation of K433 acetylation promotes PKM2 protein kinase activity and nuclear localization. *Mol Cell* **52**: 340–352.
- Ma H, Nguyen C, Lee KS, Kahn M. 2005. Differential roles for the coactivators CBP and p300 on TCF/ β -catenin-mediated survivin gene expression. *Oncogene* **24**: 3619–3631.
- Maksimoska J, Segura-Peña D, Cole PA, Marmorstein R. 2014. Structure of the p300 histone acetyltransferase bound to acetyl-coenzyme A and its analogues. *Biochemistry* **53**: 3415–3422.
- Manuyakorn A, Paulus R, Farrell J, Dawson NA, Tze S, Cheung-Lau G, Hines OJ, Reber H, Seligson DB, Horvath S, et al. 2010. Cellular histone modification patterns predict prognosis and treatment response in resectable pancreatic adenocarcinoma: Results from RTOG 9704. *J Clin Oncol* **28**: 1358–1365.
- Martínez-Balbás MA, Bauer UM, Nielsen SJ, Brehm A, Kouzarides T. 2000. Regulation of E2F1 activity by acetylation. *EMBO J* **19**: 662–671.
- Marzio G, Wagener C, Gutierrez MI, Cartwright P, Helin K, Giacca M. 2000. E2F family members are differentially regulated by reversible acetylation. *J Biol Chem* **275**: 10887–10892.
- McBrian MA, Behbahan IS, Ferrari R, Su T, Huang TW, Li K, Hong CS, Christofk HR, Vogelauer M, Seligson DB, et al. 2013. Histone acetylation regulates intracellular pH. *Mol Cell* **49**: 310–321.
- Miller RW, Rubinstein JH. 1995. Tumors in Rubinstein–Taybi syndrome. *Am J Med Genet* **56**: 112–115.
- Monteiro AN, August A, Hanafusa H. 1996. Evidence for a transcriptional activation function of BRCA1 C-terminal region. *Proc Natl Acad Sci* **93**: 13595–13599.
- Mosashvili D, Kahl P, Mertens C, Holzapfel S, Rogenhofer S, Hauser S, Büttner R, Von Ruecker A, Müller SC, Ellinger J. 2010. Global histone acetylation levels: Prognostic relevance in patients with renal cell carcinoma. *Cancer Sci* **101**: 2664–2669.
- Mullan PB, Quinn JE, Harkin DP. 2006. The role of BRCA1 in transcriptional regulation and cell cycle control. *Oncogene* **25**: 5854–5863.
- Mullighan CG, Zhang J, Kasper LH, Lerach S, Payne-Turner D, Phillips LA, Heatley SL, Holmfeldt L, Collins-Underwood JR, Ma J, et al. 2011. CREBBP mutations in relapsed acute lymphoblastic leukaemia. *Nature* **471**: 235–239.
- Nishihara A, Hanai JI, Okamoto N, Yanagisawa J, Kato S, Miyazono K, Kawabata M. 1998. Role of p300, a transcriptional coactivator, in signalling of TGF- β . *Genes Cells* **3**: 613–623.
- O’Brate A, Giannakakou P. 2003. The importance of p53 location: Nuclear or cytoplasmic zip code? *Drug Resist Updat* **6**: 313–322.
- Panagopoulos I, Fioretos T, Isaksson M, Samuelsson U, Billström R, Strömbeck B, Mitelman F, Johansson B. 2001. Fusion of the MORF and CBP genes in acute myeloid leukemia with the t(10;16)(q22;p13). *Hum Mol Genet* **10**: 395–404.
- Pao GM, Janknecht R, Ruffner H, Hunter T, Verma IM. 2000. CBP/p300 interact with and function as transcriptional coactivators of BRCA1. *Proc Natl Acad Sci* **97**: 1020–1025.
- Parks SK, Chiche J, Pouyssegur J. 2011. pH control mechanisms of tumor survival and growth. *J Cell Physiol* **226**: 299–308.
- Pasqualucci L, Dominguez-Sola D, Chiarenza A, Fabbri G, Grunn A, Trifonov V, Kasper LH, Lerach S, Tang H, Ma J, et al. 2011. Inactivating mutations of acetyltransferase genes in B-cell lymphoma. *Nature* **471**: 189–195.
- Petrij F, Giles RH, Dauwerse HG, Saris JJ, Hennekam RC, Masuno M, Tommerup N, van Ommen GJ, Goodman RH, Peters DJ, et al. 1995. Rubinstein–Taybi syndrome caused by mutations in the transcriptional co-activator CBP. *Nature* **376**: 348–351.
- Polesskaya A, Naguibneva I, Fritsch L, Duquet A, Ait-Si-Ali S, Robin P, Vervisch A, Pritchard LL, Cole P, Harel-Bellan A. 2001. CBP/p300 and muscle differentiation: No HAT, no muscle. *EMBO J* **20**: 6816–6825.
- Prieur A, Besnard E, Babled A, Lemaitre JM. 2011. p53 and p16(INK4A) independent induction of senescence by chromatin-dependent alteration of S phase progression. *Nat Commun* **2**: 473.
- Pugh BF. 2006. HATs off to PIC assembly. *Mol Cell* **23**: 776–777.
- Ramos YFM, Hestand MS, Verlaan M, Krabbendam E, Ariyurek Y, van Galen M, van Dam H, van Ommen GJB, den Dunnen JT, Zantema A, et al. 2010. Genome-wide assessment of differential roles for p300 and CBP in transcription regulation. *Nucleic Acids Res* **38**: 5396–5408.
- Rebel VI, Kung AL, Tanner EA, Yang H, Bronson RT, Livingston DM. 2002. Distinct roles for CREB-binding protein and p300 in hematopoietic stem cell self-renewal. *Proc Natl Acad Sci* **99**: 14789–14794.
- Ringel AE, Wolberger C. 2013. A new RING tossed into an old HAT. *Structure* **72**: 181–204.
- Roelfsema JH, Peters DJM. 2007. Rubinstein–Taybi syndrome: Clinical and molecular overview. *Expert Rev Mol Med* **9**: 1–16.
- Rotte A, Bhandaru M, Cheng Y, Sjoestroem C, Martinka M, Li G. 2013. Decreased expression of nuclear p300 is associated with disease progression and worse prognosis of melanoma patients. *PLoS ONE* **8**: 1–12.
- Sankar N, Baluchamy S, Kadeppagari RK, Singhal G, Weitzman S, Thimmapaya B. 2008. p300 provides a corepressor function by cooperating with YY1 and HDAC3 to repress c-Myc. *Oncogene* **27**: 5717–5728.
- Santer FR, Höschele PPS, Oh SJ, Erb HHH, Bouchal J, Cavaretta IT, Parson W, Meyers DJ, Cole PA, Culig Z. 2011. Inhibition of the acetyltransferases p300 and CBP reveals a targetable function for p300 in the survival and invasion pathways of prostate cancer cell lines. *Mol Cancer Ther* **10**: 1644–1655.
- Santoso B, Kadonaga JT. 2006. Reconstitution of chromatin transcription with purified components reveals a chro-

- matin-specific repressive activity of p300. *Nat Struct Mol Biol* **13**: 131–139.
- Sawada Y, Ishino M, Miura K, Ohtsuka E, Fujinaga K. 1997. Identification of specific amino acid residues of adenovirus 12 E1A involved in transformation and p300 binding. *Virus Genes* **15**: 161–170.
- Seligson DB, Horvath S, Shi T, Yu H, Tze S, Grunstein M, Kurdastani SK. 2005. Global histone modification patterns predict risk of prostate cancer recurrence. *Nature* **435**: 1262–1266.
- Seligson DB, Horvath S, McBrien MA, Mah V, Yu H, Tze S, Wang Q, Chia D, Goodglick L, Kurdastani SK. 2009. Global levels of histone modifications predict prognosis in different cancers. *Am J Pathol* **174**: 1619–1628.
- Shi Y, Mello C. 1998. A CBP/p300 homolog specifies multiple differentiation pathways in *Caenorhabditis elegans*. *Genes Dev* **12**: 943–955.
- Shi D, Pop MS, Kulikov R, Love IM, Kung AL, Grossman SR. 2009. CBP and p300 are cytoplasmic E4 polyubiquitin ligases for p53. *Proc Natl Acad Sci* **106**: 16275–16280.
- Smith JL, Freebern WJ, Collins I, De Siervi A, Montano I, Haggerty CM, McNutt MC, Butscher WG, Dzekunova I, Petersen DW, et al. 2004. Kinetic profiles of p300 occupancy in vivo predict common features of promoter structure and coactivator recruitment. *Proc Natl Acad Sci* **101**: 11554–11559.
- Sterner DE, Berger SL. 2000. Acetylation of histones and transcription-related factors. *Microbiol Mol Biol Rev* **64**: 435–459.
- Suganuma T, Kawabata M, Ohshima T, Ikeda MA. 2002. Growth suppression of human carcinoma cells by re-introduction of the p300 coactivator. *Proc Natl Acad Sci* **99**: 13073–13078.
- Tanaka Y, Naruse I, Maekawa T, Masuya H, Shiroishi T, Ishii S. 1997. Abnormal skeletal patterning in embryos lacking a single Cbp allele: A partial similarity with Rubinstein-Taybi syndrome. *Proc Natl Acad Sci* **94**: 10215–10220.
- Teo JL, Kahn M. 2010. The Wnt signaling pathway in cellular proliferation and differentiation: A tale of two coactivators. *Adv Drug Deliv Rev* **62**: 1149–1155.
- Tillinghast GW, Partee J, Albert B, Kelley JM, Burtow KH, Kelly K. 2003. Analysis of genetic stability at the EP300 and CREBBP loci in a panel of cancer cell lines. *Genes Chromosom Cancer* **37**: 121–131.
- Trouche D, Kouzarides T. 1996. E2F1 and E1A(12S) have a homologous activation domain regulated by RB and CBP. *Proc Natl Acad Sci* **93**: 1439–1442.
- Trouche D, Cook A, Kouzarides T. 1996. The CBP co-activator stimulates E2F1/DP1 activity. *Nucleic Acids Res* **24**: 4139–4145.
- Turnell AS, Stewart GS, Grand RJA, Rookes SM, Martin A, Yamano H, Elledge SJ, Gallimore PH. 2005. The APC/C and CBP/p300 cooperate to regulate transcription and cell-cycle progression. *Nature* **438**: 690–695.
- Vempati RK, Jayani RS, Notani D, Sengupta A, Galande S, Haldar D. 2010. p300-mediated acetylation of histone H3 lysine 56 functions in DNA damage response in mammals. *J Biol Chem* **285**: 28553–28564.
- Vogelauer M, Wu J, Suka N, Grunstein M. 2000. Global histone acetylation and deacetylation in yeast. *Nature* **408**: 495–498.
- Wang H, Larris B, Peiris TH, Zhang L, Le Lay J, Gao Y, Greenbaum LE. 2007. C/EBP β activates E2F-regulated genes in vivo via recruitment of the coactivator CREB-binding protein/p300. *J Biol Chem* **282**: 24679–24688.
- Waterborg JH. 2001. Dynamics of histone acetylation in *Saccharomyces cerevisiae*. *Biochemistry* **40**: 2599–2605.
- Webb BA, Chimenti M, Jacobson MP, Barber DL. 2011. Dysregulated pH: A perfect storm for cancer progression. *Nat Rev Cancer* **11**: 671–677.
- Whyte P, Williamson NM, Harlow E. 1989. Cellular targets for transformation by the adenovirus E1A proteins. *Cell* **56**: 67–75.
- Wong N, Ojo D, Yan J, Tang D. 2015. PKM2 contributes to cancer metabolism. *Cancer Lett* **356**: 184–191.
- Wu J, Lu LY, Yu X. 2010. The role of BRCA1 in DNA damage response. *Protein Cell* **1**: 117–123.
- Xiao XS, Cai MY, Chen JW, Guan XY, Kung HF, Zeng YX, Xie D. 2011. High expression of p300 in human breast cancer correlates with tumor recurrence and predicts adverse prognosis. *Chinese J Cancer Res* **23**: 201–207.
- Yan G, Eller MS, Elm C, Larocca CA, Ryu B, Panova IP, Dancy BM, Bowers EM, Meyers D, Lareau L, et al. 2013. Selective inhibition of p300 HAT blocks cell-cycle progression, induces cellular senescence, and inhibits the DNA damage response in melanoma cells. *J Invest Dermatol* **133**: 2444–2452.
- Yang XJ, Ullah M. 2007. MOZ and MORE, two large MYSTic HATs in normal and cancer stem cells. *Oncogene* **26**: 5408–5419.
- Yang XJ, Ogryzko VV, Nishikawa J, Howard BH, Nakatani Y. 1996. A p300/CBP-associated factor that competes with the adenoviral oncoprotein E1A. *Nature* **382**: 319–324.
- Yang W, Xia Y, Hawke D, Li X, Liang J, Xing D, Aldape K, Hunter T, Alfred Yung WK, Lu Z. 2012. PKM2 phosphorylates histone H3 and promotes gene transcription and tumorigenesis. *Cell* **150**: 685–696.
- Yang H, Pinello CE, Luo J, Li D, Wang Y, Zhao LY, Jahn SC, Saldanha SA, Planck J, Geary KR, et al. 2013. Small-molecule inhibitors of acetyltransferase p300 identified by high-throughput screening are potent anticancer agents. *Mol Cancer Ther* **12**: 610–620.
- Yao TP, Oh SP, Fuchs M, Zhou ND, Ch'ng LE, Newsome D, Bronson RT, Li E, Livingston DM, Eckner R. 1998. Gene dosage-dependent embryonic development and proliferation defects in mice lacking the transcriptional integrator p300. *Cell* **93**: 361–372.
- Yuan ZM, Huang Y, Ishiko T, Nakada S, Utsugisawa T, Shioya H, Utsugisawa Y, Yokoyama K, Weichselbaum R, Shi Y, et al. 1999. Role for p300 in stabilization of p53 in the response to DNA damage. *J Biol Chem* **274**: 1883–1886.
- Yuan J, Pu M, Zhang Z, Lou Z. 2009. Histone H3-K56 acetylation is important for genomic stability in mammals. *Cell Cycle* **8**: 1747–1753.
- Zimmermann H, Degenkolbe R, Bernard HU, O'Connor MJ. 1999. The human papillomavirus type 16 E6 oncoprotein can down-regulate p53 activity by targeting the transcriptional coactivator CBP/p300. *J Virol* **73**: 6209–6219.

Chapter IV

Histone Deacetylase Inhibitors Provoke a Tumor Supportive Phenotype in Pancreatic Cancer Associated Fibroblasts

This chapter is a reprint of work published in 2016 in *Oncotarget*. Briefly, this collaborative study investigates the efficacy of HDAC inhibitors (HDACi) in the treatment of pancreatic cancer. An effect of HDAC inhibition in induction of a tumor supportive response in cancer-associated fibroblasts is described. This can account for the low efficacy of this treatment in pancreatic cancer. The potential use of combinatorial therapy for improving HDACi treatment is discussed.

I contributed intellectually and provided technical assistance as well as critical revision of the article.

Histone deacetylase inhibitors provoke a tumor supportive phenotype in pancreatic cancer associated fibroblasts

Andrew H. Nguyen¹, Irmina A. Elliott¹, Nanping Wu¹, Cynthia Matsumura¹, Maria Vogelauer², Narsis Attar², Amanda Dann¹, Razmik Ghukasyan¹, Paul A. Toste¹, Sanjeet G. Patel¹, Jennifer L. Williams³, Luyi Li¹, David W. Dawson⁴, Caius Radu⁵, Siavash K. Kurdistani², Timothy R. Donahue^{1,5}

¹Department of Surgery, David Geffen School of Medicine at UCLA, Los Angeles, California, USA

²Department of Biological Chemistry, David Geffen School of Medicine at UCLA, Los Angeles, California, USA

³Department of Surgery, Harbor-UCLA Medical Center, Torrance, California, USA

⁴Department of Pathology and Laboratory Medicine, David Geffen School of Medicine at UCLA, Los Angeles, California, USA

⁵Department of Molecular and Medical Pharmacology, David Geffen School of Medicine at UCLA, Los Angeles, California, USA

Correspondence to: Timothy R. Donahue, **email:** tdonahue@mednet.ucla.edu

Keywords: histone deacetylase inhibitor, SAHA, AP-1, pancreatic cancer, cancer-associated fibroblasts

Received: October 04, 2016 **Accepted:** November 07, 2016 **Published:** November 24, 2016

ABSTRACT

Although histone deacetylase inhibitors (HDACi) are a promising class of anti-cancer drugs, thus far, they have been unsuccessful in early phase clinical trials for pancreatic ductal adenocarcinoma (PDAC). One potential reason for their poor efficacy is the tumor stroma, where cancer-associated fibroblasts (CAFs) are a prominent cell type and a source of resistance to cancer therapies. Here, we demonstrate that stromal fibroblasts contribute to the poor efficacy of HDACi's in PDAC. HDACi-treated fibroblasts show increased biological aggressiveness and are characterized by increased secretion of pro-inflammatory tumor-supportive cytokines and chemokines. We find that HDAC2 binds to the enhancer and promoter regions of pro-inflammatory genes specifically in CAFs and *in silico* analysis identified AP-1 to be the most frequently associated transcription factor bound in these regions. Pharmacologic inhibition of pathways upstream of AP-1 suppresses the HDACi-induced inflammatory gene expression and tumor-supportive responses in fibroblasts. Our findings demonstrate that the combination of HDACi's with chemical inhibitors of the AP-1 signaling pathway attenuate the inflammatory phenotype of fibroblasts and may improve the efficacy of HDACi in PDAC and, potentially, in other solid tumors rich in stroma.

INTRODUCTION

Pancreatic ductal adenocarcinoma (PDAC) is associated with poor overall prognosis and resistance to both conventional and emerging therapies. Gemcitabine is the most frequently used chemotherapy for PDAC, but at best, it increases survival by just a few weeks in both early- and advanced-stage patients [1]. Over the last 10 years, there have only been three new drugs approved by the FDA for PDAC, each of which confers only modest survival improvement in advanced-stage patients. In 2005, erlotinib, an EGFR inhibitor, was approved after being shown to increase survival by an average

of 10 days as compared to gemcitabine alone [2]. In 2014, a nanoparticle coated with albumin and packaged with paclitaxel (nab-paclitaxel) was also approved after demonstrating 2 months additional survival over gemcitabine [3]. Recently, liposomal irinotecan combined with fluorouracil/leucovorin has been approved for advanced-stage disease, also adding a modest 2 months additional survival compared to fluorouracil alone. As PDAC is predicted to become the second leading cause of cancer-related deaths in the United States within the next 10 years, there is an ever-pressing need to identify new therapies that are broadly effective against this particularly difficult to treat malignancy [4].

Histone deacetylase inhibitors (HDACi's) are a chemically diverse class of anti-cancer drugs that function by inhibiting lysine deacetylases, resulting in greater acetylation of histones by histone acetyltransferases (HATs) and transcriptional de-repression of their target genes. In tumor cells (TC), HDAC inhibition predominantly induces G1-S cell cycle arrest by increasing CDKN1A/p21 expression [5, 6]. HDACi's have shown greatest promise in the treatment of hematologic malignancies. FDA approval was granted for the pan-HDACi vorinostat (suberanilohydroxamic acid/SAHA) in 2006 [7], and class I selective HDACi romidepsin in 2009 for refractory cutaneous T-cell lymphoma [8] and in 2011 for other peripheral T-cell lymphomas [9]. In 2015, panobinostat, another pan-HDACi, was approved for the treatment of multiple myeloma [10]. However, early phase clinical trials of HDACi's, such as vorinostat/SAHA and panobinostat/LBH-589, combined with standard-of-care cytotoxic chemotherapy for solid tumors, including PDAC, did not show any therapeutic benefit [11, 12]. Although HDACi's appear to be effective against solid tumor cancer cell lines, including PDAC, in culture and *in vivo*, these preclinical results have not been reproduced in early phase clinical trials [13].

As compared to most hematologic malignancies, many solid organ tumors contain a diversity of cellular and non-cellular components in the peritumoral microenvironment, collectively referred to as the "tumor-associated stroma." PDAC has the highest stromal volume that comprises approximately 80 percent of the tumor mass, including a cellular compartment comprised predominantly of cancer-associated fibroblasts (CAFs). In PDAC, CAFs contribute to treatment resistance by synthesizing extracellular matrix proteins that impede drug delivery, and also secrete cytokines and chemokines, which act on neighboring TCs via paracrine signaling. These secreted factors derived from PDAC CAFs increase TC proliferation, migration, invasion, and colony formation in cell culture and *in vivo* [14–16].

In this study, we hypothesized that PDAC CAFs contribute to the poor efficacy of HDACi's in PDAC and therefore evaluated the effects of HDACi's on PDAC CAFs in culture and *in vivo*. We found that PDAC CAFs treated with HDACi's paradoxically become pro-tumorigenic. SAHA transiently increased proliferation of PDAC TCs when co-cultured with CAFs, a phenotype mediated by a pro-inflammatory secretory response induced in CAFs by HDACi's. ChIP-sequencing for HDAC2 revealed enrichment upstream of pro-inflammatory genes that are also commonly regulated by the AP-1 transcription factors. Finally, blockade of this pro-inflammatory response with JNK inhibitors markedly attenuated the tumor-promoting HDACi-induced inflammatory response in these CAFs.

RESULTS

HDACi's decrease PDAC tumor cell viability in isolation but not in the presence of CAFs

In a syngeneic, orthotopic Kras^{LSL.G12D/+}; p53^{R172H/+}; PdxCre^{tg/+} (KPC) PDAC mouse model, systemic treatment with the pan-HDACi SAHA suppressed tumor growth as compared to untreated controls (Figure 1A, Supplementary Figure 1). Analysis of untreated or treated tumor explants on day 37 after implantation revealed that they were almost entirely comprised of TCs with homogeneous morphology (Supplementary Figure 1B) and without the typical dense fibrotic stroma typical of human PDAC histology (Supplementary Figure 2). Therefore, we hypothesized that SAHA was effective in this model because of the lack of the typical stroma which comprises up to 80% of human PDAC.

We observed that immortalized PDAC cells are sensitive to HDACi in culture. MIA PaCa-2 cells were highly sensitive to SAHA with an IC₅₀ of 4 μ M (Figure 1B). PANC-1 cells were also sensitive after 96h, albeit with a higher IC₅₀ (10 μ M) (Figure 1B). In contrast to TCs, two patient-derived primary PDAC CAF lines were extremely resistant to SAHA across a wide range of doses (Figure 1C). The resistance was not unique to SAHA as CAFs were also resistant to either the Class I selective HDACi entinostat (MS-275) or the pan-HDACi panobinostat (LBH-589), both of which decreased MIA PaCa-2 viability (Supplementary Figure 3). Interestingly, hTERT immortalized PDAC CAFs were found to be highly sensitive to SAHA, which is similar to MIA PaCa-2 cancer cells with an IC₅₀ of 4 μ M (Figure 1C). For this reason, in subsequent experiments, we utilized only early passage non-immortalized patient-derived primary PDAC CAFs.

We next asked if the presence of fibroblasts affected TC sensitivity to HDACi's. Using a 3D TC:CAF co-culture model on Matrigel, GFP-expressing PANC-1 TCs formed 3D tumor-like spheres only when cultured in the presence of CAFs (Figure 1D) where CAFs are evenly distributed among TCs (Supplementary Figure 4). PANC-1 cells cultured in the absence of fibroblasts formed only small clusters of cells rather than a larger sphere (Supplementary Figure 5). To quantify tumor cell proliferation while in TC:CAF co-culture, measurements of fluorescence from GFP expressing cancer cells was performed. Fluorescence measurements using a multimode microplate reader in this heterocellular model were validated with the Cell Titer Glo assay as an accurate measure of TC numbers (Supplementary Figure 6). Additionally, GFP-expressing TCs were treated with SAHA and the Cell Titer Glo assay was performed and we observed the addition of SAHA did not affect the linear relationship between GFP fluorescence measurements

and cellular viability (Supplementary Figure 7). While PANC-1 cells cultured alone on plastic (Figure 1B) or Matrigel (Supplementary Figure 8) were sensitive to HDACi, both longer exposure and higher doses were required to suppress TC proliferation in the 3D TC:CAF co-culture model (Figure 1D). Intriguingly, PANC-1 cells in the TC:CAF model were more proliferative with SAHA treatment at early time points during continuous treatment compared to untreated controls (see days 1 and 2 in Figure 1D). Taken together, these results suggest that the HDACi-treated PDAC TCs benefit from the presence of tumor supportive CAFs.

HDACi-treated CAFs enhance aggressiveness of neighboring tumor cells via a paracrine mechanism

We next determined how HDACi-treated CAFs modulate various TC phenotypes through a series of cell culture and *in vivo* models. First, both MIA PaCa-2 and PANC-1 TCs were more proliferative when cultured in conditioned media (CM) from CAFs pre-treated with HDACi than CM from untreated controls as measured by plate fluorescence (Figure 2A–2B). Similarly, PANC-1 TCs grew faster in the TC:CAF Matrigel model with

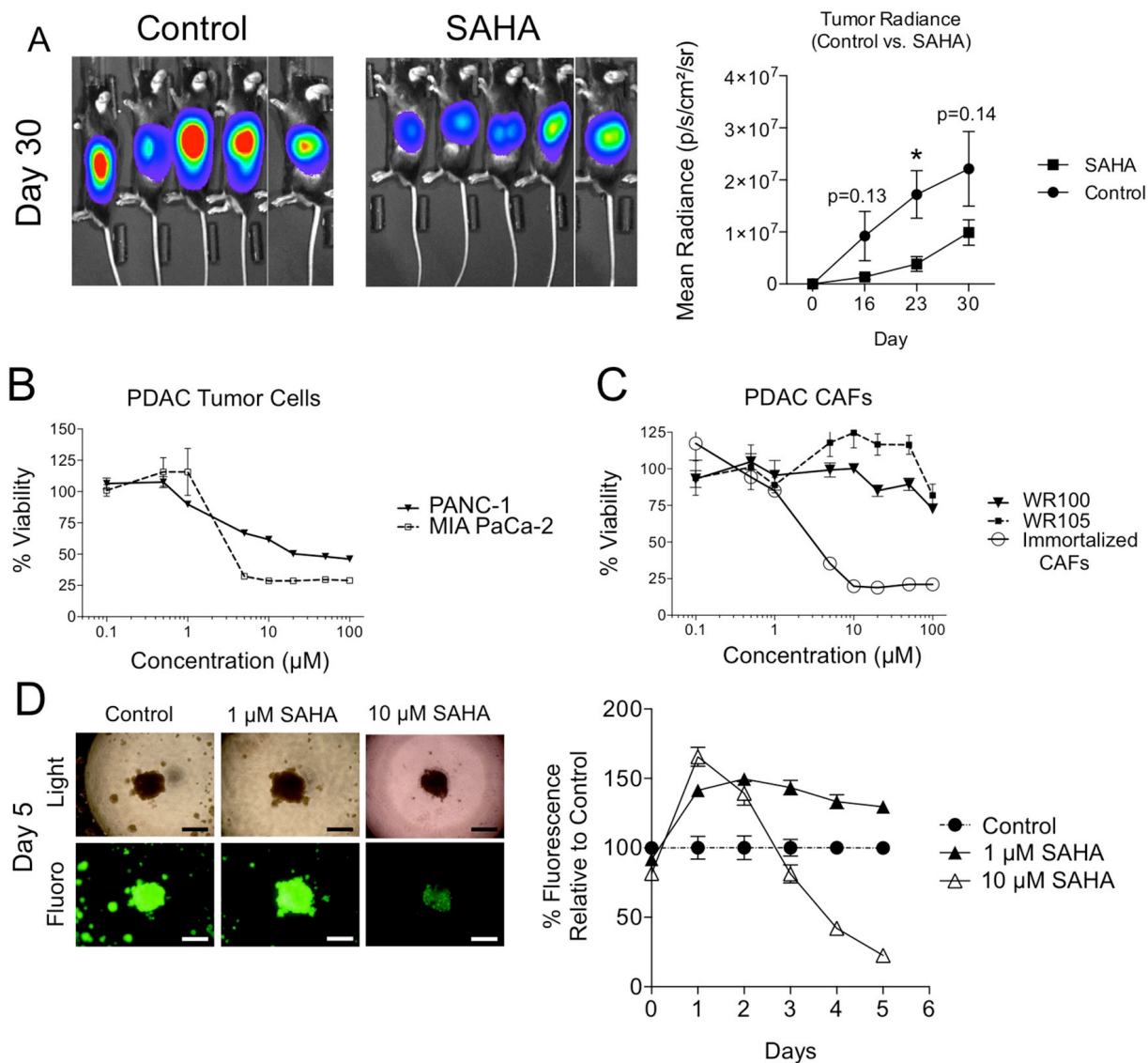


Figure 1: Effect of HDAC inhibition on PDAC tumor cell viability in isolation and in 3D co-culture with CAFs. **A.** KPC-luc cells were implanted in the pancreata of C57BL/6 mice and mice were treated with oral gavage of SAHA 5 times weekly beginning on Day 7. Luminescence measurements were measured on days 16, 23, and 30 in SAHA treated and control mice. Error bars represent SEMs. *P < 0.05. **B.** MTT assay of PANC-1 and MIA PaCa-2 PDAC tumor cell viability at various doses of SAHA for 96h. **C.** MTT assay of WR100 and WR105 primary PDAC fibroblasts and immortalized CAFs at various doses of SAHA for 96h. **D.** Images of PANC-1-GFP/PDAC fibroblast co-culture under fluorescence and light microscopy (left) (4X; scale: 300 μm) and 5 day time course of relative fluorescence of PANC-1-GFP/PDAC CAF co-cultures with treatment of SAHA. Fluorescence is normalized to untreated control cell co-cultures.

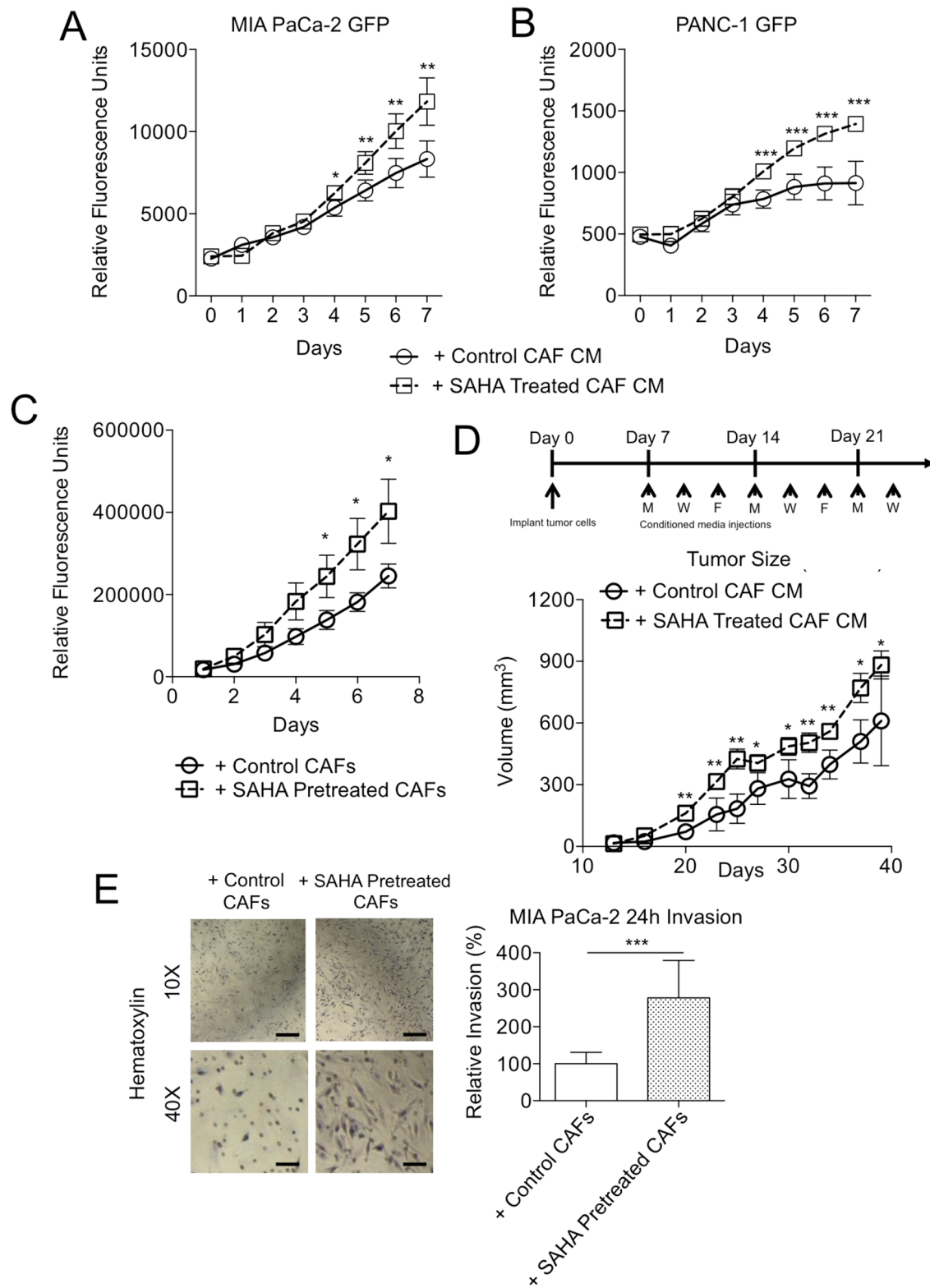


Figure 2: HDACi-treated fibroblasts enhance tumor cell malignant phenotypes. Fluorescence measurements of **A**. MIA PaCa-2-GFP and **B**. PANC-1-GFP cells cultured with conditioned media (without drug) from CAFs pre-treated with or without SAHA for 7 days. **C**. Fluorescence measurements of PANC-1-GFP 3D co-cultured (without drug) for 7 days with CAFs pre-treated +/- SAHA. **D**. Schematic of *in vivo* experimental design (above) and tumor volume (below) of subcutaneous flank MIA PaCa-2 tumors of 8 tumors per group injected thrice weekly with conditioned media from cultured CAFs +/- SAHA. *P < 0.05, **P < 0.01. **E**. Light microscopy images (left) (10X; scale: 100 μ m, 40X; scale 10 μ m) and relative invasion (right) of MIA PaCa-2 invasion with control or 10 μ M SAHA pre-treated PDAC CAFs after 24h in a modified Boyden chamber. *P < 0.05, **P < 0.01, ***P < 0.001.

CAFs that had been pre-treated with SAHA than untreated controls (Figure 2C). Finally, we also examined if HDACi-treatment of the same patient-derived CAFs could also enhance tumor growth *in vivo*. MIA PaCa-2 cells were implanted in bilateral subcutaneous flanks of NOD/SCID/IL2 γ mice and tumors were supplemented thrice weekly with CM (without drug) from cultured CAFs pre-treated +/- SAHA (Figure 2D). Consistent with the cell culture results, tumor growth was accelerated, particularly at earlier time points, in mice injected with SAHA-treated CAF CM.

In addition to enhancing cell proliferation, pretreatment of CAFs with HDACi increased the invasion of co-cultured TCs. CAFs were included in this assay, as their presence has been shown to be important for the process of TC invasion [17]. We observed significantly greater invasion of MIA PaCa-2 cells when cultured in the presence CAFs that had been pre-treated with SAHA as compared to untreated control CAFs (Figure 2E). Taken together, these results suggest that HDACi treatment causes CAFs to become more supportive of tumor growth and aggressiveness in cell culture and *in vivo* through a paracrine mechanism.

SAHA treatment increases expression of tumor-supportive, pro-inflammatory mediators in CAFs

A key mechanism by which CAFs modify the behavior of neighboring TCs is via release of pro-inflammatory factors into the tumor microenvironment [15, 16, 18, 19]. Given our findings with CM from HDACi-treated CAFs that indicated a paracrine mechanism of action, we explored whether pro-inflammatory mediators were increased following HDACi-treatment of CAFs. We initially compared the composition of CM from PDAC CAFs treated with SAHA vs. untreated controls using a membrane-based antibody cytokine array and found HDACi treatment was associated with increased production of pro-inflammatory mediators CXCL1 and IL-8 (Figure 3A), which are known to enhance TC malignant phenotypes [20]. These findings were further validated in a panel of pro-inflammatory genes by quantitative RT-PCR which demonstrated SAHA treatment caused a dose-dependent increase in the expression of this panel of inflammatory genes linked to the tumor-supportive

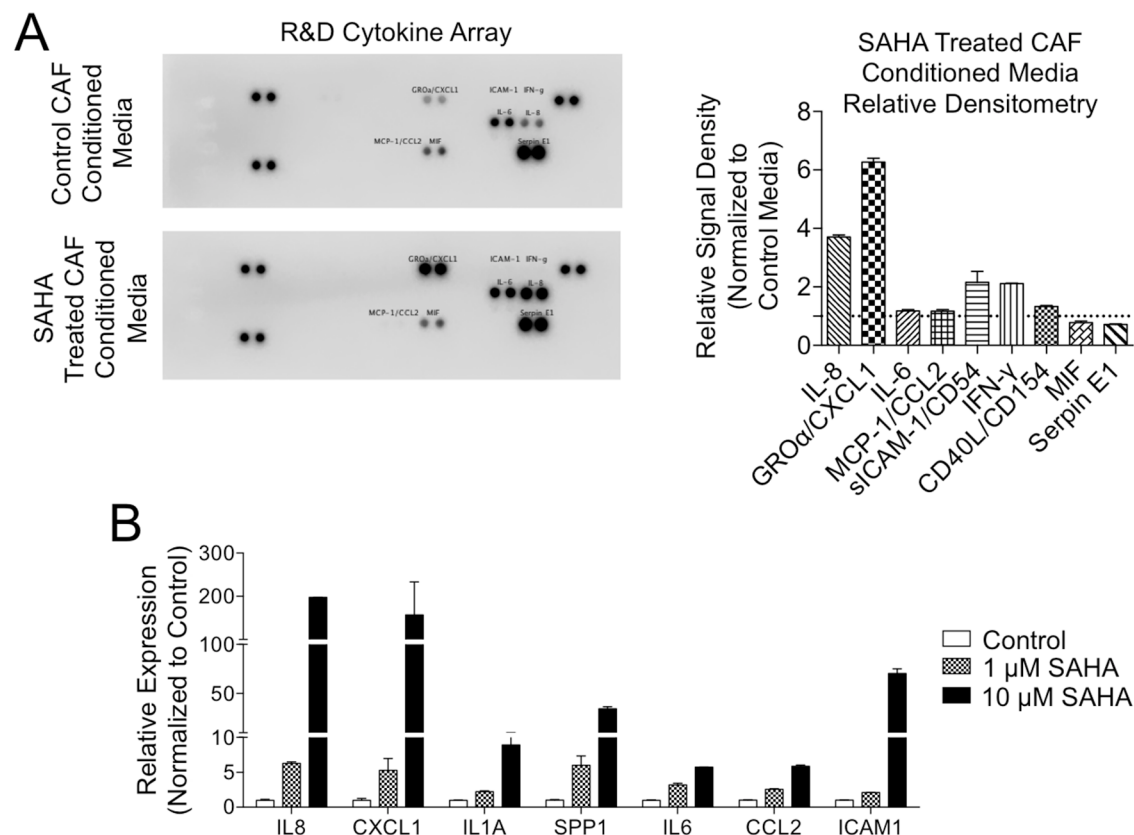


Figure 3: HDACi treatment increases secretion of tumor supportive pro-inflammatory mediators in PDAC CAFs. A. Secretion of pro-inflammatory cytokines was assessed after 24h in control and 10 μ M SAHA treated CAFs by cytokine array (left) with relative densitometry measurements (right). B. Gene expression of inflammatory mediators was determined by qRT-PCR in PDAC CAFs treated for 24h with SAHA.

senescence associated secretory phenotype (SASP) [16, 21], including IL8, CXCL1, IL1A, SPP1, IL6, CCL2, and ICAM1 (Figure 3B). To determine if the enhanced expression of pro-inflammatory mediators was unique to the pan-HDACi SAHA, we next treated primary PDAC CAFs with class I selective HDACi entinostat/MS-275 or the highly potent pan-HDACi panobinostat/LBH-589 (Supplementary Figure 9), each of which also increased the expression of the same panel of genes.

HDACi effects on gene expression are cell-type specific

We next determined the mechanism by which HDACi's increase the expression of pro-inflammatory genes in PDAC CAFs. Histone hyperacetylation through HDAC inhibition results in a permissive transcriptional landscape and the expression of HDAC-regulated genes [22]. In PDAC CAFs, we found that increasing doses of HDACi resulted in increased global histone acetylation (Figure 4A) with the threshold for histone hyperacetylation occurring in the range of 5–10 μ M SAHA; therefore, 10 μ M HDACi was used for subsequent experiments.

To determine whether HDACs may directly suppress the expression of pro-inflammatory genes in CAFs, we performed ChIP-Seq for HDAC2 in primary PDAC CAFs and the PANC-1 TC line. HDAC2 is known to have a role in cell cycle dysregulation in cancer [23, 24]; it is highly expressed in PDAC and associated with resistance to therapy and apoptosis [25, 26]. However, the role of HDAC2 in CAFs is not well defined. In CAFs, we found that HDAC2 binding is enriched in the regulatory regions primarily within 2 Kb of the transcription start site of a large group of pro-inflammatory genes, which was not present in PANC-1 cells (Figure 4B).

In contrast, using GREAT gene ontology analysis [27], HDAC2 binding in PANC-1 TCs occurs in genes predominantly involved in growth factor signaling and cell cycle regulation (Supplementary Figure 10). Induction of cell cycle-related CDKN1A/p21 expression by HDACi's in TCs is believed to be a key mechanism for the resultant cell cycle arrest [5, 22, 28].

These distinct HDAC2 binding patterns in CAFs and TCs may explain differential effects HDACi's have on these two cell types. We next used the HOMER Motif Analysis to identify the enrichment of transcription factor motifs in ChIP-Seq data [29], and found that HDAC2 binds to motifs associated with the AP-1 transcription both PANC-1 TCs and in CAFs although AP-1 motifs were more frequent in CAFs (Figure 4C). These findings were similarly replicated in a search using the Cistrome SeqPos Motif Analysis [30], which identified the c-JUN/AP-1 related binding motifs to be present in the vicinity of HDAC2 binding in CAFs (Supplementary Figure 11).

We further broadly queried common transcription factors that regulate a panel of pro-inflammatory genes

upregulated after HDACi treatment in CAFs using the ENCODE ChIP-Seq Significance Tool [31]. This tool identifies transcription factors that commonly regulate sets of genes by searching publically available ChIP-Seq data sets from the ENCODE Project. We searched for DNA binding factors present within 5,000 base pairs upstream and downstream of the transcription start site of the seven SASP pro-inflammatory genes consistently increased with HDACi treatment in our studies: IL8, CXCL1, IL1A, SPP1, IL6, CCL2, and ICAM1 (Figure 4D). This tool identified STAT3, c-FOS (a component of AP-1), and GATA2 ($q < 0.05$) to be in regulatory regions of these genes. As AP-1 is a well known regulator of inflammation [32] and our HDAC2 ChIP-Seq studies suggest the greatest association of HDAC2 to AP-1 transcription factor binding motifs, we chose to further investigate blockade of the upstream pathways of AP-1 signaling to inhibit the CAF-mediated inflammatory response to HDACi's.

JNK1 inhibition potently suppresses pro-inflammatory, tumor-supportive changes in HDACi-treated CAFs

A key step in forming the active AP-1 transcription factor includes the phosphorylation of c-JUN by Janus N-terminal Kinases (JNKs) to allow heterodimerization of the c-Fos/c-JUN complex. JNK has been implicated as a key regulator of a feed-forward loop of inflammatory signaling, amplifying the production of pro-inflammatory cytokines including IL-8 [33]. JNK inhibition has additionally been shown to effectively inhibit PDAC growth in culture and *in vivo*, using transgenic [34] and human tumor xenograft models [35]. Our previous results have also shown that inhibition of stress response kinases, including JNK, attenuates the inflammatory response in CAFs to DNA damaging chemotherapies [16]. Thus, taken together with our *in silico* results with HDAC2 ChIP-Seq, we focused the remainder of our studies on JNK inhibition as a potentially effective co-therapy with HDACi.

The JNK family of kinases consists of three different isoforms (JNK 1, 2, or 3), which regulate a diverse set of pathways with variable activity based on cell-specific context [36]. We examined a panel of non-specific and isoform-specific JNK inhibitors. We found that SP600125 inhibited c-JUN activation (decreased p-c-JUN) (Figure 5A) and was markedly effective at suppressing inflammatory genes induced by HDACi treatment in a dose-dependent manner (Figure 5B). SP600125, the potent ATP competitive JNK specific inhibitor, is known to decrease expression of inflammatory mediators [37]. JNK-IN-8, which inhibits JNK1/2, suppressed c-JUN phosphorylation (p-c-JUN, Figure 5A) and silenced HDACi-induced inflammatory gene expression in a dose-dependent manner (Figure 5C). In contrast, JNK-IN-9 (a JNK2/3 specific inhibitor) and SR3576 (a JNK3 specific inhibitor) failed to block c-JUN phosphorylation

(Figure 5A) or suppress HDACi-induced gene expression changes in PDAC CAFs (Figure 5D-5E), indicating that JNK1 inhibitors specifically block c-JUN activation and expression of inflammatory mediators in response to HDACi in PDAC CAFs.

We next examined the functional impact of dual HDAC and JNK inhibition in two heterocellular PDAC culture models. First, to determine the effects of JNK inhibition specifically in SAHA-treated CAFs on TC behavior, CM was generated from CAFs pre-treated with

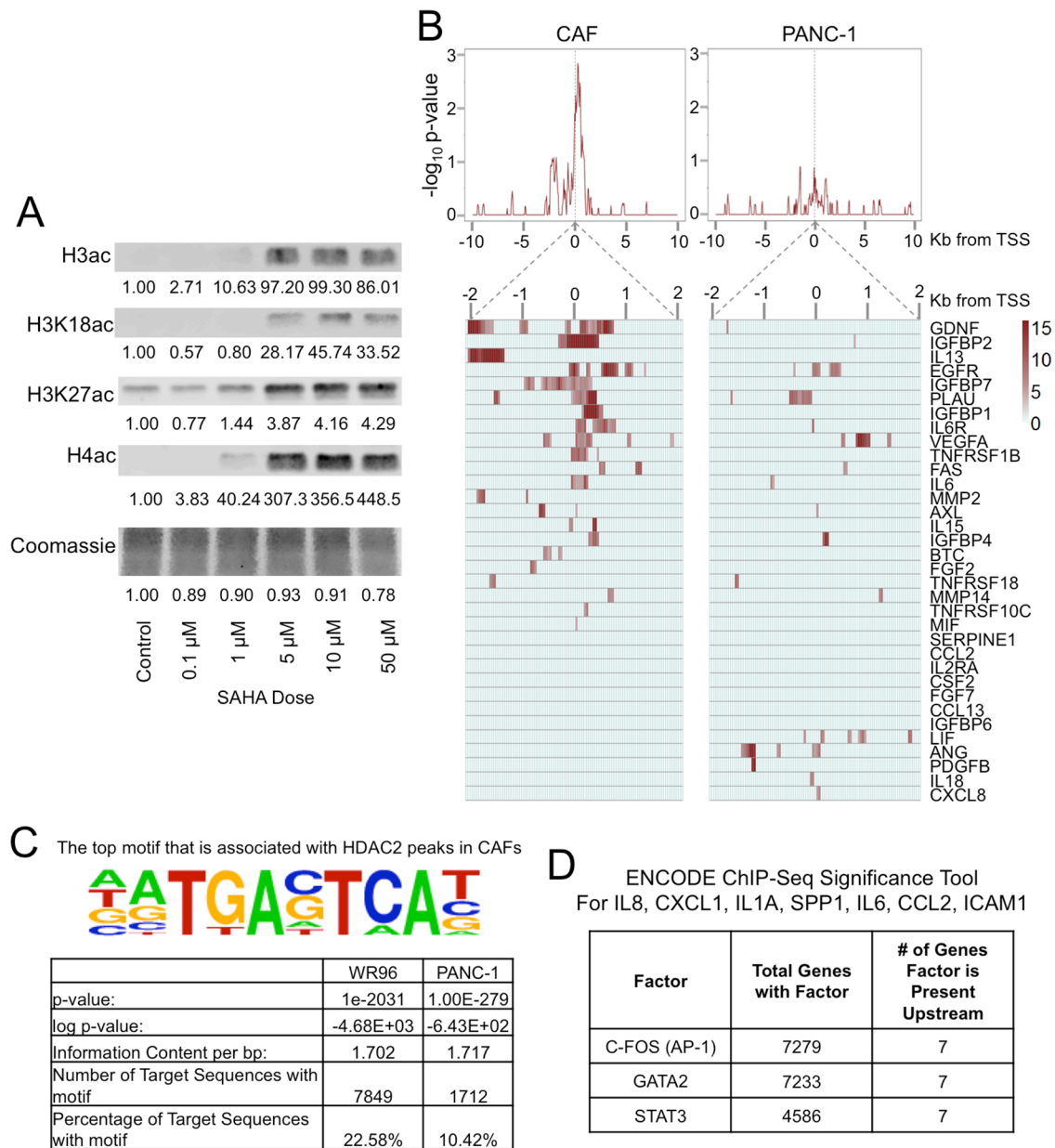


Figure 4: HDAC inhibition causes histone hyperacetylation in CAFs. **A.** Near-infrared western blots of histone extracts of PDAC CAFs treated at various doses of SAHA for 24h. Quantitative near-infrared fluorescent western blots were performed using the LI-COR Odyssey Fc imaging system with densitometry measurements were performed relative to untreated control cell blots are reported. **B.** HDAC2 ChIP-Seq was performed in primary PDAC CAFs and PANC-1 TCs. Average profile Distribution of HDAC2 binding \pm 10 Kb from the transcription start site (TSS) of pro-inflammatory genes (top) and heat map of HDAC2 distribution \pm 2.5 Kb from the TSS (below) of individual pro-inflammatory genes using significant peaks ($P = 10^4$ over three 50 bp windows). **C.** Transcription factor binding motif analysis using HOMER (Hypergeometric Optimization of Motif EnRichment). The top motif identified with HDAC2 peaks in CAFs was found to be associated with AP-1 transcription factor as displayed ($P = 1.0 \times 10^{-2031}$). This motif was present in 22% of HDAC2 peak sequences in fibroblasts. **D.** Factors bound to chromatin common among 7 pro-inflammatory genes within 5,000 base pairs of the transcription start site of these genes were identified using the ENCODE ChIP-Seq Significance Tool ($q < 0.05$). STAT3, C-FOS (a component of the AP-1 heterodimer), and GATA2 were found to commonly bind in gene regulatory regions in the vicinity of the TSS of all 7 genes.

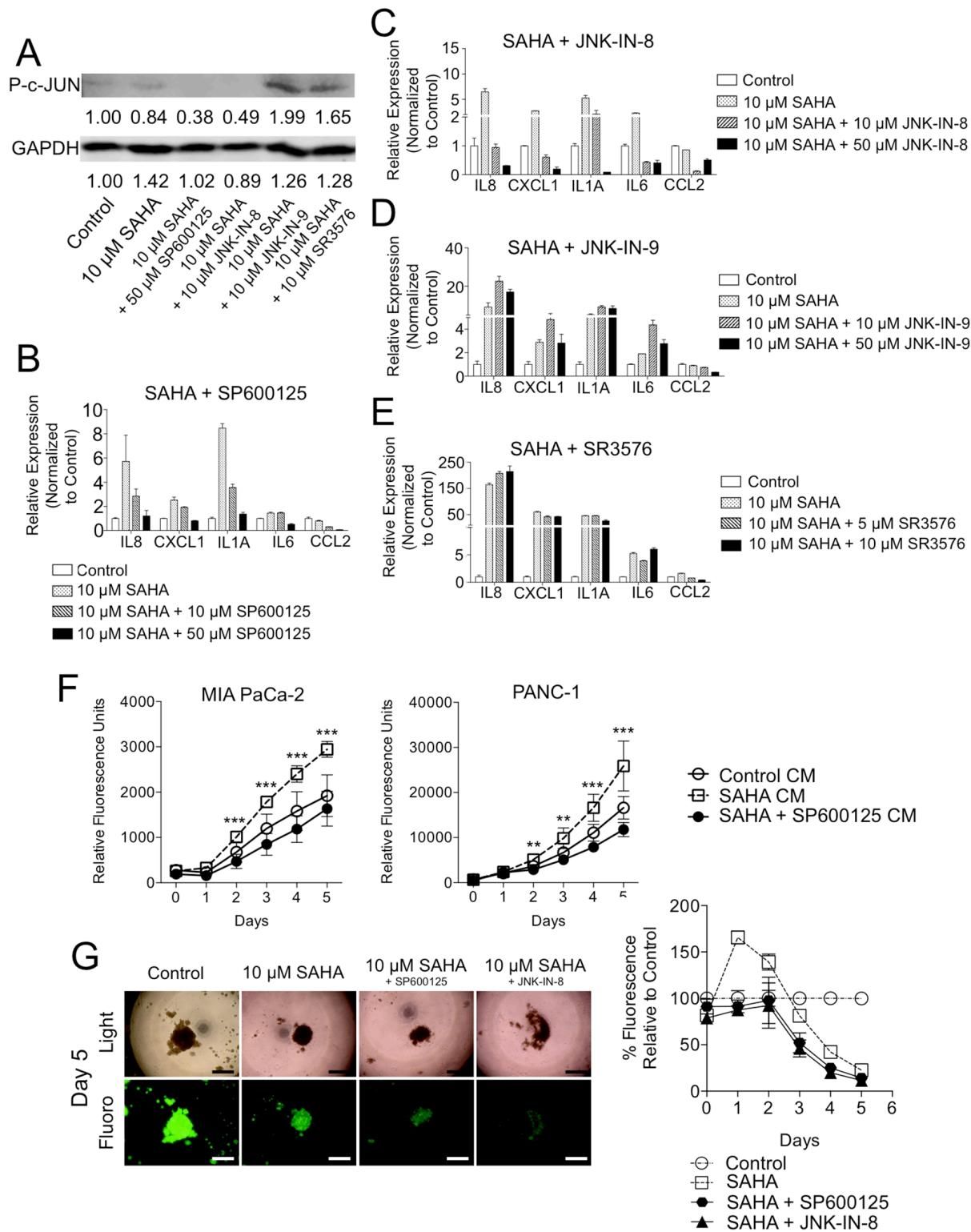


Figure 5: Chemical inhibition of JNK suppresses tumor supportive effects of HDACi in CAFs. A. PDAC CAFs were treated with SAHA +/- various JNK inhibitors and western blots for P-c-JUN and GAPDH was performed of cell lysates with measurements of relative densitometry reported below blot signals. qRT-PCR was performed of PDAC CAFs treated with SAHA and various doses of B. SP600125, C. JNK-IN-8, D. JNK-IN-9, or E. SR3576. F. Fluorescence measurements of GFP-expressing MIA PaCa-2 (left) and PANC-1 (right) cells grown in conditioned media (without drug) from i) naïve CAFs or ii-iii) CAFs pretreated with 10 μ M SAHA +/- 50 μ M SP600125. T-tests were performed to compare 10 μ M SAHA CM and 10 μ M SAHA + 50 μ M SP600125 CM groups (**P < 0.01, ***P < 0.001). G. PANC-1-GFP / CAF 3D co-cultures were treated with SAHA +/- JNK inhibitors: 50 μ M SP600125 or 10 μ M JNK-IN-8 and fluorescence measurements were performed daily (4X; scale: 300 μ m).

SAHA +/- SP600125. Viability of both PANC-1 and MIA PaCa-2 cells were decreased when cultured in CM from SP600125/SAHA treated CAFs as compared with SAHA controls (Figure 5F). Next, to evaluate the phenotype of TCs in the presence of CAFs and dual SAHA/JNK inhibitor treatment, the 3D TC:CAF co-culture model was employed (Figure 5G). Here, addition of SP600125 suppressed the SAHA-induced spike in CAF co-cultured PANC-1 TC proliferation on Days 1 and 2 (Figure 1D and 5G). Taken together, these data show that JNK inhibition can overcome the SAHA-induced tumor-supportive inflammatory response from CAFs, thus potentially isolating the beneficial effects on TCs and overall efficacy of HDACi's in this notoriously difficult to treat cancer and other solid tumors with a CAF laden stromal compartment.

DISCUSSION

HDAC inhibitors effectively kill PDAC TCs in culture and pre-clinical *in vivo* models but have been unsuccessful in early phase clinical trials. Here we show that the poor clinical efficacy of HDACi's may be mediated partly by their effect on the PDAC stromal microenvironment.

As depicted in our proposed model (Figure 6), primary human PDAC CAFs treated with HDACi's develop a counter-productive and paradoxical tumor-supportive response, linked to the release of numerous pro-inflammatory SASP cytokines and chemokines. In part, regulation of these genes is dependent upon acetylation and deacetylation by HATs and HDACs, respectively. In CAFs, HDACs bind preferentially to enhancer and promoter regions upstream of these pro-inflammatory genes, in contrast to TCs where they directly regulate CDKN1A/p21 expression [24] as suggested by our gene ontology findings in PANC-1 TCs which identified cell cycle regulation. Inhibition of HDACs may yield a permissive landscape for the transcription factors, which include AP-1 (c-JUN/c-FOS), to drive transcription of the pro-inflammatory SASP genes in CAFs. Inhibition of JNK signaling, upstream of AP-1, attenuated the tumor supportive inflammatory response to HDACi's.

Our findings that HDAC inhibition unleashes a pro-inflammatory cytokine release rather than cell arrest or death in CAFs is consistent with previous reports. [38]. Pazolli et al. demonstrated that chemical HDAC inhibition with trichostatin A induced the expression of pro-inflammatory osteopontin, IL-6, and IL-8 in CAFs; and an HDAC1 dominant-negative mutation that causes hyperactivation of its target genes caused a similar pro-inflammatory phenotype [39]. Additionally, it has also been shown that HDAC inhibition exaggerated the pro-inflammatory cellular response to toll-like receptor mediated ligation [40, 41], which is suggested to occur as a result of histone hyperacetylation, allowing deregulated transcription of pro-inflammatory genes.

In PDAC and other cancers characterized by a prominent desmoplastic stroma, pro-inflammatory stromal fibroblasts have been described to enhance TC survival and chemoresistance [15, 42, 43]. Our lab recently identified that this CAF phenotype can be accentuated by exposure to DNA damaging chemotherapies [16]. In the current study, we find that HDAC inhibition, which creates a permissive transcriptional landscape for pro-inflammatory gene expression, causes increased secretion of a variety of tumor supportive cytokines and chemokines from PDAC CAFs. We demonstrate that HDAC inhibition drives an inflammatory response in CAFs that is counterproductive and tumor supportive.

By identifying HDAC2 binding patterns in CAFs and querying ENCODE project data, we found that the transcription factor AP-1 may regulate the changes in gene expression enabled by HDACi's. AP-1, which becomes active via phosphorylation of c-JUN by JNKs, is a crucial component involved in the expression of tumor-supportive cytokines and chemokines. JNKs occur in three isoforms (JNK 1, 2, or 3) [36] and have been shown to be activated in inflammatory diseases, including experimental models of pancreatitis [44, 45] and cancer [46]. We propose that specifically JNK1 inhibition may be additive or synergistic with HDACi's in PDAC, as we demonstrated that both the non-specific JNK (1, 2, and 3) inhibitor SP600125 or the JNK1/2 selective inhibitor JNK-IN-8 suppress the pro-inflammatory gene expression induced in PDAC CAFs by SAHA. We also find that these JNK inhibitors reduced the presence of phosphorylated c-JUN, thus decreasing the availability of the active AP-1 heterodimer, downregulating AP-1-dependent transcription, and arresting the production of tumor-supportive inflammation. While it has been previously suggested that JNK3 is a key isoform in the amplification, but not the initiation, of inflammation signaling [33], we found that JNK2/3 or specific JNK3 inhibition was ineffective in suppressing phosphorylation of c-JUN and did not alter HDACi-induced inflammatory gene expression in PDAC CAFs. In addition, SP600125 has been previously shown to enhance G1 arrest on PDAC TCs [34] which may also prove beneficial with HDACi's that induce p21 expression and subsequent cell cycle arrest in TCs.

JNK inhibitors are a particularly attractive therapy for PDAC. In addition to our current work which illustrates their tumor suppressive effects on CAFs treated with HDACi's, they have also been previously shown to also exert anti-tumor effects directly on PDAC tumor cells: inhibiting TC proliferation in culture [34] and decreasing primary human tumor xenograft growth *in vivo* [35].

In conclusion, traditional therapies for the treatment of PDAC target rapidly proliferating TCs with cytotoxic agents. However, this TC centric view of cancer therapy can result in unanticipated and paradoxically deleterious tumor-supportive effects in the adjacent CAFs [16]. Recently, there has been greater recognition of the

contribution of the tumor stroma to cancer progression and therapy resistance. We now provide further evidence the pan-HDACi SAHA dramatically increases the expression of tumor-supportive pro-inflammatory mediators in stromal fibroblasts. We identify the AP-1 transcription

factor likely to be present at HDAC2 binding sites and in a focused chemical inhibitor screen, identify compounds that can suppress this counterproductive pro-inflammatory response. Finally, we provide experimental evidence that inflammation-suppressing JNK inhibition could

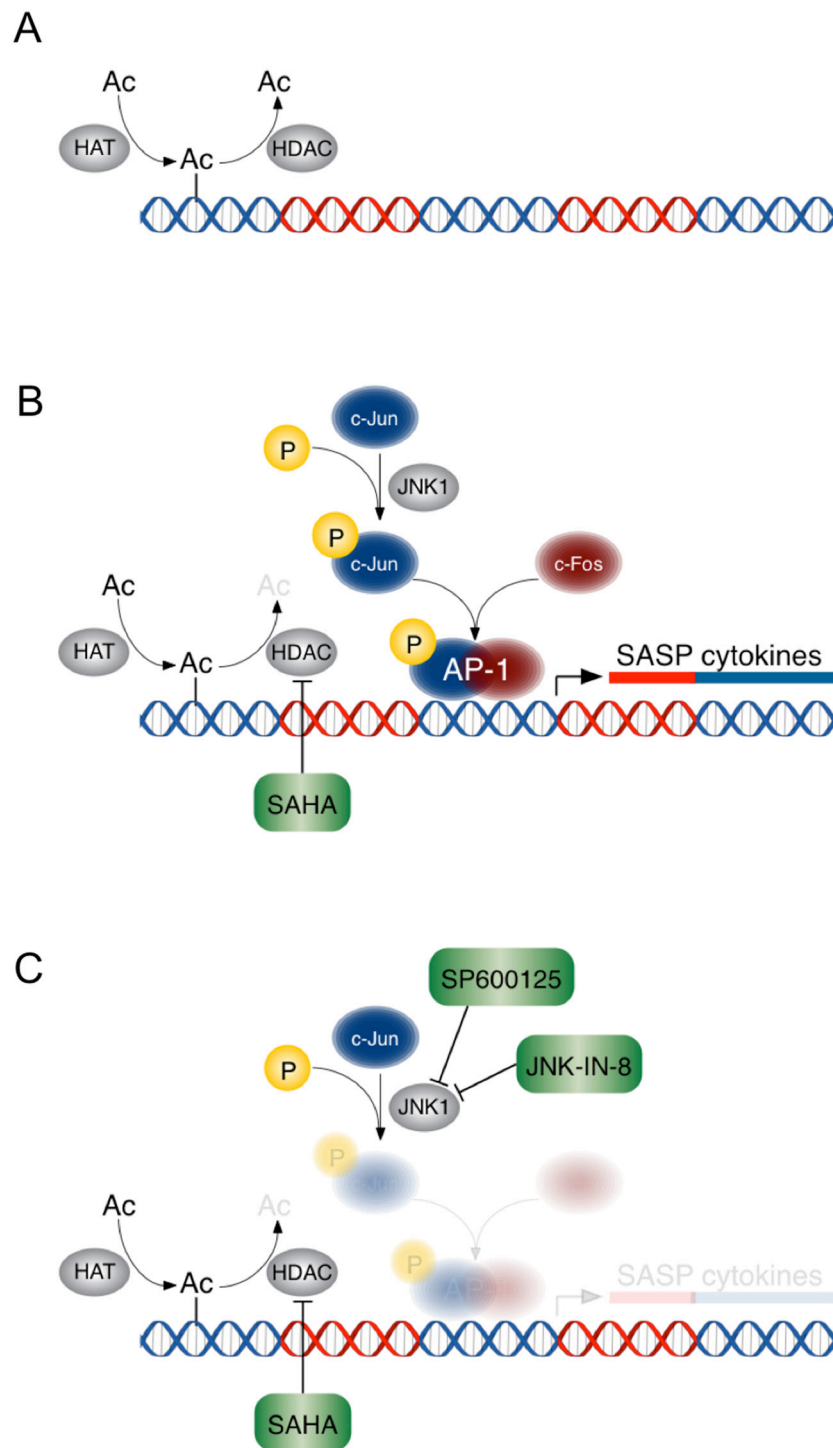


Figure 6: A schematic of the effects of HDACi's +/- JNK inhibition in PDAC CAFs. HDAC inhibition results in hyperacetylation of histones and allows permissive gene expression of AP-1 target genes. **A.** HATs and HDACs regulate DNA acetylation. **B.** HDAC inhibition creates a permissive transcriptional landscape for SASP pro-inflammatory gene expression, which is mediated by transcription factor AP-1. **C.** JNK1 inhibition prevents pro-inflammatory gene expression despite HDAC inhibition.

potentially be a rational addition to HDACi treatment in PDAC. This work provides important insights into a strategy to improve treatment outcomes in stroma-rich solid organ malignancies with HDAC inhibitors.

MATERIALS AND METHODS

Cell lines

PANC-1 and MIA PaCa-2 pancreatic cancer cells were purchased from the American Type Culture Collection (ATCC). Short tandem repeat analysis was performed by ATCC. PANC-1 GFP pancreatic cancer cells were a gift from Dr. Huan Meng (UCLA, Los Angeles, CA) and MIA PaCa-2 GFP pancreatic cancer cells were a gift from Dr. David Dawson (UCLA, Los Angeles, CA). hTERT immortalized pancreatic cancer associated fibroblasts were gifts from the laboratory of Dr. Rosa Hwang (MD Anderson, Houston, TX). KPC-luc cells were a gift from Dr. Caius Radu (UCLA, Los Angeles, CA). Kras^{LSL.G12D/+}; p53^{R172H/+}; PdxCre^{tg/+} (KPC) cells were a gift from Dr. Guido Eibl (UCLA, Los Angeles, CA). All cell lines were maintained in DMEM/F12 containing 10% FBS, 1% GlutaMax, and 1% penicillin/streptomycin and were routinely tested for Mycoplasma.

Human primary pancreatic fibroblast isolation

Fresh pancreatic tissue was obtained from the Translational Pathology Core Laboratory from patients undergoing pancreatic resection at the Ronald Reagan UCLA Medical Center. All samples were obtained from consenting patients in accordance with policies and practices of the Institutional Review Board and the Office of the Human Research Protection Program at UCLA. Tumor samples underwent mechanical and enzymatic digestion and then digested tissues were cultured in DMEM/F12 (Corning) containing 10% fetal bovine serum (FBS) (Omega Scientific), 1% GlutaMax, and 1% penicillin/streptomycin (both Life Technologies). Newly established primary fibroblast cultures were treated with 25 µg/ml Plasmocin (Invivogen) for two weeks and then maintained at 2.5 µg/ml. Because these are a finite resource, it was not feasible to use the same line in all cases. Primary pancreatic fibroblasts were used between passage numbers 3 to 6. Primary fibroblasts were characterized by wild-type KRAS status and α -smooth muscle actin positivity as previously described [47].

Chemical inhibitors

The following chemical inhibitors were dissolved in DMSO (Sigma) (unless stated otherwise) as stock solutions and then subsequently diluted in culture media: Vorinostat/SAHA (Biotang), LBH-589 (Biotang), MS-275 (Biotang), SP600125 (LC Lab), JNK-IN-8

(Selleck Chem), JNK-IN-9 (Selleck Chem), and SR3576 (ApexBio).

Conditioned media generation

Primary pancreatic fibroblasts were grown to 90% confluence. Fibroblasts were treated with HDACi, HDACi combined with a chemical inhibitor, or DMSO control for 24 hours. Plates were then washed and cells were incubated with phenol red free, serum-free DMEM/F12 containing 1% GlutaMax and 1% penicillin/streptomycin. After 24 hours incubation, conditioned media was harvested, 0.22 µm filtered, and then stored in aliquots at -20°C.

In vitro cell viability

Cells were seeded in 96-well plates with doses of HDACi's diluted in media in a total volume of 100 µl per well. At indicated time points, 10 µl of 5 mg/ml MTT (Life Technologies) in PBS was added to each well and incubated for 4 hours at 37°C and 5% CO₂. Cells were then lysed with 100 µl 10% SDS (Sigma), 0.01M HCl (Sigma) and incubated overnight at 37°C and 5% CO₂. Absorbance readings were measured at 560 nm wavelength using a Modulus II Microplate Multimode Reader (Turner BioSystems). Alternatively, cell viability was measured using the CellTiter-Glo Luminescent Cell Viability Assay (Promega) according to the manufacturer's recommendations. Experiments were performed in triplicate wells and repeated at least twice.

In vitro tumor cell-fibroblast 3D co-culture

40 µl of Matrigel (Corning) was plated in black walled, flat bottom 96 well plates (Corning) and allowed to polymerize for 30 minutes at 37°C and 5% CO₂. 5 x 10³ PANC-1 GFP cells and 1 x 10⁴ primary pancreatic fibroblasts were seeded together with HDACi's with or without other chemical inhibitors in 100 µl DMEM/F12 containing 10% FBS, 1% GlutaMax, and 1% penicillin/streptomycin and 2% Matrigel. In experiments with PANC-1 cells were cultured alone, 5 x 10³ PANC-1 GFP were used. Fluorescence readings were measured using a blue optical kit (Ex 490 nm/Em 510-570 nm) on a Modulus II Microplate Multimode Reader. Images were taken using a CX41 Inverted Microscope with a DP26 Digital Camera (Olympus). Experiments were performed in triplicate wells and repeated at least twice.

In vitro tumor cell proliferation

PANC-1 GFP and MIA PaCa-2 GFP cells were plated in black walled, flat bottom 96 well plates at 3 x 10³ cells per well in fibroblast conditioned media containing 1% FBS. Fluorescence readings were

measured daily using a blue optical kit (Ex 490 nm/Em 510-570 nm) on a Modulus II Microplate Multimode Reader. Experiments were performed in triplicate wells and repeated at least twice.

***In vivo* xenograft tumor growth**

All mouse experiments were conducted in accordance with protocols approved by the Institutional Animal Care and Use Committee at the University of California, Los Angeles. 5×10^5 PDAC tumor cells were resuspended in 1:1 diluted Matrigel in DMEM/F12 1% GlutaMax and 1% penicillin/streptomycin and then injected in 100 μ l volumes in the subcutaneous flank five 6-8 week old sex-matched NOD/SCID/IL2 γ mice. Alternatively, in our orthotopic KrasLSL.G12D/+; p53R172H/+; PdxCretg/+ (KPC) PDAC mouse model, KPC tumor cells in 40 μ l suspensions were implanted in the pancreata of 6-8 week old sex-matched C57BL/6 mice. For conditioned media supplementation experiments, beginning at day 7, tumors were supplemented thrice weekly with 50 μ l peri-tumoral injections of conditioned media. For SAHA treatment experiments, mice were treated 5 times weekly with 40 mg/kg SAHA in PBS by oral gavage. Subcutaneous tumors were measured weekly by dial caliper or *in vivo* bioluminescence and mice were sacrificed when tumor diameters approached 15 mm.

***In vitro* tumor cell-fibroblast invasion assay**

MIA PaCa-2 and primary pancreatic fibroblasts were each seeded at 5×10^4 cells per Matrigel-coated 8 μ m pore PET membrane 24-well cell culture inserts (Corning) in conditioned media supplemented with 0.1% FBS. 10% FBS conditioned media was placed in the bottom wells and cells were allowed to invade for 24 hours. After completion of invasion, cells on the lower surface of the membrane were fixed and stained with hematoxylin. Images were taken using a CX41 Inverted Microscope with a DP26 Digital Camera. Invaded tumor cells were quantified in five 20X microscope visual fields based on distinct differences in morphology between primary pancreatic fibroblasts and MIA PaCa-2 cells. Experiments were performed in triplicate wells and repeated at least twice.

Chemiluminescent cytokine array

Primary pancreatic fibroblasts were treated for 24 hours with HDACi or with DMSO alone and media was subsequently harvested. Media was assayed using the Human Cytokine Array Panel A (R&D Systems), according to manufacturer's instructions. Membranes were developed using standard chemiluminescent techniques and images were captured using the Odyssey Fc Imaging

System (LI-COR). Pixel density was calculated using Image Studio software (LI-COR).

Gene expression by quantitative real-time PCR

Total RNA was isolated from cells using the Quick-RNA MiniPrep kit (Zymo). Reverse transcription was performed using the High Capacity cDNA Reverse Transcription kit (Life Technologies). Quantitative PCR was performed using EvaGreen qPCR Master Mix (Lambda Biotech). RNA expression values were normalized to 36B4 control gene and then calculated as relative expression to control. Primers used are reported in Supplementary Table 1.

ChIP-Seq

Chromatin Immunoprecipitation (ChIP) was performed as described previously [48] using α HDAC2 antibody from Bethyl laboratories (Cat#A300-705/Lot#1). Sequencing libraries were constructed from 0.2ng of input and immunoprecipitated DNA using the KAPA DNA Library Preparation Kit (KapaBiosystems). Sequencing on an Illumina HiSeq 2000 sequencer yielded between 13 and 30 million reads. Analysis of sequence data was as previously described [49], except that the genome was tiled into 50 bp windows.

Western blots

Western blots were performed using the LI-COR Odyssey infrared blot system, according to manufacturer's instructions. Blots were performed on acid-extracted histones or whole cell lysates. The following antibodies were used: p-c-JUN (Ser63) Lot #6 (Cell Signaling), GAPDH Lot #PJ20538 (ThermoFisher), acetyl-Histone-H3 Lot #2370129 (Millipore), acetyl-Histone-H4 Lot #2302181 (Millipore), H3K18ac Lot #30508004 (Active Motif), H3K27ac Lot #GR167613-1 (Abcam). LI-COR IRDye 700 and 800 nm channel secondary antibodies were used. Western blots were imaged using the Odyssey Fc Imaging System in 700 and 800 nm channels and densitometry analysis was performed using the LI-COR Image Studio software.

Statistical analyses

Data are presented as the mean \pm standard error of the mean unless otherwise stated. Statistical significance was calculated via the Student's t-test. Values of ≤ 0.05 were considered statistically significant. Statistical analyses were performed using Prism 6 Software (GraphPad). Transcription binding significance of the ENCODE ChIP-Seq Significance Tool results are calculated by a hypergeometric test with a multiple hypothesis correction [31].

Abbreviations

HDAC - histone deacetylase, HDACi – histone deacetylase inhibitor, PDAC – pancreatic ductal adenocarcinoma, CAF – cancer-associated fibroblast, HAT – histone acetyltransferase, SAHA - suberanilohydroxamic acid, ChIP - chromatin immunoprecipitation, KPC - KrasLSL.G12D/+; p53R172H/+; PdxCretg/+, TC – tumor cell, CM – conditioned media, JNK - janus N-terminal kinase.

CONFLICTS OF INTEREST

We do not have any financial or other interests that pose a conflict of interest to the work presented in this submission.

GRANT SUPPORT

Dr. Nguyen was supported by a T32 Training Award from the National Institute of Health (NIH T32DK07180-39) and the Gerald S. Levey Surgical Research Award.

REFERENCES

1. Burris H, Storniolo AM. Assessing clinical benefit in the treatment of pancreas cancer: gemcitabine compared to 5-fluorouracil. *European journal of cancer*. 1997; 33:S18-22.
2. Moore MJ, Goldstein D, Hamm J, Figer A, Hecht JR, Gallinger S, Au HJ, Murawa P, Walde D, Wolff RA, Campos D, Lim R, Ding K, et al. Erlotinib plus gemcitabine compared with gemcitabine alone in patients with advanced pancreatic cancer: a phase III trial of the National Cancer Institute of Canada Clinical Trials Group. *Journal of clinical oncology*. 2007; 25:1960-1966.
3. Von Hoff DD, Ervin T, Arena FP, Chiorean EG, Infante J, Moore M, Seay T, Tjulandin SA, Ma WW, Saleh MN, Harris M, Reni M, Dowden S, et al. Increased survival in pancreatic cancer with nab-paclitaxel plus gemcitabine. *The New England journal of medicine*. 2013; 369:1691-1703.
4. Rahib L, Smith BD, Aizenberg R, Rosenzweig AB, Fleshman JM, Matrisian LM. Projecting cancer incidence and deaths to 2030: the unexpected burden of thyroid, liver, and pancreas cancers in the United States. *Cancer research*. 2014; 74:2913-2921.
5. Gui CY, Ngo L, Xu WS, Richon VM, Marks PA. Histone deacetylase (HDAC) inhibitor activation of p21WAF1 involves changes in promoter-associated proteins, including HDAC1. *Proceedings of the National Academy of Sciences of the United States of America*. 2004; 101:1241-1246.
6. Ju R, Muller MT. Histone deacetylase inhibitors activate p21(WAF1) expression via ATM. *Cancer research*. 2003; 63:2891-2897.
7. Kelly WK, O'Connor OA, Krug LM, Chiao JH, Heaney M, Curley T, MacGregore-Cortelli B, Tong W, Secrist JP, Schwartz L, Richardson S, Chu E, Olgac S, et al. Phase I study of an oral histone deacetylase inhibitor, suberoylanilide hydroxamic acid, in patients with advanced cancer. *Journal of clinical oncology*. 2005; 23:3923-3931.
8. Piekarz RL, Frye R, Turner M, Wright JJ, Allen SL, Kirschbaum MH, Zain J, Prince HM, Leonard JP, Geskin LJ, Reeder C, Joske D, Figg WD, et al. Phase II multi-institutional trial of the histone deacetylase inhibitor romidepsin as monotherapy for patients with cutaneous T-cell lymphoma. *Journal of clinical oncology*. 2009; 27:5410-5417.
9. Piekarz RL, Frye R, Prince HM, Kirschbaum MH, Zain J, Allen SL, Jaffe ES, Ling A, Turner M, Peer CJ, Figg WD, Steinberg SM, Smith S, et al. Phase 2 trial of romidepsin in patients with peripheral T-cell lymphoma. *Blood*. 2011; 117:5827-5834.
10. Richardson PG, Hungria VT, Yoon SS, Beksac M, Dimopoulos MA, Elghandour A, Jedrzejczak WW, Guenther A, Nakorn TN, Siritanaratkul N, Schlossman RL, Hou J, Moreau P, et al. Panobinostat plus bortezomib and dexamethasone in previously treated multiple myeloma: outcomes by prior treatment. *Blood*. 2016; 127:713-721.
11. Qiu T, Zhou L, Zhu W, Wang T, Wang J, Shu Y, Liu P. Effects of treatment with histone deacetylase inhibitors in solid tumors: a review based on 30 clinical trials. *Future oncology*. 2013; 9:255-269.
12. Koutsounas I, Giaginis C, Theocharis S. Histone deacetylase inhibitors and pancreatic cancer: are there any promising clinical trials? *World journal of gastroenterology*. 2013; 19:1173-1181.
13. Dovzhanskiy DI, Arnold SM, Hackert T, Oehme I, Witt O, Felix K, Giese N, Werner J. Experimental *in vivo* and *in vitro* treatment with a new histone deacetylase inhibitor belinostat inhibits the growth of pancreatic cancer. *BMC cancer*. 2012; 12:226.
14. Olive KP, Jacobetz MA, Davidson CJ, Gopinathan A, McIntyre D, Honess D, Madhu B, Goldgraben MA, Caldwell ME, Allard D, Frese KK, Denicola G, Feig C, et al. Inhibition of Hedgehog signaling enhances delivery of chemotherapy in a mouse model of pancreatic cancer. *Science*. 2009; 324:1457-1461.
15. Hwang RF, Moore T, Arumugam T, Ramachandran V, Amos KD, Rivera A, Ji B, Evans DB, Logsdon CD. Cancer-associated stromal fibroblasts promote pancreatic tumor progression. *Cancer research*. 2008; 68:918-926.
16. Toste PA, Nguyen AH, Kadera BE, Duong M, Wu N, Gawlas I, Tran LM, Bikhchandani M, Li L, Patel SG, Dawson DW, Donahue TR. Chemotherapy-induced Inflammatory Gene Signature and Pro-tumorigenic

- Phenotype in Pancreatic CAFs via Stress-associated MAPK. *Molecular cancer research*. 2016.
17. Brentnall TA, Lai LA, Coleman J, Bronner MP, Pan S, Chen R. Arousal of cancer-associated stroma: overexpression of palladin activates fibroblasts to promote tumor invasion. *PLoS one*. 2012; 7:e30219.
 18. Kalluri R, Zeisberg M. Fibroblasts in cancer. *Nature reviews Cancer*. 2006; 6:392-401.
 19. Erez N, Truitt M, Olson P, Arron ST, Hanahan D. Cancer-Associated Fibroblasts Are Activated in Incipient Neoplasia to Orchestrate Tumor-Promoting Inflammation in an NF-kappaB-Dependent Manner. *Cancer cell*. 2010; 17:135-147.
 20. Coussens LM, Werb Z. Inflammation and cancer. *Nature*. 2002; 420:860-867.
 21. Coppe JP, Desprez PY, Krtolica A, Campisi J. The senescence-associated secretory phenotype: the dark side of tumor suppression. *Annual review of pathology*. 2010; 5:99-118.
 22. Glaser KB, Staver MJ, Waring JF, Stender J, Ulrich RG, Davidsen SK. Gene expression profiling of multiple histone deacetylase (HDAC) inhibitors: defining a common gene set produced by HDAC inhibition in T24 and MDA carcinoma cell lines. *Molecular cancer therapeutics*. 2003; 2:151-163.
 23. Jung KH, Noh JH, Kim JK, Eun JW, Bae HJ, Xie HJ, Chang YG, Kim MG, Park H, Lee JY, Nam SW. HDAC2 overexpression confers oncogenic potential to human lung cancer cells by deregulating expression of apoptosis and cell cycle proteins. *Journal of cellular biochemistry*. 2012; 113:2167-2177.
 24. Huang BH, Laban M, Leung CH, Lee L, Lee CK, Salto-Tellez M, Raju GC, Hooi SC. Inhibition of histone deacetylase 2 increases apoptosis and p21Cip1/WAF1 expression, independent of histone deacetylase 1. *Cell death and differentiation*. 2005; 12:395-404.
 25. Fritsche P, Seidler B, Schuler S, Schnieke A, Gottlicher M, Schmid RM, Saur D, Schneider G. HDAC2 mediates therapeutic resistance of pancreatic cancer cells via the BH3-only protein NOXA. *Gut*. 2009; 58:1399-1409.
 26. Schuler S, Fritsche P, Diersch S, Arlt A, Schmid RM, Saur D, Schneider G. HDAC2 attenuates TRAIL-induced apoptosis of pancreatic cancer cells. *Molecular cancer*. 2010; 9:80.
 27. McLean CY, Bristor D, Hiller M, Clarke SL, Schaar BT, Lowe CB, Wenger AM, Bejerano G. GREAT improves functional interpretation of cis-regulatory regions. *Nature biotechnology*. 2010; 28:495-501.
 28. Richon VM, Sandhoff TW, Rifkind RA, Marks PA. Histone deacetylase inhibitor selectively induces p21WAF1 expression and gene-associated histone acetylation. *Proceedings of the National Academy of Sciences of the United States of America*. 2000; 97:10014-10019.
 29. Heinz S, Benner C, Spann N, Bertolino E, Lin YC, Laslo P, Cheng JX, Murre C, Singh H, Glass CK. Simple combinations of lineage-determining transcription factors prime cis-regulatory elements required for macrophage and B cell identities. *Molecular cell*. 2010; 38:576-589.
 30. Liu T, Ortiz JA, Taing L, Meyer CA, Lee B, Zhang Y, Shin H, Wong SS, Ma J, Lei Y, Pape UJ, Poidinger M, Chen Y, et al. Cistrome: an integrative platform for transcriptional regulation studies. *Genome biology*. 2011; 12:R83.
 31. Auerbach RK, Chen B, Butte AJ. Relating genes to function: identifying enriched transcription factors using the ENCODE ChIP-Seq significance tool. *Bioinformatics*. 2013; 29:1922-1924.
 32. Manning AM, Davis RJ. Targeting JNK for therapeutic benefit: from junk to gold? *Nature reviews Drug discovery*. 2003; 2:554-565.
 33. Biton S, Ashkenazi A. NEMO and RIP1 control cell fate in response to extensive DNA damage via TNF-alpha feedforward signaling. *Cell*. 2011; 145:92-103.
 34. Takahashi R, Hirata Y, Sakitani K, Nakata W, Kinoshita H, Hayakawa Y, Nakagawa H, Sakamoto K, Hikiba Y, Ijichi H, Moses HL, Maeda S, Koike K. Therapeutic effect of c-Jun N-terminal kinase inhibition on pancreatic cancer. *Cancer science*. 2013; 104:337-344.
 35. Zhong Y, Naito Y, Cope L, Naranjo-Suarez S, Saunders T, Hong SM, Goggins MG, Herman JM, Wolfgang CL, Iacobuzio-Donahue CA. Functional p38 MAPK identified by biomarker profiling of pancreatic cancer restrains growth through JNK inhibition and correlates with improved survival. *Clin Cancer Res*. 2014; 20:6200-6211.
 36. Davis RJ. Signal transduction by the JNK group of MAP kinases. *Cell*. 2000; 103:239-252.
 37. Bennett BL, Sasaki DT, Murray BW, O'Leary EC, Sakata ST, Xu W, Leisten JC, Motiwala A, Pierce S, Satoh Y, Bhagwat SS, Manning AM, Anderson DW. SP600125, an anthrapyrazolone inhibitor of Jun N-terminal kinase. *Proceedings of the National Academy of Sciences of the United States of America*. 2001; 98:13681-13686.
 38. Brinkmann H, Dahler AL, Popa C, Serewko MM, Parsons PG, Gabrielli BG, Burgess AJ, Saunders NA. Histone hyperacetylation induced by histone deacetylase inhibitors is not sufficient to cause growth inhibition in human dermal fibroblasts. *The Journal of biological chemistry*. 2001; 276:22491-22499.
 39. Pazolli E, Alspach E, Milczarek A, Prior J, Piwnicka-Worms D, Stewart SA. Chromatin remodeling underlies the senescence-associated secretory phenotype of tumor stromal fibroblasts that supports cancer progression. *Cancer research*. 2012; 72:2251-2261.
 40. Halili MA, Andrews MR, Labzin LI, Schroder K, Matthias G, Cao C, Lovelace E, Reid RC, Le GT, Hume DA, Irvine KM, Matthias P, Fairlie DP, et al. Differential effects of

- selective HDAC inhibitors on macrophage inflammatory responses to the Toll-like receptor 4 agonist LPS. *Journal of leukocyte biology*. 2010; 87:1103-1114.
41. Aung HT, Schroder K, Himes SR, Brion K, van Zuylen W, Trieu A, Suzuki H, Hayashizaki Y, Hume DA, Sweet MJ, Ravasi T. LPS regulates proinflammatory gene expression in macrophages by altering histone deacetylase expression. *FASEB journal*. 2006; 20:1315-1327.
 42. Knoop RF, Sparn M, Waldmann J, Plassmeier L, Bartsch DK, Lauth M, Hudemann C, Fendrich V. Chronic pancreatitis and systemic inflammatory response syndrome prevent impact of chemotherapy with gemcitabine in a genetically engineered mouse model of pancreatic cancer. *Neoplasia*. 2014; 16:463-470.
 43. Kelly MG, Alvero AB, Chen R, Silasi DA, Abrahams VM, Chan S, Visintin I, Rutherford T, Mor G. TLR-4 signaling promotes tumor growth and paclitaxel chemoresistance in ovarian cancer. *Cancer research*. 2006; 66:3859-3868.
 44. Sledzinski M, Borkowska A, Sielicka-Dudzin A, Halon M, Wozniak M, Spodnik JH, Antosiewicz AH, Antosiewicz J. Cerulein-induced acute pancreatitis is associated with c-Jun NH(2)-terminal kinase 1-dependent ferritin degradation and iron-dependent free radicals formation. *Pancreas*. 2013; 42:1070-1077.
 45. Liu M, Shi L, Chen M, Chen S, Zou X. Effects of c-Jun N-terminal kinase signaling pathway on severe acute pancreatitis-associated lung injury. *Pancreas*. 2012; 41:358-366.
 46. Wang J, Kuitatse I, Lee AV, Pan J, Giuliano A, Cui X. Sustained c-Jun-NH2-kinase activity promotes epithelial-mesenchymal transition, invasion, and survival of breast cancer cells by regulating extracellular signal-regulated kinase activation. *Molecular cancer research*. 2010; 8:266-277.
 47. Kadera BE, Li L, Toste PA, Wu N, Adams C, Dawson DW, Donahue TR. MicroRNA-21 in pancreatic ductal adenocarcinoma tumor-associated fibroblasts promotes metastasis. *PloS one*. 2013; 8:e71978.
 48. Stock JK, Giadrossi S, Casanova M, Brookes E, Vidal M, Koseki H, Brockdorff N, Fisher AG, Pombo A. Ring1-mediated ubiquitination of H2A restrains poised RNA polymerase II at bivalent genes in mouse ES cells. *Nature cell biology*. 2007; 9:1428-1435.
 49. Ferrari R, Su T, Li B, Bonora G, Oberai A, Chan Y, Sasidharan R, Berk AJ, Pellegrini M, Kurdistani SK. Reorganization of the host epigenome by a viral oncogene. *Genome research*. 2012; 22:1212-1221.

Chapter V

The Histone H3-H4 Tetramer is a Copper Reductase Enzyme

This chapter is unpublished and under peer review. It describes a novel function of the eukaryotic chromatin. Briefly, this work reveals that the eukaryotic nucleosome functions as a major nucleocytoplasmic oxidoreductase catalyzing the reduction of Cu^{2+} to Cu^{1+} , that provides cuprous ions for cellular and mitochondrial biology. The significance of this function for understanding eukaryotic evolution and cellular physiology is discussed. I co-authored this manuscript and contributed to the conception and design of the experiments and the preparation of the initial draft for submission. I conducted growth assays, inductively-coupled plasma mass spectrometry and mRNA-sequencing independently as well as in collaboration with Oscar Campos and Dr. Maria Vogelauer.

The Histone H3-H4 Tetramer is a Copper Reductase Enzyme

Narsis Attar^{1,2,3}, Oscar A. Campos^{1,2,3}, Maria Vogelauer^{1,2}, Yong Xue², Stefan Schmollinger⁴, Linda Yen⁵, Shannon Zikovich², Jade Dardine², Michael F. Carey^{2,3}, Sabeeha S. Merchant⁴, and Siavash K. Kurdistani^{2,3,6,7,*}

¹Co-first author, listed alphabetically

²Department of Biological Chemistry, David Geffen School of Medicine, University of California Los Angeles, Los Angeles, CA 90095, USA

³Molecular Biology Institute, University of California Los Angeles, Los Angeles, CA 90095, USA

⁴Institute for Genomics and Proteomics, Department of Chemistry and Biochemistry, University of California Los Angeles, Los Angeles, CA 90095, USA

⁵Department of Molecular, Cell, and Developmental Biology, University of California Los Angeles, Los Angeles, CA 90095, USA

⁶Eli and Edythe Broad Center of Regenerative Medicine and Stem Cell Research, David Geffen School of Medicine, University of California Los Angeles, Los Angeles, CA 90095, USA

⁷Lead Contact

*Correspondence: Siavash Kurdistani
310.794.5194
skurdistani@mednet.ucla.edu

Summary

The histone H3-H4 tetramer forms a putative metal-binding region of unknown function at the interface of the two apposing H3 proteins. We report that mutating a highly conserved histidine residue in the H3-H3' interface impairs cellular activities such as mitochondrial respiration and Sod1 function that depend on availability of reduced copper. The impairment of copper homeostasis is not due to altered gene expression or total copper abundance but is consistent with decreased levels of cuprous ions, suggesting histones may directly affect copper's oxidation state. Indeed, the intact nucleosome or the H3-H4 tetramer assembled *in vitro* from recombinant histones exhibits robust copper reductase activity, catalyzing Cu^{2+} to Cu^{1+} . We propose that eukaryotic chromatin is an oxidoreductase enzyme, which provides bioavailable copper for cellular and mitochondrial chemistry. As the emergence of eukaryotes coincided with increased oxidation and therefore decreased bioavailability of essential metals, the enzymatic function of histones could have facilitated eukaryogenesis.

Keywords

Histones, Nucleosome, Copper, Mitochondria, Respiration, SOD1, Oxidoreductase, Enzyme, Eukaryogenesis

Introduction

Eukaryotic genomes are nearly universally packaged in the form of chromatin, a nucleoprotein structure that protects the DNA and facilitates its compaction while also regulating DNA-based processes. The core histones H2A, H2B, H3 and H4—the main protein components of chromatin—evolved from histone-like proteins in archaea such as the HMf-1 and HMf-2 proteins of *Methanothermobacter thermautotrophicus* (Sandman et al., 1990). The H3-H4 tetramer bound to DNA, also known as a tetrasome, docks with two H2A-H2B dimers to form the canonical 146 bp eukaryotic nucleosome. However, archaeal histones wrap only ~60 bp of DNA to form structures similar to the H3-H4 tetrasome (Pereira et al., 1997). Unlike eukaryotic chromatin, archaeal histones lack extended N-terminal tails and are typically devoid of post-translational modifications (Forbes et al., 2004); and thus could not contribute to gene regulation in the way that eukaryotes employ histone modifications. Although the archaeal nucleosomes could provide basic forms of regulation by restricting access of proteins to the DNA (Soares et al., 1998), the rationale for evolution of histones in certain archaeal species, with typically small genomes ranging from 1-3 Mbp, has been unclear. Histones may have evolved in archaea to maintain the integrity of the genome in the harsh environments in which they thrive (Li et al., 1998). But not all archaea that live in extreme environments contain nucleosome-like structures (Brochier-Armanet et al., 2011). Here we reveal a novel function of histones in copper homeostasis that could provide a basis for their evolutionary origin.

Eukaryotes derive from the merger of a histone-containing archaeon with a bacterium approximately 1.5-2 billion years ago (Koonin, 2015). A histone-based genome packaging system is thought to have been fortuitously present in the archaeal ancestor (Sandman and Reeve, 1998). In such a scenario, histones could only later have facilitated evolution of eukaryotic complexity in part by compacting an expanding genome size (Sandman and Reeve, 1998). It is possible,

however, that the presence of histones in our archaeal ancestor was not incidental, rather essential for the emergence of early eukaryotes. So far, no viable scenario has been put forth to account for a possible contribution of histones to the development of features in early eukaryotes including the endosymbiotic evolution of mitochondria.

The emergence of eukaryotes coincided roughly with accumulation of molecular oxygen (Anbar, 2008), which resulted in significant alterations in the abundance and oxidation states of transition metals. For instance, before the great oxidation event, iron (Fe) and copper (Cu) were present in their reduced and therefore bioavailable forms, with iron being much more prevalent than copper (Saito et al., 2003). The earliest eukaryotes appeared when iron and copper were being increasingly oxidized and less bioavailable yet more toxic in presence of oxygen (Saito et al., 2003). This presented a formidable challenge for acquisition or intracellular usage of these essential metals by organisms that had evolved in a previously reducing environment. Whether early eukaryotes relied partly on histones to meet this challenge has not been considered.

Copper is an essential element in eukaryotes and serves as a co-factor for numerous enzymes that function in key intra- and extra-cellular processes (Nevitt et al., 2012). Copper is required for mitochondrial respiration as a co-factor for cytochrome c oxidase, the last enzyme (complex IV) in the mitochondrial electron transport chain (ETC), and for Cu, Zn-superoxide dismutase 1 (Sod1), which catalyzes disproportionation of superoxide radicals to prevent oxidative damage (Nevitt et al., 2012). Copper is imported through dedicated transporters and distributed to its cellular destinations via protein chaperones. In *Saccharomyces cerevisiae*, *CTR1* (Copper Transport) encodes the main high-affinity copper transporter that mediate nearly all copper import in limited copper conditions (Dancis et al., 1994). Protein chaperones such as Ccs1 (Copper Chaperone for SOD1) and Cox17 (Cytochrome c Oxidase) are then required for delivery of copper to Sod1 or cytochrome c oxidase, respectively (Culotta et al., 1997; Glerum et al., 1996).

As a co-factor, copper is utilized in its cupric (Cu^{2+}) or cuprous (Cu^{1+}) forms but only the latter is bound by chaperones, indicating that its oxidation state is important for proper intracellular trafficking (Pufahl et al., 1997). The intracellular ratio of oxidized vs. reduced copper and how this proportion is established are unknown, although evidence suggests that most, but not all, exists as Cu^{1+} bound to protein and non-protein ligands (Rae et al., 1999; Yang et al., 2005). Copper may also serve as a signaling element to regulate specific biochemical pathways such as lipolysis (Krishnamoorthy et al., 2016). The utility of copper, however, must be balanced against its toxicity caused by displacement of other metals in proteins or its redox activity (Macomber and Imlay, 2009). Organisms have therefore evolved homeostatic mechanisms for careful provision of copper to meet specific demands. Several diseases in humans, including cancer, neurodegenerative diseases like Amyotrophic Lateral Sclerosis (ALS), Alzheimer's, Wilson, Menkes and others, involve disruption of copper homeostasis (Bleackley and Macgillivray, 2011; Turski and Thiele, 2009).

As early as 1986, it was noted that the eukaryotic nucleosome has a potential metal-binding structure comprising amino acid residues in the C-terminal regions of the two apposing histone H3 proteins. These residues include cysteine 110 (H3C110) and histidine 113 (H3H113) (Saavedra, 1986) (Figure 1A). Several hydrogen bonds involving residues in and around the H3-H3' interface, including those that constitute the putative metal-binding pocket, form a 4-helix bundle that is also required for the assembly of the H3-H4 tetramer (Luger et al., 1997). Interestingly, the evolutionary conservation of individual or pairs of amino acids in this region is not readily explained by their contributions to the thermodynamic stability of the nucleosome alone. This observation suggests that "a novel function" provided by the H3-H3' interface is driving the surprising conservation (Ramachandran et al., 2011). The functional significance of a potential metal-binding structure in H3, and whether a metal-binding function could explain the evolutionary conservation, have not been investigated.

Two lines of reasoning prompted us to investigate whether histone H3 may play a role in cellular copper homeostasis. First, the coincidence of eukaryotic emergence and geochemical alterations of transition metals raised the possibility of histones having a role in enhancing intracellular metal homeostasis. Second, a functioning complex IV in the ETC of the bacterial ancestor of mitochondria at the time of its merger may have depended on the intracellular provision of cuprous ions by the archaeal host—as it occurs today in eukaryotes. Here, we provide biochemical, molecular and genetic data that histone H3 is required for efficient use of copper inside cells. We show that recombinant *Xenopus laevis* H3-H4 tetramer, identical at the protein level to the human H3.2-H4 tetramer, catalyzes reduction of cupric to cuprous ions. Our data suggest that the catalytic site likely forms at the interface of the two histone H3 proteins as mutations in this region alter or abolish the *in vitro* enzymatic activity of the H3-H4 tetramer; and cause defects in mitochondrial respiration and Sod1 activity—both of which depend on the availability of intracellular cuprous ions—in *S. cerevisiae*. Alterations in gene expression, nucleosome assembly, or total cellular copper quota could not explain these phenotypes. Rather, the phenotypes are consistent with decreased levels of Cu^{+1} and can be recapitulated by decreasing intracellular reducing power. Our data reveal that in eukaryotes, DNA wraps around an enzyme that catalyzes reduction of copper for utilization by various cellular and mitochondrial proteins. This notion has a profound impact in the fields of evolution and the molecular biology of the eukaryotic cell and may be relevant to a range of human pathologies in which alterations of copper-dependent processes are implicated (Bleackley and Macgillivray, 2011; Turski and Thiele, 2009)

Results

Mutation of histone H3 histidine 113 to asparagine (H3H113N) has little effect on global chromatin accessibility or gene expression. Since the H3-H3' interface contributes to the stability of the H3-H4 tetramer, we first determined the impact of mutating H3H113, a highly-conserved residue that is also found in archaeal histones (Figure 1B), on chromatin accessibility and global gene expression. Mutation of this residue to alanine (*H3H113A*) or glutamine (*H3H113Q*) is lethal in yeast for unknown reasons (Huang et al., 2009). However, we noticed that in the COSMIC (Forbes et al., 2015) and ExAC (Lek et al., 2016) databases H3H113 is mutated to asparagine (*H3H113N*) in certain individuals, suggesting that this mutation may be tolerated in yeast as well. We used CRISPR/Cas9 to generate a *S. cerevisiae* strain with H113N mutations in both copies of histone H3 genes (*HHT1* and *HHT2*) in their chromosomal loci under their natural promoters without any other genetic disruption. This strain, $H3^{H113N}$, is viable but exhibits a 2-fold increase in growth doubling time compared to wildtype (WT) in rich media (Figures 1C and 1D). Asf1 (Anti-Silencing Function) is a histone chaperone that binds to the H3-H4 dimer through interactions with H3H113 and other residues, and is required for nucleosome assembly and disassembly (Adkins et al., 2004; Agez et al., 2007). We also assessed the phenotype of an *ASF1* deletion strain (*asf1Δ*) to exclude potential disruption to Asf1-H3/H4 dimer interactions and consequent alteration in chromatin structure as underlying factors for the phenotypes of the $H3^{H113N}$ strain. Deletion of *ASF1* also increases doubling time (Figures 1C and 1D) but to a lesser extent than did the *H3H113N* mutation. Analysis of global chromatin structure by Micrococcal nuclease (MNase) revealed essentially similar digestion patterns for WT, $H3^{H113N}$ and *asf1Δ* strains, with the latter two being slightly less accessible at lower MNase concentrations (Figure 1E). Global gene expression patterns were also essentially similar between WT and $H3^{H113N}$ grown in yeast extract peptone dextrose (YPD) or in synthetic complete (SC) medium with no gene having a statistically significant difference at a Benjamini-Hochberg false discovery rate (FDR) of <10% (Figure 1F). Thus, the *H3H113N* mutation has no significant effect on steady state genome-wide gene expression or chromatin accessibility.

The H3H113 residue is required for efficient use of copper for mitochondrial respiration.

We reasoned that if the putative metal binding pocket at the H3-H3' interface is disrupted, the cell might suffer from aberrant metal ion homeostasis. To assess copper homeostasis, we examined the ability of $H3^{H113N}$ to grow on non-fermentable carbon sources and therefore rely on mitochondrial respiration for growth. Although $H3^{H113N}$ displays a growth defect compared to WT in YPD, it did not display a further defect under respiratory conditions where non-fermentable ethanol and glycerol were substituted for dextrose (YPEG) (Figure 2A). In rich media conditions, abundant copper uptake might mask an underlying deficiency in copper utilization. We therefore deleted *CTR1*, the main copper importer in yeast, to disrupt copper availability in the context of WT and $H3H113N$ histones. The *ctr1* Δ mutant is unable to grow on YPEG with baseline copper abundance (Figure 2A, lower panel). Addition of 20 μ M copper rescues the *ctr1* Δ respiratory growth defect but only in the background of WT histone H3 (Figure 2A). Four times more exogenous copper is required to rescue the growth defect of *ctr1* Δ in the presence of $H3H113N$ mutant histones (Figure 2A). The rescue of *asf1* Δ *ctr1* Δ is achieved at similar levels of copper as *ctr1* Δ alone, and therefore does not phenocopy $H3^{H113N}$ *ctr1* Δ (Figure 2A). Combination of $H3H113N$ mutation with deletion of *MAC1* ($H3^{H113N}$ *mac1* Δ), a copper-sensing transcription factor required for expression of copper transport genes including *CTR1* (Graden and Winge, 1997), also increased the amount of exogenous copper required for growth on YPEG compared to *mac1* Δ alone (Figure 2B). Addition of iron, zinc, or manganese did not rescue the growth defects of strains with *ctr1* Δ , confirming the specific copper deficiency (Figure S1A). The copper-mediated rescue of growth in these mutants is indeed dependent on mitochondrial respiration because deletion of *Cox17*, which functions downstream of *Ctr1* for eventual delivery of copper to cytochrome *c* oxidase (Glerum et al., 1996), prevented rescue even if >100-fold more exogenous copper is provided compared to *ctr1* Δ strains (Figure S1B). In liquid YPEG culture, $H3^{H113N}$ *ctr1* Δ also lagged behind *ctr1* Δ in growth and oxygen (O_2) consumption at several medium copper

concentrations (Figure 2C). These results indicate that the histone *H3H113N* mutation decreases copper availability for respiratory growth when copper is limiting.

The *H3^{H113N}ctr1Δ* respiratory deficiency is not due to copper buffering capacity, intracellular levels of copper or gene expression differences. Cup1 is a metallothionein that binds and stores copper and thereby buffers the cytotoxic effects of high concentrations of copper (Jensen et al., 1996). *CUP1* is amplified to varying copy numbers in laboratory strains of yeast (Karin et al., 1984). To exclude the possibility that an increased Cup1 capacity for sequestering copper accounts for the inability of *H3^{H113N}ctr1Δ* to efficiently utilize copper for mitochondrial respiration, we introduced a stop codon (F8stop) in every copy of the *CUP1* gene using CRISPR/Cas9. As expected, loss of Cup1 sensitizes cells to high concentrations of copper (data not shown) but the *cup1^{F8stop}H3^{H113N}ctr1Δ* strain still required more copper than did *cup1^{F8stop}ctr1Δ* to grow on YPEG (Figure S1C).

There were also no differences in intracellular levels of copper or iron between WT and *H3^{H113N}* strains in the same stage of growth in YPD (Figure S1D) or YPEG (Figure 2D) as measured by inductively coupled plasma mass spectrometry (ICP-MS). Deletion of *CTR1* lowered the intracellular levels of copper as expected and to the same extent with or without the *H3H113N* mutation (Figures 2D and S1D). Addition of excess copper to YPEG increased intracellular levels of copper to similar levels in both *ctr1Δ* and *H3^{H113N}ctr1Δ* strains (Figure 2D), suggesting that the *H3^{H113N}ctr1Δ* growth defect relative to *ctr1Δ* is not due to an inability to uptake copper through alternative routes (Hassett et al., 2000).

Analysis of gene expression by mRNA-seq revealed very similar global gene expression profiles in WT and *H3^{H113N}* strains in YPEG (Figure S1E). The *H3^{H113N}* strain showed comparable changes in gene expression as those observed in WT, including upregulation of genes that

function in the ETC and the TCA cycle as well as copper or iron regulons, all of which are required for growth on YPEG (Figures 2E and S1F). Thus, the *H3H113N* mutation does not interfere with either sensing of non-fermentable carbon sources or establishing the proper gene expression profiles for their metabolism. The inability of *H3^{H113N}ctr1Δ* to utilize copper for growth in non-fermentative media is therefore not caused by altered expression of genes important for respiratory growth.

Diminishing reducing power phenocopies the respiratory deficiency of *H3^{H113N}ctr1Δ* mutant. The increased copper requirement of *H3^{H113N}ctr1Δ* for growth on YPEG despite having normal levels of intracellular copper raised the possibility that the levels of cuprous ions, which are required for cuproprotein assembly, is lower in *H3^{H113N}ctr1Δ* compared to *ctr1Δ*. However, there are difficulties associated with reliable determination of the oxidation state of intracellular copper in yeast. To indirectly address the effects of the copper oxidation state, we reasoned that decreasing cellular reducing power might phenocopy the respiratory deficiency of *H3^{H113N}ctr1Δ* by limiting the availability of electrons for reduction of Cu^{2+} . To disrupt the cellular redox state, we placed the expression of gamma glutamylcysteine synthetase (*GSH1*), which catalyzes the first step in glutathione (GSH) biosynthesis, under the control of the *GAL1* promoter in *ctr1Δ* to generate the *ctr1Δp^(GAL1)-GSH1* strain. In media without galactose, the expression of *GSH1* is turned off, leading to decreased glutathione levels, a major source of reducing equivalents in the cell. The *ctr1Δp^(GAL1)-GSH1* strain required more copper to grow on YPEG than *ctr1Δ* alone (Figure 2F), reminiscent of the *H3^{H113N}ctr1Δ* phenotype (Figure 2A). These data are consistent with decreased availability of cuprous ions, as opposed to decreased abundance of elemental copper, as an explanation for the respiratory deficiency of the *H3^{H113N}ctr1Δ* or *ctr1Δp^(GAL1)-GSH1* strains compared to *ctr1Δ* alone.

The H3H113 residue is required for copper-dependent rescue of the *ccs1*Δ lysine auxotrophy. We next investigated whether the role of H3H113 residue in copper homeostasis is unique to mitochondrial function or if it more generally regulates copper utilization. Deletion of *SOD1* or *CCS1*, the chaperone that delivers copper to Sod1, results in lysine auxotrophy in yeast when grown in the presence of oxygen (Lin and Culotta, 1996) (Figure 3A). We found that while the lysine auxotrophy of *ccs1*Δ is rescued by addition of excess exogenous copper, the *H3^{H113N}ccs1*Δ growth in media lacking lysine is not fully restored even in presence of 500 μM copper (Figure 3A). Deletion of *ASF1* has no effect on copper-dependent rescue of *ccs1*Δ (Figure 3A). In stark contrast to the *H3H113N* mutation, reducing intracellular levels of copper by deletion of *CTR1* does not increase the requirement of *ccs1*Δ for exogenous copper (Figure 3B). This indicates that Ccs1-mediated function(s) are more dependent on an intact H3-H3' interface than on total levels of intracellular copper.

Addition of manganese, zinc or iron did not rescue *ccs1*Δ growth, confirming the specific disruption of copper utilization (Figure S2A). The rescue of *ccs1*Δ strains by exogenous copper is likely through recovering Sod1 function since similar amounts of copper did not rescue the lysine auxotrophy of *sod1*Δ with or without *H3H113N* mutation (Figure S2B). Similar to growth on agar plates, *H3^{H113N}ccs1*Δ showed little improvement in growth in lysine-deficient liquid media supplemented with copper compared to *ccs1*Δ alone (Figure 3C). The increased copper requirement of *H3^{H113N}ccs1*Δ is not due to increased Cup1 buffering capacity (Figure S2C), or decreases in intracellular copper or iron levels (Figures 3D and S2D). There were also no significant differences in global gene expression profiles of *ccs1*Δ versus *H3^{H113N}ccs1*Δ (Figure S2E) including genes involved in lysine biosynthesis, which were induced in lysine deficient media, copper homeostasis or antioxidant defense (Figures 3E and S2F). Hypoxic conditions restored the growth of *ccs1*Δ and *sod1*Δ in media lacking lysine, confirming the oxygen-dependent toxicity underlying the lysine auxotrophy. The *H3H113N* mutation had no effect on the rescue of

ccs1 Δ and *sod1* Δ lysine auxotrophy by hypoxic conditions (Figure S2G), indicating that the *H3H113N* defect in lysine synthesis only manifests when copper-dependent Sod1 function is required. Altogether, these results indicate that extra copper can rescue *ccs1* Δ lysine auxotrophy, and that introduction of *H3H113N* mutation decreases the ability of *ccs1* Δ strain to use copper efficiently.

Consistent with these results, we also found that the growth of *H3^{H113N}ctr1* Δ (*note that this is the copper transporter deletion*) on lysine deficient media is adversely affected relative to *ctr1* Δ (Figures 3F). Addition of the copper chelator bathocuproinedisulfonic acid (BCS) to decrease copper uptake exacerbates the growth defect of *H3^{H113N}ctr1* Δ on lysine-deficient media much more so than that of *ctr1* Δ (Figures 3F and S2H). This indicates that in limiting copper conditions the *H3H113N* mutation makes cells auxotrophic for lysine. Since as little as 2% of functional Sod1 is required for adequate lysine biosynthesis (Corson et al., 1998), our findings altogether suggest *H3H113N* significantly impairs efficiency of copper utilization.

Recombinant histone H3-H4 tetramer is a copper reductase. Since the phenotypes of strains with the *H3H113N* mutation were consistent with loss of cuprous ion species, we hypothesized that histone H3 may be an enzyme that maintains cuprous ions for the cell by catalyzing reduction of Cu^{2+} to Cu^{1+} . To test this hypothesis, we assembled and purified a histone H3-H4 tetramer from recombinant *Xenopus laevis* histones H3 and H4, which are identical to human H3.2 and H4 histones respectively, using the standard salt dialysis method (Figure S3A) (Luger et al., 1999). We also empirically developed a colorimetric assay to measure production of Cu^{1+} based on the ability of the copper chelator neocuproine (NC) to chelate Cu^{1+} quantitatively. The NC $\cdot\text{Cu}^{1+}$ complex has a yellow color that absorbs light at 448 nm (Figure S3B). We used tris(2-carboxyethyl)phosphine (TCEP) as a source of electrons (i.e., reducing co-factor) because of its low rate of spontaneous copper reduction. Most other commonly used reducing agents directly

reduced copper in our assay condition (see Methods). We performed the assay by first mixing the tetramer, TCEP and NC in 100 mM NaCl and then adding cupric chloride (CuCl_2) in a sodium tricine buffer (pH=7.4). Upon addition of copper, we observed a time-dependent increase in production of Cu^{1+} as indicated by increasing yellow coloration of the reaction mixture containing the H3-H4 tetramer but not the control buffer (Figure 4A). Figure 4B shows a typical reaction profile for a tetramer versus buffer alone. The earliest measurement is 2.2 seconds (s) after addition of copper by which time a significant fraction of copper is already reduced (Figure 4B). The reaction plateaus at later time points due to near full consumption of TCEP. Because ~75% of total Cu^{1+} produced occurs within the first 30 seconds (Figure 4B inset), we focused on this time interval in subsequent experiments. The line and shadings represent the mean and standard deviations of at least three assays, respectively. We detected no significant activity in the absence of TCEP and increasing activity with increasing amounts of TCEP, indicating that TCEP provides the electrons for reduction of copper (Figure 4C). The enzymatic activity is specific to the tetramer since unassembled histone H3 and another histone protein such as the *S. cerevisiae* H2A do not show activity (Figure 4D). The tetramer's enzymatic activity is heat labile as boiling the tetramer prior to the assay abolished copper reduction (Figure 4E). We did not detect iron reductase activity when using FeCl_3 and a ferrous ion chelator, indicating that the reaction is specific to copper under these conditions (data not shown).

Within the H3-H4 tetramer, the H3C110 residues may become oxidized to form a disulfide bond (Camerini-Otero and Felsenfeld, 1977), in the process causing the reduction of a second reaction component. This raises the possibility that any set of cysteine residues capable of forming a disulfide bond *per se* may facilitate reduction of copper in our reaction conditions. To address this possibility, we performed the copper reduction assay with RNase A, which contains four disulfide bonds (Klink et al., 2000), and detected no significant copper reductase activity above background (Figure 4F).

Finally, we assembled mononucleosomes using recombinant core histones and the 601 nucleosome positioning DNA fragment using standard salt gradient dialysis (Figure S4) (Peterson, 2008). The nucleosome was also able to reduce copper using TCEP as the reducing co-factor (Figure 4G). Altogether, these data indicate that the *Xenopus* histone H3-H4 tetramer, in free or nucleosome form, is an enzyme with copper reductase activity.

The kinetic properties of H3-H4 tetramer is comparable to eukaryotic enzymes. To establish the kinetic properties of the H3-H4 tetramer enzymatic activity, we determined the initial velocity of copper reduction at increasing concentrations of substrate (Figure 5A). Plotting the initial velocities against substrate concentrations, and curve-fitting with a Henri-Michaelis-Menten enzyme kinetics model, yielded a K_m value of $28.8 \pm 4.0 \mu\text{M}$ (Figures 5B and C), which is approximately 4.5-fold lower than median K_m values for typical eukaryotic enzymes (Bar-Even et al., 2011). Other kinetic parameters are indicated in Figure 5C. These data indicate that in our assay condition the kinetic parameters of the H3-H4 tetramer enzymatic activity are well within the range of eukaryotic enzymes (Bar-Even et al., 2011).

Mutations of the residues in the H3-H3' interface affect enzyme activity. We next examined the effects of the histone *H3C110A* or *H3H113N* mutation on the *in vitro* enzyme activity of the *Xenopus* H3-H4 tetramer. The tetramer with histone *H3C110A* mutation assembled similarly to WT tetramer as indicated by their elution profiles from the size exclusion column (Figure 6A). However, the *H3C110A* tetramer had little to no copper reductase activity in our assay condition compared to buffer alone (Figure 6B), indicating that either H3C110 is required for or the presence of alanine disrupts the *in vitro* enzymatic activity of the tetramer. The histone *H3H113N* mutation also did not affect the assembly of the tetramer (Figure 6C) but, surprisingly, had little effect on the *in vitro* copper reductase activity when TCEP was used as the reducing co-factor (Figure 6D).

Enzyme kinetic analysis indicated that the *H3H113N* tetramer has a comparable K_m value ($29.4 \pm 6.3 \mu\text{M}$) to the WT tetramer but a somewhat higher V_{max} (Figure S5). *In vitro* assembled mononucleosomes with H3H113N histones also showed comparable copper reduction activity to WT mononucleosomes (Figure 6E). These data indicate that the H3H113 residue is not required for the enzymatic activity of the *Xenopus* tetramer in our assay conditions. However, when we used dihydrolipoic acid (LA) instead of TCEP as the reducing co-factor, the H113N tetramer generated somewhat less Cu^{1+} than the WT tetramer (p value=0.023 for area under the curve, t -test) (Figure 6F). Although the H113N mutation does not abolish the enzymatic activity of the *Xenopus* tetramer, it may impair it under certain conditions. Altogether, the data indicate that H3C110 and H3H113 are important for the enzyme activity of the tetramer, and since substitutions with certain other amino acid residues did not significantly affect tetramer assembly *in vitro*, their roles in copper reduction and tetramer formation can be separated.

Decreasing histone H3 dosage impairs copper homeostasis. The finding that the H3-H4 tetramer within the nucleosome generates cuprous ions for the cell suggests that decreasing the dosage of histones, and therefore nucleosomes, should decrease availability of cuprous ions and thus the efficiency of copper usage. To test this, we deleted one of the two copies of the histone H3 and H4 genes (*hht1-hhf1* Δ) in WT cells or in the context of *ctr1* Δ . We confirmed that the *hht1-hhf1* Δ strain had less H3 and H4 proteins (Figure 7A) and increased susceptibility to chromatin digestion by MNase (Figure 7B), consistent with decreased average number of nucleosomes. Deletion of *HHT1* and *HHF1* did not significantly affect growth in YPD (Figure 7C). However, as predicted, combination of *hht1-hhf1* Δ with *ctr1* Δ required more copper for growth on YPEG (Figure 7D) and was more sensitive to depletion of copper in lysine deficient medium (Figure 7E) compared to *ctr1* Δ alone. These data indicate that the number of nucleosomes, and therefore the number of copper reductase enzymes, affects intracellular copper dependent activities.

Discussion

Histones were considered initially to only be structural constituents of the eukaryotic genome, serving to package the large amount of DNA into the confines of the nucleus. Pioneering experiments in 1980s and 90s revealed that histones also function in regulating gene expression and essentially all other processes that contend with DNA through controlling access to certain DNA sequences and post-translational modifications (Felsenfeld, 1992; Grunstein, 1997; Jenuwein and Allis, 2001). We now show that the histone H3-H4 tetramer within a nucleosome also catalyzes reduction of Cu^{2+} to Cu^{1+} , revealing eukaryotic chromatin as a major nucleocytoplasmic oxidoreductase enzyme that provides cuprous ions for cellular and mitochondrial biology. Considering the importance of copper to processes as diverse as tissue integrity, methylation cycle, iron homeostasis and melanin and neurotransmitter syntheses in mammals (Finney et al., 2014; Nevitt et al., 2012; Winston and Jaiser, 2008), the enzymatic activity of histones could have wide-ranging effects at molecular, cellular, and tissue levels with consequences for organismal physiology and disease.

The enzymatic activity of the H3-H4 tetramer suggests the protein complex has novel features that were previously unsuspected but must be fully discerned through future studies. An important feature is the location of the enzyme active site, which we favor to be at the interface of the two H3 proteins for multiple reasons. First, the H3-H3' interface appears to be under an evolutionary selective pressure beyond what is required for thermodynamic stability of the tetramer (Ramachandran et al., 2011). The active site of an enzyme could constitute such a selective pressure. Second, the positioning of H3H113 at the end of an α -helix is an arrangement that is found commonly in oxidoreductases such as thioredoxin (Hol, 1985). H3H113 may stabilize the α 2 helix dipole near the H3-H3' interface, which may enhance transfer of electrons (Galoppini and Fox, 1996). Third, the potential requirement of H3C110 for the enzymatic activity of histones

that contain it, further supports the location of the active site at the H3-H3' interface. The C110 residues from apposing H3s within the tetramer are 6.2Å apart in the crystal structure but *in vivo* can form a disulfide bond, the length of which is 2.05Å (Camerini-Otero and Felsenfeld, 1977). Interestingly, the mechanism of electron transfer by other oxidoreductase enzymes such as thioredoxin reductase (Holmgren, 1995) or ribonucleotide reductase (Kolberg et al., 2004) involves cyclical oxidation and reduction of internal cysteine residues through disulfide bond formation. Yet in others, such as Sod1, the redox reactive cysteine residues play a regulatory role rather than participating in the electron transfer reaction (Furukawa et al., 2004). Whether oxidation/reduction of H3C110 residues is directly involved in electron transfer by the H3-H4 tetramer remains to be determined. Nonetheless, formation of a disulfide linkage requires significant distortion of the conformation of the tetramer, suggesting that the structure of the tetramer, especially around the 4-helix bundle within the nucleosome, is dynamic (Luger et al., 1997). H3C110 is in the center of the bundle and buried within the nucleosome structure but is also readily accessible as evidenced by reactivity with small molecular probes (Garcia-Gimenez et al., 2013). Thus, the potential flexibility of the 4-helix bundle, redox reactivity of H3C110 and accessibility of the H3-H3' interface residues could be important for enzyme activity and/or its regulation. Fourth, the H3-H3' interface coordinates metals such as zinc, cobalt, nickel (Adamczyk et al., 2007) or mercury (Lambert et al., 1999) when incubated with these metals *in vitro*. Finally, the H3-H3' interface assembles *in vivo* only when histones are incorporated into a nucleosome. Therefore, the commencement of enzymatic activity would be inextricably coupled to the protection of DNA as it wraps on the outer surface of the nucleosome. Such a coupling may be a beneficial adaptation in species that require reduced intracellular copper as a failsafe mechanism to avoid potentially damaging effects of copper.

As a reductase, the H3-H4 tetramer must extract electrons from reducing co-factors, pass them through the protein and transfer them to copper ions at the active site. How the tetramer

achieves this is unclear but the position at which electrons are extracted from the reducing co-factor need not be near the active site. In addition, since cellular copper ions are mostly bound by proteins (Rae et al., 1999), copper is likely delivered to and taken away from histones through as-yet-to-be-identified chaperones. Furthermore, we have assessed the activity of one canonical histone H3, namely, H3.2. However, H3 has several variants with intriguing sequence differences that are functionally characterized based on their modes of incorporation into chromatin, position along the chromosome or expression pattern. Whether the histone H3 variants and/or their location across the genome (e.g., euchromatin vs. heterochromatin) influence the kinetic properties or co-factor requirements of the H3-H4 tetramer enzyme activity remain interesting but open questions. Like copper, iron is also used commonly in its ferrous form and is an important bioessential element for numerous processes including epigenetic gene regulation (Cartularo and Costa, 2014). Although we did not detect any iron reductase activity in our assay condition with H3.2-containing tetramers, we cannot rule out the ability of the tetramer with canonical or variant histones to catalyze reduction of iron in certain conditions or organisms.

We obtained our *in vivo* data from analysis of the budding yeast, arguing that the yeast nucleosome has copper reductase activity. Despite repeated efforts, we were unable to satisfactorily assemble the recombinant yeast H3-H4 tetramer, consistent with the known difficulties of using yeast histones for *in vitro* studies (Leung et al., 2016). Interestingly, *S. cerevisiae* and a number of other fungi possess histone H3 proteins that lack the cysteine residue equivalent to H3C110 in other eukaryotes (data not shown). Other than missing H3C110, the C-terminal region of yeast H3 has additional sequence differences compared to the *Xenopus*/human H3 (Figure 1B, gray highlights). It is conceivable that enzymatic activity of tetramers with histone H3 proteins that lack C110 require additional co-factors or proceed through a different reaction mechanism. This may also explain why the *H3H113N* mutation has a minor effect on the *Xenopus* tetramer *in vitro* activity, but displays robust genetic phenotypes in *S. cerevisiae* that are

consistent with having a significant impact on the yeast tetramer copper reductase activity *in vivo*. We cannot determine whether the yeast H3H113N is a hypomorphic or a null allele vis-à-vis the enzymatic activity of the yeast tetramer. But it is possible that a complete loss of enzyme function would be lethal in yeast as several residues in the vicinity of H3-H3' interface are required for viability (Dai et al., 2008).

Eukaryotes evolved from an archaeon that had a small genome but possessed ancestral histones without extended, positively-charged N-terminal tails or abundant posttranslational modifications. This evolutionary timeline questions whether the present-day functions of histones were also the reasons histones evolved to bind DNA and form chromatin in the first place; and if these functions contributed to the successful emergence of early eukaryotes. The appearance of the first eukaryotes coincided with extensive alterations in redox geochemistry with increasing levels of oxygen and decreased bioavailable forms of transition metals such as iron and copper (Anbar, 2008). This geochemical change presented a daunting challenge to cells for acquisition and intracellular maintenance of bioessential metals, which became rare and toxic in aerobic conditions. The oxidoreductase function of the H3-H4 tetramer, the ancient structural form of histones, could now provide a reasonable explanation for why the archaeal ancestor of the eukaryotes possessed histone tetramers. This enzymatic activity together with an associated intracellular transit capability for Cu^{1+} could have facilitated provision of cuprous ions to the nascent mitochondria to maintain a functioning ETC, intimately linking histones to the successful evolution of our common eukaryotic ancestor.

Author contributions

Conceptualization, N.A., O.A.C., M.V., Y.X., and S.K.K.; Methodology, N.A., O.A.C., M.V., Y.X., M.F.C., S.S.M., and S.K.K.; Investigation, N.A., O.A.C., M.V., Y.X., S.S., L.Y., J.D., S.Z. and S.K.K.; Formal Analysis, N.A., O.A.C., and M.V.; Writing – Original Draft, N.A., O.A.C., M.V., and S.K.K.; Writing – Review & Editing, N.A., O.A.C., M.V., Y.X., L.Y., S.S., M.F.C., S.S.M. and S.K.K.; Resources, N.A., O.A.C., M.V., L.Y., M.F.C., S.S.M., and S.K.K.; Visualization, N.A., O.A.C., and M.V.; Supervision, S.K.K.; Project Administration, S.K.K.; Funding Acquisition, M.F.C., S.S.M., and S.K.K.

Acknowledgements

We thank Heather Christofk for useful discussions, Mayo Thompson for proofreading, Marco Morselli for assistance in RNA-seq library preparation, and the UCLA Broad Stem Cell Center Sequencing Core. This work was supported by NIH grants CA178415 to S.K.K., GM074701 to M.F.C., GM42143 to S.S.M., and CA188592 to M.V. O.A.C was supported by the Whitcome and Dissertation Year Fellowships from UCLA. N.A. was supported by the NCI Ruth L. Kirschstein NRSA for Individual MD/PhD Degree Fellows F30 CA186619 and NIH training grant T32 GM8042. S.Z. was supported by the Amgen Scholars Program.

References

- Adamczyk, M., Poznanski, J., Kopera, E., and Bal, W. (2007). A zinc-finger like metal binding site in the nucleosome. *FEBS Lett.* *581*, 1409-1416.
- Adkins, M.W., Howar, S.R., and Tyler, J.K. (2004). Chromatin disassembly mediated by the histone chaperone Asf1 is essential for transcriptional activation of the yeast PH05 and PH08 genes. *Mol. Cell* *14*, 657-666.
- Agez, M., Chen, J., Guerois, R., van Heijenoort, C., Thuret, J.Y., Mann, C., and Ochsenbein, F. (2007). Structure of the histone chaperone ASF1 bound to the histone H3 C-terminal helix and functional insights. *Structure* *15*, 191-199.
- Anbar, A.D. (2008). Oceans. Elements and evolution. *Science* *322*, 1481-1483.

- Bar-Even, A., Noor, E., Savir, Y., Liebermeister, W., Davidi, D., Tawfik, D.S., and Milo, R. (2011). The moderately efficient enzyme: Evolutionary and physicochemical trends shaping enzyme parameters. *Biochemistry* *50*, 4402-4410.
- Bleackley, M.R., and Macgillivray, R.T. (2011). Transition metal homeostasis: from yeast to human disease. *Biometals* *24*, 785-809.
- Brachmann, C.B., Davies, A., Cost, G.J., Caputo, E., Li, J.C., Hieter, P., and Boeke, J.D. (1998). Designer deletion strains derived from *Saccharomyces cerevisiae* S288C: a useful set of strains and plasmids for PCR-mediated gene disruption and other applications. *Yeast* *14*, 115-132.
- Brochier-Armanet, C., Forterre, P., and Gribaldo, S. (2011). Phylogeny and evolution of the Archaea: one hundred genomes later. *Cur. Opin. Microbiol.* *14*, 274-281.
- Camerini-Otero, R.D., and Felsenfeld, G. (1977). Histone H3 disulfide dimers and nucleosome structure. *Proc. Natl. Acad. Sci. USA* *74*, 5519-5523.
- Cartularo, L., and Costa, M. (2014). Role of iron in epigenetic regulation of gene expression. In *Nutrition and Epigenetics*, E. Ho, and F. Domann, eds. (CRC Press), pp. 253-272.
- Corson, L.B., Strain, J.J., Culotta, V.C., and Cleveland, D.W. (1998). Chaperone-facilitated copper binding is a property common to several classes of familial amyotrophic lateral sclerosis-linked superoxide dismutase mutants. *Proc. Natl. Acad. Sci. USA* *95*, 6361-6366.
- Culotta, V.C., Klomp, L.W.J., Strain, J., Casareno, R.L.B., Krems, B., and Gitlin, J.D. (1997). The copper chaperone for superoxide dismutase. *J. Biol. Chem.* *272*, 23469-23472.
- Dai, J., Hyland, E.M., Yuan, D.S., Huang, H.L., Bader, J.S., and Boeke, J.D. (2008). Probing nucleosome function: A highly versatile library of synthetic histone H3 and H4 mutants. *Cell* *134*, 1066-1078.
- Dancis, A., Yuan, D.S., Haile, D., Askwith, C., Eide, D., Moehle, C., Kaplan, J., and Klausner, R.D. (1994). Molecular characterization of a copper transport protein in *Saccharomyces cerevisiae*: an unexpected role for copper in iron transport. *Cell* *76*, 393-402.
- Davey, C.A., Sargent, D.F., Luger, K., Maeder, A.W., and Richmond, T.J. (2002). Solvent mediated interactions in the structure of the nucleosome core particle at 1.9 angstrom resolution. *J. Mol. Biol.* *319*, 1097-1113.
- Dorigo, B., Schalch, T., Bystricky, K., and Richmond, T.J. (2003). Chromatin fiber folding: Requirement for the histone H4 N-terminal tail. *J. Mol. Biol.* *327*, 85-96.
- Felsenfeld, G. (1992). Chromatin as an essential part of the transcriptional mechanism. *Nature* *355*, 219-224.
- Finney, J., Moon, H.J., Ronnebaum, T., Lantz, M., and Mure, M. (2014). Human copper-dependent amine oxidases. *Arch. Biochem. Biophys.* *546*, 19-32.
- Forbes, A.J., Patrie, S.M., Taylor, G.K., Kim, Y.B., Jiang, L., and Kelleher, N.L. (2004). Targeted analysis and discovery of posttranslational modifications in proteins from methanogenic archaea by top-down MS. *Proc. Natl. Acad. Sci. USA* *101*, 2678-2683.
- Forbes, S.A., Beare, D., Gunasekaran, P., Leung, K., Bindal, N., Boutselakis, H., Ding, M.J., Bamford, S., Cole, C., Ward, S., et al. (2015). COSMIC: exploring the world's knowledge of somatic mutations in human cancer. *Nucleic Acids Res.* *43*, D805-D811.
- Furukawa, Y., Torres, A.S., and O'Halloran, T.V. (2004). Oxygen-induced maturation of SOD1: a key role for disulfide formation by the copper chaperone CCS. *EMBO J.* *23*, 2872-2881.

- Galoppini, E., and Fox, M.A. (1996). Effect of the electric field generated by the helix dipole on photoinduced intramolecular electron transfer in dichromophoric alpha-helical peptides. *J. Am. Chem. Soc.* *118*, 2299-2300.
- Garcia-Gimenez, J.L., Olaso, G., Hake, S.B., Bonisch, C., Wiedemann, S.M., Markovic, J., Dasi, F., Gimeno, A., Perez-Quilis, C., Palacios, O., et al. (2013). Histone h3 glutathionylation in proliferating mammalian cells destabilizes nucleosomal structure. *Antioxid. Redox Signal.* *19*, 1305-1320.
- Glerum, D.M., Shtanko, A., and Tzagoloff, A. (1996). Characterization of COX17, a yeast gene involved in copper metabolism and assembly of cytochrome oxidase. *J. Biol. Chem.* *271*, 14504-14509.
- Goldstein, A.L., and McCusker, J.H. (1999). Three new dominant drug resistance cassettes for gene disruption in *Saccharomyces cerevisiae*. *Yeast* *15*, 1541-1553.
- Graden, J.A., and Winge, D.R. (1997). Copper-mediated repression of the activation domain in the yeast Mac1p transcription factor. *Proc. Natl. Acad. Sci. USA* *94*, 5550-5555.
- Grunstein, M. (1997). Histone acetylation in chromatin structure and transcription. *Nature* *389*, 349-352.
- Hassett, R., Dix, D.R., Eide, D.J., and Kosman, D.J. (2000). The Fe(II) permease Fet4p functions as a low affinity copper transporter and supports normal copper trafficking in *Saccharomyces cerevisiae*. *Biochem. J.* *351*, 477-484.
- Hol, W.G. (1985). The role of the alpha-helix dipole in protein function and structure. *Prog. Biophys. Mol. Biol.* *45*, 149-195.
- Holmgren, A. (1995). Thioredoxin structure and mechanism: conformational changes on oxidation of the active site sulfhydryls to a disulfide. *Structure* *3*, 239-243.
- Huang, H.L., Maertens, A.M., Hyland, E.M., Dai, J.B.A., Norris, A., Boeke, J.D., and Bader, J.S. (2009). HistoneHits: A database for histone mutations and their phenotypes. *Genome Res.* *19*, 674-681.
- Jensen, L.T., Howard, W.R., Strain, J.J., Winge, D.R., and Culotta, V.C. (1996). Enhanced effectiveness of copper ion buffering by CUP1 metallothionein compared with CRS5 metallothionein in *Saccharomyces cerevisiae*. *J. Biol. Chem.* *271*, 18514-18519.
- Jenuwein, T., and Allis, C.D. (2001). Translating the histone code. *Science* *293*, 1074-1080.
- Karin, M., Najarian, R., Haslinger, A., Valenzuela, P., Welch, J., and Fogel, S. (1984). Primary structure and transcription of an amplified genetic locus: the Cup1 locus of yeast. *Proc. Natl. Acad. Sci. USA* *81*, 337-341.
- Kim, D., Perte, G., Trapnell, C., Pimentel, H., Kelley, R., and Salzberg, S.L. (2013). TopHat2: accurate alignment of transcriptomes in the presence of insertions, deletions and gene fusions. *Genome Biol.* *14*, R36.
- Klink, T.A., Woycechowsky, K.J., Taylor, K.M., and Raines, R.T. (2000). Contribution of disulfide bonds to the conformational stability and catalytic activity of ribonuclease A. *Eur. J. Biochem.* *267*, 566-572.
- Kolberg, M., Strand, K.R., Graff, P., and Andersson, K.K. (2004). Structure, function, and mechanism of ribonucleotide reductases. *Biochim. Biophys. Acta* *1699*, 1-34.

- Koonin, E.V. (2015). Origin of eukaryotes from within archaea, archaeal eukaryome and bursts of gene gain: eukaryogenesis just made easier? *Philos. Trans. R. Soc. Lond. B. Biol. Sci.* **370**, 20140333.
- Krishnamoorthy, L., Cotruvo, J.A., Jr., Chan, J., Kaluarachchi, H., Muchenditsi, A., Pendyala, V.S., Jia, S., Aron, A.T., Ackerman, C.M., Wal, M.N., et al. (2016). Copper regulates cyclic-AMP-dependent lipolysis. *Nat. Chem. Biol.* **12**, 586-592.
- Lambert, S.J., Nicholson, J.M., Chantalat, L., Reid, A.J., Donovan, M.J., and Baldwin, J.P. (1999). Purification of histone core octamers and 2.15 Å X-ray analysis of crystals in KCl/phosphate. *Acta Crystallogr. D. Biol. Crystallogr.* **55**, 1048-1051.
- Lek, M., Karczewski, K.J., Minikel, E.V., Samocha, K.E., Banks, E., Fennell, T., O'Donnell-Luria, A.H., Ware, J.S., Hill, A.J., Cummings, B.B., et al. (2016). Analysis of protein-coding genetic variation in 60,706 humans. *Nature* **536**, 285-291.
- Leung, A., Cheema, M., Gonzalez-Romero, R., Eirin-Lopez, J.M., Ausio, J., and Nelson, C.J. (2016). Unique yeast histone sequences influence octamer and nucleosome stability. *FEBS Lett.* **590**, 2629-2638.
- Li, W.T., Grayling, R.A., Sandman, K., Edmondson, S., Shriver, J.W., and Reeve, J.N. (1998). Thermodynamic stability of archaeal histones. *Biochemistry* **37**, 10563-10572.
- Lin, S.J., and Culotta, V.C. (1996). Suppression of oxidative damage by *Saccharomyces cerevisiae* ATX2, which encodes a manganese-trafficking protein that localizes to Golgi-like vesicles. *Mol. Cell. Biol.* **16**, 6303-6312.
- Longtine, M.S., McKenzie, A., Demarini, D.J., Shah, N.G., Wach, A., Brachat, A., Philippsen, P., and Pringle, J.R. (1998). Additional modules for versatile and economical PCR-based gene deletion and modification in *Saccharomyces cerevisiae*. *Yeast* **14**, 953-961.
- Luger, K., Mader, A.W., Richmond, R.K., Sargent, D.F., and Richmond, T.J. (1997). Crystal structure of the nucleosome core particle at 2.8 Å resolution. *Nature* **389**, 251-260.
- Luger, K., Rechsteiner, T.J., and Richmond, T.J. (1999). Preparation of nucleosome core particle from recombinant histones. *Methods Enzymol.* **304**, 3-19.
- Macomber, L., and Imlay, J.A. (2009). The iron-sulfur clusters of dehydratases are primary intracellular targets of copper toxicity. *Proc. Natl. Acad. Sci. USA* **106**, 8344-8349.
- Mann, R.K., and Grunstein, M. (1992). Histone H3 N-terminal mutations allow hyperactivation of the yeast Gal1 gene in vivo. *EMBO J.* **11**, 3297-3306.
- Nevitt, T., Ohrvik, H., and Thiele, D.J. (2012). Charting the travels of copper in eukaryotes from yeast to mammals. *Biochim. Biophys. Acta* **1823**, 1580-1593.
- Pereira, S.L., Grayling, R.A., Lurz, R., and Reeve, J.N. (1997). Archaeal nucleosomes. *Proc. Natl. Acad. Sci. USA* **94**, 12633-12637.
- Peterson, C.L. (2008). Salt gradient dialysis reconstitution of nucleosomes. *CSH Protoc.* **2008**, pdb.prot5113.
- Pufahl, R.A., Singer, C.P., Peariso, K.L., Lin, S.J., Schmidt, P.J., Fahrni, C.J., Culotta, V.C., PennerHahn, J.E., and O'Halloran, T.V. (1997). Metal ion chaperone function of the soluble Cu(I) receptor Atx1. *Science* **278**, 853-856.
- Rae, T.D., Schmidt, P.J., Pufahl, R.A., Culotta, V.C., and O'Halloran, T.V. (1999). Undetectable intracellular free copper: The requirement of a copper chaperone for superoxide dismutase. *Science* **284**, 805-808.

- Ramachandran, S., Vogel, L., Strahl, B.D., and Dokholyan, N.V. (2011). Thermodynamic stability of histone H3 is a necessary but not sufficient driving force for its evolutionary conservation. *PLoS Comput. Biol.* 7, e1001042.
- Rando, O.J. (2010). Genome-wide mapping of nucleosomes in yeast. *Methods Enzymol.* 470, 105-118.
- Ryan, O.W., Skerker, J.M., Maurer, M.J., Li, X., Tsai, J.C., Poddar, S., Lee, M.E., DeLoache, W., Dueber, J.E., Arkin, A.P., et al. (2014). Selection of chromosomal DNA libraries using a multiplex CRISPR system. *Elife* 3, e03703.
- Saavedra, R.A. (1986). Histones and metal-binding domains. *Science* 234, 1589-1589.
- Saito, M.A., Sigman, D.M., and Morel, F.M.M. (2003). The bioinorganic chemistry of the ancient ocean: the co-evolution of cyanobacterial metal requirements and biogeochemical cycles at the Archean-Proterozoic boundary? *Inorg. Chim. Acta* 356, 308-318.
- Sandman, K., Krzycki, J.A., Dobrinski, B., Lurz, R., and Reeve, J.N. (1990). HMf, a DNA-binding protein isolated from the hyperthermophilic archaeon *Methanothermus fervidus*, is most closely related to histones. *Proc. Natl. Acad. Sci. USA* 87, 5788-5791.
- Sandman, K., and Reeve, J.N. (1998). Origin of the eukaryotic nucleus. *Science* 280, 501-503.
- Schindelin, J., Arganda-Carreras, I., Frise, E., Kaynig, V., Longair, M., Pietzsch, T., Preibisch, S., Rueden, C., Saalfeld, S., Schmid, B., et al. (2012). Fiji: an open-source platform for biological-image analysis. *Nat. Methods* 9, 676-682.
- Schmitt, M.E., Brown, T.A., and Trumppower, B.L. (1990). A rapid and simple method for preparation of RNA from *Saccharomyces cerevisiae*. *Nucleic Acids Res.* 18, 3091-3092.
- Soares, D., Dahlke, I., Li, W.T., Sandman, K., Hethke, C., Thomm, M., and Reeve, J.N. (1998). Archaeal histone stability, DNA binding, and transcription inhibition above 90 degrees C. *Extremophiles* 2, 75-81.
- Storici, F., and Resnick, M.A. (2006). The delitto perfetto approach to in vivo site-directed mutagenesis and chromosome rearrangements with synthetic oligonucleotides in yeast. *Methods Enzymol.* 409, 329-345.
- Turski, M.L., and Thiele, D.J. (2009). New roles for copper metabolism in cell proliferation, signaling, and disease. *J. Biol. Chem.* 284, 717-721.
- Winston, G.P., and Jaiser, S.R. (2008). Copper deficiency myelopathy and subacute combined degeneration of the cord - why is the phenotype so similar? *Med. Hypotheses* 71, 229-236.
- Xu, G., Deng, N., Zhao, Z., Judeh, T., Flemington, E., and Zhu, D. (2011). SAMMate: a GUI tool for processing short read alignments in SAM/BAM format. *Source Code Biol. Med.* 6, 2.
- Yang, L.C., McRae, R., Henary, M.M., Patel, R., Lai, B., Vogt, S., and Fahrni, C.J. (2005). Imaging of the intracellular topography of copper with a fluorescent sensor and by synchrotron x-ray fluorescence microscopy. *Proc. Natl. Acad. Sci. USA* 102, 11179-11184.

Figure Legends

Figure 1. Mutation of histone H3 histidine 113 to asparagine has little effect on global chromatin accessibility or gene expression in *S. cerevisiae*. (A) Left: *X. laevis* nucleosome core particle structure (PDB:1KX5) (Davey et al., 2002) viewed down the DNA superhelix axis. Histone H3, H4, H2A and H2B are shown in metallic orange, blue, green and red, respectively. The square box delineates the H3-H3' interface. Right: Interface residues H113 and C110, one from each of the histone H3 molecules, are highlighted. (B) Alignment of the c-terminal region of *S. cerevisiae* histone H3, human non-centromeric histone H3 variants, and *M. fervidus* HMf-1 and HMf-2. (C) Spot test growth assay and (D) average doubling times from steady-state growth in liquid SC media. Bar graphs show mean \pm standard deviation (SD) from 3-6 replicate cultures. (E) Quantitative representation of the signal intensity profiles from chromatin digested with the indicated amounts of MNase. A.U.: arbitrary units. (F) Scatterplots of average global gene expression values from exponentially growing cells in SC and YPD, with Spearman's rank correlation coefficient (r_s) as indicated. * $P < 0.05$, ** $P \leq 0.01$, *** $P \leq 0.001$.

Figure 2. $H3^{H113N}$ diminishes copper utilization for respiratory growth. See also Figure S1. (A and B) Spot test assays in respiratory media (YPEG) with the indicated amounts of CuSO_4 . Baseline copper concentration in YP media is $\sim 1 \mu\text{M}$. (C) Growth and oxygen consumption assays in liquid YPEG with increasing amounts of CuSO_4 . Bar and line graphs show mean population doublings \pm SD and oxygen consumption rates after 24 hrs, respectively, from three independent experiments. P value representations are shown in black and red for growth and oxygen consumption measurements, respectively. (D) Intracellular copper and iron content of cells grown in the indicated media for 3-4 doublings for WT and $H3^{H113N}$ and 12 hrs for *ctr1* Δ strains. Bar graphs represent mean \pm SD from 3-6 replicate cultures. #The *ctr1* Δ strains, which do not grow in non-fermentable media, were incubated in YPEG and assessed for metal content for

reference. **(E)** Average mRNA expression levels for three gene sets (Table S3) comparing fermentative (YPD) and respiratory (YPEG) growth conditions from two independent experiments. **(F)** Same as (A). *P<0.05, **P≤0.01, ***P≤0.001.

Figure 3. *H3^{H113N}* is deficient in utilizing copper to rescue *ccs1Δ* lysine auxotrophy. See also Figure S2. **(A and B)** Spot test assays in the indicated media. Baseline copper concentration in SC media is ~ 0.16 μM **(C)** Growth assay in the indicated liquid media shown as average population doublings (± SD) after 24 hrs from three independent experiments. **(D)** Intracellular copper and iron content of cells grown in the indicated media for 3-4 doublings for WT and *H3^{H113N}* and 24 hrs for *ccs1Δ* strains. Bar graphs represent mean ± SD from 3-6 replicate cultures. #The *ccs1Δ* strains, which grow minimally in SC-lys media, were assessed for metal content for reference. **(E)** Average mRNA expression levels for three gene sets (Table S3) in cells growing exponentially in the indicated media after 24 hrs from two independent experiments. **(F)** Spot test assays on SC or SC-lys plates containing 1 mM and 10 μM copper chelator (BCS), respectively. *P<0.05, **P≤0.01, ***P≤0.001.

Figure 4. The human H3.2/H4 tetramer is a copper reductase. See also Figures S3 and S4 **(A)** Photographic representation of *in vitro* copper reductase assay at indicated times. Control buffer or H3.2/H4 tetramer were reacted with 100 μM TCEP and 1 mM CuCl₂. Note that reduction of copper occurs as soon as it is added to the tetramer reaction mix. **(B)** Reaction profiles of 1 μM H3.2/H4 tetramer or buffer reacted with 1 mM CuCl₂ and 20 μM TCEP. Lines and shading represent the mean ± SD of 3-5 assays. Inset shows data from the initial 30 seconds of the same reaction. **(C)** Same as in (B) but with the indicated TCEP concentrations. **(D)** Same as in (B) including the reaction profiles of 1 μM monomeric histone H3.2 and *S.cerevisiae* histone H2A. **(E)** Same as in (B) except that the H3.2/H4 tetramer and control buffer were incubated at 100°C for 15 minutes. **(F)** Same as in (B) but with FPLC purified RNase A and its control buffer. **(G)** Same

as in (B) but with 0.4 μM assembled nucleosome (instead of H3.2/H4 tetramer) and its control buffer.

Figure 5. Enzymatic parameters of the H3.2/H4 tetramer. (A) Reaction profiles of 1 μM the WT tetramer with 20 μM TCEP and the indicated CuCl_2 concentrations. Lines and shading represent the mean \pm SD of 4-5 assays. (B) Henri-Michaelis-Menten curve of initial velocities of reactions shown in A. (C) Calculated enzymatic parameters of the tetramer from the curve in (B).

Figure 6. Targeted mutations in the H3-H3' interface alter the enzyme activity of the tetramer but not its assembly. See also Figures S4 and S5. (A and C) FPLC elution profiles of the indicated H3.2/H4 tetramers and a protein standard. (B and D) Reaction profiles of 1 μM of the indicated H3.2/H4 tetramers or control buffers, combined with 1 mM CuCl_2 in the presence of 20 μM TCEP. Lines and shading represent the mean \pm SD of 3-5 assays. (F) Same as in (C) but with 0.4 μM assembled H3H113N nucleosome or its control buffer. (G) Same as in (C), but showing the reaction profile with 20 μM dihydrolipoic acid.

Figure 7. Deletion of one copy of histone H3 and H4 genes renders cells defective in utilizing copper for respiratory growth. (A) Western blots of histone H3 and H4 and coomassie-stained 15% SDS-PAGE (showing gel segment for 25-75 kDa) including the relative signal intensity for the indicated strains. (B) Quantitative representation of the signal intensity profiles from chromatin digested with the indicated amounts of MNase. A.U.: arbitrary units. (C) Average doubling times (\pm SD) from steady-state growth in liquid YPD from three replicate cultures. (D) Average population doublings (\pm SD) for growth in liquid YPEG with increasing amounts of CuSO_4 after 36 hrs from three replicate cultures. (E) Average population doublings (\pm SD) for growth in liquid SC-lys with increasing amounts of BCS after 24 hrs from three replicate cultures. * $P < 0.05$, ** $P \leq 0.01$, *** $P \leq 0.001$.

Figure 1

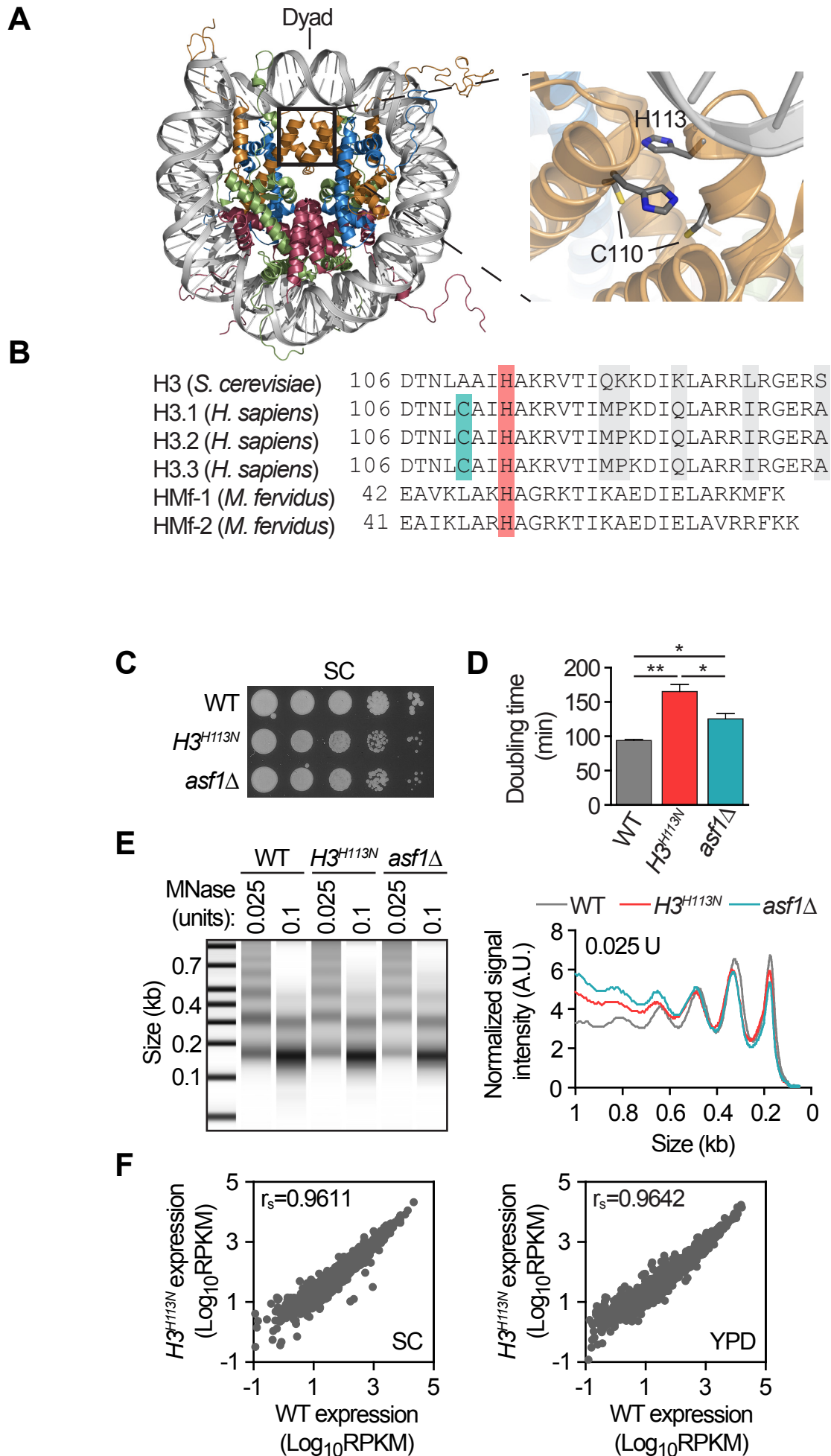


Figure 2

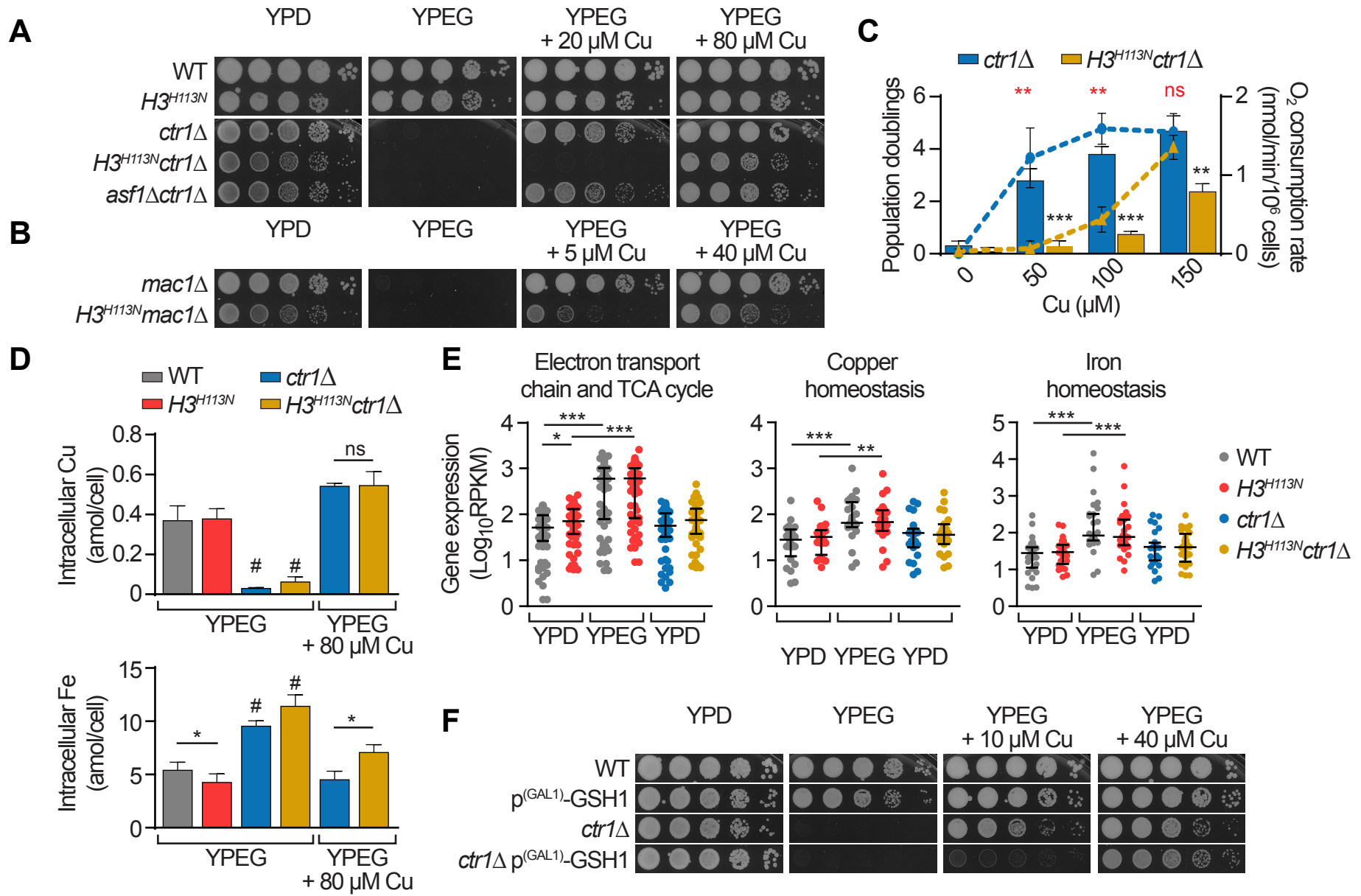


Figure 3

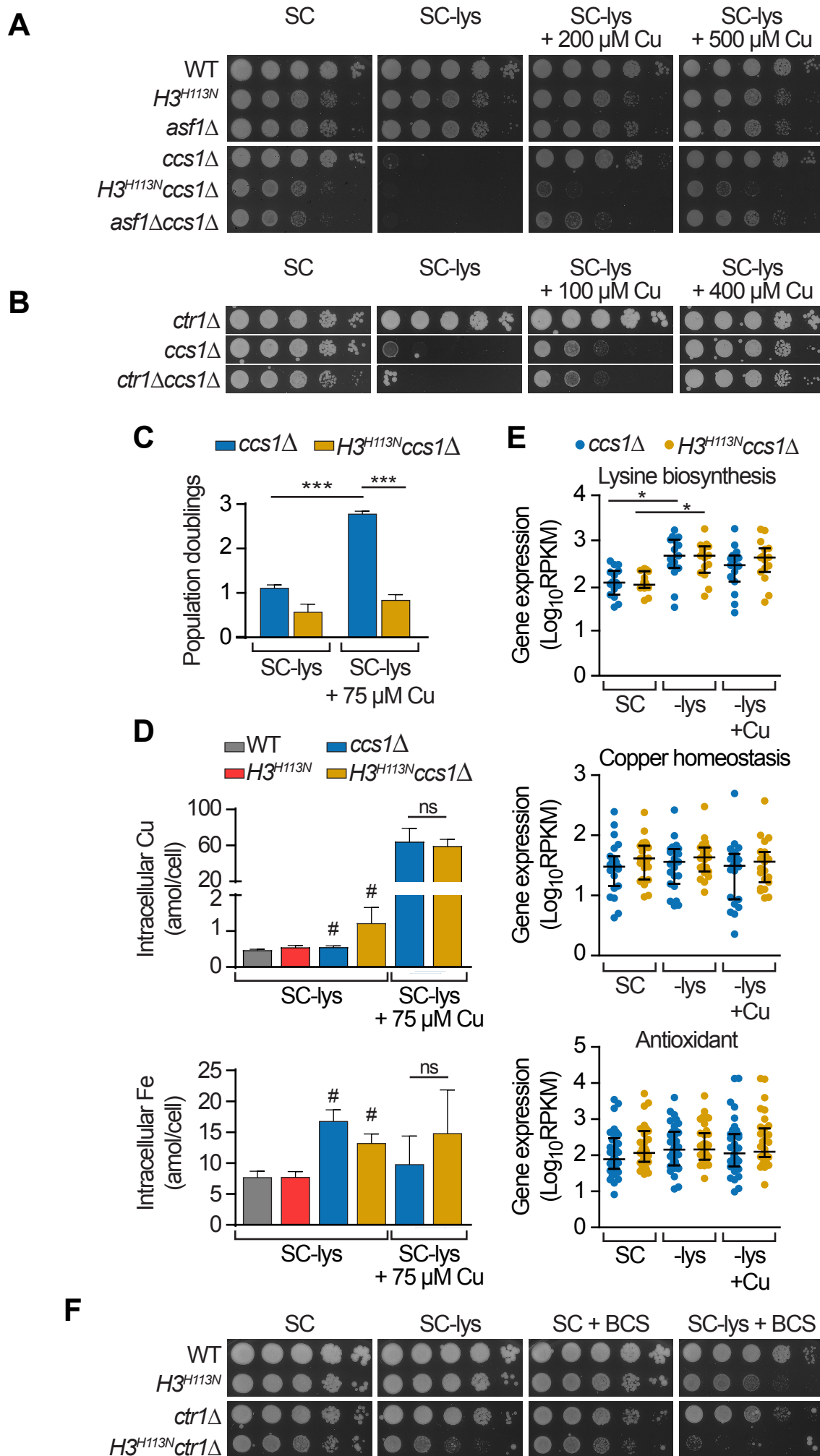


Figure 4

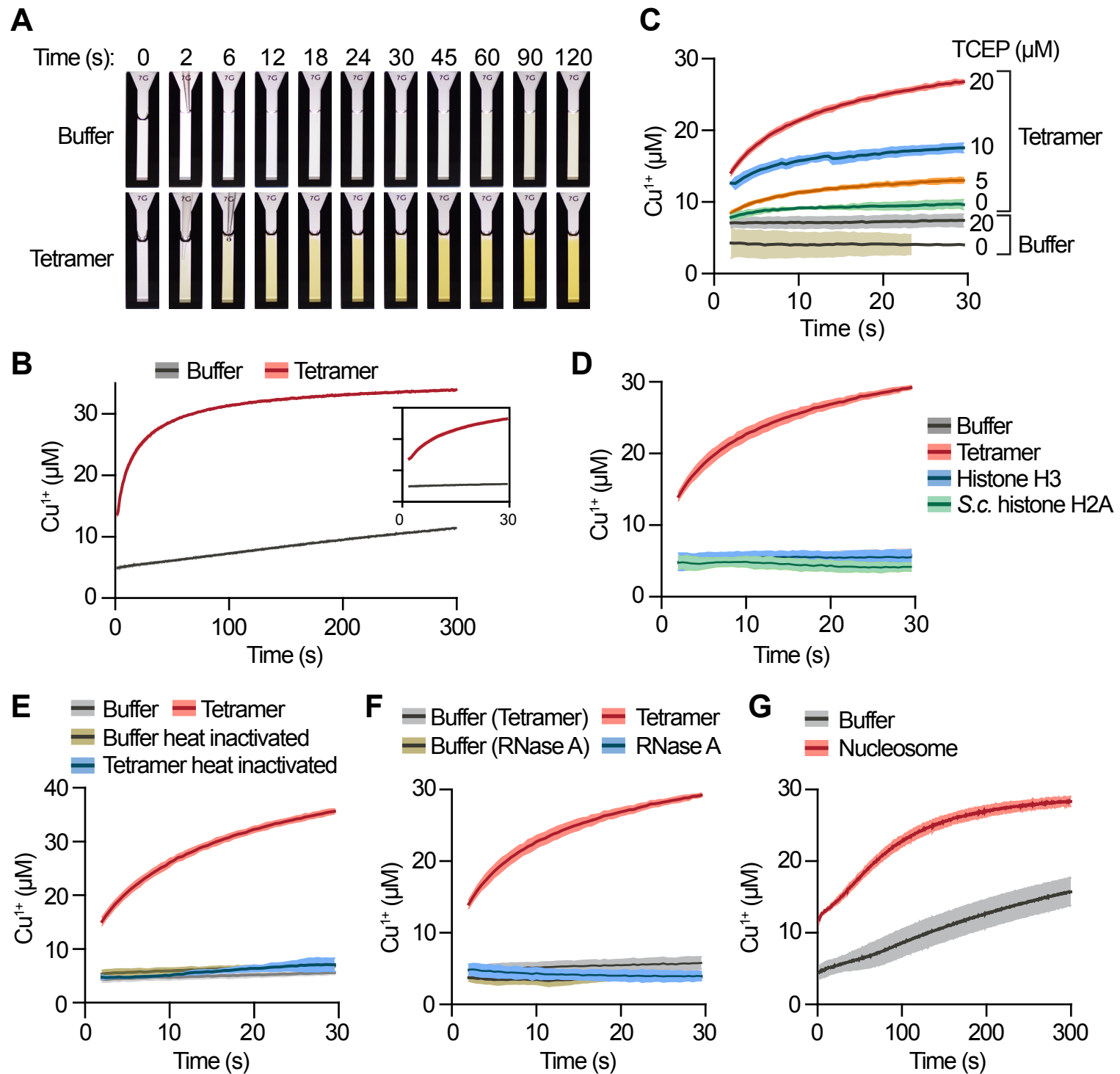
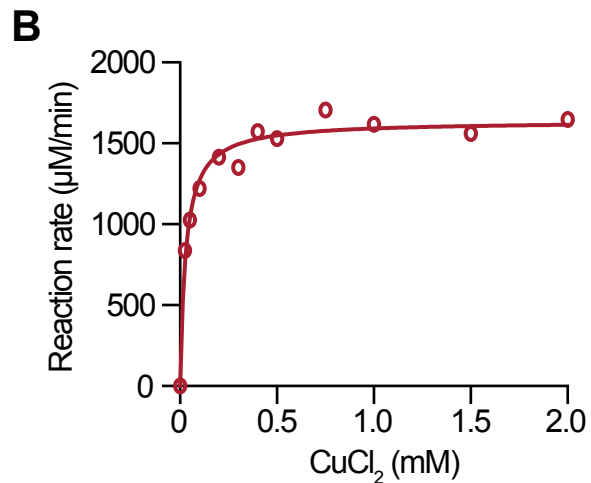
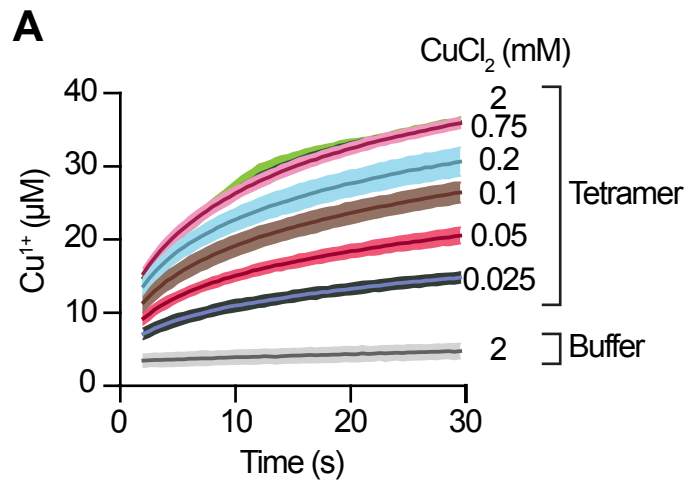


Figure 5



C

Enzyme Parameters	Value ± SD
K_m (µM)	28.8 ± 4
V_{max} (µM/min)	1638 ± 32.2
k_{cat} (sec ⁻¹)	27.3 ± 0.5
k_{cat}/K_m (M ⁻¹ sec ⁻¹)	9.5×10^{-5}

Figure 6

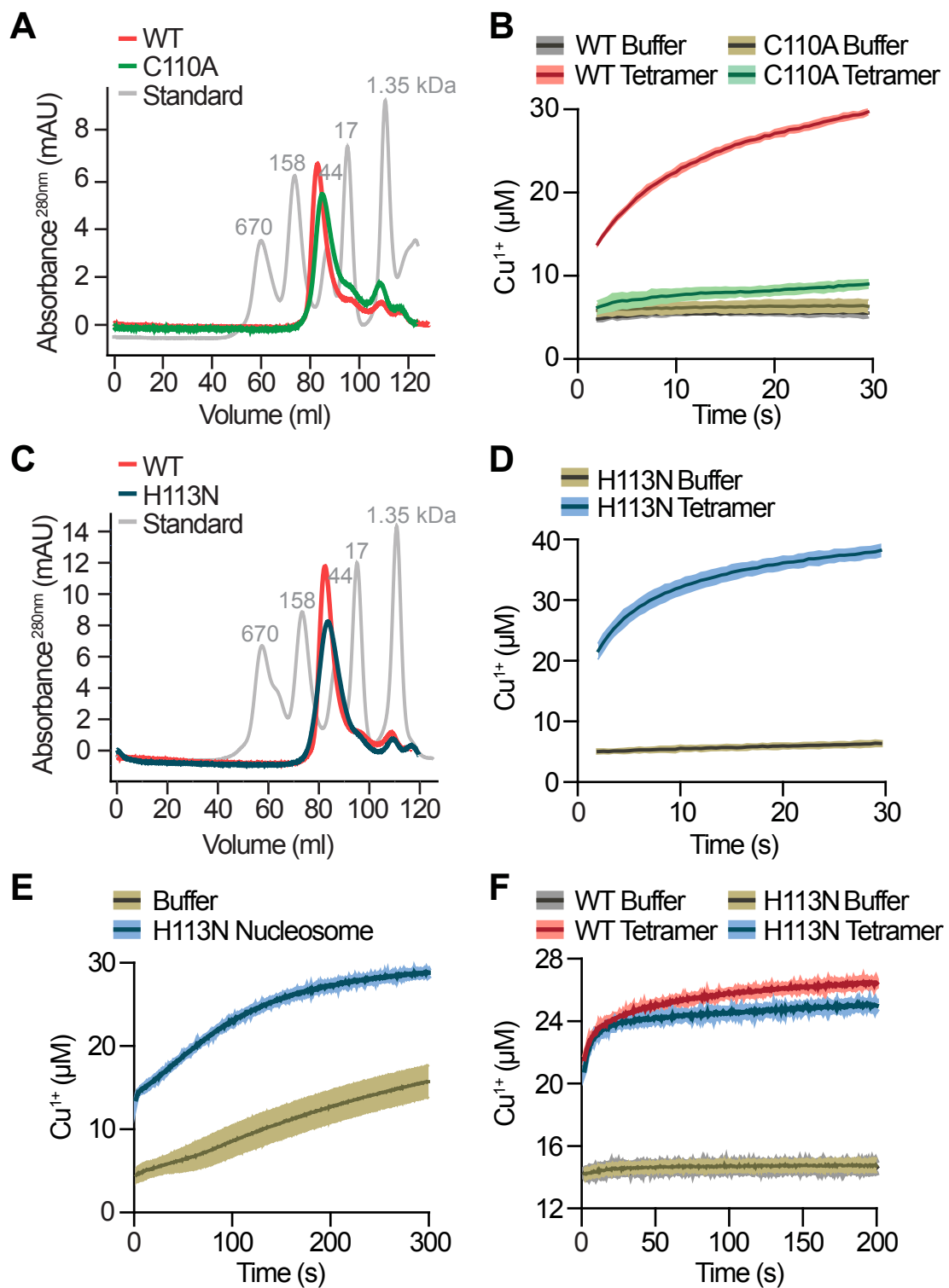
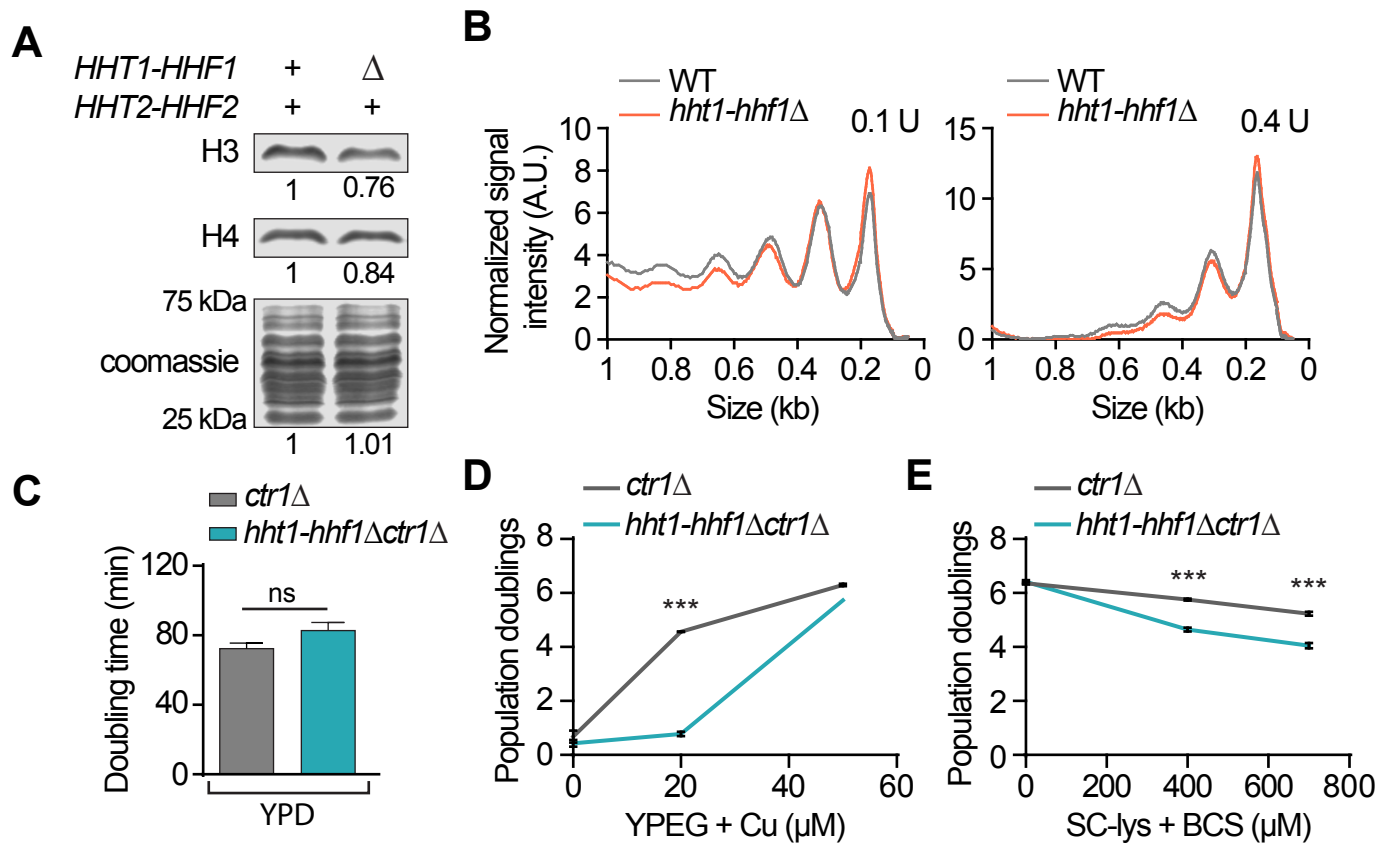


Figure 7



SUPPLEMENTAL INFORMATION 1
(SUPPLEMENTAL FIGURE LEGENDS, FIGURES AND TABLES)

The Histone H3-H4 Tetramer is a Copper Reductase Enzyme

Narsis Attar^{1,2,3}, Oscar A. Campos^{1,2,3}, Maria Vogelauer^{1,2}, Yong Xue², Stefan Schmollinger⁴, Linda Yen⁵, Shannon Zikovich², Jade Dardine², Michael F. Carey^{2,3}, Sabeeha S. Merchant⁴, and Siavash K. Kurdistani^{2,3,6,7,*}

¹Co-first author, listed alphabetically

²Department of Biological Chemistry, David Geffen School of Medicine, University of California Los Angeles, Los Angeles, CA 90095, USA

³Molecular Biology Institute, University of California Los Angeles, Los Angeles, CA 90095, USA

⁴Institute for Genomics and Proteomics, Department of Chemistry and Biochemistry, University of California Los Angeles, Los Angeles, CA 90095, USA

⁵Department of Molecular, Cell, and Developmental Biology, University of California Los Angeles, Los Angeles, CA 90095, USA

⁶Eli and Edythe Broad Center of Regenerative Medicine and Stem Cell Research, David Geffen School of Medicine, University of California Los Angeles, Los Angeles, CA 90095, USA

⁷Lead Contact

*Correspondence: Siavash Kurdistani
310.794.5194
skurdistani@mednet.ucla.edu

Supplemental Figure Legends

Figure S1, related to Figure 2. The H3H113N mutation does not affect CUP1 buffering capacity, cellular metal content, or gene expression in fermentative or non-fermentative media. (A-C) Spot test assays of the indicated strains in media as specified. Note that the *ctr1* Δ strain is respiratory deficient and cannot be rescued by exogenous manganese, zinc or iron. **(D)** Intracellular copper and iron content measured by ICP-MS for exponentially growing strains in YPD. Data are presented as mean \pm SD from 3-6 replicate cultures. **(E)** Scatterplot of average global gene expression values from exponentially growing cells in YPEG from two independent experiments, with Spearman's rank correlation coefficient (r_s) as indicated. **(F)** Heat map of average mRNA expression levels for copper homeostasis genes (data summarized in Fig 2E) from two independent experiments. * $P < 0.05$, ** $P \leq 0.01$, *** $P \leq 0.001$.

Figure S2, related to Figure 3. The H3H113N mutation does not affect CUP1 buffering capacity, cellular metal content, gene expression or oxygen sensitivity in lysine deficient media. (A-C) Spot test assays of the indicated strains in media as specified. Note that *ccs1* Δ and *sod1* Δ renders cells auxotrophic for lysine and cannot be rescued by exogenous manganese, zinc or iron. **(D)** Intracellular copper and iron content measured by ICP-MS for exponentially growing strains in YPD. Data are presented as mean \pm SD from 3-6 replicate cultures. **(E)** Scatterplot of average global gene expression values from exponentially growing cells in complete (SC) or lysine deficient (SC-lys) media from two independent experiments, with Spearman's rank correlation coefficient (r_s) as indicated. **(F)** Heat map of average mRNA expression levels for copper homeostasis genes (data summarized in Fig 3E) from two independent experiments. **(G)** Spot test assays of the indicated strains in SC or SC-lys grown in normoxic or hypoxic conditions.

(H) Average population doublings (\pm SD) for growth in the indicated media after 36 hrs from three independent experiments. * $P < 0.05$, ** $P \leq 0.01$, *** $P \leq 0.001$.

Figure S3, related to Figure 4. Experimental outline of H3.2/H4 tetramer formation and *in vitro* copper reductase assay. (A) The procedure for preparation of histones and assembly of tetramer is outlined. **(B)** Graphical representation of the copper reductase assay.

Figure S4, related to Figures 4 and 6. Electrophoretic quality control of octamers, nucleosomes, and tetramers. (A and B) Coomassie-stained 18% denaturing PAGE of the indicated tetramers. The molecular weight is indicated for reference. **(C)** Same as (A and B) but for the indicated octamers. **(D)** Ethidium bromide-stained 5% native PAGE of the un-assembled 146-bp DNA fragment (DNA) or assembled nucleosomes containing H3.2 or H3H113N. A 100-bp DNA ladder (M) is included for molecular weight reference.

Figure S5, related to Figure 6. Enzymatic parameters of the H113N tetramer. (A) Reaction profiles of 1 μ M the H113N tetramer with 20 μ M TCEP and the indicated CuCl_2 concentrations. Lines and shading represent the mean \pm SD of 4-5 assays. **(B)** Henri-Michaelis-Menten curve of initial velocities of reactions shown in A. **(C)** Calculated enzymatic parameters of the H113N tetramer from the curve in (B).

Figure S1

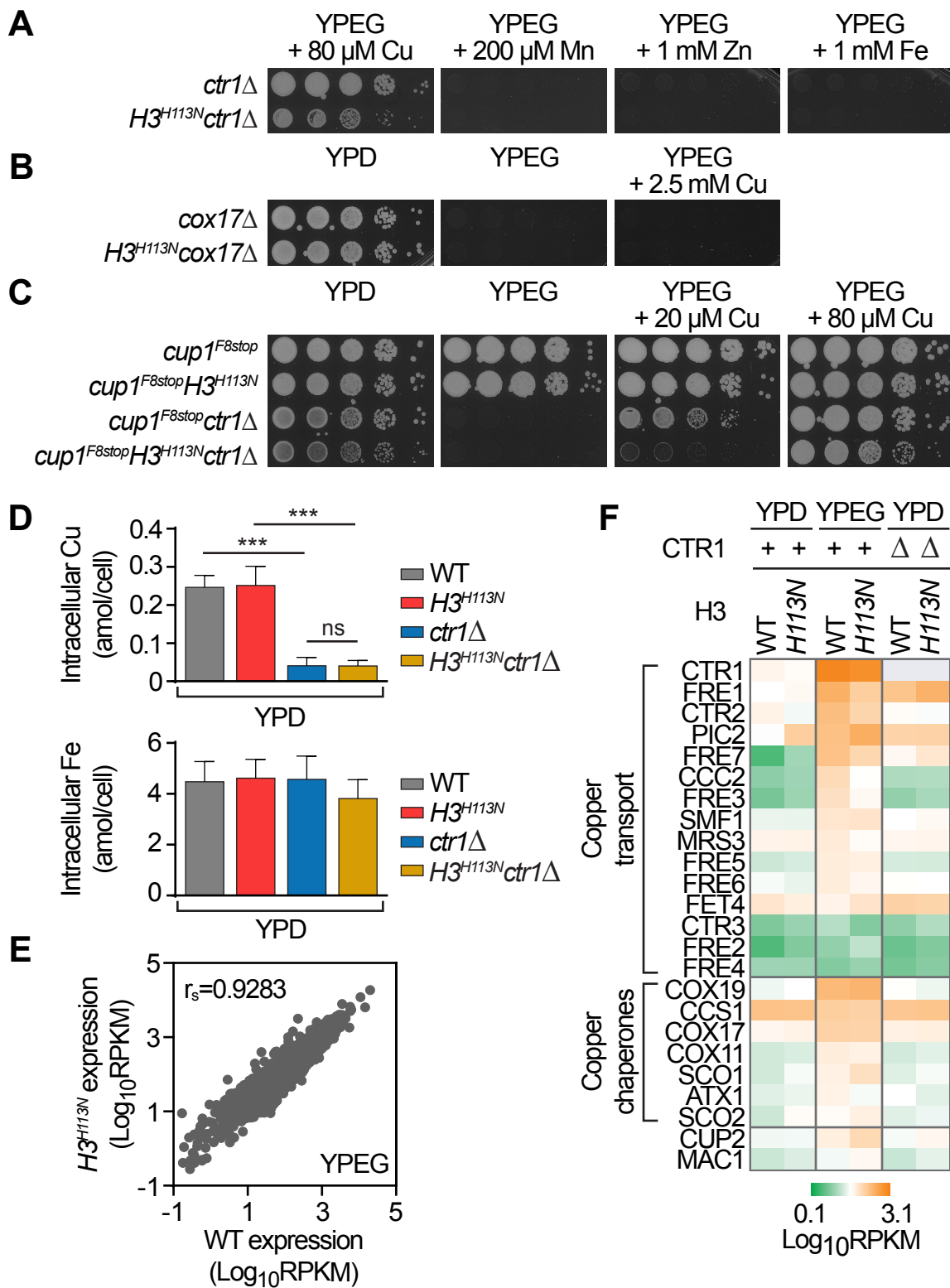


Figure S2

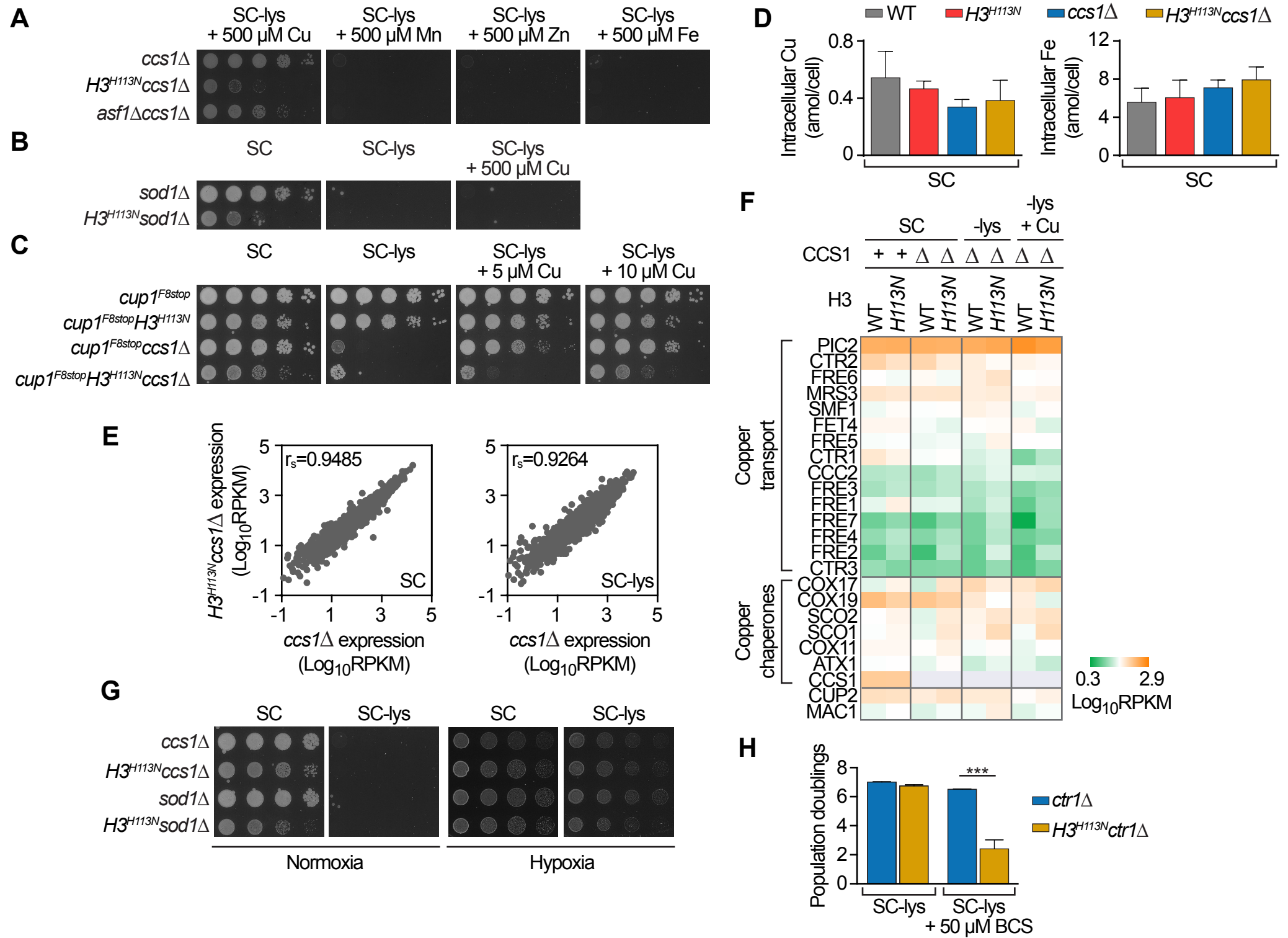
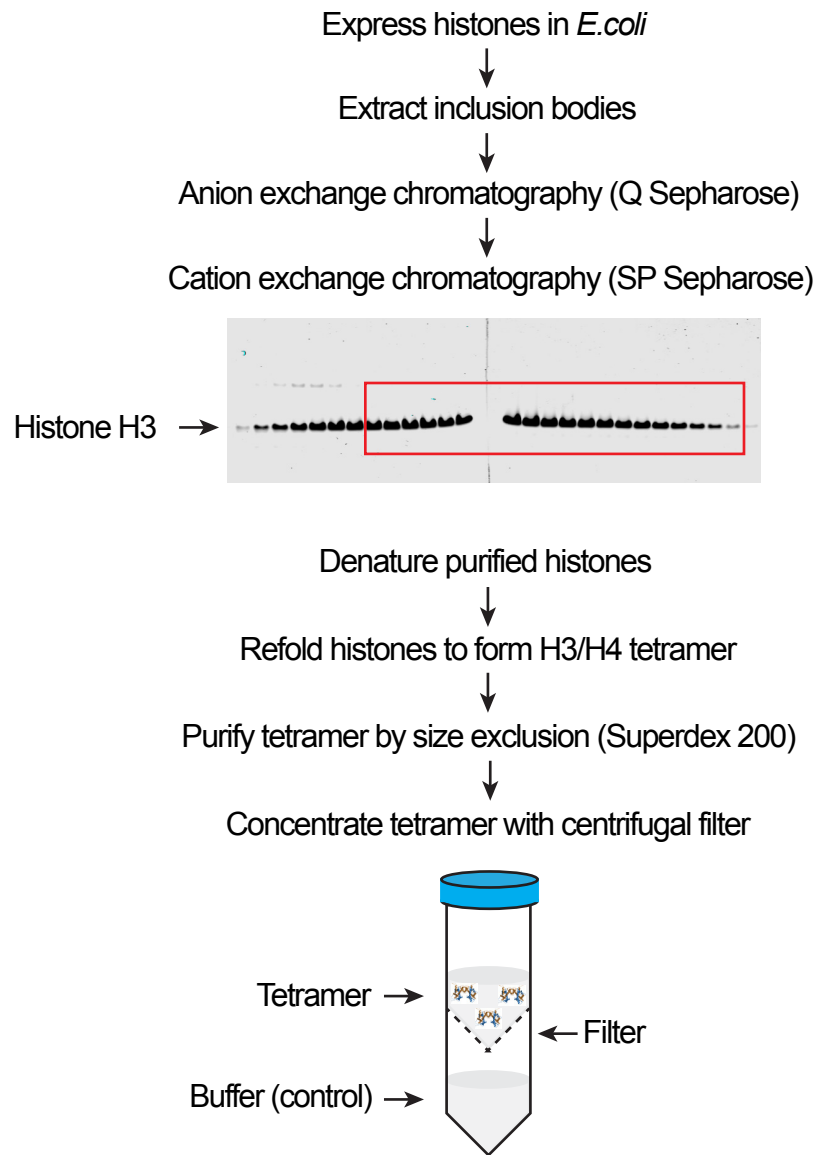


Figure S3

A



B

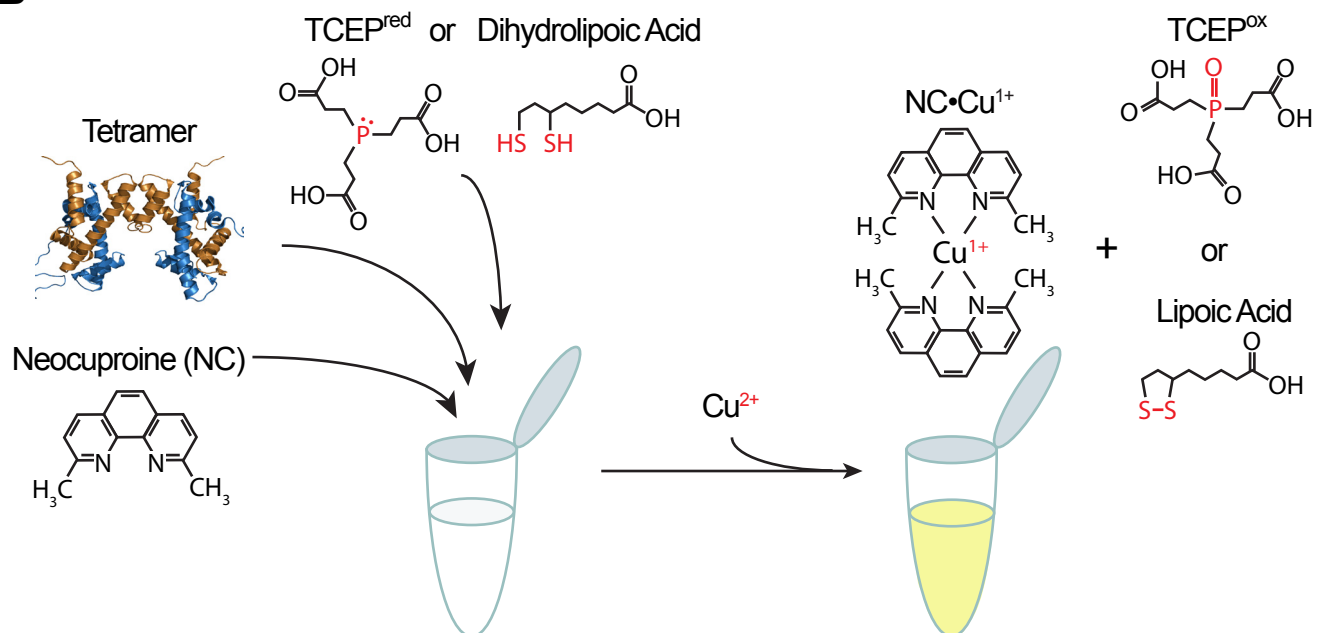
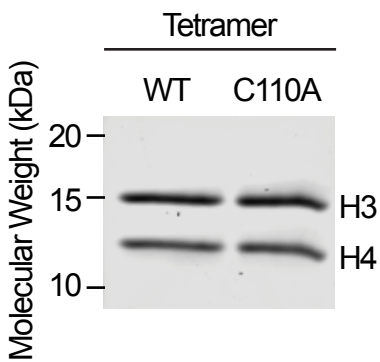
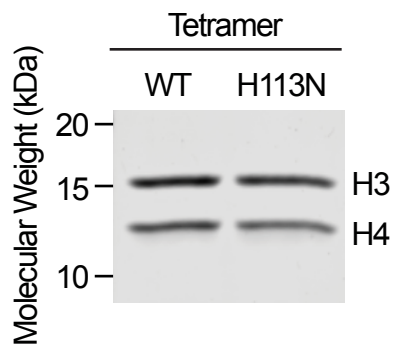


Figure S4

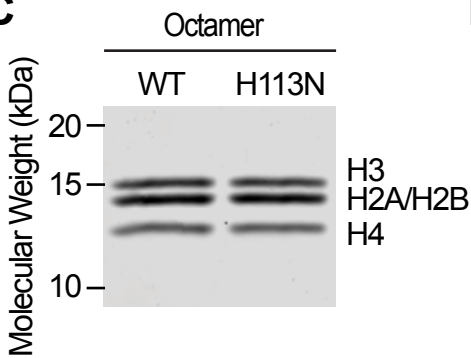
A



B



C



D

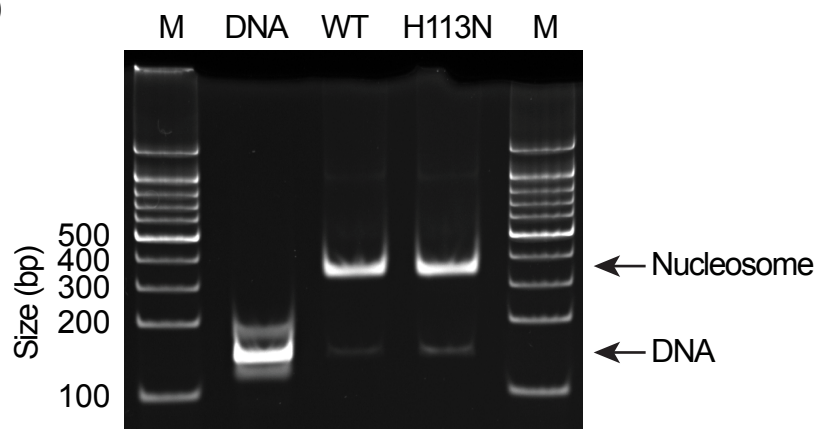


Figure S5

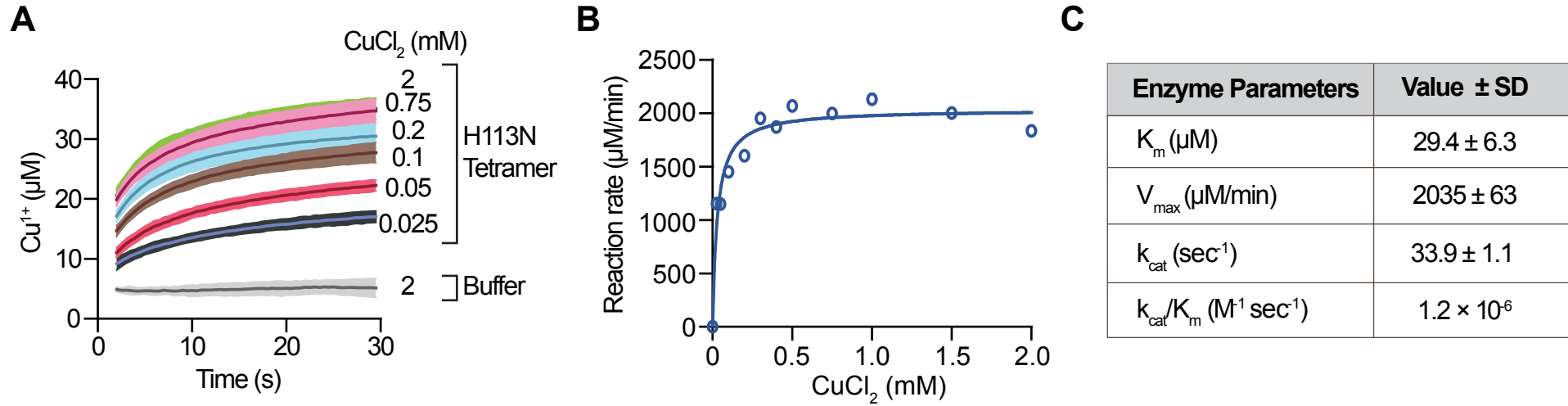


Table S1: Yeast strains used in this study

Strain name	Mutant short name	Description	Reference
BY4741	parental	<i>MATa his3Δ1 leu2Δ0 met15Δ0 ura3Δ0</i>	Brachmann et al., 1998
OCY1131	WT	<i>MATa his3Δ1 leu2Δ0 met15Δ0 ura3Δ0, (hht2Δ::ura3)Δ::HHT2</i>	This study
OCY1136	<i>H3^{H113N}</i>	<i>MATa his3Δ1 leu2Δ0 met15Δ0 ura3Δ0, (hht2Δ::ura3)Δ::HHT2-H113N HHT1-H113N</i>	This study
NAY536	<i>asf1Δ</i>	<i>MATa his3Δ1 leu2Δ0 met15Δ0 ura3Δ0, (hht2::ura3)::HHT2, asf1Δ::hphMX4</i>	This study
OCY1861	<i>ctr1Δ</i>	<i>MATa his3Δ1 leu2Δ0 met15Δ0 ura3Δ0, (hht2Δ::ura3)Δ::HHT2, ctr1Δ::hphMX4</i>	This study
OCY1862	<i>H3^{H113N} ctr1Δ</i>	<i>MATa his3Δ1 leu2Δ0 met15Δ0 ura3Δ0, (hht2Δ::ura3)Δ::HHT2-H113N HHT1-H113N, ctr1Δ::hphMX4</i>	This study
OCY2141	<i>asf1Δ ctr1Δ</i>	<i>MATa his3Δ1 leu2Δ0 met15Δ0 ura3Δ0, (hht2Δ::ura3)Δ::HHT2, asf1Δ::hphMX4, ctr1Δ::His3MX6</i>	This study
OCY2251	<i>mac1Δ</i>	<i>MATa his3Δ1 leu2Δ0 met15Δ0 ura3Δ0, (hht2Δ::ura3)Δ::HHT2, mac1Δ::His3MX6</i>	This study
OCY2252	<i>H3^{H113N} mac1Δ</i>	<i>MATa his3Δ1 leu2Δ0 met15Δ0 ura3Δ0, (hht2Δ::ura3)Δ::HHT2-H113N HHT1-H113N, mac1Δ::His3MX6</i>	This study
OCY2381	<i>p^(GAL1)-GSH1</i>	<i>MATa his3Δ1 leu2Δ0 met15Δ0 ura3Δ0, (hht2Δ::ura3)Δ::HHT2, kanMX6-PGAL1-GSH1</i>	This study
OCY2391	<i>ctr1Δ p^(GAL1)-GSH1</i>	<i>MATa his3Δ1 leu2Δ0 met15Δ0 ura3Δ0, (hht2Δ::ura3)Δ::HHT2, ctr1Δ::hphMX4, kanMX6-PGAL1-GSH1</i>	This study
OCY2131	<i>cox17Δ</i>	<i>MATa his3Δ1 leu2Δ0 met15Δ0 ura3Δ0, (hht2Δ::ura3)Δ::HHT2, cox17Δ::kanMX6</i>	This study
OCY2132	<i>H3^{H113N} cox17Δ</i>	<i>MATa his3Δ1 leu2Δ0 met15Δ0 ura3Δ0, (hht2Δ::ura3)Δ::HHT2-H113N HHT1-H113N, cox17Δ::kanMX6</i>	This study
OCY1981	<i>cup1^{F8stop}</i>	<i>MATa his3Δ1 leu2Δ0 met15Δ0 ura3Δ0, (hht2Δ::ura3)Δ::HHT2, cup1-F8stop</i>	This study
OCY1983	<i>cup1^{F8stop} H3^{H113N}</i>	<i>MATa his3Δ1 leu2Δ0 met15Δ0 ura3Δ0, (hht2Δ::ura3)Δ::HHT2, cup1-F8stop, HHT1-H113N HHT2-H113N</i>	This study
OCY2181	<i>cup1^{F8stop} ctr1Δ</i>	<i>MATa his3Δ1 leu2Δ0 met15Δ0 ura3Δ0, (hht2Δ::ura3)Δ::HHT2, cup1-F8stop, ctr1Δ::His3MX6</i>	This study
OCY2182	<i>cup1^{F8stop} H3^{H113N} ctr1Δ</i>	<i>MATa his3Δ1 leu2Δ0 met15Δ0 ura3Δ0, (hht2Δ::ura3)Δ::HHT2, cup1-F8stop, HHT1-H113N HHT2-H113N, ctr1Δ::His3MX6</i>	This study
NAY553	<i>ccs1Δ</i>	<i>MATa his3Δ1 leu2Δ0 met15Δ0 ura3Δ0, (hht2::ura3)::HHT2, ccs1Δ::kanMX6</i>	This study
NAY554	<i>H3^{H113N} ccs1Δ</i>	<i>MATa his3Δ1 leu2Δ0 met15Δ0 ura3Δ0, (hht2::ura3)::HHT2-H113N HHT1-H113N, ccs1Δ::kanMX6</i>	This study
NAY597	<i>asf1Δ ccs1Δ</i>	<i>MATa his3Δ1 leu2Δ0 met15Δ0 ura3Δ0, (hht2Δ::ura3)Δ::HHT2, asf1Δ::hphMX4, ccs1Δ::His3MX6</i>	This study
NAY551	<i>sod1Δ</i>	<i>MATa his3Δ1 leu2Δ0 met15Δ0 ura3Δ0, (hht2::ura3)::HHT2, sod1Δ::hphMX4</i>	This study
NAY552	<i>H3^{H113N} sod1Δ</i>	<i>MATa his3Δ1 leu2Δ0 met15Δ0 ura3Δ0, (hht2::ura3)::HHT2-H113N HHT1-H113N, sod1Δ::hphMX4</i>	This study
OCY2211	<i>cup1^{F8stop} ccs1Δ</i>	<i>MATa his3Δ1 leu2Δ0 met15Δ0 ura3Δ0, (hht2Δ::ura3)Δ::HHT2, cup1-F8stop, ccs1Δ::kanMX6</i>	This study
OCY2212	<i>cup1^{F8stop} H3^{H113N} ccs1Δ</i>	<i>MATa his3Δ1 leu2Δ0 met15Δ0 ura3Δ0, (hht2Δ::ura3)Δ::HHT2, cup1-F8stop, HHT1-H113N HHT2-H113N, ccs1Δ::kanMX6</i>	This study
OCY1135	<i>hht1-hhf1Δ</i>	<i>MATa his3Δ1 leu2Δ0 met15Δ0 ura3Δ0, (hht2Δ::URA3)Δ::HHT2, hht1-hhf1Δ::hphMX4</i>	This study
OCY2421	<i>ctr1Δ</i>	<i>MATa his3Δ1 leu2Δ0 met15Δ0 ura3Δ0, (hht2Δ::URA3)Δ::HHT2, ctr1Δ::His3MX6</i>	This study

NAY564	<i>hht1-hhf1Δctr1Δ</i>	<i>MATa his3Δ1 leu2Δ0 met15Δ0 ura3Δ0, (hht2Δ::URA3)Δ::HHT2, hht1-hhf1Δ::hphMX4, ctr1Δ::His3MX6</i>	This study
---------------	------------------------	----------------------------------------------------------------------------------------------------	------------

Table S2: Oligonucleotide primers used in this study

Name	Sequence	Description
Δhht2-CORE-F	TTCCAAGTGTCTTCCCCTTTTACTAAAGGATCCAAGCAAACACTCCACAGAGCTCGTTTTTCGACACTGG	Targeted HHT2 deletion using pCORE
Δhht2-CORE-R	ATGTCCCCCAGTCTAAATGCATAGAAAAAAAAAAATCCCGCTTATATTCCTTACCATTAAAGTTGATC	
pRM-HHT2-F	TGTTTTGTGACTTCCACTTTGG	Targeted HHT2 reintroduction using pRM200 or pYX55
pRM-HHT2-R	AAAAGGAGATGTTTGTATGATGTCC	
pCAS-amp-uni-R	AAAGTCCCATTTCGCCACCCG	Universal primer for pCAS sgRNA change
pCAS-HHT1-H113-gRNA-F	AGTGACACGCTTGGCGTGAAGTTTTAGAGCTAGAAATAGC	HHT1-H113 target sgRNA change on pCAS
pCAS-HHT2-H113-gRNA-F	TTTGTTTGAAGACACTAATCGTTTTAGAGCTAGAAATAGC	HHT2-H113 target sgRNA change on pCAS
pCAS-CUP1-F8-gRNA-F	TTAATTAAGTTCAAAATGAGTTTTAGAGCTAGAAATAGC	CUP1-F8 target sgRNA change on pCAS
HHT1-H113N-mutrep-F	CGAAGCCTACTTAGTCTCTTTATTTGAAGATACCAACTTGGCTGCCATTAATGCCAAGCG	Template for HDR to introduce HHT1-H113N
HHT1-H113N-mutrep-R	TCTTCTAGCCAACTTGATATCCTTCTTTTGGATAGTGACACGCTTGGCATTAAATGGCAGC	
HHT2-H113N-mutrep-F	CTTCTGCTATCGGTGCTTTGCAAGAAATCCGTCGAAGCATACTTAGTCTCTTTGTTGAAGACACTAATCTTGCTGCTATT	Template for HDR to introduce HHT2-H113N
HHT2-H113N-mutrep-R	ACCTCTTAGTCTTCTGGCCAATTTGATATCCTTCTTTTGGATAGTAACACGCTTAGCGTTAATAGCAGCAAGATTAGTGT	
CUP1-F8stop-mutrep-F	ACAATCAATCAATCAATCATCACATAAAATGTTTCAGCGAATTAATTAAGTGC AAAATGA	Template for HDR to introduce CUP1-F8stop
CUP1-F8stop-mutrep-R	ATTTTTGCAGCTACCACATTGGCATTGGCACTCATGACCTTCATTTTGTTCAGT TAATTAA	
Δasf1-Hph-U2	TAACAGCGTACTCTCCCTACCATCCAATTGAAACATAAGATATAGAAAAGCCAGCTGAAGCTTCGTACGC	Targeted ASF1 deletion using pAG32
Δasf1-Hph-D2	TAAAGTGACTCTCTTGCAGGTACCATTAATCTTATAACCCATAAATTCATAGGCCACTAGTGGATCTG	
Δctr1-Hph-U2	ATAGAAAAATAAAAAAAGTGATTATATTTGACATTCAAAACCGCTGAAGCTTCGTACGC	Targeted CTR1 deletion using pAG32
Δctr1-Hph-D2	TGGAAGAAGAAGATATAGGTGGACGAACCTTGCTAGTTAATAGGCCACTAGTGGATCTG	
Δctr1-His-F1	ATAGAAAAATAAAAAAAGTGATTATATTTGACATTCAAAACCGATCCCCGGGT TAATTAA	Targeted CTR1 deletion using pFA6a-His3MX6
Δctr1-His-R1	TGGAAGAAGAAGATATAGGTGGACGAACCTTGCTAGTTAGAATTCGAGCTCGTTTAAAC	
Δmac1-His-F1	CTTGTTTTTAACTTGAAACAGTCTGGTAAGTTCTTCAAGCTCTATCAGAGCGG ATCCCCGGTTAATTAA	

Δmac1-His-R1	ATTTTCATTCCTGTTGCCTCAATGTGTTTTCTATCTGTATTTACGTGATTGAA TTCGAGCTCGTTTAAAC	Targeted MAC1 deletion using pFA6a-His3MX6
Kan-PGAL-GSH1-F4	CTTGTAGAAGCTGAAAATTGAGCAGATTTAGTATAGGGCTGAATTCGAGCTCG TTTAAAC	Targeted p ^(GAL1) -GSH1 insertion using pFA6a-kanMX6-PGAL1
Kan-PGAL-GSH1-R2	ACTCAAACCACTGCAAAGGCGTGCCCAAAGCTAAGAGTCCCATTTTGAGATCC GGGTTTT	
Δcox17-Kan-F1	AGTGTACACAATCAGATAACTACACAATCAATTATACCCACGGATCCCCGGGT TAATTAA	Targeted COX17 deletion using pFA6a-kanMX6
Δcox17-Kan-R1	ATATATACAAGAAATGGTTGTTCGGCAGACTGTCAGTAAGAGAATTCGAGCTCG TTTAAAC	
Δccs1-Kan-F1	ATATCTTTGCAAGGCAGAAACCCATTTCGATCAGCACAAAACGGATCCCCGGGT TAATTAA	Targeted CCS1 deletion using either pFA6a-kanMX6 or pFA6a-His3MX6
Δccs1-Kan-R1	TTATATCTGTATTACGCTACGTTGTGCTATCTTGGATGTTGAATTCGAGCTCG TTTAAAC	
Δsod1-Hph-U2	AACAGGCAAGAAAAGCAATCGCGCAAAACAAATAAAAACATAATTAATTTATACCA GCTGAAGCTTCGTACGC	Targeted SOD1 deletion using pAG32
Δsod1-Hph-D2	CTTACTACTTACTTACATACGGTTTTTATTCAAGTATATTATCATTAACAATA GGCCACTAGTGGATCTG	
Δhht1-hhf1-Hph-U2	ATATTTGCTTGTTGTTACCGTTTTCTTAGAATTAGCTAAAAGAATACCCTCCT TGACAGTCTT	Targeted HHT1-HHF1 locus deletion using pAG32
Δhht1-hhf1-Hph-D2	TTTTGTTCGTTTTTTACTAAAACCTGATGACAATCAACAAAATACGACTCACTA TAGGGAGACCG	
xIH3-A102G-F	GAGGCTTATCTGGTCGGACTCTTTGAGGACACCA	Mutagenesis primers to generate H3.2 (A102G)
xIH3-A102G-R	TGGTGTCTCAAAGAGTCCGACCAGATAAGCCTC	
xIH3-H113N-F2	AACCTGTGCGCCATCAACGCCAAGAGGGTCACCA	Mutagenesis primers to generate H3.2-H113N
xIH3-H113N-R2	TGGTGACCCTCTTGCGTTGATGGCGCACAGGTT	
xIH3-C110A-F	GAGGACACCAACCTGGCCGCCATCCACGCCAAG	Mutagenesis primers to generate H3.2-C110A
xIH3-C110A-R	CTTGCGTGGATGGCGGCCAGGTTGGTGTCTCTC	
601_146bp_F	CTGGAGAATCCCCGGTGC	Primers to amplify "601" sequence
601_146bp_R	CAGGATGTATATATCTGACACGTGC	

Table S3: Gene sets for gene expression analysis

Gene set	Genes
Copper homeostasis	ATX1, CCC2, CCS1, COX11, COX17, COX19, CTR1, CTR2, CTR3, CUP2, FET4, FRE1, FRE2, FRE3, FRE4, FRE5, FRE6, FRE7, MAC1, MRS3, PIC2, SCO1, SCO2, SMF1
Iron homeostasis	AFT1, AFT2, ARN1, ARN2, ATX1, CCC2, CTH1, FET3, FET4, FET5, FIT1, FIT2, FIT3, FRE1, FRE2, FRE3, FRE4, FRE5, FRE6, FRE7, FRE8, FTH1, FTR1, HMX1, SIT1, SMF1, SMF3, TIS11
Electron transport chain and TCA cycle	ACO1, ACO2, AIF1, CIR2, CIT1, CIT2, CIT3, COR1, COX13, COX4, COX5A, COX5B, COX6, COX7, COX8, COX9, CYC1, CYC7, CYT1, DAL7, DLD2, DLD3, FUM1, ICL1, IDH1, IDH2, IDP1, IDP2, IDP3, KGD1, KGD2, LSC1, LSC2, MAS1, MDH1, MDH2, MDH3, MLS1, MTC3, NDI1, QCR10, QCR2, QCR6, QCR7, QCR8, QCR9, RIP1, SDH1, SDH2, SDH3, SDH4, SDH5, SHH3, SHH4, TAZ1, YJL045W, YJL045W, YMR31
Lysine biosynthesis	ACO2, ARO8, HOM2, HOM3, HOM6, KGD2, LYS1, LYS12, LYS14, LYS2, LYS20, LYS21, LYS4, LYS5, LYS9
Antioxidant	AHP1, CCP1, CCS1, CTA1, CTT1, CUP1-1, CUP1-2, DOT5, ECM4, GLR1, GPX1, GPX2, GRX1, GRX2, GRX6, GRX7, GRX8, GTO1, GTT1, HYR1, MRP1, PRX1, RSM26, SCO1, SCO2, SOD1, SOD2, SRX1, TRR1, TRR2, TRX1, TRX2, TRX3, TSA1, TSA2, URE2

SUPPLEMENTAL INFORMATION 2
(STAR METHODS AND KEY RESOURCES TABLE)

The Histone H3-H4 Tetramer is a Copper Reductase Enzyme

Narsis Attar^{1,2,3}, Oscar A. Campos^{1,2,3}, Maria Vogelauer^{1,2}, Yong Xue², Stefan Schmollinger⁴, Linda Yen⁵, Shannon Zikovich², Jade Dardine², Michael F. Carey^{2,3}, Sabeeha S. Merchant⁴, and Siavash K. Kurdistani^{2,3,6,7,*}

¹Co-first author, listed alphabetically

²Department of Biological Chemistry, David Geffen School of Medicine, University of California Los Angeles, Los Angeles, CA 90095, USA

³Molecular Biology Institute, University of California Los Angeles, Los Angeles, CA 90095, USA

⁴Institute for Genomics and Proteomics, Department of Chemistry and Biochemistry, University of California Los Angeles, Los Angeles, CA 90095, USA

⁵Department of Molecular, Cell, and Developmental Biology, University of California Los Angeles, Los Angeles, CA 90095, USA

⁶Eli and Edythe Broad Center of Regenerative Medicine and Stem Cell Research, David Geffen School of Medicine, University of California Los Angeles, Los Angeles, CA 90095, USA

⁷Lead Contact

*Correspondence: Siavash Kurdistani
310.794.5194
skurdistani@mednet.ucla.edu

STAR METHODS

CONTACT FOR REAGENT AND RESOURCE SHARING

Please direct request for resources to Siavash Kurdistanani (skurdistani@mednet.ucla.edu).

EXPERIMENTAL MODEL AND SUBJECT DETAILS

Strains and general growth conditions

Haploid *Saccharomyces cerevisiae* strains used in this study are based on the BY4741 (S288C background, MATa) (Brachmann et al., 1998) strain, and are listed in Table S1. All strains were maintained on standard YPD (1% Yeast extract, 2% Peptone, 2% Glucose) plates and were grown at 30°C for varying amounts of time in all experiments as described below. Unless otherwise noted, all yeast experiments were initiated by growing cells overnight to dense cultures in various media conditions. The cells were subsequently diluted in fresh media as described below. Bacteria for histone expression were BL21(DE3)pLysS cells and BL21(DE3) (Agilent). Transformed bacteria were grown on 2xTY media (1.6% Bacto Tryptone, 1% Yeast Extract, 0.5% NaCl) supplemented with 100 µg/mL ampicillin.

Oligonucleotides, plasmids, and strain generation for yeast experiments

All yeast strains were generated by the standard lithium acetate-based yeast transformation procedures. DNA fragments used for gene replacement deletions or promoter integrations were generated by PCR from plasmid templates listed in the Key Resources table. DNA fragments used as homology-directed repair templates for CRISPR-Cas9 mutagenesis were generated by primer extension to generate 100 bp-long oligonucleotides. Primers used to generate CRISPR repair templates and to amplify selectable markers containing 40 bp-long gene-flanking homology regions for gene-specific targeting are listed in Table S2.

The histone H3 His113Asn (H3H113N) mutation was generated in both chromosomal loci (*HHT1* and *HHT2*) in a stepwise and marker-less manner. First, using the *delitto perfetto* approach (Storici and Resnick, 2006), H113N was introduced into the *HHT2* locus. The entire *HHT2* coding region was first replaced with a KanMX4-KIURA3 cassette, with selection on Geneticin.

Subsequently, the KanMX4-KIURA3 was precisely replaced with either the WT *HHT2* as a control (essentially restoring the BY4741 strain, but distinguished as OCY1131 here to account for its history of temporarily lacking *HHT2*), or with an *HHT2* variant harboring the H113N mutation (340-CAC-342 becomes 340-AAC-342), with counter-selection on 5-fluoroorotic acid. DNA fragments used for the reintroduction of WT *HHT2* or *hht2-H113N* were generated by PCR using plasmids containing the WT *HHT2* (pRM200) (Mann and Grunstein, 1992) or *hht2-H113N* (pYX55) as templates. The pYX55 plasmid was generated by site-directed mutagenesis of the WT *HHT2* on pRM200 using the Agilent Lightning quick change mutagenesis kit, as directed by the manufacturer, and using primers listed in Table S2.

Second, the H113N mutation was introduced in *HHT1* using the CRISPR-Cas9 system optimized for *S. cerevisiae* (Ryan et al., 2014). The pCAS plasmid, containing both the Cas9 gene from *Streptococcus pyogenes* and a single guide RNA, was a gift from Jamie Cate (Ryan et al., 2014). To target Cas9 to the *HHT1* region containing H113, the 20 bp targeting sequence at the 5' end of the sgRNA was changed by PCR. First, pCAS was PCR-amplified with Phusion High-Fidelity DNA Polymerase (NEB) using a 5'-phosphorylated reverse primer immediately upstream of the target sequence, and a forward primer containing the 20 nucleotide *HHT1* region surrounding H113 on its 5' end. The PCR product was treated with DpnI endonuclease (NEB) and re-circularized with T4 DNA ligase (NEB) according to manufacturers' protocols. The H113N mutation (340-CAC-342 becomes 340-AAT-342) was then introduced in yeast by co-transformation with the *HHT1-H113*-targeting pCAS plasmid, and a 100-nt double stranded homology-directed repair template containing the mutation. Successful mutagenesis at both *HHT1* and *HHT2* was confirmed by sequencing of the entire gene coding locus.

Subsequent deletions of *ASF1*, *CTR1*, *MAC1*, *COX17*, *CCS1*, *SOD1*, and *HHT1-HHF1* genes, as well as insertion of the GAL1 promoter upstream of *GSH1* were generated by standard yeast gene replacement and targeted insertion methodology using selectable marker integration (Goldstein and McCusker, 1999; Longtine et al., 1998). Successful integrations and deletions

were confirmed by PCR. Importantly, combinations of H113N with these gene deletions were generated in the strain already containing the H113N mutation in both histone H3 copies (OCY1136).

The only exception is the generation of strains in which Cup1 is disrupted, alone or in combination with H113N. Because of the multi-copy CUP1 gene, and the complexity of the locus with respect to the flanking RSC30 gene, we disrupted the gene by introduction of a stop codon at Phe8 at all CUP1 copies. Introduction of the stop codon was performed using the CRISPR-Cas9 system as described above for generating *hht1-H113N*, and correct mutagenesis was confirmed by sequencing. Lastly, H113N was introduced in both *HHT1* and *HHT2* using the same CRISPR-Cas9 approach for both loci in the strain already containing the *cup1-F8stop* mutation. Primers used to generate the targeting sgRNAs and the repair templates introducing mutations are listed in Table S2.

Oligonucleotides, plasmids for histone expression and nucleosome assembly

Plasmids for expression of *Xenopus laevis* histones are from (Luger et al., 1997). The histone H3 plasmid from this reference contains an H3-G102A mutation, which was corrected to the WT G102 by site directed mutagenesis (QuikChange, Agilent) using primers xIH3-A102G-F and xIH3-A102G-R, resulting in plasmid pH3.2. C110 of histone H3.2 was mutated to alanine using primers xIH3-C110A_F and xIH3-C110A-R to produce pH3.2-C110A. H3H113 was mutated to asparagine using primers xIH3-H113N-F2 and xIH3-H113N-R2, resulting in pH3.2-H113N. A plasmid containing 12 tandem 177 bp repeats of the 601 sequence for nucleosome positioning was kindly provided by Craig L. Peterson (Dorigo et al., 2003). Plasmids used are listed in the Key Resources table, and primers for mutagenesis are listed in Table S2.

METHOD DETAILS

Steps were taken to reduce trace metal contamination in glassware. We found these steps to be critical for reliability and reproducibility of all data involving transition metals, especially for the H3-H4 tetramer enzyme activity. Failure to properly remove trace metal contaminants may

result in tetramers with no in vitro enzyme activity. In some cases, as described below, BioUltra grade reagents were used to ensure lowest possible trace metal contaminants.

Preparation of solutions and glassware

Buffers and solutions for the *in vitro* enzyme assays were treated with 10% hydrochloric acid for at least 12 hrs (acid-washed glassware) followed by further acid washing for 1 hr in 10% nitric acid. Acid-washed glassware was rinsed thoroughly before solution preparation. Buffers and solutions were prepared from BioUltra quality products and also treated with Chelex 100 (Sigma) to further reduce contaminating transition metals. Powder components were added without the use of metal spatulas to further avoid metal contamination. After components were dissolved, solutions were filtered through 0.2 μm membranes and stored in acid-washed glass containers or single-use polypropylene containers. Standard RC dialysis tubing for dialysis (Spectrumlabs.com) was washed in 1L of 10 mM EDTA (99.99% trace metal basis – Sigma) for 1h at 80°C, transferred to fresh 1L of 10 mM EDTA at 80°C and let cool slowly at room temperature for 16 hours. Clean membranes were dehydrated for 30 min in 95% EtOH and stored at 4°C in 47% EtOH, 5 mM EDTA. Before usage, the tubing strips were rehydrated in H₂O for several hours at room temperature.

All liquid media for yeast experiments were prepared in glassware that was treated with 10% hydrochloric acid for at least 12 hrs (acid-washed glassware). For yeast media, addition of all components was done without the use of metal spatulas. Media was filtered through 0.2 μm membranes and additional components, BCS and CuSO₄, were added from separately filtered stock solutions. Fermentative media was either YPD (1% Yeast Extract, 2% Peptone, 2% glucose), SC (synthetic complete media with 2% glucose) or SC lacking lysine. Non-fermentative media was YPEG (1% Yeast Extract, 2% Peptone, 3% ethanol, 3% glycerol).

Agar media was prepared similarly using acid-washed glassware. Additional media components listed in figures were added after autoclaving and dissolving of agar, and just before pouring of plates. Agar media for hypoxic growth were supplemented with ergosterol and Tween-

80. A stock solution of ergosterol at 2 mg/ml was prepared in a solution of 50% ethanol and 50% Tween-80 and added to the media after autoclaving to achieve a final concentration of 20 µg/ml ergosterol, 0.5% Tween-80 and 0.5% ethanol.

Liquid culture growth curves

To determine doubling times shown in Fig 1 and Fig 7, following an overnight growth in SC or YPD media, cells were diluted to $OD_{600} = 0.2$ in fresh media, and grown at 30°C for up to 10 hrs. Cell density of the culture was measured every 2 hrs and doubling times were calculated from 2-8 hrs of growth, when cells were growing exponentially.

In growth experiments shown in Fig 2 and Fig 7D, following an overnight growth in YPD media, cells were diluted to $OD_{600} = 0.4$ in YPEG containing various concentrations of $CuSO_4$, and incubated at 30°C. Growth experiments shown in Fig 3 and Fig S2 were done similarly in SC-lys media containing various concentrations of $CuSO_4$. For growth shown in Fig 7E, following an overnight growth in SC-lys containing various concentrations of BCS, cells were diluted to $OD_{600} = 0.2$ in the respective media and incubated at 30°C. At 24 or 36 hrs, culture densities were measured and the total numbers of doublings in that period were calculated.

Spot tests

Following an overnight growth, cells were diluted to $OD_{600} = 0.3-0.4$ in YPD and grown at 30°C for 4-5 hrs to log phase ($OD_{600} = 1-2$). Cells were subsequently pelleted by centrifugation, washed and resuspended in water to $OD_{600} = 5$. Cells were then 10-fold serially diluted and 5 µL of cells were spotted on agar plates containing media and additives as indicated in the figures. Cells were incubated at 30°C for up to 7 days and imaged daily using an Epson document scanner. Because of differing growth rates in the various media conditions, images shown in the figures were captured when sufficient growth had occurred and growth differences could be assessed, and this ranged between 2-7 days. The exception is for media conditions that prevented growth (e.g. *ctr1*Δ strains in YPEG), in which images shown were captured at 3 days of incubation. Experiments in hypoxic conditions (Fig S2) were done using a 2.5 L sealable jar

and anaerobic gas generating sachets (AnaeroGen) designed to rapidly (i.e. within 30 minutes) generate an anaerobic environment achieving atmospheric oxygen of <1%. Following growth in liquid media as described above, cells were pelleted by centrifugation, washed and resuspended in water to $OD_{600} = 10$. Cells were then 5-fold serially diluted and 5 μ L of cells were spotted on agar plates with the media indicated in the figure. Media for normoxic and hypoxic conditions (Fig S2G) was supplemented with 20 μ g/ml ergosterol and 0.5% Tween-80 to support growth in low-oxygen conditions. The plates were then placed in the sealed hypoxic jar for 7 days at 30°C before capturing images, while normoxic control plates were incubated as usual.

Images shown are representative examples of at least two replicates performed on different days with the same clones.

Micrococcal nuclease digestion

Micrococcal nuclease (MNase) digestion assays were performed to assess chromatin accessibility as an indicator of nucleosome assembly and abundance. MNase digestion was performed similarly to as described previously (Rando, 2010). Following an overnight growth in SC media, strains indicated in Fig 1 and Fig 7 were diluted to $OD_{600} = 0.25$ in 100 mL of fresh SC. Cells were grown at 30°C for ~2 doublings, at which point 37% formaldehyde (Sigma) was added to each culture to a final concentration of 2%. Cells were fixed for 30 min at 30°C. Cells were then transferred to centrifuge bottles and 2.5 M glycine was added to quench formaldehyde reactivity to a final concentration of 125 mM. Cells were pelleted by centrifugation at 3700 rpm, for 10 min, at 4°C and subsequently resuspended in water. A volume corresponding to 2×10^9 cells was transferred to new 15 mL conical tubes, pelleted and washed with water, and resuspended to $OD_{600} = 12.5$ in Zymolyase buffer (1 M Sorbitol, 50 mM Tris pH 7.5) on ice. β -mercaptoethanol was added to a concentration of 10 mM. To initiate cell wall digestion, 2 mg of Zymolyase 100-T was added and cells were incubated at 30°C for 35 min. Spheroplasts were pelleted by centrifuging at 3700 rpm for 10 min at 4°C, and resuspended in 2 mL of MNase digestion buffer (1 M sorbitol, 50 mM NaCl, 10 mM Tris pH 7.5, 5 mM $MgCl_2$, 1 mM $CaCl_2$, 500 μ M spermidine,

0.075% Igepal CA-630, 10 mM BME). Resuspended spheroplasts were then equally distributed to 4 tubes, and varying amounts of MNase were added as indicated in the figures. Samples were incubated at 37°C for 20 min, at which point MNase was inactivated by the addition of 5X stop solution (5% SDS, 50 mM EDTA). Proteins were then digested by addition of 160 ug of proteinase K (Sigma), and formaldehyde crosslinks reversed, by incubation at 65°C for ~12 hrs.

DNA was purified by standard phenol-chloroform extraction methods. One volume of phenol:chloroform:isoamyl alcohol (25:24:1) was added to each sample, and the samples were centrifuged at 16,000xg for 5 min to separate the aqueous and phenol phases. The upper aqueous phase was transferred to a new tube, 3 M sodium acetate pH 5.5 was added to 300 mM final concentration, and nucleic acids were precipitated with isopropanol. Nucleic acid pellets were then resuspended in 60 µL Qiagen buffer EB (10 mM Tris, pH 8.5). MNase-digested DNA samples were treated with 10 ug of RNase A (Roche) for 1 hr at 37°C. Lastly, DNA samples were purified using the Wizard SV PCR purification kit (Promega) according to the manufacturer's protocol, and eluted in 30 µL of Qiagen buffer EB. Final DNA concentrations were determined using the Qubit DNA broad range assay (ThermoFisher) according to the manufacturer's protocol. ScreenTape images shown and quantified are representative examples of three replicate MNase digestions from separately grown cultures of the same cell clones.

MNase accessibility analysis

MNase-digested DNA samples were normalized by concentration, and visualized using the DNA ScreenTape assay on the TapeStation 2200 instrument (Agilent), according to the manufacturer's protocol. Using TapeStation Analysis software (Agilent) gel images were exported, without contrast adjustment, and saved in TIFF format. Pixel intensities along a line perpendicular to DNA bands and through the center of each lane were then quantified using FIJI (ImageJ 1.48k).

SDS-PAGE and Western Blotting

Whole cell protein extracts were prepared from 500 million cells growing exponentially in YPD medium. Cell pellets were resuspended in 2 mL of 0.2 M NaOH and incubated at room

temperature for 15 minutes. The samples were then centrifuged at 12,000 rpm for 5 minutes; pellets were resuspended in 200 μ L of SDS-PAGE loading buffer (50 mM Tris-HCl pH 6.8, 2% SDS, 10% glycerol, 1% β -mercaptoethanol) and boiled for 5 minutes. Lysates were cleared by centrifugation at 13,000 rpm for 5 minutes to remove debris. For SDS-PAGE and western blots shown in Fig 7, 4 μ g of lysate was used. Western blots were performed using the LI-COR Odyssey system. Primary antibodies to histone H3 and H4 were diluted in the recommended Odyssey buffer at 1:5000 and 1:800, respectively, and blots were incubated in diluted antibody at 4°C overnight. Signal quantifications were obtained using Image Studio Lite software.

Sample preparation for inductively-coupled plasma mass spectrometry (ICP-MS)

Cells from dense overnight cultures in SC or YPD media were diluted to $OD_{600} = 0.2-0.4$ and grown at 30°C for ~3 doublings in SC or YPD, or for 18 and 24 hrs in YPEG and SC-lys, respectively. Three replicate cultures were prepared for each sample. Cells ($4-12 \times 10^8$) were collected by centrifugation, and cell pellets were washed twice in 1 mM EDTA to remove cell surface-associated metals. This was followed by one wash in Nanopure Diamond filtered water to remove residual EDTA. Cell pellets were then stored at -20°C for 1-3 weeks prior to preparation for ICP-MS.

Plastic bottles and cylinders used for preparation of solutions for sample digestion were treated with 7-10% ACS grade nitric acid for 5 days at 50°C. Acid-washed materials were rinsed thoroughly with Nanopure water before use. Frozen cell pellets were thawed at room temperature and packed by centrifugation at 3000xg. Pellets were overlaid slowly (not to disrupt the pellet) with 70% Optima Grade nitric acid and digested at 65°C for 12-16 hrs. Prior to mass spectrometry, the digested samples were diluted with Nanopure water to a final concentration of 2% nitric acid and a final volume of 3-5 mL.

Inductively-coupled plasma mass spectrometry

Total Fe and Cu content was measured by inductively coupled plasma mass spectrometry on the Agilent 8800 ICP-QQQ in MS/MS mode. The most abundant isotopes of iron and copper

(i.e. Fe⁵⁶ and Cu⁶³) were used to determine the total cellular iron and copper levels. Iron was measured both directly, with hydrogen present in the collision/reaction cell, and indirectly, after mass-shift to FeO with oxygen present in the cell. While both methods produced similar results, the data presented here for iron are from oxygen mass-shift mode. Copper was measured directly in oxygen-mode. The metal content was determined in comparison to an environmental calibration standard (Agilent 5183-4688), which contains 100x higher concentration of Fe compared to Cu, more accurately reflecting biological samples. Every run was calibrated individually, ⁴⁵Sc or ⁸⁹Y were used as internal standards to compare the calibration with the analyzed samples. Average counts of 5 technical replicates were used for each calibration standard and each individual biological sample. The deviation in between technical replicates never exceeded 5%. Standard deviation in figures reflects the standard deviation between biological replicates (n = 3 - 6). Prepared calibration standards ranged from 10 ppt to 500 ppb for ⁶³Cu and 1 ppb - 50 ppm for ⁵⁶Fe. All Cu and Fe measurements in our study were within the calibrated linear ranges for Cu and Fe and well above the lower limits of detection, which were determined from multiple blank samples. We used ICP MassHunter software for ICP-MS data analysis.

RNA extraction

Following an overnight growth, cells were diluted in the various media conditions indicated in the figures. Cells grown in SC were diluted to OD₆₀₀ = 0.05 and grown for 5 doublings at 30°C, at which point they were growing exponentially. Cells grown in YPD and YPEG were diluted to OD₆₀₀ = 0.2 and grown for 3-4 doublings at 30°C, at which point they were growing exponentially. Cells in SC-lys media, with or without extra CuSO₄, were diluted to OD₆₀₀ = 0.4 and incubated at 30°C for 24 hrs, at which point they had reached OD₆₀₀ = 0.6–1.6. Approximately 1.5x10⁸ cells were collected by centrifugation and frozen at -20°C until further processing. RNA was extracted using previously published methods (Schmitt et al., 1990) with some modifications. Frozen cell pellets, without significant thawing, were resuspended in 440 µL of AE buffer (50 mM Na acetate

pH 5.2, 10 mM EDTA, 1% SDS), and RNA was extracted by addition of 440 μ L of 5:1 phenol:chloroform pH 4.5 (ThermoFisher) and incubation at 65°C for 4 min. Samples were then rapidly frozen in dry ice-ethanol, and centrifuged at 16,000xg to separate the aqueous and phenol phases. The aqueous supernatant (350 μ L) was transferred to a new tube, and re-extracted by addition of 300 μ L of 25:24:1 phenol:chloroform:isoamyl alcohol, and centrifuged as above to separate phases. 250 μ L was transferred to a new tube, 25 μ L of 3 M Na acetate pH 5.2 was added, and nucleic acids were ethanol-precipitated. Nucleic acid pellets were then resuspended in 100 μ L of nuclease-free water and stored at -20°C until further processing. RNA concentration was measured by Nanodrop 2000 microvolume spectrophotometer. Typical yield from this extraction method was about 30 μ g of total RNA. RNA extracted for subsequent RNA-seq analysis are from two replicates of cells grown on different days with different media batches. The exceptions are cells grown in SC (Fig 1) which are from three replicates, and cells grown in SC-lys+75 μ M CuSO₄ (Fig 3 and S2) which is from one experiment.

Sample preparation for poly-A RNA sequencing

Prior to preparing RNA-seq libraries for Illumina HiSeq sequencing, contaminating DNA was digested, and RNA quality was assessed. Total RNA (10 μ g) was treated with Turbo DNase according to the manufacturer's "Routine DNase treatment" procedures, in 50 μ L reaction volumes. Samples were incubated at 37°C for 30 min. Following DNase treatment and reagent inactivation, total RNA concentration was determined using the Qubit RNA broad range assay (ThermoFisher) according to the manufacturer's protocol. RNA quality was then assessed using the RNA ScreenTape assay on the TapeStation 2200 instrument (Agilent), according to the manufacturer's protocol with undiluted RNA samples. Using TapeStation Analysis software (Agilent), RNA Integrity Number equivalent (RINe) scores, which reflects the ratio of abundances of 28S, 18S, and sub-18S RNAs, were calculated. Only samples with RINe scores greater than 9 (out of 10) were used for sequencing library preparation.

RNA-sequencing libraries were then prepared either manually with the KAPA Stranded mRNA-seq library prep kit (KAPA Biosystems), or with automation, using the Illumina TruSeq Stranded mRNA Library Kit for NeoPrep (Illumina). Both library preparation procedures first isolate polyA⁺ mRNAs using oligo-dT beads. Isolated polyA⁺ RNAs are then chemically fragmented, and random primers are used in the first cDNA reverse transcription step. For both approaches, libraries were prepared according to the manufacturer's protocols, with the following important parameters. For libraries constructed using the KAPA kit, 250 ng of DNase-treated total RNA was used as input. Following the mRNA capture step, RNA was fragmented for 8 min at 94°C, which was designed to generate average library insert sizes of 100-200 bp. Illumina HiSeq-compatible adapters were ligated at reaction concentrations of 25 nM and ligation was performed for 15 min at 20°C. Following adapter ligation and post-ligation purification, library fragments were amplified with 15 PCR cycles, using the manufacturer's provided thermal cycling times and temperatures. For libraries constructed using Illumina's Neoprep automated library preparation system, 70 ng of DNase-treated total RNA was used as input. To maximize library product, we disabled the default library normalization step that occurs at the end of the automated library construction and quantification. The number of library amplification cycles was set to 15.

RNA-seq libraries were assessed for correct fragment size and the presence of adapter dimers, using the DNA ScreenTape assay on the TapeStation 2200 instrument (Agilent), according to the manufacturer's protocol. Average library sizes of ~270 bp were observed and deemed correct. Using TapeStation Analysis software (Agilent), library DNA concentrations were estimated. Libraries were then pooled for multiplexed sequencing at equimolar ratios. Because some libraries contained more than 1% adapter dimers, by concentration, the library pools were further purified using Agencourt RNAClean XP beads. One volume of beads, thoroughly resuspended, was added to the library pool, and allowed to incubate for 15 min at room temperature without perturbation. Beads were then magnetically isolated, and washed twice with 70% ethanol. Beads were air-dried for 5 min, and resuspended, off the magnet, in 30 µL of

resuspension buffer provided in TruSeq library preparation kits (Illumina, RSB, part # 15026770). Eluted DNA was transferred to a fresh 1.5 mL microcentrifuge tube. Bead-purified library pool DNA concentration was then measured using the Qubit DNA broad range assay (ThermoFisher) according to the manufacturer's protocol, and total DNA concentration was adjusted to 10 nM for Illumina sequencing.

mRNA-sequencing and data processing

High throughput sequencing was performed on Illumina's HiSeq 4000 system, with single-end 50 bp insert reads, and dedicated index reads. Total read count per library ranged from ~1.5-9 million. De-multiplexed reads, in FASTQ file format, were aligned to the R64-1-1 S288C reference genome assembly (sacCer3), downloaded from the UCSC database, using Tophat 2.0.9 (Kim et al., 2013). The "-g 1" parameter was used to limit the number of alignments for each read to one, the top-scoring alignment. In the case of a tie, the read was randomly distributed to one of the tied top-scoring alignments. Percentage of reads aligned once was greater than 90% in all cases.

Gene expression analysis

Gene expression values, in reads per kilobase per million mapped reads (RPKMs), for 6692 annotated open reading frames were calculated using SAMMate 2.7.4 (Xu et al., 2011). In calculating RPKM values, only reads that align to annotated exons were considered. Reads aligning to introns or intergenic regions were not counted in normalizing the read counts to the total number of mapped reads. Many of the 6692 annotated ORFs have no attributed function, localization, mutant phenotypes or interactions and are often labeled as "dubious" or "putative" in the Saccharomyces Genome Database (SGD). Furthermore, these putative ORFs typically have low expression values. We removed 1648 such ORFs from further analysis, and used the remaining 5044 ORFs for comparisons between groups.

RNA-sequencing gene sets

Genes that were analyzed as part of functional groups in Figure 2 and 3 are listed in table S3. Each gene set was constructed by downloading and merging gene ontology term gene lists from AmiGO 2 in March 2017. For the “copper homeostasis” and “iron homeostasis” gene sets, we further modified the lists by adding or removing genes based on literature review. The “copper homeostasis” set was generated starting with the following list: GO 0006878 – Cellular copper ion homeostasis. The “iron homeostasis” set was generated by starting with the following list: GO 0055072 – Iron ion homeostasis. The “electron transport and TCA cycle” set was generated by merging the following lists: GO 0022904 – Respiratory electron transport chain, and GO 0006099 – Tricarboxylic acid cycle. The “lysine biosynthesis” set was based on the following list: GO 0006553 – Lysine metabolic process. The “antioxidant” set was based on the following list: GO 0016209 – Antioxidant activity.

Oxygen consumption assay

Oxygen consumption rates were measured in whole cells using the Fiber Optic Oxygen Monitor, Model 110 (Instech laboratories Inc., Plymouth Meeting, PA). Cells from dense overnight cultures in YPD media were diluted in YPEG to $OD_{600} = 0.4$ and grown at 30°C for 24 hrs. Cells were then collected by centrifugation, and pellets concentrated in fresh YPEG media to achieve $OD_{600} = 1.5$ in a final volume of 500 μ L. The cell suspension was placed in an airtight chamber for oxygen consumption measurement. Oxygen level is sensed by the quenching of fluorescence of an indicator dye. The increase in fluorescence represents a decrease in oxygen levels in the sealed chamber and is a measure of cellular oxygen consumption. Cells were recorded for 5 minutes and the rate of oxygen consumption was determined for a one-minute steady state period during which fluorescence signal increased linearly.

Histone purification

Histone purification was performed essentially as described in (Luger et al., 1999) with some modifications. Histone H2A, H2B or H3 expression plasmids were transformed into BL21(DE3)pLysS cells (Agilent) and histone H4 expression plasmids into BL21(DE3). The entire

transformation reaction was plated onto 2xTY plates containing 100 µg/mL ampicillin. After 16 hrs of growth, the resistant cells were added to 1 L of 2xTY containing 100 µg/mL ampicillin and grown to $OD_{600} = 0.6$. A 100 µL aliquot was taken and analyzed by PAGE as a negative control sample. Expression was then induced with 0.4 µg/mL isopropyl β-D-1-thiogalactopyranoside for 3 hrs. A 50 µL aliquot was analyzed by PAGE to control expression levels. The remaining culture was centrifuged at 5000 rpm for 15 min and the pellet resuspended in 14 mL of Wash Buffer (50 mM Tris pH7.5, 100 mM NaCl, 1 mM EDTA, 1 mM Benzamidine and 5 mM β-mercaptoethanol), flash frozen and stored at -80°C. Frozen cells were thawed at 37°C and sonicated for 3 seconds on, 5 seconds off cycles for a total of 4-6 minutes at intensity setting 6 with a 550 Sonic Dismembrator (Fisher Scientific). All the following steps were conducted on ice. The lysate was centrifuged in a Sorvall SS-34 rotor at 4°C at 17000 rpm for 15 min and the supernatant was discarded. The pellet, which contains inclusion bodies, was resuspended in 20 mL Wash Buffer containing 1% Triton X-100 using a pre-chilled Dounce homogenizer and collected by centrifugation at 17000 rpm. This wash step was repeated once followed by two washes without Triton X-100. The clean inclusion bodies were solubilized in 100 µL of DMSO and further resuspended in 15 mL Unfolding Buffer (7 M Guanidinium-HCl, 20 mM Tris-HCl pH 7.5, 10 mM DTT). Histones were extracted for 2 hrs. Debris was removed by centrifugation at 17000 rpm for 20 minutes and the supernatant, containing extracted histones, was dialyzed at 4°C two times into 1 L of SAU200 Buffer (7 M Urea, 20 mM NaOAc pH 5.2, 200 mM NaCl, 1 mM EDTA, 5 mM β-Mercaptoethanol) for 1 hr, followed by one overnight dialysis. Histones in SAU200 Buffer were centrifuged in a Sorvall SS-34 at 10000 rpm for 10 min at 4°C to eliminate possible debris. The histones were then pre-cleared by running the preparation over a Hi-Trap Q-Sepharose column (GE healthcare), after which they were loaded onto a Hi-Trap SP-Sepharose column (GE healthcare) and eluted by a salt gradient from SAU200 Buffer (buffer A) to SAU600 Buffer (same as SAU200, but 600 mM NaCl) (buffer B). Aliquots of 1 mL were collected and 3 µL of each was analyzed by PAGE on a 15% gel. Fractions

containing pure histones were pooled and dialyzed 3 times against 4 L of 2 mM β -mercaptoethanol in water. Histones were then divided into aliquots, flash frozen and lyophilized.

Tetramer and nucleosome assembly

Please see above for critical notes on preparation of acid-washed glassware and buffers with low trace metal contaminants.

H3/H4 tetramer and H2A/H2B/H3/H4 octamer assembly was performed as described in (Luger et al., 1999) with some adjustments. Equimolar amounts of H3 and H4 (tetramer) or H2A, H2B, H3 and H4 (octamer) were dissolved in Unfolding Buffer (see above) at a concentration of 2 mg/mL total protein content and incubated for 1 hr with rotation at room temperature. Refolding was achieved by 2X 1 hr dialysis at 4°C against 1 L of Low Salt Refolding Buffer (500 mM NaCl, 10 mM Tris-HCl pH 7.5, 1 mM EDTA, 5 mM β -mercaptoethanol) (Tetramer) or High Salt Refolding Buffer (2 M NaCl, 10 mM Tris-HCl pH 7.5, 1 mM EDTA, 5 mM β -mercaptoethanol) (Octamer), followed by one dialysis >16 h. The refolded tetramer/octamer was centrifuged for 1 min at full speed at 4°C to eliminate any insoluble particles and purified by size exclusion chromatography on a HiLoad 16/600 Superdex 200 column (GE healthcare) at 1 ml/min in Low Salt SE-Buffer (500mM NaCl, 10 mM Tris-HCl pH7.5) (tetramer) or High Salt SE-Buffer (2 M NaCl, 10 mM Tris-HCl pH7.5) (octamer). Fractions containing the tetramer/octamer were concentrated using Amicon Ultra–15/Ultracel-10K centrifugal filters (Millipore). The flow-through buffer was used as negative control (“buffer”) in the copper reductase assay, described below (see also supplementary figure 3).

Nucleosome assembly was performed using a 0.95:1 molar ratio of octamer to DNA and following the protocol described in (Peterson, 2008). The 146 bp fragment of the 601 nucleosomal positioning sequence (Lowary and Widom, 1998) was PCR amplified using primers 601_146bp_F and 601_146_R. The amplified fragment was ethanol precipitated and the recovered DNA was purified by a 4 hr incubation in 500 mM NaCl/12% PEG6000 followed by a 20 min centrifugation at 16000xg at 4°C . The resulting pellet was resuspended in 100 μ L of 0.3 M NaOAc and

precipitated by addition of 250 μ l of 100% EtOH. The purified 146 bp DNA fragment (150 μ g/ml) was incubated with histone octamer (160.4 μ g/ml) in 2 M NaCl and dialyzed at 4°C for at least 6 hrs (and up to 16 hrs) consecutively into 1 L of the following buffers: Buffer 1 (1 M NaCl, 10 mM Tris-HCl pH7.5, 1 mM EDTA, 5 mM β -mercaptoethanol), Buffer 2 (0.8 M NaCl, 10 mM Tris-HCl pH7.5, 1 mM EDTA, 5 mM β -mercaptoethanol), Buffer 3 (0.6 M NaCl, 10 mM Tris-HCl pH7.5, 1 mM EDTA, 5 mM β -mercaptoethanol), Buffer 4 (0.0025 M NaCl, 10 mM Tris-HCl pH7.5, 1 mM EDTA, 5 mM β -mercaptoethanol). The assembled nucleosomes were further dialyzed 3 times for 1 hr each in 1 L of Buffer 5 (0.0025 M NaCl, 1 mM Tris-HCl pH7.5) at 4°C. Proper nucleosome assembly was confirmed by native PAGE and nucleosomes were used for copper reductase assay within a few hrs.

***In vitro* copper reductase assay**

The H3/H4 tetramer, or the same volume of control buffer, was resuspended to a final concentration of 1 μ M in 100 mM NaCl, 1 mM Neocuproine (Sigma) and 20 μ M BioUltra tris(2-carboxyethyl)phosphine (TCEP, Sigma), unless otherwise stated. The reaction was started by adding a mix of CuCl₂ and Tricine-HCl, pH 7.5, at final concentrations of 1 mM and 5 mM, respectively. The reaction was monitored by measuring absorbance at 448 nm every 0.5 seconds using a Hewlett-Packard HP8453 diode-array UV/Visible spectrophotometer. Nicotinamide Adenine Dinucleotide (NADH), Nicotinamide Adenine Dinucleotide Phosphate (NADPH), Dithiobutylamine (DTBA), Tris(hydroxypropyl)phosphine (THP) and glutathione (GSH) were also used as reducing co-factors, but showed high spontaneous reduction of copper (data not shown). Hence, TCEP was the reducing co-factor of choice during these studies, unless otherwise stated. Nucleosomes (0.4 μ M) were assayed under identical reaction conditions except for that the reaction was started with a mix of CuCl₂ and Tricine-HCl, pH 7.5, at final concentrations of 1 mM and 10 mM, respectively, and that the NaCl concentration was 300 mM.

QUANTIFICATION AND STATISTICAL ANALYSIS

The number of experimental replicates (n), and the observed significance levels are indicated in figure legends. All statistical analyses were performed using Graphpad Prism 5 or 7, unless otherwise stated. Significance values for pair-wise comparisons of doubling times (Fig 1C and 7C) were calculated using the Mann-Whitney test. Significance values for comparisons of the number of population doublings in Fig 2C, 7D and 7E and oxygen consumption rates in Fig 2C were calculated using the Holm-Sidak method for multiple t-tests, with alpha = 0.05. Significance values for comparisons of the number of population doublings in Fig 3C and S2H were calculated using a mixed model Two-Way ANOVA with Bonferroni post-hoc test for pair-wise comparisons. For inductively coupled mass spectrometry, 3-9 replicates were measured for each sample (n) from 1-3 separate experiments. Statistical testing for iron and copper measurements was done using unpaired Student's t- tests. For gene expression data, we averaged RPKM values from replicates and used mean values for calculation of global gene expression correlations (e.g. Fig 1D) and for analyzing gene sets (e.g. Fig 2E). For global correlations, Spearman's rank correlation coefficients were calculated. Significance values for pair-wise comparisons of gene expression levels of gene sets (e.g. Fig 2E) were calculated using the Mann-Whitney test. We also assessed differential gene expression, using the SAMMate RPKM values, for each gene and between WT and *H3^{H113N}* strains grown in SC media. Student's t-test was used to calculate p values with the Benjamini-Hochberg procedure to control the false discovery rate at 0.1. This analysis was performed using Microsoft Excel 2016. No genes were found to be significantly differentially expressed by this procedure. For MNase digestion profiles (Fig 1E), signal intensities measured using FIJI were scaled to DNA length using a gel migration distance-to-DNA fragment size calibration curve. Signal intensities were also normalized by dividing by the total lane intensity and multiplying by 1000. Curve fitting for enzymatic kinetic analysis was performed online using "mycurvefit" tool (<https://mycurvefit.com>), taking zero as starting value. Predicted values for 0.3 seconds were within 20% of the maximum values detected and used to calculate the initial velocities. These initial velocities were then transferred to Graphpad Prism version 5.01 and fitted

with the Michaelis-Menten non-linear regression function to determine enzymatic parameters. The “area under curve” non-linear regression function of the same software was used to determine the value of the area under progress curves for p value measurement by the t-test.

KEY RESOURCES TABLE

REAGENT or RESOURCE	SOURCE	IDENTIFIER
Antibodies		
Rabbit polyclonal anti histone H3 (C-terminal)	Active motif	Cat# 39163
Rabbit polyclonal anti histone H4	Abcam	Cat# 10158
IRDye® 800CW Goat anti-Rabbit IgG (H + L), 0.1 mg	LI-COR	Cat# 925-32211
Bacterial and Virus Strains		
BL(DE3)	Agilent Technologies	Cat# 200131
BL(DE3)pLysS	Agilent Technologies	Cat# 200132
Chemicals, Peptides, and Recombinant Proteins		
BD Bacto™ Dehydrated Culture Media Additive: Tryptone	Fisher Scientific	Cat# 211705
BD Bacto™ Dehydrated Culture Media Additive: Yeast Extract	Fisher Scientific	Cat# 212750
BD BBL™/Difco™ Bacto™ Media Additives/Ingredients/Reagents: Peptone	Fisher Scientific	Cat# 211677
BD™ Difco™ Yeast Nitrogen Base without Amino Acids and Ammonium Sulfate	Fisher Scientific	Cat# 233520
BD Bacto™ Dehydrated Agar	Fisher Scientific	Cat# 214010
SC Powder, 30 grams	Sunrise Science Products	Cat# 1300-30
SC-lys Powder, 30 grams	Sunrise Science Products	Cat# 13007-30
Ampicillin Sodium Salt	Sigma-Aldrich	Cat# A9518
Isopropyl β-D-thiogalactopyranoside	Goldbio.com	Cat# 12481C25
Ergosterol ≥95.0% (HPLC)	Sigma-Aldrich	Cat# 45480
Geneticin	Gibco	Cat# 11811-031
Bathocuproinedisulfonic acid disodium salt hydrate	Sigma-Aldrich	Cat# 146625
Copper(II) chloride	Sigma-Aldrich	Cat# C1654
Copper(II) sulfate pentahydrate	Sigma-Aldrich	Cat# C6283
Manganese Chloride Tetrahydrate (Crystalline/Certified ACS)	Fisher Scientific	Cat# M87-100
Iron(III) chloride hexahydrate	Sigma-Aldrich	Cat# 236489
Zinc sulfate heptahydrate	Sigma-Aldrich	Cat# 221376
Nitric Acid 67-69%, Optima™, for Ultra Trace Elemental Analysis	Fisher Scientific	Cat# A467
Nitric Acid (Certified ACS Plus)	Fisher Scientific	Cat# A200-212
Hydrochloric acid	Fisher Scientific	Cat# A144SI-212
Hydrochloric acid (ACS grade)	Sigma-Aldrich	Cat# 320331
ICP-MS Multi-element calibration standard	Agilent Technologies	Cat# 5183-4688
1000 ppm (µg/mL) Sulfur for ICP	Inorganic Ventures	Cat# CGS1
1000 ppm (µg/mL) Phosphorus for ICP	Inorganic Ventures	Cat# CGP1
1000 ppm (µg/mL) Scandium for ICP	Inorganic Ventures	Cat# CGSC1

100 ppm (µg/mL) Yttrium for ICP-MS	Inorganic Ventures	Cat# MSY-100PPM
Agencourt RNAClean XP beads	Beckman Coulter	Cat# A63987
Zymolyase® 100-T	Nacalai USA	Cat# 07665-55
Nuclease micrococcal from Staphylococcus aureus	Sigma-Aldrich	Cat# N5386
RNase A from bovine pancreas (RNASEA-RO ROCHE)	Sigma-Aldrich	Cat# 10109142001
Proteinase K from Tritirachium album	Sigma-Aldrich	Cat# P6556
Trizma Base (BioUltra)	Sigma-Aldrich	Cat# 93362
Sodium Chloride (BioUltra)	Sigma-Aldrich	Cat# 71376
Tris(2-carboxyethyl)phosphine hydrochloride (BioUltra)	Sigma-Aldrich	Cat# 75259
β-Mercaptoethanol (Pharmagrade)	Sigma-Aldrich	Cat# 07604
Tris(hydroxymethyl)phosphine	Sigma-Aldrich	Cat# 177881
Dihydrolipoic acid	Sigma-Aldrich	Cat# T8260
DL-Dithiothreitol	Goldbio.com	Cat# DTT25
(S)-2-Aminobutane-1,4-dithiol hydrochloride	Sigma-Aldrich	Cat# 774405
β-Nicotinamide adenine dinucleotide 2-phosphate reduced sodium salt	Sigma-Aldrich	Cat# N9660-15VL
β-Nicotinamide adenine dinucleotide reduced disodium salt hydrate	Sigma-Aldrich	Cat# N8129
L-Glutathione reduced	Sigma-Aldrich	Cat# G4251
Neocuproine	Sigma-Aldrich	Cat# N1501
Chelex 100 (Mol. Biol. Grade Resin)	Biorad	Cat# 142-1253
Ethylenediaminetetraacetic acid (99.99% trace metal basis)	Sigma-Aldrich	Cat# 431788
Poly(ethyleneglycol) 3500	Sigma-Aldrich	Cat# 202444
Poly(ethyleneglycol) 6000 (BioUltra)	Sigma-Aldrich	Cat# 81255
Sodium hydroxide (semiconductor grade)	Sigma-Aldrich	Cat# 306575
Sodium Acetate Trihydrate	Fisher Scientific	Cat# S209-500
Urea	Affimetrix/USB	Cat# 23036
Guanidine hydrochloride	Sigma-Aldrich	Cat# G3272
Critical Commercial Assays		
Stranded mRNA-Seq Kit, with KAPA mRNA Capture Beads	KAPA Biosystems	Cat# KK8420
TruSeq Stranded mRNA Library Prep Kit for NeoPrep	Illumina	Cat# NP-202-1001
D1000 ScreenTape	Agilent Technologies	Cat# 5067-5582
D1000 Sample Buffer	Agilent Technologies	Cat# 5067-5602
RNA ScreenTape	Agilent Technologies	Cat# 5067-5576
RNA ScreenTape Sample Buffer	Agilent Technologies	Cat# 5067-5577
Qubit dsDNA BR Assay Kit	ThermoFisher Scientific	Cat# Q32850
TURBO DNA-free Kit	ThermoFisher Scientific	Cat# AM1907

Quickchange II sitedirected mutagenesis kit	Agilent Technologies	Cat# 200523
Deposited Data		
Raw and analyzed data	This study	GEO: GSE100034
Experimental Models: Organisms/Strains		
See Table S1		
Oligonucleotides		
See Table S2		
Recombinant DNA		
pCORE (KanMX4-KIURA3)	(Storici and Resnick, 2006)	Addgene plasmid #72231
pRM200 (HHT2-HHF2, TRP1)	(Mann and Grunstein, 1992)	N/A
pYX55 (<i>HHT2-H113N</i> -HHF2, TRP1)	This study	N/A
pCAS (LYP1 sgRNA, kanMX)	(Ryan et al., 2014)	Addgene plasmid #60847
pCASK-HHT1-H113 (HHT1-H113 sgRNA, kanMX)	This study	N/A
pCASK-HHT2-H113 (HHT2-H113 sgRNA, kanMX)	This study	N/A
pCASK-CUP1-F8 (CUP1-F8 sgRNA, kanMX)	This study	N/A
pET3a-H3	(Luger et al., 1997)	N/A
pET3a-H4	(Luger et al., 1997)	N/A
pET3a-H2A	(Luger et al., 1997)	N/A
pET3a-H2B	(Luger et al., 1997)	N/A
pH3.2	This study	N/A
pH3.2-C110A	This study	N/A
pH3.2-H113N	This study	N/A
p601-12-177	(Dorigo et al., 2003)	N/A
Software and Algorithms		
SAMMate 2.7.4	(Xu et al., 2011)	http://sammate.sourceforge.net/
Tophat 2.0.9	(Kim et al., 2013)	https://ccb.jhu.edu/software/tophat/index.shtml
Agilent 2200 TapeStation Software A.02.01	Agilent Technologies	http://www.genomics.agilent.com/article.jsp?pagelid=9100002

MassHunter	Agilent Technologies	http://www.agilent.com/en-us/products/software-informatics/masshunter-suite/masshunter-masshunter-software
Prism	GraphPad Software	https://www.graphpad.com/scientific-software/prism/
Image Studio Lite	LI-COR	https://www.licor.com/bio/products/software/image_studio_lite/index.html
My Curve Fit (beta)	My Assays Ltd.	https://mycurvefit.com/
FIJI	(Schindelin et al., 2012; Schindelin et al., 2012)	https://imagej.net/Fiji/Downloads
Other		
AnaeroGen sachet	Thermo Scientific	Cat# AN0025
Falcon™ 15mL Conical Centrifuge Tubes	Corning Inc.	Cat# 352097
Spectra/Por standard RC dialysis tubing (50mm Nominal Flat Width)	Spectumlabs.com	Cat# 132665
Spectra/Por standard RC dialysis tubing (23mm Nominal Flat Width)	Spectumlabs.com	Cat# 132650
Hi-Trap Q-HP column	GE Healthcare	Cat# 17-1154-01
Hi-Trap SP-HP column	GE Healthcare	Cat# 17-1152-01
HiLoad 16/600 Superdex 200 column	GE Healthcare	Cat# 28989335
Amicon Ultra–15/Ultracel-10K centrifugal filters	Millipore	Cat# UFC901024

Chapter VI

Nucleosome Copper Reductase Activity is Required for SOD1 Function in Supporting Iron Metabolism

This chapter was written for inclusion in this dissertation. More investigations pertaining to this chapter is currently underway. Briefly, this chapter describes the role of the nucleosome copper reductase activity in iron metabolism. The novel function of the copper-dependent superoxide dismutase in mediating this connection is revealed. The significance of this role of copper in iron metabolism and the potential mechanistic links are discussed. This work also highlights the potentially far-reaching affects of the enzymatic activity of the nucleosome in cellular physiology and disease through its impact on iron-dependent essential processes.

I authored this chapter for inclusion in my dissertation. I am responsible for the literature review, drafting the article and the conception and design of the experiments. I conducted the experiments in collaboration with Oscar Campos.

The Nucleosome Copper Reductase Activity is Required for Sod1 Function to Support Iron Metabolism

Summary

The link between copper and iron metabolism has been described in many organisms, mainly through the role of copper in uptake and acquisition of iron. Here we describe the impact of nucleosome copper reductase activity on cellular iron requirement. We provide genetic and molecular evidence that impairment of the nucleosome copper reductase activity makes cells sensitive to iron deficiency. This is not due to disruption of the copper-dependent iron uptake machinery in *Saccharomyces Cerevisiae*. Instead, we have discovered a novel function of the Cu-Zn superoxide dismutase (SOD1) in supporting growth under iron-deficient conditions. This function of SOD1 is dependent on provision of cuprous ions by the nucleosome.

Introduction

Iron, one of the most abundant elements on Earth and a catalyst for the formation of life on this planet, is an essential metal for all biological systems. The use of iron as a co-factor in cellular functions is ubiquitous. It is required for wide-ranging processes including DNA replication and repair, ribosome biogenesis, metabolic catalysis, and oxygen transport^{1,2}. Iron may exist in several oxidation states, -2 to +6, with +2 (ferrous) and +3 (ferric) being the most common and biologically relevant. The redox property of iron makes it suitable for a variety of cellular chemistry involving electron loss or gain³.

Biological systems utilize iron either as diiron clusters (2 Fe²⁺ ions) or in prosthetic groups such as iron-sulfur clusters and heme. The speciation of iron and its redox state in the cell is an important determinant of its bioavailability. The bioavailability of iron is also affected by its oxidation state⁴. Oxidized iron (Fe³⁺) is the prominent form found in the aerobic environment established on Earth since the Great Oxygenation Event. The ferric form of iron is poorly soluble and forms precipitates with inorganic molecules such as phosphate⁵. Organisms have devised mechanisms for enhancing the bioavailability and acquisition of Fe³⁺. These include cell-surface reduction of iron to soluble Fe²⁺, acidification of the extracellular environment to solubilize ferric iron, and the use of ferric-binding siderophores^{4,6}.

Assimilatory iron reduction—the process of enzymatic iron reduction for uptake and intracellular incorporation—has been found in nearly all organisms. Most ferric reductases in eukaryotes are associated with cellular membranes that make Fe²⁺ available for a variety of iron transport systems⁶. However, a major iron uptake pathway requires its conversion back to Fe³⁺ once ferric reductases have reduced it to soluble Fe²⁺. This system involves a multicopper ferroxidase that oxidizes Fe²⁺ to Fe³⁺ for transport by specific ferric transporters⁷. The copper-dependent mechanism

of iron acquisition partly accounts for the interdependency observed between the homeostasis of these two metals in eukaryotes as well as a number of bacteria. This system has been well-defined in *Saccharomyces Cerevisiae* and includes the multicopper ferroxidase, Fet3, coupled to the ferric transporter Ftr1. Fet3 contains four copper ions and depends on the redox property of copper for its iron oxidase activity^{7,8}. Fet3-Ftr1 system serves as the high affinity iron uptake machinery in yeast and is induced under iron-limiting conditions. A second homologous ferroxidase, Fet5, is involved in mobilization of iron from the vacuole, a major organelle for metal storage⁹. The analogous multicopper ferroxidases in mammals, hephaestin and ceruloplasmin, are also involved in iron uptake and iron mobilization between organs¹⁰.

Given the requirement of copper for iron uptake, disruption of copper homeostasis may impact iron metabolism. The significance of the molecular link between copper and iron homeostasis is highlighted by iron disorders resulting from copper deficiency or genetic lesions in ceruloplasmin¹¹. Copper is an essential transition metal and its homeostasis is tightly regulated to ensure efficient utilization while preventing toxicity. In addition to abundance, bioavailability of copper is a critical consideration for all copper-dependent processes. Copper, much like iron, is a redox active transition metal and is utilized as a co-factor either in its cupric (Cu^{2+}) or in cuprous (Cu^{1+}) form for redox chemistry. The oxidation state of copper is also important for proper intracellular trafficking, which is mediated by chaperons that carry the cuprous form of copper¹². Thus reduced copper is the bioavailable form of copper.

It is presumed that the reducing environment of the eukaryotic cell is responsible for maintaining the pool of cuprous ions. This presumption is based on the unproven idea that the reducing state of the cytoplasm non-specifically affects oxidation state of all things within it. In the case of copper, the recently described function of the yeast and human nucleosome as a cupric reductase provides evidence for an active mechanism for ensuring copper is reduced for use by the

cell and mitochondria (Attar 2017, submitted). The enzymatic function of the eukaryotic nucleosome was shown to be important for two copper-dependent pathways, mitochondrial respiration and superoxide dismutase activity. Here, we asked whether the nucleosome copper reductase activity provides bioavailable copper for iron homeostasis.

We provide genetic and molecular evidence that mutation of H3H113 to asparagine in the H3-H3' dimerization interface of the nucleosome, the likely active site for the cupric reductase activity, leads to poor survival in iron-limiting conditions in *S. Cerevisiae*. This phenotypic defect cannot be accounted for by diminished intracellular iron levels or iron uptake capacity, suggesting that the copper-dependent iron transport system is unaffected by the H3H113N mutation. Interestingly, we found that Cu-Zn superoxide dismutase 1 (Sod1) contributes to the ability of cells to survive iron limitation. The previously unrecognized role of Sod1 in iron deficiency is dependent on the provision of reduced copper ions by the nucleosome. Our data reveal a novel pathway through which the eukaryotic nucleosome copper reductase activity contributes to iron metabolism via maintaining Sod1 function without affecting iron uptake and acquisition.

The link between Sod1 function and the integrity of iron metabolism described here has important implications for understanding the pathogenic mechanisms underlying many diseases with alterations in these two cellular activities. Sod1 is implicated in certain human pathologies, most notably amyotrophic lateral sclerosis, as well as Parkinson's disease and cancer^{13,14}. The occurrence of iron deficiency is widespread and has implication for diseases ranging from anemias to neurodegeneration and numerous chronic diseases¹⁵. The role of histones in providing copper for Sod1 functions, including its role in iron metabolism, can provide new insights into such diseases and a novel perspective for understanding the role of copper in iron homeostasis.

Results

Histone H3 H113 residue is required for growth in iron limiting conditions. Histidine residue 113 in histone H3 lies at the interface between the two H3 molecules at the core of the nucleosome. We previously showed that the mutation of this histidine to asparagine (H113N) disrupts copper-dependent processes in *S. Cerevisiae* through potential defects in the copper reductase activity of the nucleosome. Given the copper dependency of the high affinity iron uptake system through the function of Fet3 in *S. Cerevisiae*, we asked whether the H113N mutation results in diminished iron uptake abilities and survival in iron-limiting conditions.

We examined the ability of $H3^{H113N}$ mutant to grow in iron-deplete media using the iron chelator, bathophenanthrolinedisulfonic acid (BPS), which limits iron availability for cellular uptake. Although $H3^{H113N}$ has a slower growth rate than the wild type counterpart (WT) in rich media, it does not show enhanced sensitivity to iron depletion, even at BPS concentrations that significantly reduce growth (Figure 1A).

Upon iron depletion, a comprehensive cellular response is mediated by the iron-responsive transcription factor Aft1, that induces the expression of multiple iron uptake systems and downregulates non-essential iron consuming processes^{16,17}. We reasoned the function of the multicopper ferroxidase, Fet3, may still be dependent on nucleosome copper reduction but a defect may be difficult to detect given the robust presence of other iron uptake systems and the hypomorphic nature of the H113N allele. To test the functionality of Fet3 more directly, we deleted the copper-transporting P-type ATPase, Ccc2, that is needed to provide copper into the endomembrane system for constitution of enzymatically active Fet3¹⁸. As expected *ccc2Δ* strains are more sensitive to iron depletion when compared with the wildtype counterpart. The combination of H3H113N with *ccc2Δ* exacerbates the growth defect in iron-limiting conditions (Figure 1B). This defect is rescued by addition of excess copper to the media suggesting a copper-related deficiency in

H3^{H113N}cc2Δ compare to *cc2Δ* alone in iron-limiting conditions. Deletion of *AFT1* to disable the overall transcriptional response to iron depletion significantly reduces growth in iron-limited media. The defect of *aft1Δ* strain in iron limitation is recovered by addition of exogenous copper; however, more copper is needed to achieve a similar rescue in *H3^{H113N}aft1Δ* (Figure 1B). This further highlights the copper-dependent defect in strains harboring H3H113N.

Deletion of *CTR1*, a primary copper transporter renders cells sensitive to iron depletion, confirming the known requirement of copper for Fet3 activity and iron uptake¹⁸ (Figure 1C). Similar to *cc2Δ* and *aft1Δ* backgrounds, the H3H113N mutation significantly reduces growth in iron depletion when combined with *ctr1Δ*. The greater defect of *H3^{H113N}ctr1Δ* compared with *ctr1Δ* is recovered by addition of excess exogenous copper (Figure 1C).

The reduced survival upon iron limitation in the context of H113N histone H3 is not due to differences in gene expression, since strains harboring H3H113N mutation have similar global gene expression patterns as the WT counterpart (Figure 1D). Importantly, the expression of genes involved in iron homeostasis and the induction of the iron-deficiency response mediated by Aft1 is similar between strains with WT and H113N histone H3 (Figure 1E). Altogether our data suggest that H3H113 is required to contend with iron-limiting conditions, likely through the nucleosome copper reductase activity and provision of bioavailable copper.

Diminished survival of H3H113N-harboring strains in iron limitation is not due to differences in total cellular iron content or iron uptake capacity. We hypothesized that defective iron uptake due to decreased copper provision for Fet3 may be the reason H3H113N mutant sensitizes cells to iron limitation. To determine the mechanism by which nucleosome copper reductase activity may be contributing to iron homeostasis, we first measured intracellular iron

content using inductively-coupled mass spectrometry (ICP-MS). Deletion of *AFT1* or *CTR1* results in an expected reduction in steady-state levels of intracellular iron in rich media (Figure 2A). When grown in BPS-containing media, a further reduction in iron levels is detected (Figure 2A). However, strains harboring H3H113N have similar levels of intracellular iron as the WT counterpart both in iron-replete and iron-deplete conditions. Surprisingly, addition of exogenous copper to low iron media, which we show to enhance growth, does not lead to a detectable increase in intracellular iron levels (Figure 2A). These findings challenge the idea of a defect in iron uptake or accumulation as the underlying problem in $H3^{H113N}ctr1\Delta$ and $H3^{H113N}aft1\Delta$.

Steady-state iron measurements in *aft1* Δ and *ctr1* Δ backgrounds, especially in low iron conditions, are significantly lower than the wildtype counterparts. These measurements in some cases fall close to or below the lower limit of the linear range in our ICP-MS experiments. This poses a technical problem for accurate detection of differences between strains. But even if H3H113N-harboring strains have lower levels of iron than their WT counterparts, it is unclear how such small differences would be biologically meaningful.

We therefore decided to assess the high affinity iron uptake machinery by testing the ability of strains with WT or H113N histone H3 to functionally induce this system in response to a period of iron limitation. To do so, strains were grown in BPS-containing media to deplete iron, leading to induction of the iron deficiency response and upregulation of iron uptake mechanisms, most notably the Fet3-mediated high affinity uptake system. After a period of growth in low iron, cells were transferred to iron-replete media and intracellular iron was measured. Total cellular iron content during the depletion phase is reduced equally in both WT and $H3^{H113N}$ (Figure 2B). Upon iron addback, an increase in intracellular iron is observed as a result of the activation of the iron deficiency response during the depletion phase. However, WT and $H3^{H113N}$ increase intracellular iron to the same level (Figure 2B). Similarly, iron uptake after a period of depletion in the background of

ctr1Δ or *ccc2Δ* is identical between strains harboring WT and H113N histone H3 (Figure 2C). To further limit copper availability for Fet3 activation, copper chelator Bathocuproinedisulfonic acid (BCS) was used during iron addback for experiments done with *ccc2Δ* strains. However, even in such copper-limiting media no iron uptake defect was observed in *H3^{H113N}ccc2Δ* compared with *ccc2Δ* (Figure 2C). These findings are in agreement with steady-state measurements also revealing wildtype levels of iron in the context of H3H113N. Despite diminished survival conferred by H3H113N mutation in iron-limiting conditions, we failed to reveal a defect in iron uptake capacity and iron accumulation in this context. This suggests that the copper-related defect of *H3^{H113N}* strains in coping with iron depletion cannot be accounted for by limited Fet3 activity for iron uptake.

Sod1, not the multicopper ferroxidase Fet3, is dependent on H3H113 for supporting iron metabolism. Since the functionality of the high affinity iron uptake system and hence Fet3 is intact in *H3^{H113N}*, we wondered whether other components of iron metabolism are dependent on utilization of copper. The Fet3-related multicopper ferroxidase, Fet5, and the ferric transporter Fth1 form a complex analogous to Fet3-Ftr1 on the vacuolar membrane. Fet5 uses the same copper-dependent redox mechanism as Fet3 for transport of iron across the vacuolar membrane into the cytoplasm¹⁹. This intracellular iron transport system is induced by iron limitation in an Aft1-dependent manner and can contribute to iron metabolism by allowing the utilization of stored vacuolar iron⁹. We deleted *FET3* alone and in combination with *FET5* in the context of WT or H113N histone H3. Deletion of *FET3* renders cells defective in low iron conditions, while deletion of *FET5* has a minor effect alone and does not enhance the growth defect of *fet3Δ* strains (Figure 3A). Interestingly, the growth defect in low iron associated with H3H113N is observed in absence of *FET3* (Figure 3A). In addition, exogenous copper can rescue the growth defect of *fet3Δ* strains

(Figure 3A). These genetic data further support the iron uptake results and suggest the contribution of histones to a Fet3-independent, copper-dependent pathway for iron metabolism.

Iron metabolism and utilization depends not only on the intracellular concentration but also proper trafficking, storage and speciation of iron⁴. An essential species of iron used ubiquitously as a co-factor in all forms of life is the iron-sulfur (Fe-S) cluster prosthetic group²⁰. The properties of Fe-S clusters such as oxidation states and the local protein environment are important for the function of these co-factors in diverse biological reactions²¹. The activity of these co-factors is therefore sensitive to oxidants. Superoxide dismutase 1, as one of the major cytosolic antioxidant defense systems, is important for protecting Fe-S clusters²¹⁻²³. For instance, Sod1 is required for maintaining the activity of Fe-S cluster containing enzymes in certain amino acid biosynthetic pathways, explaining the auxotrophy of *sod1Δ* for those amino acids²².

The integrity of Fe-S clusters and the potential protective role of Sod1 may be even more imperative when iron is limiting. Since the nucleosome copper reductase activity has been shown to be required for optimal Sod1 function, we questioned whether in iron limitation suboptimal Sod1 function underlies the poor survival of strains harboring H3H113N. Deletion of SOD1 in the context of WT or H113N histone H3 results in a growth defect in iron limitation suggesting a requirement of this enzyme for iron metabolism (Figure 3B). In contrast to what we observed in strain backgrounds null for components of the iron regulon, *H3^{H113N}sod1Δ* does not show any additional defect in iron-deplete conditions compared to *sod1Δ* alone (Figure 3B). This suggests that the enhanced defect in coping with iron depletion conferred by H3H113N may be attributed to Sod1.

Addition of exogenous copper rescues the growth defect of *sod1Δ* and *H3^{H113N}sod1Δ* similarly, through the activation of an intact Fet3-Ftr1 uptake system in both strains (Figure 3B). Combination of FET3 and SOD1 deletion leads to an even greater growth defect in low iron than

the deletion of either gene alone (Figure 3C). Interestingly, the double deletion abrogates the copper-mediated rescue in low iron media regardless of the histone allele (Figure 3C). This finding strongly indicates that the added exogenous copper is utilized by these two independent pathways to support growth in iron limitation. While both high-affinity iron uptake system and Sod1-mediated antioxidant defense are required for supporting growth under iron limitation, the enzymatic activity of the nucleosome only impacts the latter. These data indicate that the enzymatic activity of the nucleosome can have far-reaching effects on numerous biological processes through supporting Sod1 activity and the iron metabolome.

Discussion

The link between iron and copper metabolism has been appreciated for decades. The notion that copper can interfere with iron metabolism through competition for uptake or displacement of protein-bound iron is certainly a consideration when copper is in excess or improperly handled^{24,25}. The more intricate dependence of iron homeostasis on copper is an intriguing topic of study. The discovery of multicopper ferroxidases involved in iron acquisition and homeostasis in numerous organisms have provided a molecular explanation for this connection^{26,27}.

More recently, sparse evidence suggesting a connection between iron homeostasis and oxidative stress that goes beyond iron-mediated oxidative stress have been put forth. Deficiencies in iron homeostasis achieved by limiting iron abundance, either via deletion of components of the iron regulon in yeast (e.g. Fet3) or use of iron chelators, have been shown to render cells sensitive to oxidants²⁸. Although other interpretations can be offered, these findings can suggest a vulnerability to oxidative damage in iron deprivation or a requirement of iron for antioxidant defense. Conversely, oxidative stress partially induces the iron deficiency response and plays a role in activating Aft1 in yeast^{28,29}. Although more work is required to understand the underlying

mechanisms, these findings suggest a regulatory link between iron metabolism and cellular redox states.

Superoxide dismutase 1, a major contributor to redox homeostasis, has been shown to affect iron homeostasis as its deletion results in upregulation of genes involved in iron uptake³⁰. Vulnerability of iron-sulfur clusters to oxidation in the absence of Sod1 anti-oxidant activity is suggested to account for these observations. It is well established that disruptions in Fe-S cluster biogenesis or abundance, as may be the case in absence of Sod1, lead to the activation of the iron regulon^{31,32}. Reactive oxygen species can oxidize Fe-S clusters and bring about remarkable conformational changes leading to disassembly, inactivation or interconversion between different Fe-S cluster forms²¹. In all cases, the activity of these essential iron co-factors can be diminished or altered by oxidative stress and may be dependent on the function of Sod1. We now provide evidence for the requirement of the highly conserved eukaryotic Cu-Zn Sod1 for surviving iron limitation in the model organism *S. Cerevisiae*. This requirement may reflect the importance of Sod1 function in protecting Fe-S clusters when iron is limiting. We further reveal a novel role of the copper reductase enzymatic activity of the nucleosome in iron metabolism through supporting Sod1 function, rather than supporting the high affinity iron uptake system.

The role of copper in ensuring proper iron metabolism has so far been mainly appreciated by its impact on the function of multicopper ferroxidases. The involvement of superoxide dismutase in supporting the iron metabolome reveals another layer of connection between these two metals. This finding expands the interdependency between the functions and homeostasis of iron and copper in eukaryotes.

The newly discovered function of histones in copper homeostasis may open a window into other possible links between bioavailability of copper and iron metabolism. A potential crosstalk between the nucleosome and the iron metabolome can be hypothesized which could regulate the

copper reductase activity in response to cellular iron status. In such crosstalk regulation, lower levels of iron may increase the nucleosome copper reductase activity to meet the demand for cuprous ions by Sod1 to protect the remaining Fe-S clusters from oxidative damage. Whether the nucleosome can more directly affect iron metabolism is also an intriguing notion. Although the reductase activity of the nucleosome seems to be specific to copper, the possibility of iron reduction cannot be fully ruled out. Nucleosome-catalyzed ferric reduction can theoretically result in significant changes in the overall iron redox of the cell and thus its utilization in prosthetic groups such as heme and Fe-S clusters.

Our data indicate that provision of Cu^{1+} by nucleosomes for intracellular copper-dependent processes may be specific; however, it is unclear what determines this specificity. We postulate the idea of functional separation between potentially distinct intracellular pools of copper. It is intriguing to investigate whether such putative functional separation stems from compartmentalization of copper or of copper-dependent cellular components. Copper-dependent processes in the mitochondrial and cytoplasmic compartments, respiration and Sod1 function, respectively, but not the endomembrane compartment (i.e. Fet3 activation) seem to be dependent on the copper reductase activity of the nucleosome. However, it is important to note that the lack of defect in iron uptake in our system may not completely rule out the dependency of this copper-mediated pathway on the nucleosome copper reductase activity. The H113N mutation investigated in this study may represent a mild disruption of the copper reductase activity, whereby still maintaining sufficient cuprous ion generation for utilization by Fet3. Further investigation of the nucleosome enzymatic activity is required to address this possibility.

Viewing this through an evolutionary lens, one might also hypothesize that the specificity is driven by a potential advantage bestowed on the bacterial symbiont and/or the host during eukaryogenesis by histone copper reductase activity. The archaeal host for endosymbiosis possessed

ancestral nucleosomes³³ which may have harbored copper reductase capacity. Histones, by supplying copper specifically for respiration and Sod1 function, can more directly support and tolerate mitochondrion-related processes such as the electron transport chain. Respiration by the mitochondria can be a source of oxidants which may impose an additional pressure for protection of Fe-S clusters³⁴. Iron-sulfur clusters are not only synthesized in the mitochondria but are also required for mitochondrial respiration²⁰. The integrity of Fe-S clusters is therefore a critical parameter for mitochondrial function and even more so for cellular fitness in the face of mitochondrial respiration. Histones may have been important for mediating this fitness while supporting the symbiont by providing copper for electron transport chain and Sod1. Whether or not this function served as an evolutionary force for the presence of histones in early eukaryotes, it is clear that our knowledge of the nucleosome copper reductase activity in modern eukaryotes is limited. More investigation is warranted to better understand the impact of this novel function of histones on metal homeostasis. Nonetheless, given the essential nature of iron for diverse cellular processes, the enzymatic activity of the nucleosome in supporting iron metabolism can have far-reaching effects for eukaryotic biology, human physiology and disease.

FIGUR LEGENDS

Figure 1. H3H113N mutation reduces fitness in iron limiting conditions. A) Spot growth assays in iron-replete SC (synthetic complete media) and iron-deplete SC achieved using the iron chelator bathophenanthrolinedisulfonic acid (BPS). B) and C) Spot growth assays in iron-deplete media with and without additional exogenous CuSO₄. Iron and copper concentrations in SC are ~ 1.2 and 0.25 μM, respectively. D) Scatterplots of average global gene expression values from exponentially growing cells in SC and SC containing BPS, with Spearman's rank correlation coefficient (r_s) as indicated. E) Average mRNA expression levels for genes involved in iron homeostasis in iron replete and deplete growth conditions from two independent experiments.

Figure 2. Histone H3 H113 residue is not required for iron accumulation or iron uptake in response to iron deprivation. A) Intracellular iron content of cells grown in the indicated media for 3-4 doublings. Bar graphs represent mean ± SD from 3-6 replicate cultures. B) and C) Assay for iron uptake capacity showing intracellular iron content from exponentially growing cells in SC and cells grown in SC containing BPS for 2-3 doublings followed by incubation in SC for 1 population doubling (B) or 1 hour (C). Note: the copper chelator Bathocuproinedisulfonic acid (BCS) is used to deplete copper during iron addback for experiments done with *wc2Δ* strains to further limit copper availability for Fet3 activation.

Figure 3. Sod1 is protective in iron deficient conditions and is dependent on the copper reductase activity of the nucleosome in contrast to Fet3. A) Spot growth assays in SC and SC containing BPS with and without additional CuSO₄. B) and C) same as (A) for the indicated strains.

Methods

Spot tests

Following an overnight growth, cells were diluted to $OD_{600} = 0.3-0.4$ in YPD and grown at 30°C for 4-5 hrs to log phase ($OD_{600} = 1-2$). Cells were subsequently pelleted by centrifugation, washed and resuspended in water to $OD_{600} = 5$. Cells were then 10-fold serially diluted and $5\ \mu\text{L}$ of cells were spotted on agar plates containing media and additives as indicated in the figures. Cells were incubated at 30°C for up to 7 days and imaged daily using an Epson documentscanner. Because of differing growth rates in the various media conditions, images shown in the figures were captured when sufficient growth had occurred and growth differences could be assessed, and this ranged between 2-7 days.

RNA extraction

Following an overnight growth, cells were diluted in the various media conditions indicated in the figures. Cells grown in SC were diluted to $OD_{600} = 0.05$ and grown for 5 doublings at 30°C , at which point they were growing exponentially. Approximately 1.5×10^8 cells were collected by centrifugation and frozen at -20°C until further processing. RNA was extracted using previously published methods (Schmitt et al., 1990) with some modifications. Frozen cell pellets, without significant thawing, were resuspended in $440\ \mu\text{L}$ of AE buffer (50 mM Na acetate pH 5.2, 10 mM EDTA, 1% SDS), and RNA was extracted by addition of $440\ \mu\text{L}$ of 5:1 phenol:chloroform pH 4.5 (ThermoFisher) and incubation at 65°C for 4 min. Samples were then rapidly frozen in dry ice-ethanol, and centrifuged at $16,000 \times g$ to separate the aqueous and phenol phases. The aqueous supernatant ($350\ \mu\text{L}$) was transferred to a new tube, and re extracted by addition of $300\ \mu\text{L}$ of

25:24:1 phenol:chloroform:isoamyl alcohol, and centrifuged as above to separate phases. 250 μ L was transferred to a new tube, 25 μ L of 3 M Na acetate pH 5.2 was added, and nucleic acids were ethanol-precipitated. Nucleic acid pellets were then resuspended in 100 μ L of nuclease-free water and stored at -20°C until further processing. RNA concentration was measured by Nanodrop 2000 microvolume spectrophotometer. Typical yield from this extraction method was about 30 μ g of total RNA. RNA extracted for subsequent RNA-seq analysis are from two replicates of cells grown on different days with different media batches.

Sample preparation for poly-A RNA sequencing

Prior to preparing RNA-seq libraries for Illumina HiSeq sequencing, contaminating DNA was digested, and RNA quality was assessed. Total RNA (10 μ g) was treated with Turbo DNase according to the manufacturer's "Routine DNase treatment" procedures. RNA-sequencing libraries were then prepared either manually with the KAPA Stranded mRNA-seq library prep kit (KAPA Biosystems), or with automation, using the Illumina TruSeq Stranded mRNA Library Kit for NeoPrep (Illumina). Both library preparation procedures first isolate polyA+ mRNAs using oligo-dT beads. Isolated polyA+ RNAs are then chemically fragmented, and random primers are used in the first cDNA reverse transcription step. For both approaches, libraries were prepared according to the manufacturer's protocols.

mRNA-sequencing and data processing

High throughput sequencing was performed on Illumina's HiSeq 4000 system, with singleend 50 bp insert reads, and dedicated index reads. Total read count per library ranged from ~1.5-9 million. De-multiplexed reads, in FASTQ file format, were aligned to the R64-1-1 S288C reference genome assembly (sacCer3), downloaded from the UCSC database, using Tophat 2.0.9 (Kim et al., 2013).

The “-g 1” parameter was used to limit the number of alignments for each read to one, the top-scoring alignment. In the case of a tie, the read was randomly distributed to one of the tied top-scoring alignments. Percentage of reads aligned once was greater than 90% in all cases.

Gene expression analysis

Gene expression values, in reads per kilobase per million mapped reads (RPKM), for 6692 annotated open reading frames were calculated using SAMMate 2.7.4 (Xu et al., 2011). In calculating RPKM values, only reads that align to annotated exons were considered. Reads aligning to introns or intergenic regions were not counted in normalizing the read counts to the total number of mapped reads. Many of the 6692 annotated ORFs have no attributed function, localization, mutant phenotypes or interactions and are often labeled as “dubious” or “putative” in the Saccharomyces Genome Database (SGD). Furthermore, these putative ORFs typically have low expression values. We removed 1648 such ORFs from further analysis, and used the remaining 5044 ORFs for comparisons between groups.

Sample preparation for inductively-coupled plasma mass spectrometry (ICP-MS)

Cells from dense overnight cultures in SC media were diluted to OD₆₀₀ = 0.2-0.4 and grown at 30°C for ~3 doublings in SC or SC containing the iron chelator, bathophenanthrolinedisulfonic acid (BPS). Three replicate cultures were prepared for each sample. Cells (4-12 x 10⁸) were collected by centrifugation, and cell pellets were washed twice in 1 mM EDTA to remove cell surface-associated metals. This was followed by one wash in Nanopure Diamond filtered water to remove residual EDTA. Cell pellets were then stored at -20°C for 1-3 weeks prior to preparation for ICP-MS. Plastic bottles and cylinders used for preparation of solutions for sample digestion were treated with 7-10% ACS grade nitric acid for 5 days at 50°C. Acid-washed materials were rinsed

thoroughly with Nanopure water before use. Frozen cell pellets were thawed at room temperature and packed by centrifugation at 3000xg. Pellets were overlaid slowly (not to disrupt the pellet) with 70% Optima Grade nitric acid and digested at 65°C for 12-16 hrs. Prior to mass spectrometry, the digested samples were diluted with Nanopure water to a final concentration of 2% nitric acid and a final volume of 3-5 mL.

Inductively-coupled plasma mass spectrometry

Total Fe content was measured by inductively coupled plasma mass spectrometry on the Agilent 8800 ICP-QQQ in MS/MS mode. The most abundant isotopes of iron (i.e. Fe56) was used to determine the total cellular iron and copper levels. Iron was measured both directly, with hydrogen present in the collision/reaction cell, and indirectly, after mass-shift to FeO with oxygen present in the cell. While both methods produced similar results, the data presented here for iron are from oxygen mass-shift mode. The metal content was determined in comparison to an environmental calibration standard (Agilent 5183-4688) reflecting biological samples. Every run was calibrated individually, 45Sc or 89Y were used as internal standards to compare the calibration with the analyzed samples. Average counts of 5 technical replicates were used for each calibration standard and each individual biological sample. The deviation in between technical replicates never exceeded 5%. Standard deviation in figures reflects the standard deviation between biological replicates (n = 3 - 6). Prepared calibration standards ranged from 1 ppb - 50 ppm for ⁵⁶Fe. All Fe measurements in our study were well above the lower limits of detection, which was determined from multiple blank samples. We used ICP MassHunter software for ICP-MS data analysis.

Liquid cultures for iron uptake assays

To assess iron uptake capacity, following an overnight growth in SC media, cells were diluted to

OD600 = 0.2 in fresh media with or without the iron chelator, bathophenanthrolinedisulfonic acid (BPS), and grown at 30°C for 2-3 doublings. Cell density of the culture was measured after this period and cells were collected from growth in SC media for preparation for ICP-MS. Cells grown in presence of BPS were washed with Nanopure Diamond filtered water and diluted to OD600 = 0.5 in fresh SC media. Cells were grown at 30°C for 1 hour or 1 doubling after which point they were collected for ICP-MS.

Figure 1

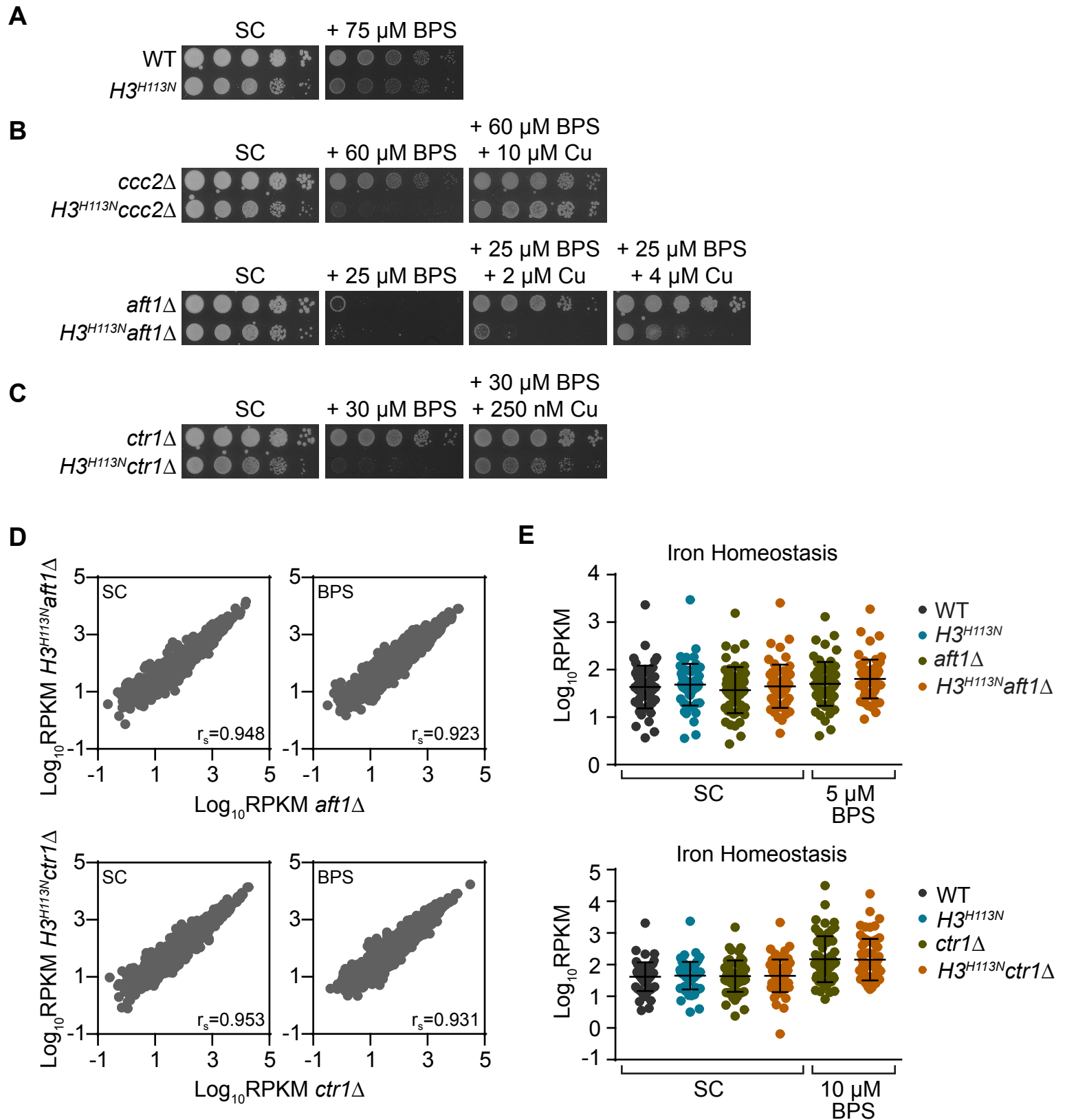
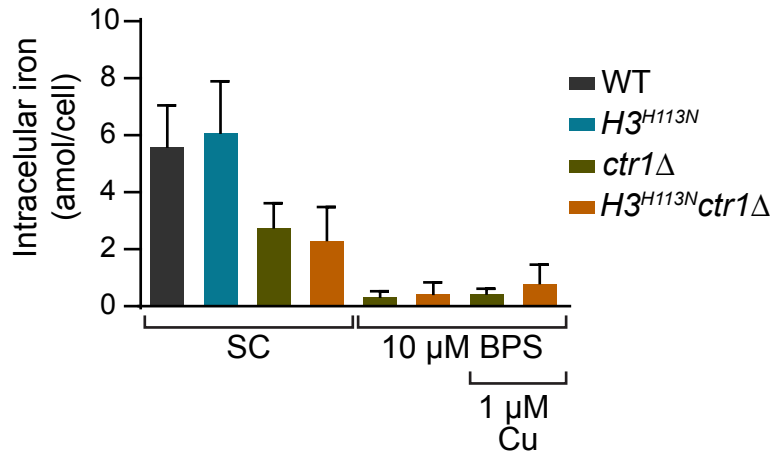
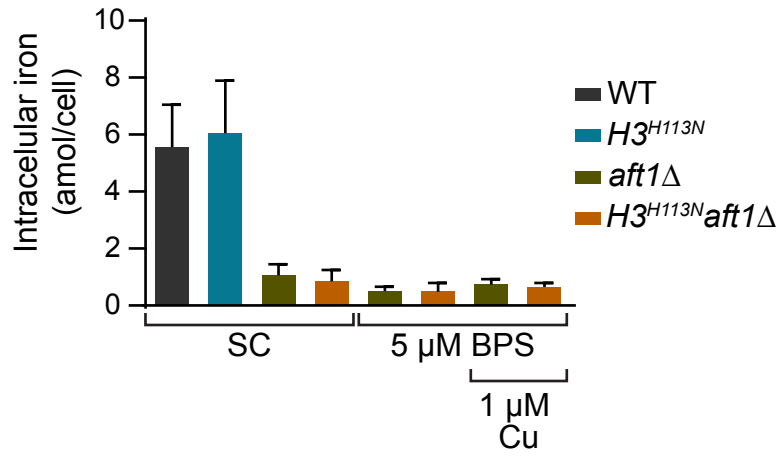
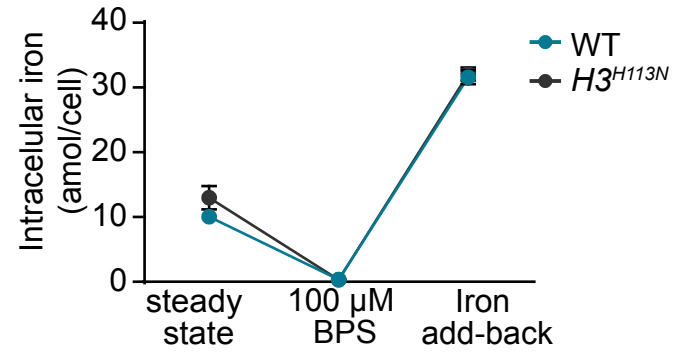


Figure 2

A



B



C

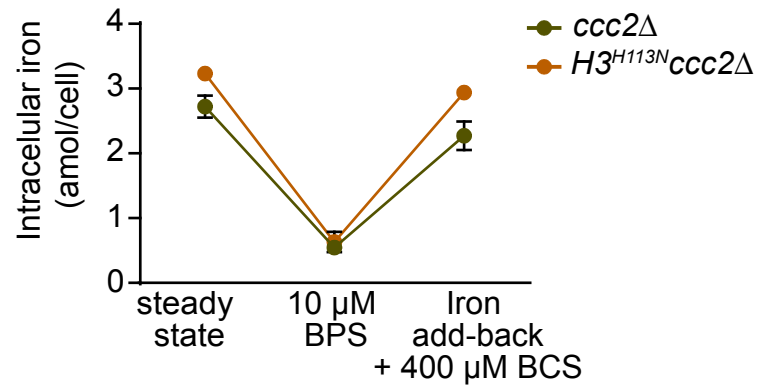
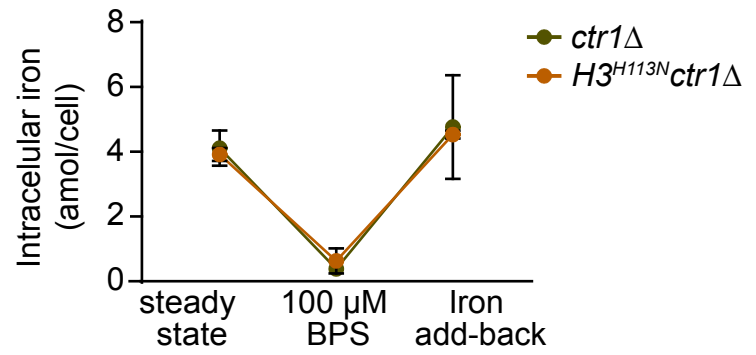
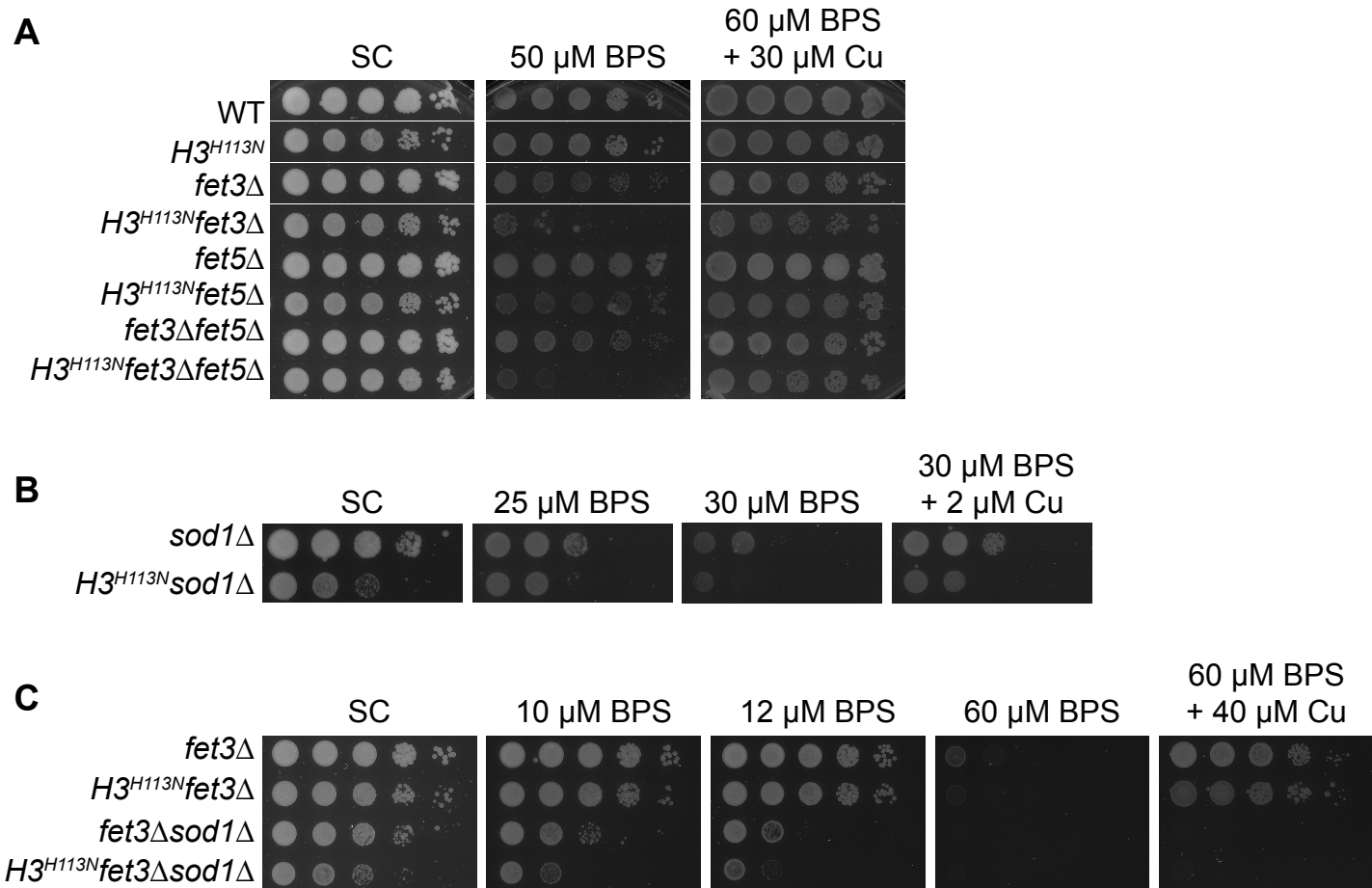


Figure 3



References

1. Zhang, C. Essential functions of iron-requiring proteins in DNA replication, repair and cell cycle control. *Protein Cell* **5**, 750–760 (2014).
2. Lieu, P. T., Heiskala, M., Peterson, P. A. & Yang, Y. The roles of iron in health and disease. *Molecular Aspects of Medicine* **22**, 1–87 (2001).
3. Aisen, P., Enns, C. & Wessling-Resnick, M. Chemistry and biology of eukaryotic iron metabolism. *Int. J. Biochem. Cell Biol.* **33**, 940–959 (2001).
4. Outten, A. C. D. and C. E. *The Iron Metallome in Eukaryotic Organisms.* **12**, (2013).
5. Hong Enriquez, R. P. & Do, T. N. Bioavailability of Metal Ions and Evolutionary Adaptation. *Life* **2**, 274–285 (2012).
6. Schroder, I., Johnson, E. & De Vries, S. Microbial ferric iron reductases. *FEMS Microbiology Reviews* **27**, 427–447 (2003).
7. Taylor, A. B., Stoj, C. S., Ziegler, L., Kosman, D. J. & Hart, P. J. The copper-iron connection in biology: structure of the metallo-oxidase Fet3p. *Proc. Natl. Acad. Sci. U. S. A.* **102**, 15459–64 (2005).
8. Kosman, D. J. Molecular mechanisms of iron uptake in fungi. *Mol. Microbiol.* **47**, 1185–1197 (2003).
9. Urbanowski, J. L. & Piper, R. C. The iron transporter Fth1p forms a complex with the Fet5 iron oxidase and resides on the vacuolar membrane. *J. Biol. Chem.* **274**, 38061–38070 (1999).
10. Hellman, N. E. & Gitlin, J. D. CERULOPLASMIN METABOLISM AND FUNCTION. *Annu. Rev. Nutr* **22**, 439–58 (2002).
11. Frieden, E. Ceruloplasmin, A Link Between Copper and Iron Metabolism.
12. Palumaa, P. Copper chaperones. the concept of conformational control in the metabolism of copper. *FEBS Letters* **587**, 1902–1910 (2013).
13. Saccon, R. a., Bunton-Stasyshyn, R. K. a, Fisher, E. M. C. & Fratta, P. Is SOD1 loss of function involved in amyotrophic lateral sclerosis? *Brain* **136**, 2342–2358 (2013).
14. Papa, L., Hahn, M., Marsh, E. L., Evans, B. S. & Germain, D. SOD2 to SOD1 switch in breast cancer. *J. Biol. Chem.* **289**, 5412–5416 (2014).
15. Kotze, M., Van Velden, D., Van Rensburg, S. & Erasmus, R. Pathogenic Mechanisms Underlying Iron Deficiency and Iron Overload: New Insights for Clinical Application. *J. Int. Fed. Clin. Chem. Lab. Med.* (2009).

16. Rutherford, J. C. & Bird, A. J. Metal-Responsive Transcription Factors That Regulate Iron , Zinc , and Copper Homeostasis in Eukaryotic Cells MINIREVIEW Metal-Responsive Transcription Factors That Regulate Iron , Zinc , and Copper Homeostasis in Eukaryotic Cells. *Eukaryotic cell* **3**, 1–13 (2004).
17. Kaplan, C. D. & Kaplan, J. Iron Acquisition and Transcriptional Regulation. doi:10.1021/cr9001676
18. Yuan, D. S. *et al.* The Menkes/Wilson disease gene homologue in yeast provides copper to a ceruloplasmin-like oxidase required for iron uptake. *Biochemistry* **92**, 2632–2636 (1995).
19. Spizzo, T., Byersdorfer, C., Dueterhoeft, S. & Eide, D. The yeast FET5 gene encodes a FET3 -related multicopper oxidase implicated in iron transport.
20. Lill, R. Function and biogenesis of iron–sulphur proteins. *Nature* **460**, 831–838 (2009).
21. Rouault, T. A. & Tong, W.-H. Iron–sulphur cluster biogenesis and mitochondrial iron homeostasis. *Nat. Rev. Mol. Cell Biol.* **6**, 345–351 (2005).
22. Wallace, M. A. *et al.* Superoxide inhibits 4Fe-4S cluster enzymes involved in amino acid biosynthesis. Cross-compartment protection by CuZn-superoxide dismutase. *J. Biol. Chem.* **279**, 32055–32062 (2004).
23. Popović-Bijelić, A. *et al.* Iron-sulfur cluster damage by the superoxide radical in neural tissues of the SOD1G93A ALS rat model. *Free Radic. Biol. Med.* **96**, 313–322 (2016).
24. Arredondo, M., Martínez, R., Núñez, M. T., Ruz, M. & Olivares, M. Inhibition of iron and copper uptake by iron, copper and zinc. in *Biological Research* **39**, 95–102 (2006).
25. Foster, a. W., Osman, D. & Robinson, N. J. Metal Preferences and Metallation. *J. Biol. Chem.* **289**, 28095–28103 (2014).
26. Lang, M., Braun, C. L., Kanost, M. R. & Gorman, M. J. Multicopper oxidase-1 is a ferroxidase essential for iron homeostasis in *Drosophila melanogaster*. *Proc. Natl. Acad. Sci.* **109**, 13337–13342 (2012).
27. Vashchenko, G. & Macgillivray, R. T. A. Multi-Copper Oxidases and Human Iron Metabolism. *Nutrients* **5**, 2289–2313 (2013).
28. Castells-Roca, L., Mühlhoff, U., Lill, R., Herrero, E. & Bellí, G. The oxidative stress response in yeast cells involves changes in the stability of Aft1 regulon mRNAs. *Mol. Microbiol.* **81**, 232–248 (2011).
29. Pujol-Carrion, N., Belli, G., Herrero, E., Nogues, A. & de la Torre-Ruiz, M. A. Glutaredoxins Grx3 and Grx4 regulate nuclear localisation of Aft1 and the oxidative stress response in *Saccharomyces cerevisiae*. *J. Cell Sci.* **119**, 4554–4564 (2006).

30. De Freitas, J. M., Liba, A., Meneghini, R., Valentine, J. S. & Gralla, E. B. Yeast Lacking Cu-Zn Superoxide Dismutase Show Altered Iron Homeostasis ROLE OF OXIDATIVE STRESS IN IRON METABOLISM*.
31. Outten, C. E. & Albetel, A. N. Iron sensing and regulation in *Saccharomyces cerevisiae*: Ironing out the mechanistic details. *Current Opinion in Microbiology* **16**, 662–668 (2013).
32. Rutherford, J. C. *et al.* Activation of the iron regulon by the yeast Aft1/Aft2 transcription factors depends on mitochondrial but not cytosolic iron-sulfur protein biogenesis. *J. Biol. Chem.* **280**, 10135–10140 (2005).
33. Sandman, K., Krzycki, J. A., Dobrinski, B., Lurzt, R. & Reeve, J. N. Hmf, a DNA-binding protein isolated from the hyperthermophilic archaeon *Methanothermobacter ferredoxinus*, is most closely related to histones (DNA-protein complex/thermal stability/molecular evolution/histone sequence conservation). *Biochemistry* **87**, 5788–5791 (1990).
34. Turrens, J. F. Mitochondrial formation of reactive oxygen species. *J. Physiol.* **552**, 335–344 (2003).